Πανεπιστήμιο Ιωαννίνων
Σχολή Θετικών Επιστημών
Τμήμα Φυσικής

Φαινομενολογική Ανάλυση Μοντέλων Σωματιδιακής Σκοτεινής Ύλης

Δημήτριος Καραμήτρος

Διδακτορική Διατριβή

Ιωάννινα 2017

University of Ioannina
School of natural science
Department of Physics

Phenomenological Analysis of Particle Dark Matter Models

Dimitrios Karamitros

PhD Thesis

Ioannina 2017

Three-member advisory committee:

1. Athanasios Dedes (Supervisor)
   Associate Professor, Physics Department, University of Ioannina.
2. Kyriakos Tamvakis
   Professor, Physics Department, University of Ioannina.
3. Leandros Perivolaropoulos
   Professor, Physics Department, University of Ioannina.

Seven-member PhD examination committee:

1. Athanasios Dedes– Associate Professor, Physics Department, University of Ioannina.
2. Kyriakos Tamvakis– Professor, Physics Department, University of Ioannina.
3. Leandros Perivolaropoulos– Professor, Physics Department, University of Ioannina.
4. Ioannis Vergados– Emeritus Professor, Physics Department, University of Ioannina.
5. George Leontaris– Professor, Physics Department, University of Ioannina.
6. Ioannis Rizos– Professor, Physics Department, University of Ioannina.
7. Vassilis Spanos– Associate Professor, Department of Physics, University of Athens.

Dedicated to my family and those who supported me

Η παρούσα διδακτορική διατριβή έχει συγχρηματοδοτηθεί από την Ευρωπαϊκή Ένωση (Ευρωπαϊκό Κοινωνικό Ταμείο–ΕΚΤ) και από εθνικούς πόρους μέσω του Επιχειρησιακού Προγράμματος «Εκπαίδευση και Δια Βίου Μάθηση» του Εθνικού Στρατηγικού Πλαισίου Αναφοράς (ΕΣΠΑ) – Ερευνητικό Χρηματοδοτούμενο Έργο: ΘΑΛΗΣ. Επένδυση στην κοινωνία της γνώσης μέσω του Ευρωπαϊκού Κοινωνικού Ταμείου, MIS:375734

Περίληψη

Σήμερα, υπάρχουν αναμφισβήτητα στοιχεία για την ύπαρξη σκοτεινής ύλης, πιθανότατα με τη μορφή ηλεκτρικά ουδέτερων, σταθερών σωματιδίων. Ωστόσο, παρά την αυξανόμενη πειραματική και θεωρητική δραστηριότητα, η ακριβής φύση των σωματιδίων της σκοτεινής ύλης παραμένει άγνωστη. Στην παρούσα εργασία παρουσιάζουμε τρία μοντέλα που προβλέπουν ένα σωματίδιο σκοτεινής ύλης. Σε κάθε μοντέλο, εστιάζοντας στις πιο φυσικές περιπτώσεις, μελετάμε τις φαινομενολογικές επιπτώσεις του σωματιδίου σκοτεινής ύλης καθώς επίσης και των συνοδών σωματιδίων.

Στο πρώτο κεφάλαιο, συζητούμε εν συντομία το Καθιερωμένο Πρότυπο της φυσικής των στοιχειωδών σωματιδίων, την κοσμολογία και την σκοτεινή ύλη. Ξεκινάμε επιδεικνύοντας τη μορφή της συμμετρίας βαθμίδας του Καθιερωμένου Προτύπου. Στη συνέχεια εισάγουμε το σωματιδιακό περιεχόμενο και την προέλευση των διαφόρων μαζών μέσω του μηχανισμού Higgs. Στη συνέχεια, συζητάμε τη βασική διατύπωση του Καθιερωμένου Κοσμολογικού Μοντέλου. Εισάγουμε τη μετρική Friedman-Roberson-Walker, και συζητήστε την επέκταση και τη θερμική ιστορία του Σύμπαντος. Τέλος, συζητάμε το πρόβλημα της σκοτεινής ύλης. Παρουσιάζουμε τα στοιχεία για την ύπαρξη της σκοτεινής ύλης καθώς και τα γενικά χαρακτηριστικά του αντίστοιχου υποθετικού σωματιδίου. Στη συνέχεια, παρουσιάζουμε δύο μηχανισμούς που εξηγούν την εξέλιξη της αριθμητικής πυκνότητας του σωματιδίου αυτού. Κλείνοντας αυτό το κεφάλαιο, συζητούμε εν συντομία διάφορα πειράματα και παρατηρησιακές προσπάθειες που επικεντρώνονται στην ανίχνευση σωματιδίων σκοτεινής ύλης.

Στο δεύτερο κεφάλαιο, παρουσιάζουμε το απλούστερο φερμιονικό μοντέλο σκοτεινής ύλης, που αποτελείται από ένα σωματίδιο Majorana (S) το οποίο είναι singlet κάτω απο τη συμμετρία βαθμίδας του Καθιερωμένου Προτύπου. Δεδομένου ότι δεν υπάρχουν πιθανές επανακανονικοποιήσιμες αλληλεπιδράσεις μεταξύ του σωματιδίου αυτού και του Καθιερωμένου Προτύπου (λόγω μίας συμμετρίας Z_2), παρουσιάσαμε τον μοναδικό $d = 5$ μη-επανακανονικοποιήσιμο τελεστή που περιγράφει την αλληλεπίδραση μεταξύ του σωματιδίου S και του μποζονίου Higgs. Στη συνέχεια, εξετάζουμε την παραγωγή της αφθονίας των σωματιδίων S, μέσω των μηχανισμών freeze-out και freeze-in, σε δύο διαφορετικές περιοχές μάζας.

Στο τρίτο κεφάλαιο, μελετάμε μια επέκταση του Καθιερωμένου Προτύπου που αποτελείται από έναν φερμιονικό σκοτεινό τομέα. Αυτός ο σκοτεινός τομέας αποτελείται από δυο Weyl doublets με αντίθετο υπερφορτίο και ένα Majorana triplet. Υπό την υπόθεση μιας συμμετρίας Z_2, αυτά τα σωματίδια αλληλεπιδρούν πάντα ανά ζεύγη, επομένως το ελαφρύτερο ουδέτερο σωματίδιο είναι υποψήφιο σωματίδιο σκοτεινής ύλης. Δείχνουμε ότι οι όροι Yukawa αυτού του σκοτεινού τομέα είναι συμμετρικοί κάτω από μία συμμετρία που είναι υπεύθυνη για την καταστολή της ενεργού διατομής της ελαστικής σκέδασης νουκλεονίων-σκοτεινής ύλης, δεδομένου ότι οι αλληλεπιδράσεις μεταξύ του σωματιδίου σκοτεινής ύλης και του Higgs καθώς και του Z δεν υπάρχουν σε πρώτη προσέγγιση. Εστιάζοντας σε αυτό το συμμετρικό όριο, το ελαφρύτερο ουδέτερο φερμιόνιο αυτού του σκοτεινού τομέα μπορεί να εξηγήσει φυσικά την παρατηρούμενη πυκνότητα σκοτεινής ύλης, με μάζα στην κλίμακα των ασθενών φορέων.

Επιπλέον, δείχνουμε ότι τα νέα φορτισμένα φερμιόνια είναι υπεύθυνα για την καταστολή του πλάτους διάσπασης του μποζονίου Higgs σε δύο φωτόνια. Τέλος, δείχνουμε ότι το σωματίδιο σκοτεινής ύλης αυτού του μοντέλου μπορεί να παραχθεί και να ανιχνευθεί στο LHC στο εγγύς μέλλον.

Στο Κεφάλαιο 4, θεωρούμε έναν σκοτεινό τομέα που αποτελείται από ένα ζεύγος Weyl $SU(2)_L$-doublets με αντίθετα υπερφορτία. Αντιμετωπίζοντας αυτόν τον σκοτεινό τομέα ως όριο χαμηλής ενέργειας ενός ολοκληρωμένου μοντέλου με μια ενέργεια αποκοπής στην κλίμακα TeV, εκτελούμε μια λεπτομερή φαινομενολογική ανάλυση, συμπεριλαμβανομένων όλων των επανακανονικοποιήσιμων και μη-επανακανονικοποιήσιμων τελεστών $d = 5$ μεταξύ των σωματιδίων του σκοτεινού τομέα και του Καθιερωμένου Προτύπου. Διαπιστώνουμε ότι το σωματίδιο σκοτεινής ύλης μπορεί να έχει μια μάζα κοντά στην ηλεκτρασθενή κλίμακα, υπακούοντας σε όλους τους πειραματικούς και παρατηρησιακούς περιορισμούς, υπό την προϋπόθεση ότι υπάρχουν σημαντικές διπολικές αλληλεπιδράσεις μεταξύ των σωματιδίων του σκοτεινού τομέα και των μποζονίων βαθμίδας. Τέλος, συζητούμε πιθανή ανίχνευση του σωματιδίου σκοτεινής ύλης στις έρευνες 'χαμένης' ενέργειας του LHC. Δείχνουμε ότι οι ενεργές διατομές για τις τρέχουσες αναζητήσεις mono-X είναι αρκετά μικρές, με το κανάλι mono-jet να είναι το πιο πιθανό για μελλοντική ανίχνευση.

Στη συνέχεια, στο πέμπτο κεφάλαιο, εισάγουμε ένα ελάχιστο μοντέλο που προβλέπει ένα σωματίδιο σκοτεινής ύλης που αποκτά με φυσικό τρόπο μάζα κάτω απο τη GeV κλίμακα. Το μοντέλο αυτό είναι ένα two Higgs doublet model συμμετρικό κάτω από μια συμμετρία Peccei-Quinn (PQ), το οποίο αποτελείται από δύο Weyl φερμιόνια $SU(2)_L$-doublets και ένα singlet. Οι doublets είναι ουδέτερες κάτω από την συμμετρία PQ και είναι αποσυνδεδεμένες απο το πλάσμα καθ ΄όλη την ιστορία του Σύμπαντος. Το σωματίδιο σκοτεινής ύλης είναι το singlet, το οποίο είναι φορτισμένο κάτω από την συμμετρία PQ, και επομένως άμαζο. Η μάζα του σωματιδίου αυτού δημιουργείται κυρίως μέσω κβαντικών διορθώσεων, λόγω ενός όρου που σπάει την PQ. Δείχνουμε ότι η παραγωγή μάζας είναι συμβατή με την παραγωγή σκοτεινής ύλης μέσω του μηχανισμού freeze-in, χωρίς να βασίζεται στην λεπτομερή ρύθμιση των παραμέτρων.

Τέλος, συνοψίζουμε τα αποτελέσματα αυτής της εργασίας και συζητούμε πιθανές μελλοντικές κατευθύνσεις του έργου που παρουσιάστηκε.

Outline

Nowadays, there is irrefutable evidence for the existence of dark matter (DM), probably in the form of electrically neutral, stable particles. However, despite the increasing experimental and theoretical efforts, the exact nature of the dark matter particle(s) remains unknown. In this thesis, we present three models predicting a dark matter particle. In each model, focusing on the most natural cases, we study the phenomenological implications of the DM candidate particle as well as its parters.

In the first chapter, we briefly discuss the Standard Model (SM) of particle physics, cosmology and dark matter. We start by demonstrating the form of the SM gauge invariance. Then we introduce its particle content and explain the origin of the various masses via the Higgs mechanism. Afterwards, we discuss the basic formulation of the Standard Cosmological Model. We introduce the Friedman-Roberson-Walker metric, and discuss the expansion and thermal history of the Universe. Finally, we discuss the dark matter problem. We present the evidence for the existence of dark matter as well as the general characteristics of the hypothetical corresponding particle. Then, we present two mechanisms that explain the evolution of the DM number density. Closing this chapter, we briefly discuss various experimental and observational efforts that focus on the detection of DM signatures.

In the second chapter, we present the simplest fermionic DM model, which consists of one Majorana gauge singlet (S). Since there are no possible interactions between the DM particle and the SM at the renormalizable level (due to a Z_2 symmetry), we introduced the only $d = 5$ non-renormalizable operator available, describing the interaction between the DM particle and the Higgs boson. Then, we examine the production of the relic abundance for the S-particle, via the freeze-out and freeze-in mechanism, in two distinct mass regions.

In the third chapter, we study an extension of the SM that consists of a fermionic dark sector. This dark sector is composed of two Weyl iso-doublets with opposite hypercharge and a Majorana iso-triplet. Under the assumption of a Z_2 symmetry, these particles always interact in pairs, therefore the lightest neutral particle is a DM candidate. We show that the Yukawa terms of this dark sector are symmetric under a custodial symmetry, which is responsible for the suppression of the DM-nucleon cross section, since the tree-level interactions between the DM particle and the Higgs as well as the Z-boson vanish. Focusing on this symmetric limit, the lightest neutral fermion of this dark sector can naturally explain the observed DM density, with a mass at the electroweak scale. Furthermore, we show that the new charged fermions are responsible for a suppression of the branching ratio of the Higgs boson to two photons. Finally, we show that the DM particle of this model can be produced and detected at the LHC in the near future.

In Chapter 4, we consider a dark sector consisting on a pair of Weyl $SU(2)_L$-doublets with opposite hypercharges. Treating this dark sector as a low-energy limit of a UV-

complete model with a cutoff energy at the TeV scale, we perform a detail phenomenological analysis, including both renormalizable and non-renormalizable $d = 5$ interactions between the dark sector particles and the SM. We find that the DM particle can have a mass near the electroweak scale, while evading all experimental and observational constraints, provided that sizeable dipole interactions between the dark sector particles and the gauge bosons are present. We, then, discuss potential detection of the DM particle at missing energy searches at the LHC. We show that the cross sections for the current mono-X searches are suppressed, with the mono-jet channel being the most promising probe for future detection.

Next, in the fifth chapter, we introduce a minimal model that predicts a DM particle with a naturally obtained sub-GeV mass. This model is a Peccei-Quinn (PQ)-symmetric two-Higgs doublet model, which consists of two Weyl fermionic $SU(2)_L$-doublets and a majorana gauge singlet. The iso-doublets are neutral under the PQ-symmetry and assumed to be decoupled throughout the history of the Universe. The DM particle is the gauge singlet, which is charged under the PQ-symmetry, and therefore massless at tree level. The mass of the DM particle is generated predominantly at one-loop level, by a soft PQ-braking term in the scalar potential. We show that the mass generation is compatible with DM production via the freeze-in mechanism at the early Universe, without relying on parameter fine tuning.

In closing, we summarise the results of this thesis and discuss possible future directions of the work presented.

Contents

1 Introduction **1**
- 1.1 The Standard Model of Particle Physics . . . 1
- 1.2 Basics of Cosmology . . . 8
  - 1.2.1 Geometry of the Expanding Universe . . . 9
  - 1.2.2 Thermodynamics of the Early Universe . . . 12
- 1.3 Dark Matter . . . 19
  - 1.3.1 Why Dark Matter? . . . 19
  - 1.3.2 General Remarks on Dark Matter . . . 20
  - 1.3.3 Dark Matter Production Mechanisms . . . 20
  - 1.3.4 Dark Matter Candidates . . . 25
  - 1.3.5 Dark Matter Searches . . . 26

2 A Warming up Example **29**
- 2.1 Freeze-in . . . 29
- 2.2 Freeze-out . . . 35

3 Doublet-Triplet Fermionic Dark Matter **39**
- 3.1 Introduction . . . 39
- 3.2 Model Details . . . 42
  - 3.2.1 The spectrum . . . 44
  - 3.2.2 The interactions . . . 45
  - 3.2.3 A custodial symmetry . . . 47
  - 3.2.4 Lightest Neutral fermion interactions under the symmetry . . . 47
  - 3.2.5 Analytical expressions for the new interactions under the symmetry 50
  - 3.2.6 Composition of the lightest Neutral Fermion . . . 52
- 3.3 Estimate of Electroweak Corrections . . . 53
- 3.4 The Thermal Relic Dark Matter Abundance . . . 56
- 3.5 Direct DM Detection . . . 59
- 3.6 Higgs boson decays to two photons . . . 63
- 3.7 Vacuum Stability . . . 66
- 3.8 Heavy fermion production and decays at LHC . . . 67
  - 3.8.1 Production . . . 67
  - 3.8.2 Decays . . . 69
- 3.9 Conclusions . . . 70

4 Effective Theory for Electroweak Doublet Dark Matter **73**
- 4.1 Introduction and Motivation . . . 73
- 4.2 Symmetries and the effective theory . . . 76
  - 4.2.1 Custodial symmetry . . . 76
  - 4.2.2 Charge conjugation symmetry . . . 77
  - 4.2.3 The discrete Z_2-symmetry . . . 78

4.2.4 Symmetric limits used in the analysis . . . 78
4.3 Phenomenology . . . 79
4.3.1 Mass Spectrum . . . 79
4.3.2 Dark Matter Particle Interactions . . . 81
4.4 "Earth" constraints in the Dark Sector . . . 83
4.4.1 Nucleon-WIMP direct detection experimental bounds . . . 83
4.4.2 LEP bounds . . . 85
4.4.3 $h \to \gamma\gamma$ . . . 85
4.4.4 Electroweak oblique corrections . . . 88
4.5 Cosmological and astrophysical constraints . . . 91
4.5.1 A close look at the relic density . . . 91
4.5.2 Cosmological constraints due to relic density . . . 96
4.5.3 Gamma-rays . . . 98
4.5.4 Neutrino flux from the Sun . . . 101
4.6 LHC searches . . . 101
4.6.1 LHC constraints at 8 TeV . . . 102
4.6.2 Mono-jet searches at 13 TeV . . . 103
4.7 Conclusions . . . 105

5 Radiative Light Dark Matter 107
5.1 Introduction . . . 107
5.2 Radiative Mechanism . . . 109
5.2.1 The Model . . . 109
5.2.2 One-Loop Radiative Mass . . . 110
5.3 Dark Matter Abundance . . . 113
5.3.1 Boltzmann Equation for $\boldsymbol{Y_S}$ . . . 114
5.3.2 Approximate Results for $\boldsymbol{\Omega_S h^2}$ . . . 115
5.4 Results . . . 115
5.4.1 Solving the Strong CP Problem . . . 117
5.4.2 Detection of RLDM . . . 118
5.5 Conclusions . . . 119

6 Conclusions and Future Directions 121

7 Appendix 125
A One-loop Vertex . . . 125
B Non-renormalizable operators . . . 126
B.1 $d = 5$ non-renormalizable operators . . . 126
B.2 $d = 6$ non-renormalizable operators . . . 128

1 Introduction

1.1 The Standard Model of Particle Physics

The Standard Model (SM) of particle physics [1–6] describes interactions between the known particles as a renormalizable Quantum Field Theory (QFT). In this section we are going to briefly discuss the structure and formulation of the SM while introducing the various conventions that are going to be useful throughout this thesis[1].

The gauge symmetry of the SM is an $SU(3)_c \times SU(2)_L \times U(1)_Y$ gauge group broken down to $SU(3)_c \times U(1)_{\rm EM}$.[2] The SM particles are either fermions (spin-1/2) or bosons (spin-0 or 1). The fermions constitute the matter sector while the vector bosons (spin-1) are responsible for the mediation of forces. Furthermore, the recently discovered [23,24] Higgs boson (spin-0), as we shall see later, is responsible for the masses of the particles [25–27].

There are three generations of fermions in the SM which consist of leptons and quarks. Leptons are neutral (singlets) under the $SU(3)_c$ symmetry and charged under the electroweak one, $SU(2)_L \times U(1)_Y$. This leads to particles that are charged only under $U(1)_{\rm EM}$, where e, μ, τ are negatively charged while the corresponding neutrinos ν_e, ν_μ, ν_τ are neutral. The quarks are charged (triplets) under $SU(3)_c$ as well as $SU(2)_L \times U(1)_Y$. The charges of the quarks are as follows: $Q = 2/3$ for u, c, t and $Q = -1/3$ for d, s, b.

The boson content of the SM consists of the gauge and Higgs bosons. The gauge bosons are associated with the generators of the corresponding Lie algebra of the gauge group. The gluons are responsible for the mediation of the strong interactions ($SU(3)_c$) interaction, hence there are eight of them. The electroweak gauge bosons are $W^{1,2,3}$ and B associated with $SU(2)_L$ and $U(1)_Y$, respectively. After electroweak symmetry breaking the gauge bosons mix resulting to the weak gage bosons $W^\pm$, Z and the photon A.

In any QFT the fundamental object is the Lagrangian. In this section we'll construct the Lagrangian which describes the interactions between the particles. Furthermore, we will discuss the Higgs mechanism which gives masses to the SM particles.

The Free Dirac Lagrangian

In order to introduce the interactions between the particles of the SM, it would be helpful to discuss first the Lagrangian which describes the free fermions. This Lagrangian is

$$\mathcal{L} = \bar{\psi}(i\partial\!\!\!/ - m)\psi, \tag{1.1}$$

where ψ is the fermion field, $\partial\!\!\!/ \equiv \gamma_\mu \partial^\mu$, $\bar{\psi} \equiv \psi^\dagger \gamma^0$. The γ matrices obey $\{\gamma^\mu,\, \gamma^\nu\} = 2g^{\mu\nu}$. A common representation for these matrices is

[1] There is a vast number of reviews and textbooks on the subject of gauge theories and QFT, among them refs. [7–22].

[2] The meaning of the indices will be apparent in the following analysis.

$$\gamma^\mu = \begin{pmatrix} \mathbf{0} & \sigma^\mu \\ \bar{\sigma}^\mu & \mathbf{0} \end{pmatrix}, \tag{1.2}$$

with $\mathbf{0}$ being 2×2 matrix with vanishing components and

$$\sigma^\mu \equiv (\mathbf{1}, \sigma^i) \text{ and } \bar{\sigma}^\mu \equiv (\mathbf{1}, -\sigma^i), \tag{1.3}$$

where $\sigma^{i=1,2,3}$ are the Pauli matrices and $\mathbf{1}$ the 2×2 unit matrix.

This is the 4-component spinor notation, which is the most widely used notation when dealing with fermions. There is another notation available which is usually helpful for fermions where the particle and the antiparticle are identical (these are referred as Majorana fermions). This notation emerges from further decomposing the one shown above, *i.e.* decomposing[3] γ^μ to σ^μ and $\bar{\sigma}^\mu$. In this notation the fermion field is written as

$$\psi = \begin{pmatrix} \psi_L \\ \psi_R \end{pmatrix}, \tag{1.4}$$

where ψ_L (ψ_R) is the left- (right-) handed component of the spinor field. We define here an additional γ-matrix

$$\gamma^5 = \begin{pmatrix} -\mathbf{1} & \mathbf{0} \\ \mathbf{0} & \mathbf{1} \end{pmatrix}, \tag{1.5}$$

which can be used to construct left and right projection operators

$$P_L \equiv \frac{1}{2}(1 - \gamma^5) \text{ and } P_R \equiv \frac{1}{2}(1 + \gamma^5), \tag{1.6}$$

which can be used to isolate the left- and right-handed spinor components. The left- and right-handed fermion fields transform independently under two-dimensional nontrivial irreducible representations of the Lorentz algebra, *i.e.* the left- (right-) handed component transform under $SU(2)_L$ ($SU(2)_R$) in the fundamental representation. The left and right components can be conveniently written as

$$\psi_L = \chi \text{ and } \psi_R = \eta^\dagger, \tag{1.7}$$

where we omit the $SU(2)$ Lorentz indices for simplicity. It is worth noting that in this notation the right-handed fermions are just the conjugate fields of the left-handed ones. Thus, particles can be defined only by their left-handed components.

With this definition, the Dirac Lagrangian (1.1) becomes

$$\mathcal{L} = i\chi^\dagger \bar{\sigma}^\mu \partial_\mu \chi + i\eta^\dagger \bar{\sigma}^\mu \partial_\mu \eta - m(\chi\eta + \chi^\dagger \eta^\dagger). \tag{1.8}$$

It is clear that χ and η describe different particles with the same mass. It will become clear in the following paragraph that χ and η have also opposite charges, hence they describe the particle-antiparticle system.

As mentioned above, the 2-component notation is very useful when dealing with Majorana fermions. These fermions are described by only one field, ξ, and the corresponding free Lagrangian is

[3] For a complete description of this notation see ref. [28].

$$\mathcal{L} = i\xi^\dagger \bar{\sigma}^\mu \partial_\mu \xi - \frac{1}{2} m(\xi\xi + \xi^\dagger \xi^\dagger). \tag{1.9}$$

It is noteworthy that the Dirac Lagrangian of eq. (1.8) describes two particles (χ and η) with the same mass, while the Majorana Lagrangian describes only one fermion (ξ). As it turns out, Majorana fermions are neutral (more general, transform under real or pseudo-real representation of a group) under all transformations, *i.e.* a Majorana fermion is its own antiparticle. On the other hand, Dirac fermions are charged, which means that χ and η describe a particle-antiparticle pair.

Quantum Electrodynamics

To construct the Lagrangian of Quantum Electrodynamics (QED) we start with the Dirac Lagrangian, describing free electrons

$$\mathcal{L} = \bar{\psi}(i\not{\partial} - m_e)\psi \ , \tag{1.10}$$

where m_e is the electron mass.

The Lagrangian (1.10) is symmetric under the global transformation $\psi(x) \to e^{i\alpha}\psi(x)$. To introduce interactions we start from the Dirac Lagrangian and require invariance under a local gauge transformation $\psi(x) \to e^{ie\alpha(x)}\psi(x)$. Then ∂_μ is replaced with the covariant derivative $D_\mu = \partial_\mu - ieA_\mu(x)$, with $A_\mu(x)$ a vector field with transformation $A_\mu(x) \to A_\mu(x) + \partial_\mu\alpha(x)$. Here we identify $A_\mu(x)$ as the electromagnetic 4-potential. Thus we introduce to the Lagrangian an invariant (kinetic) term that describes this field. This term is $-\frac{1}{4}(F_{\mu\nu}F^{\mu\nu})$, where $F_{\mu\nu} = \partial_\mu A_\nu(x) - \partial_\nu A_\mu(x)$. Finally, the Lagrangian for QED is:

$$\mathcal{L}_{\text{QED}} = \bar{\psi}(i\gamma^\mu\partial_\mu - m_e)\psi - \frac{1}{4}(F_{\mu\nu}F^{\mu\nu}) + e\bar{\psi}\gamma^\mu\psi A_\mu \ , \tag{1.11}$$

where e is the absolute value of the electron charge. From the above, it is clear that apart from the kinetic terms of the electron and photon fields, there is an interaction term. Although QED is the minimal example of a gauge theory, the procedure to generate the interaction and the form of the Lagrangian is rather generic.

In the 2-component notation, and using identities given in [28], the interaction term of the QED Lagrangian becomes

$$\mathcal{L}_{\text{int}} = e\chi^\dagger\bar{\sigma}^\mu\chi A_\mu - e\eta^\dagger\bar{\sigma}^\mu\eta A_\mu \ , \tag{1.12}$$

where it is clear that the χ and η spinors describe particles with opposite electric charge and the same mass as in eq. (1.8), *i.e.* electron-positron system.

In closing, Noether's theorem states that there is a conserved current, associated with this symmetry. For the gauge transformation $\psi \to \psi + ie\alpha(x)\psi$, the conserved (electromagnetic) current is

$$J^\mu_{\text{QED}} = \bar{\psi}\gamma^\mu\psi \ . \tag{1.13}$$

The vanishing of the derivative of the current eq. (1.13) leads to electric charge conservation.

$SU(2)$ Yang-Mills

Consider the Dirac Lagrangian (1.1) with ψ being an $SU(2)$ doublet. The free Dirac Lagrangian is invariant under the transformation $\psi \to e^{ig\vec{T}\cdot\vec{\alpha}}\psi$, $\vec{T}$ satisfies the $SU(2)$ Lie algebra

$$[T_i, T_j] = i\epsilon_{ijk}T_k \ , \tag{1.14}$$

where ϵ_{ijk} is the total antisymmetric tensor and $T_{1,2,3}$ are the $SU(2)$ generators. In the fundamental representation these are

$$T_1 = \frac{1}{2}\begin{pmatrix} 0 & 1 \\ 1 & 0 \end{pmatrix} \ , \ T_2 = \frac{1}{2}\begin{pmatrix} 0 & -i \\ i & 0 \end{pmatrix} \ , \ T_3 = \frac{1}{2}\begin{pmatrix} 1 & 0 \\ 0 & -1 \end{pmatrix} \ . \tag{1.15}$$

As in QED we promote this symmetry to a local one, *i.e.* a transformation law $\psi \to e^{ig\vec{T}\cdot\vec{\alpha}(x)}\psi$. The covariant derivative for this $SU(2)$ case is

$$D_\mu = \partial_\mu + ig\vec{T}\cdot\vec{W}_\mu \ , \tag{1.16}$$

where $\vec{W}$ is the gauge boson associated with the $SU(2)$ symmetry and transforms as $T^iW^i_\mu \to T^i \cdot W^i_\mu - g\epsilon^{ijk}\alpha_i W^j T^k + T_i(\partial_\mu \alpha^i(x))$. The invariant kinetic term for the vector fields W^i_μ is

$$\mathcal{L}^{(\mathrm{kin})}_{\mathrm{YM}} = -\frac{1}{4}(W^i_{\mu\nu}W^{i\mu\nu}) \ , \tag{1.17}$$

with

$$W^i_{\mu\nu} = \partial_\mu W^i_\nu - \partial_\nu W^i_\mu + g\epsilon^{ijk}W^j_\mu W^k_\nu \ . \tag{1.18}$$

Since $SU(2)$ is non-Abelian, this kinetic term includes also self-interaction of the W bosons. Finally, the gauge invariant Lagrangian, which describes the fields ψ, W^i_μ and their interactions, becomes now

$$\mathcal{L}_{\mathrm{YM}} = \bar{\psi}(i\gamma^\mu\partial_\mu - m)\psi - \frac{1}{4}(W^i_{\mu\nu}W^{i\mu\nu}) + g\bar{\psi}\gamma^\mu\vec{T}\cdot\vec{W}_\mu\psi \ . \tag{1.19}$$

Quantum Chromodynamics

Quantum Chromodynamics (QCD) is the theory that describes the strong interactions. The gauge symmetry of QCD is $SU(3)$ and conventionally we refer to this symmetry as $SU(3)_c$, where c refers to color. The Lagrangian is similar to eq. (1.19) with

$$\epsilon_{ijk} \to f_{abc}, \ \vec{W}_\mu \to G^a_\mu \ , \vec{T} \to t^a \text{ and } g \to g_s \ , \tag{1.20}$$

where f_{abc} is the structure constant of $SU(3)$, G is the gluon field, $a, b, c = 1, 2...8$, t^a are the $SU(3)$ Lie algebra generators and g_s is the strong gauge coupling.

Electroweak interactions

The gauge symmetry of the electroweak (EW) interactions is $SU(2)\times U(1)$ with covariant derivative

$$D_\mu = \partial_\mu - ig\vec{T}\cdot\vec{W}_\mu - ig'\frac{1}{2}YB_\mu \ , \tag{1.21}$$

where Y is the hypercharge, g and g' are the $SU(2)$ and $U(1)$ gauge couplings, respectively. Conventionally, we refer to the EW gauge symmetry as $SU(2)_L \times U(1)_Y$, where L indicates that only the left-handed components of the SM fermions transform under the $SU(2)$, and Y referring to the hypercharge.

It is convenient to rotate the fields $W_{3\mu}$ and B_μ to Z_μ and A_μ, so that they do not mix after symmetry breaking. This can be achieved by the rotation

$$\begin{pmatrix} W_{3\mu} \\ B_\mu \end{pmatrix} = \begin{pmatrix} c_W & s_W \\ -s_W & c_W \end{pmatrix} \begin{pmatrix} Z_\mu \\ A_\mu \end{pmatrix} , \tag{1.22}$$

where s_W and c_W are $sin(\theta_W)$ and $cos(\theta_W)$, respectively and using

$$T_1 W_{1\mu} + T_2 W_{2\mu} = T^+ W_\mu^+ + T^- W_\mu^- , \tag{1.23}$$

where $W_\mu^\pm = \frac{1}{\sqrt{2}}(W_{1\mu} \mp iW_{2\mu})$, $T^\pm = \frac{1}{\sqrt{2}}(T_1 \pm iT_2)$ the covariant derivative becomes

$$D_\mu = \partial_\mu - ig(T^+ W_\mu^+ + T^- W_\mu^-) - i\frac{g}{c_W}(T_3 + Qs_W^2)Z_\mu - iQeA_\mu , \tag{1.24}$$

with $e = s_W g = g' c_W$ and $Q = T_3 + \frac{1}{2}Y$ is the electric charge of each particle in units of the electron charge, e. The kinetic terms for the gauge bosons are as in QED and the $SU(2)$ Yang-Mills. Thus, the covariant derivative of the SM finally becomes

$$D_\mu = \partial_\mu - ig_s t^a G_\mu^a - ig(T^+ W_\mu^+ + T^- W_\mu^-) - i\frac{g}{c_W}(T_3 + Qs_W^2)Z_\mu - iQeA_\mu . \tag{1.25}$$

Fermions of Standard Model

As already explained, there are three generations of fermions, each containing quarks and leptons. Each fermion is described only by it's charges (representations) under the SM gauge group. The representation under the $SU(3)_c$ is quite straightforward. Quarks are $SU(3)_c$ triplets, while leptons are singlets. The case is more involved for the electroweak gauge group, since the left- and right-handed components transform in a differed way (chiral fermions) under $SU(2)_L \times U(1)_Y$. The left-handed fields are doublets under the $SU(2)_L$, while the right-handed ones are singlets.

Table 1.1: *Representations of one fermion generation under the SM gauge group.*

fermion	$SU(3)_c$	$SU(2)_L$	$U(1)_Y$
L_L	1	2	-1
l_R	1	1	-2
q_L	3	2	1/3
u_R	3	1	4/3
d_R	3	1	-2/3

In Table 1.1 we show the representations of a fermion generation under the SM gauge group. Notice that there is one right-handed lepton while there are two right-handed quarks. This, as we shall see next leads to massless neutrinos. Following the procedure shown in the previous paragraphs, all the interactions between the fermions and the

gauge bosons can be computed. The compact form of the quark and lepton interaction Lagrangian (in 4-component notation), suppressing the gauge indices, is

$$\begin{aligned}\mathcal{L} = & - \frac{1}{4}G^{a\mu\nu}G^a_{\mu\nu} - \frac{1}{4}W^{i\mu\nu}W^i_{\mu\nu} - \frac{1}{4}B^{\mu\nu}B_{\mu\nu} \\ & + i\sum_{i=1,2,3}\left[\bar{L}_{iL}\not{D}L_{iL} + \bar{l}_{iR}\not{D}l_{iR} + \bar{q}_{iL}\not{D}q_{iL} + \bar{u}_{iR}\not{D}u_{iR} + \bar{d}_{iR}\not{D}d_{iR}\right], \quad (1.26)\end{aligned}$$

where $\not{D} = \gamma^\mu D_\mu$ with D_μ being the covariant derivative of the SM given in eq. (1.25).

Table 1.2: *Representations of one fermion generation under the SM gauge group in 2-component notation. Note that the "bars" above the $SU(2)_L$ singlets are part of the fermion names.*

fermion	$SU(3)_c$	$SU(2)_L$	$U(1)_Y$
L	1	2	-1
$\bar{l}$	1	1	2
q	3	2	1/3
$\bar{u}$	$\bar{3}$	1	-4/3
$\bar{d}$	$\bar{3}$	1	2/3

One can make use of the 2-component notation by defining only the charges of left-handed fermions and antifermions as in Table 1.2. Then the fermion part of the Lagrangian, again suppressing the gauge indices, becomes

$$\mathcal{L}_{\text{fermion}} = i\sum_{i=1,2,3}\left[L_i^\dagger\bar{\sigma}^\mu D_\mu L_i + \bar{l}_i^\dagger\bar{\sigma}^\mu D_\mu\bar{l}_i + q_i^\dagger\bar{\sigma}^\mu D_\mu q_i + \bar{u}_i^\dagger\bar{\sigma}^\mu D_\mu\bar{u}_i + \bar{d}_i^\dagger\bar{\sigma}^\mu D_\mu\bar{d}_i\right], \quad (1.27)$$

Notice the absence of masses in the SM Lagrangian. This is because there are no allowed mass terms, by the gauge symmetry. Masses of particles are generated by breaking the gauge symmetry via the Higgs mechanism.

The Higgs mechanism

We saw that interactions emerge from gauge symmetries. But in the SM gauge symmetry there are no gauge invariant mass terms for the known fermions and vector bosons. Thus, somehow, we would like to break this symmetry in order to give masses to these particles. The discovery of the Higgs boson showed that this can be done by breaking the EW symmetry $SU(2)_L \times U(1)_Y$ to the electromagnetic one, *i.e.* $U(1)_{EM}$. In the following we briefly discuss this mechanism and show how the masses of the SM particles are generated.

The field responsible for the spontaneous symmetry breaking of the EW gauge symmetry, is the Higgs field, H. This field is neutral under the strong interactions and $SU(2)_L$ doublet with $U(1)_Y$ charge = 1. The EW symmetric Lagrangian describing this field is

$$\mathcal{L} = |D_\mu H|^2 + \mu^2|H|^2 - \frac{\lambda}{2}|H|^4, \quad (1.28)$$

The first term of this Lagrangian contains the interactions between H and the gauge bosons as well as the kinetic term. The last two terms are related to the potential

$$V(H, H^\dagger) = -\mu^2|H|^2 + \frac{\lambda}{2}|H|^4 \,. \tag{1.29}$$

The EW symmetry is broken when the ground state of the potential is non-zero. Since our goal is to break this symmetry, in order to allow for masses to be generated, we assume that $\mu^2 > 0$ and $\lambda > 0$. Thus the potential is minimized for $\langle H \rangle = \sqrt{\frac{\mu^2}{\lambda}}$. The EW gauge group breaks to the $U(1)_{EM}$ if the field H is expanded as

$$H = \begin{pmatrix} G^+ \\ H^0 \end{pmatrix} \rightarrow \begin{pmatrix} G^+ \\ \\ v + \dfrac{h + iG^0}{\sqrt{2}} \end{pmatrix} \,, \tag{1.30}$$

where $v \equiv \langle H \rangle$ is the vacuum expectation value (VEV) of the Higgs field, G^+ and G^0 are the goldstone bosons (in the unitary gauge these are rotated away by an $SU(2)$ transformation), and h the Higgs boson. With this expansion and eq. (1.25), we find various interaction terms and the following mass terms for $W^\pm$, Z and h

$$\mathcal{L}_{mass} = \frac{1}{2}g^2v^2W^{+\mu}W^-_\mu + \frac{1}{4}\left(\frac{g}{c_W}v\right)^2 Z_\mu Z^\mu + \lambda v^2 h^2 \,. \tag{1.31}$$

Thus the masses are $m_W = \dfrac{g}{\sqrt{2}}v$, $m_Z = \dfrac{g}{\sqrt{2}c_W}v = \dfrac{m_W}{c_W}$ and $m_h = \sqrt{2\lambda}v$. Note that there is no photon mass term, so the $U(1)_{EM}$ subgroup of the EW gauge group remains unbroken.

Fermion masses

The fermions of SM are ordered in generations, each generation contains one lepton and one quark family. Each lepton family consists of one left handed $SU(2)_L$ doublet $L_{iL} = \begin{pmatrix} \nu_i \\ l_i \end{pmatrix}_L$ and one right handed singlet, l_{iR}. Neutrinos do not have right handed components, therefore remain massless.[4] In the same way, left handed quarks are $SU(2)_L$-doublets $q_{iL} = \begin{pmatrix} u_i \\ d_i \end{pmatrix}_L$, and the right handed ones, u_{iR} and d_{iR}, are iso-singlets.

In order to generate fermion masses we need to find gauge invariant (Yukawa) terms of the form $(\bar{\psi}_L H \psi_R + \text{H.c.})$. After EW symmetry breaking, expanding H around its VEV, the fermion masses will appear proportional to $v(\bar{\psi}_L\psi_R + \text{H.c.})$. That is, the Yukawa terms for the leptons are

$$\mathcal{L}_{\text{y}}^{\text{Lepton}} = -\sum_{i=1,2,3} Y_i^{(\text{l})} \bar{L}_{iL} H l_{iR} + \text{H.c.} \,, \tag{1.32}$$

where $Y_i^{(\text{l})}$ is a Yukawa coupling, $i = 1$ corresponds to the electron (e), $i = 2$ the muon (μ) and $i = 3$ the tau (τ). Expanding H around its VEV, the Lagrangian (1.32) gives us the lepton mass terms

[4] This assumption can be relaxed.

$$\mathcal{L}_{\rm mass}^{\rm Lepton} = -\sum_{i=1,2,3} Y_i^{(\rm l)} v \bar{L}_{iL} l_{iR} + \text{H.c.} \tag{1.33}$$

That is, the lepton masses are $m_i = Y_i^{(\rm l)} v$. It is clear that, as mentioned above, neutrinos remain massless.

Quarks acquire masses in the same way. The invariant Yukawa terms for quarks are

$$\mathcal{L}_{\rm y}^{\rm Quark} = -\sum_{i,j=1,2,3} Y_{ij}^{(\rm u)}\, \bar{q}_{Li} (2i\, T_2\, H^*) u_{Rj} \; - \sum_{i,j=1,2,3} Y_{ij}^{(\rm d)}\, \bar{q}_{Li}\, H\, d_{Rj} + \text{H.c.}\,, \tag{1.34}$$

where $Y_{ij}^{(\rm u,\,d)}$ are Yukawa coupling represented by 3×3 (complex) matrices, $q_{Li} = \begin{pmatrix} u_i \\ d_i \end{pmatrix}_L$ and the singlets $q_{Rj} = u_{Rj}$, d_{Rj}. Thus, the mass terms are

$$\mathcal{L}_{\rm mass}^{\rm Quark} = -\sum_{i,j=1,2,3} Y_{ij}^{(\rm u)}\, v\; \bar{u}_{Li} u_{Rj} \; - \sum_{i,j=1,2,3} Y_{ij}^{(\rm d)}\, v\; \bar{d}_{Li} d_{Rj} + \text{H.c.} \tag{1.35}$$

Finally, we can see that the mass matrices for quarks are

$$M_{ij}^{(\rm u)} = Y_{ij}^{(\rm u)}\, v \;\; \text{and} \;\; M_{ij}^{(\rm d)} = Y_{ij}^{(\rm d)}\, v\,. \tag{1.36}$$

These matrices are not necessarily diagonal. We can diagonalize them by multiplying with some unitary matrices,[5] $V_{L,R}$ and $U_{L,R}$ defined by the following relations:

$$V_L^\dagger M^{(\rm u)} V_R = \begin{pmatrix} m_u & 0 & 0 \\ 0 & m_c & 0 \\ 0 & 0 & m_t \end{pmatrix} \;\; \text{and} \;\; U_L^\dagger M^{(\rm d)} U_R = \begin{pmatrix} m_d & 0 & 0 \\ 0 & m_s & 0 \\ 0 & 0 & m_b \end{pmatrix}\,. \tag{1.37}$$

The interaction terms of the SM Lagrangian eq. (1.26) can be written in the basis where the mass matrices are diagonal, as:

$$\begin{pmatrix} u_1 \\ u_2 \\ u_3 \end{pmatrix}_{L,R} = V_{L,R} \begin{pmatrix} u \\ c \\ t \end{pmatrix}_{L,R} \;\; \text{and} \;\; \begin{pmatrix} d_1 \\ d_2 \\ d_3 \end{pmatrix}_{L,R} = U_{L,R} \begin{pmatrix} d \\ s \\ b \end{pmatrix}_{L,R}\,, \tag{1.38}$$

where the mass of the up-quark (u) is m_u, the mass of the charm-quark (c) is m_c, etc.

Closing, we note that the same procedure can be followed in the 2-component spinor notation, resulting to the same mixing matrices and masses. This has been carried out in ref. [28].

1.2 Basics of Cosmology

The Universe seems to be *isotropic* and *homogeneous* at large scales ($\sim 10 Mpc$) and has been expanding for about 13.7 billion years. Currently, observations show that the Universe consists [29] of the known particles ($\sim 5\%$), Dark Matter ($\sim 25\%$) and Dark

[5] This is the so-called "singular value decomposition" (SVD), which ensures that the resulting diagonal matrix has non-negative real elements. SVD is explained in ref. [28].

Energy ($\sim 70\%$). In this section we will discuss the basic formulation of the Standard Cosmological Model.[6]

1.2.1 Geometry of the Expanding Universe

The Metric of the Universe

The geometry of an expanding isotropic Universe is described by the Friedman-Roberson-Walker (FRW) metric defined by the invariant line element squared (in polar coordinates)

$$ds^2 = dt^2 - a(t)^2\Big[\frac{dr^2}{1-kr^2} + r^2(d\theta^2 + sin^2\theta\, d\phi^2)\Big] \,, \tag{1.39}$$

where $a(t)$ is an expansion parameter called the scale factor and k is the curvature parameter. This metric has the consequence that the velocity of an object depends on the distance between the object and the observer as

$$\vec{v} = a(t)\frac{d\vec{r}}{dt} + \frac{da(t)}{dt}\vec{r} = a(t)\left(\dot{\vec{r}} + H\vec{r}\right) \,, \tag{1.40}$$

where H is the *Hubble* parameter defined as the expansion rate of the Universe:

$$H(t) \equiv \frac{\dot{a}(t)}{a(t)} \,. \tag{1.41}$$

Redshift

At first approximation, the particles follow a free-falling path described by the geodesic equation

$$\frac{du^\mu}{ds} + \Gamma^\mu_{\alpha\beta} u^\alpha u^\beta = 0 \,, \tag{1.42}$$

where $u^\mu \equiv \frac{dx^\mu}{ds}$ is the four velocity of a particle with x^μ its spacetime path and s the proper time. Also $\Gamma^\mu_{\alpha\beta}$ are the Christoffel-symbols

$$\Gamma^\mu_{\alpha\beta} \equiv \frac{1}{2} g^{\mu\sigma}\left(\partial_\alpha g_{\beta\sigma} + \partial_\beta g_{\alpha\sigma} - \partial_\sigma g_{\alpha\beta}\right) \,, \tag{1.43}$$

with $\partial_\mu \equiv \dfrac{\partial}{\partial x^\mu}$ and $g_{\mu\nu}$ the FRW metric defined by eq. (1.39).

The geodesic equation (1.42) can be alternatively written in terms of the particle's momentum, $P^\mu = mu^\mu$, as [7]

$$P^\alpha \frac{\partial P^\mu}{\partial x^\alpha} = -\Gamma^\mu_{\alpha\beta} P^\alpha P^\beta \,. \tag{1.44}$$

Since in a homogeneous gravitational background $\partial_i P^0 = 0$, the $\mu = 0$ component of eq. (1.44) becomes

$$P^0 \frac{dP^0}{dt} = -\Gamma^0_{\alpha\beta} P^\alpha P^\beta \,. \tag{1.45}$$

[6] See also refs. [30–32].

[7] If $m = 0$ the parameter s is some affine parameter defined from $P^\mu = \frac{dx^\mu}{ds}$. As a result eq. (1.44) still holds.

This equation results in the evolution of the energy of free-falling particles. From eq. (1.43) for the FRW metric, the energy (P^0) follows

$$E\frac{dE}{dt} = -H|\vec{p}|^2 \,, \tag{1.46}$$

where $|\vec{p}|^2 = a^2|\vec{P}|^2$, with $|\vec{p}|^2 = E^2 - m^2$. This shows us that (using $EdE = pdp$)

$$\frac{|\dot{\vec{p}}|}{|\vec{p}|} = -H \,, \tag{1.47}$$

which in turn means that the momentum $|\vec{p}|$ falls as

$$|\vec{p}| \sim \frac{1}{a} \,. \tag{1.48}$$

One important result from eq. (1.48) is the redshift. Since the wavelength of a photon is $\lambda \sim 1/|\vec{p}|$, if a photon of wavelength λ_1 is emitted at $t = t_1$, today (at $t = t_0$) its wavelength (λ_0) would be

$$\lambda_0 = \frac{a(t_0)}{a(t_1)}\lambda_1 \,. \tag{1.49}$$

Therefore, since the Universe expands ($a(t_0) > a(t_1)$), photons redshift ($\lambda_0 > \lambda_1$).

We define here the redshift parameter as

$$z \equiv \frac{\lambda_0 - \lambda_1}{\lambda_1} = \frac{a(t_0)}{a(t_1)} - 1 \,. \tag{1.50}$$

For nearby light sources, the redshift parameter can be expanded as

$$z = (t_0 - t_1)H_0 \,. \tag{1.51}$$

where $H_0 \equiv H(t = t_0)$ is called the Hubble constant (today), which is parametrized as

$$H_0 \approx 2.1h \times 10^{-42}\text{GeV} \,, \tag{1.52}$$

with h being a dimensionless expansion parameter.

Eq. (1.51) shows that the light gets redshifted proportionally to the source-observer distance and so by measuring the redshift we can determine the distance that light travelled $d \equiv |t_1 - t_0|$ (in $c = 1$ units).

Dynamics of the Expansion

The evolution of the Universe is described by the Einstein equation

$$R_{\mu\nu} - \frac{1}{2}Rg_{\mu\nu} = 8\pi G(T_{\mu\nu} + T^{\Lambda}_{\mu\nu}) \,, \tag{1.53}$$

where, $T_{\mu\nu}$ the energy-momentum tensor, $T^{\Lambda}_{\mu\nu}$ the dark energy part of the energy-momentum tensor, $R_{\mu\nu}$ the Ricci tensor and $R \equiv R^{\mu}_{\mu}$. The Ricci tensor is defined as

$$R_{\mu\nu} \equiv \partial_\alpha\Gamma^\alpha_{\mu\nu} - \partial_\nu\Gamma^\alpha_{\mu\alpha} + \Gamma^\alpha_{\alpha\beta}\Gamma^\beta_{\mu\nu} - \Gamma^\alpha_{\mu\beta}\Gamma^\beta_{\nu\alpha} \,. \tag{1.54}$$

Homogeneity and isotropy dictate that the energy-momentum tensor is of the form

$$T^{\mu}{}_{\nu} = \begin{pmatrix} \rho & 0 & 0 & 0 \\ 0 & -P & 0 & 0 \\ 0 & 0 & -P & 0 \\ 0 & 0 & 0 & -P \end{pmatrix} , \tag{1.55}$$

where ρ is the total (matter and radiation, *i.e.* $\rho_r + \rho_m$) energy density and P the pressure, which are going to be defined in the next paragraph.

The dark energy part of the energy-momentum tensor is defined as

$$T^{\Lambda}_{\mu\nu} \equiv \rho_\Lambda g_{\mu\nu} , \tag{1.56}$$

with $\rho_\Lambda \equiv \frac{\Lambda}{8\pi G}$ being the dark energy density (Λ is the so-called the cosmological constant).

The energy-momentum tensor obeys the conservation equation

$$\partial_\mu T^{\mu}{}_{\nu} + \Gamma^{\mu}_{\mu\alpha} T^{\alpha}{}_{\nu} - \Gamma^{\alpha}_{\mu\nu} T^{\mu}{}_{\alpha} = 0 , \tag{1.57}$$

which leads to the continuity equation

$$\dot{\rho} + 3H(\rho + P) = 0 . \tag{1.58}$$

The continuity equation can be written in a more familiar form as

$$dU = -P dV , \tag{1.59}$$

with $U \equiv \rho V$ (total energy) and $V \sim \alpha^3$ (volume).

After some algebra, the Einstein equation (1.53) give us the so-called "Friedman equations"[8]:

$$H^2 = \frac{8\pi G}{3}(\rho + \rho_\Lambda) - \frac{k}{a^2} , \tag{1.60}$$

$$\frac{\ddot{a}}{a} = -\frac{4\pi G}{3}(\rho + 3P - 2\rho_\Lambda) . \tag{1.61}$$

We define the critical density as

$$\rho_{cr} \equiv \frac{3H_0^2}{8\pi G} , \tag{1.62}$$

which is the total energy density at $t = t_0$ for a flat Universe ($k = 0$). We also define dimensionless density parameters today for the various components (radiation, matter, dark energy) of the Universe

$$\Omega_i \equiv \frac{\rho_{0,\,i}}{\rho_{cr}} , \tag{1.63}$$

where i is r for radiation, m for matter, Λ for dark energy.

We note that, from eq. (1.48), the energy density of relativistic particles (radiation) scales as $\rho_r = E/V \sim 1/a^4$, while the energy density of non-relativistic (matter) particles

[8] Two of Eqs.(1.58), (1.60) and (1.61) are independent.

$\rho_m = m/V \sim 1/a^3$. Furthermore, the density of dark energy is conserved (Λ is a constant). Thus, the first Friedman equation (1.60) can be written as

$$\frac{H^2}{H_0^2} = \Omega_r a^{-4} + \Omega_m a^{-3} + \Omega_\Lambda + \Omega_k a^{-2} \,, \tag{1.64}$$

where we have also defined $\Omega_k \equiv -\frac{k}{(a_0 H_0)^2}$ and $a_0 \equiv 1$.

Today we are able to observationally determine [29] the various density parameters, resulting to $\Omega_r \approx 9.4 \times 10^{-5}$, $\Omega_m \approx 0.32$, $\Omega_\Lambda \approx 0.68$. That is, $\Omega_r + \Omega_m + \Omega_\Lambda \approx 1$ and $\Omega_k \approx 0$. Also, since $a(t) < 1$ and k does not depend on time, Ω_k is negligible throughout the history of the Universe. Therefore, throughout this thesis we assume that the Universe is flat ($k = 0$), without loss of generality.

1.2.2 Thermodynamics of the Early Universe

At early times, the Universe was (approximately) in thermal equilibrium. This means that the interactions between the particles were faster than the expansion of the Universe, *i.e.* the interaction rate was larger than the Hubble parameter $\Gamma > H$. At later times, as the Universe expanded and cooled, particles started to decouple giving rise to the various cosmological abundances, including dark matter (DM) which is the focus of this thesis.

There are some events that took place in the early Universe which have affected its present state (see refs. [30–34]), namely

- *Inflation,* $T \sim 10^{15}$GeV *(?).*[9] The small temperature fluctuations of the Cosmic Microwave Background (CMB), show that the Universe started in thermal equilibrium. However, it is impossible that the entire Universe was in thermal (causal) contact, since the speed of light is finite. This is the so-called horizon problem (see ref [31, 32, 35, 36] for more information). Also, the origin of the observed temperature fluctuations of the CMB is unknown. If we assume that there was an epoch of exponential expansion of the Universe (inflation), these problems are resolved. Inflation explains how all the regions of Universe were at first in causal contact as well as the magnification of quantum (zero-point) fluctuations to the ones measured today. At the end of this epoch, the field responsible for the rapid expansion of the Universe (inflaton) decayed to the known particles. The temperature at the end of the inflaton decay is called the reheating temperature of the Universe, T_{RH}.
- *Radiation dominated Universe,* $T = T_{RH} - 1$eV. After the decay of the inflaton, the energy content of the Universe was dominated by relativistic particles in equilibrium. The Universe remained radiation dominated up to $T \sim 1$eV, where most of the content of the Universe became non-relativistic.
- *EW phase transition,* $T \sim 100$GeV. As the temperature of Universe dropped below ~ 100GeV , the Higgs field developed a VEV, resulting to the known particle masses.
- *Baryogenesis,* $T \sim 100$GeV *(?).* In the SM it is impossible to create a particle without creating its antiparticle. This means that the Universe as we know shouldn't exist, because every particle would find an antiparticle and annihilate to photons. Therefore it is natural to assume that at some point the number of particles became larger then the number of antiparticles (this procedure is described in ref. [37]). One attractive scenario is electroweak baryogenesis (for a review see ref. [38]), where

[9] The temperature of the inflation era is unknown, hence the question mark.

baryogenesis happens at the temperature where the Higgs develops a VEV, *i.e.* $T \sim 100\text{GeV}$.

- *DM relic abundance,* $T = ?$. At some point, probably during the radiation dominated phase, the number of DM particles stabilized, resulting to the current DM abundance.
- *Quark confinement,* $T \sim 1\text{GeV}$. At low energies, the QCD coupling becomes strong enough. Therefore quarks and gluons form bound states.
- *Neutrino decoupling,* $T \sim 1\text{MeV}$. The temperature where the interactions between neutrinos and the rest of the plasma, became slower than the expansion rate of the Universe.
- *Electron–positron annihilation,* $T \sim 0.5\text{MeV}$. Electrons and positrons annihilate to photons, increasing the temperature of the photons, thus creating a small deviation between the photon and neutrino temperature ($\frac{T_\gamma}{T_\nu} \approx \left(\frac{11}{4}\right)^{1/3}$).
- *Neucleosynthesis,* $T \sim 0.1\text{MeV}$. After electron-positron annihilation, light elements formed during a process called Big Bang Neucleosynthesis (BBN).
- *Matter-radiation equality,* $T \approx 1\text{eV}$. As the Universe cooled, radiation redshifted to the point where the Universe started to be dominated by its matter content.
- *Recombination and photon decoupling,* $T \sim 0.3 - 0.2\text{eV}$. the available energy is smaller than the ionising energy of the hydrogen atom, Therefore, the remaining free electrons, combined with hydrogen, which lead to the photon decoupling. The photons remained free until today form the CMB.
- *Reionization,* $T \sim 2.5 - 7\text{meV}$. After recombination, structure formation started. In dense regions, stars started to form and the resulting radiation ionised their surrounding hydrogen.
- *Dark Energy dominated Universe,* $T \sim 0.3\text{meV}$. The matter energy density became equal to the dark energy density. Until today the Universe is dominated by the dark energy content.
- *Today.* The current temperature of the photons is $T_0 = 0.24\text{meV}$.

Basic Quantities

Before moving to the discussion of DM, it would be helpful to introduce various quantities that are necessary to describe the thermal history of the Universe. The number density (n), the energy density (ρ) and the pressure (P) of a particle species (i) are defined as

$$n_i = g_i \int \frac{d^3\vec{p}}{(2\pi)^3} f_i(E) \,, \tag{1.65}$$

$$\rho_i = g_i \int \frac{d^3\vec{p}}{(2\pi)^3} f_i(E) E \,, \tag{1.66}$$

$$P_i = \int g_i \frac{d^3\vec{p}}{(2\pi)^3} f_i(E) \frac{|\vec{p}|^2}{3E} \,, \tag{1.67}$$

where $f_i(E)$ is the (homogeneous and isotropic) phase space distribution function and g_i the number of internal degrees of freedom.[10] The equilibrium distribution function at temperature T and chemical potential μ is

[10] For example, $g = 2$ for the electron, $g = 1$ for the neutrinos (they are massless), etc.

$$f_i(E) = \Big[e^{(E-\mu)/T} \pm 1\Big]^{-1} , \tag{1.68}$$

with + for fermions and − for bosons.

Entropy

The second law of thermodynamics (for vanishing chemical potential) implies that

$$TdS = dU + PdV = \frac{\partial U}{\partial T}dT + \left[\frac{\partial U}{\partial V} + P\right]dV , \tag{1.69}$$

where S is the entropy of the system. In equilibrium $dS = 0$ (*i.e.* eq. (1.59)). Entropy obeys the integrability condition

$$\frac{\partial^2 S}{\partial T \partial V} = \frac{\partial^2 S}{\partial V \partial T} . \tag{1.70}$$

By this integrability condition and the definition of the energy density ($\rho \equiv \frac{\partial U}{\partial V}$), the second law of thermodynamics obtains the form

$$dS = d\Big[\frac{\rho + P}{T}V\Big] . \tag{1.71}$$

Thus we can define the entropy density in terms of ρ, T and P as

$$s \equiv \frac{\rho + P}{T} . \tag{1.72}$$

At equilibrium $a^3 s$ is constant, which means that the entropy density scales as

$$s \sim a^{-3} . \tag{1.73}$$

Useful Relations

In the relativistic limit ($T \gg m$), for vanishing chemical potential, the number density, energy density and pressure for a particle species (i) become [30–32]

$$n_i = \; g_i \frac{\zeta(3)}{\pi^2} T^3 \times \begin{cases} 1, \text{ for bosons} \\ 3/4, \text{ for fermions} \end{cases} , \tag{1.74}$$

$$\rho_i = \; g_i \frac{\pi^2}{30} T^4 \times \begin{cases} 1, \text{ for bosons} \\ 7/8, \text{ for fermions} \end{cases} , \tag{1.75}$$

$$P_i = \; \frac{\rho_i}{3} , \tag{1.76}$$

where $\zeta(3) \approx 1.2$. The total entropy density in this limit, from eqs. (1.72), (1.75) and (1.76), becomes

$$s = \frac{2\pi^2}{45} g_{\star S} T^3, \tag{1.77}$$

with $g_{\star S}$ referred as the *effective relativistic degrees of freedom*, defined as

$$g_{\star S} \equiv \sum_{\text{i=bosons}} g_i \left(\frac{T_i}{T}\right)^3 + \sum_{\text{i=fermions}} \frac{7}{8} g_i \left(\frac{T_i}{T}\right)^3 , \tag{1.78}$$

where we have also allowed for particles to be decoupled from the thermal bath with temperatures T_i.

Observe that if the Universe is in equilibrium and its energy content is dominated by relativistic particles, eqs. (1.73) and (1.75) indicate that the temperature would scale as $T \sim 1/a$.

In the non-relativistic limit ($T \ll m$) of the n, ρ and P are [30–32]:

$$n_i = g_i \left(\frac{mT}{2\pi}\right)^{3/2} e^{-m/T} , \tag{1.79}$$

$$\rho_i = m_i\, n_i , \tag{1.80}$$

$$P_i = T\, n_i , \tag{1.81}$$

which show that, compared to the relativistic ones, all these quantities are negligible. Thus the contribution of non-relativistic particles to the entropy density is exponentially suppressed. This means that if a particle becomes non-relativistic while at equilibrium, its entropy is transferred to the relativistic ones, *e.g.* via decays or annihilations.

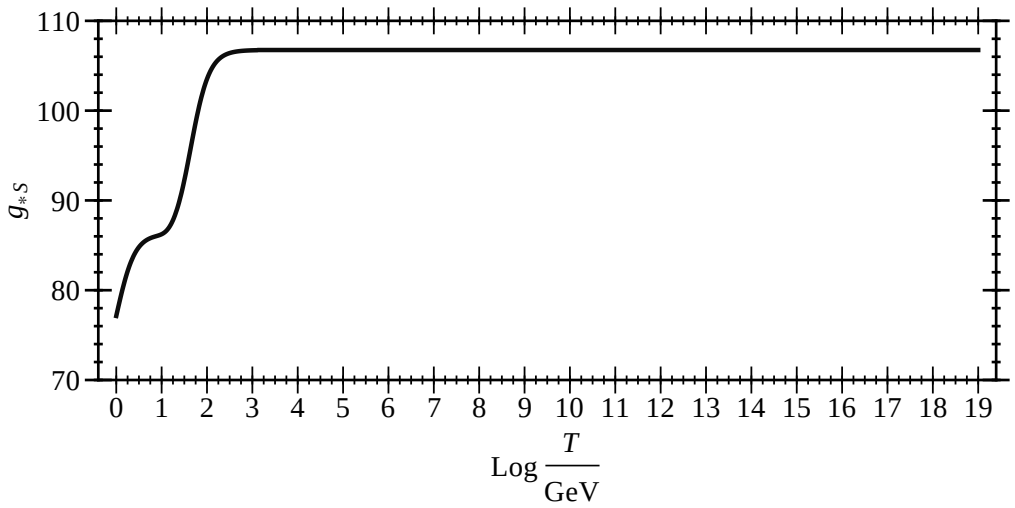

Figure 1.1: *The effective relativistic degrees of freedom of the SM as a function of the logarithm of the temperature.*

The dependence of effective relativistic degrees of freedom (1.78) of the SM particles on the logarithm of temperature, from $T = M_{Pl}$ to $T = 1$ GeV, is shown in Fig. 1.1. Observe that for temperatures above ~ 100 GeV, $g_{\star S}$ is constant, while for smaller temperatures and near mass thresholds, $g_{\star S}$ decreases exponentially. This helps to understand the decoupling process of a particle species. At T near mass thresholds, particles start to become non-relativistic (*i.e.* $g_{\star S}$ decreases), thus annihilating to lighter particles. The decoupling of these particles (usually) happens while they are in equilibrium. This means

that during the decoupling of a particle species, the temperature scaling departs from the usual $T \sim a^{-1}$, in order to take into account these annihilations while keeping the entropy constant. Therefore, from eqs. (1.73), (1.75) and (1.78), the temperature scales as

$$T \sim g_{\star S}^{-1/3} a^{-1}. \tag{1.82}$$

Finally, if the energy of the Universe is dominated by relativistic particles, the first Friedman equation (1.60) becomes

$$H = \left(\frac{8\pi^3}{90 M_{Pl}^2} g_\star\right)^{1/2} T^2 \approx 1.66 g_\star^{1/2} \frac{T^2}{M_{Pl}}\,, \tag{1.83}$$

where we have used $M_{Pl} \equiv G^{-1/2}$ with $M_{Pl} \approx 1.22 \times 10^{19}$GeV the "Planck mass". Also we have defined $g_\star$ as

$$g_\star \equiv \sum_{\text{i=bosons}} g_i \left(\frac{T_i}{T}\right)^4 + \sum_{\text{i=fermions}} \frac{7}{8} g_i \left(\frac{T_i}{T}\right)^4\,. \tag{1.84}$$

If all relativistic particles are in equilibrium, then $g_\star = g_{\star S}$.

Boltzmann Equation

The evolution of the distribution functions $f_i(E)$ of the particle species of the Universe is described by the Boltzmann equation. The Boltzmann equation for a particle i is written as

$$\frac{df_i}{dt} = \frac{\partial x^\alpha}{\partial t}\frac{\partial f_i}{\partial x^\alpha} + \frac{\partial p^\alpha}{\partial t}\frac{\partial f_i}{\partial p^\alpha} = \left(\frac{\partial}{\partial t} - H\frac{|\vec{p}|^2}{E}\frac{\partial}{\partial E}\right) f_i = I^{(\text{coll})}\,, \tag{1.85}$$

where we have used eq. (1.46) and the assumptions of homogeneity and isotropy. The r.h.s. of eq. (1.85) is the collision integral which, for all possible processes $i + X \leftrightarrow Y$, is given by

$$\begin{aligned} I_i^{(\text{coll})} =& \frac{1}{2E_i}\sum_{X,Y}\int d\Pi_X\, d\Pi_Y\, (2\pi)^4 \delta^{(4)}(p + \sum p_X - \sum p_Y)\times \\ & \left[\langle|M_{Y\to i+X}|^2\rangle \prod_Y f_Y \prod_X (1 \pm f_X)\,(1 \pm f_i) - \langle|M_{i+X\to Y}|^2\rangle f_i \prod_X f_X \prod_Y (1 \pm f_Y)\right], \end{aligned} \tag{1.86}$$

with $+$ for bosons (Bose enhancement effect), $-$ for fermions (Fermi blocking effect), $f_{i,X,Y}$ the various distributions functions, $\langle|M_{i+X\leftrightarrow Y}|^2\rangle$ the matrix elements squared, averaged over all internal degrees of freedom (divided by appropriate symmetry factors for identical particles). The integration is performed over the Lorentz invariant phase space of X and Y, with $d\Pi_{X,Y}$ defined as

$$d\Pi_{X,Y} \equiv g_{X,Y} \prod_{X,Y} \frac{d^3\vec{p}_{X,Y}}{(2\pi)^3 2E_{X,Y}}\,. \tag{1.87}$$

The Boltzmann equation in this form is rarely useful in calculations relevant to DM. Since DM is assumed to be non-relativistic today, its energy density is given by eq. (1.80). The evolution of the number density (of a particle species i) is given by the integrating the

Boltzmann equation over the momentum of i and multiplying with its internal degrees of freedom ($g_i \int \frac{d^3\vec{p}}{(2\pi)^3}$)

$$\frac{dn_i}{dt} + 3Hn_i = g_i \int \frac{d^3\vec{p}}{(2\pi)^3} I_i^{(\text{coll})} \ . \tag{1.88}$$

Noting that away from mass thresholds the entropy is conserved ($\frac{ds}{dt} = -3Hs$), the l.h.s. can be written as

$$\frac{dn_i}{dt} + 3Hn_i = s\frac{dY_i}{dt} + 3HsY + Y\frac{ds}{dt} = s\frac{dY_i}{dt} \ , \tag{1.89}$$

with Y being the yield defined as

$$Y_i \equiv \frac{n_i}{s} \ . \tag{1.90}$$

The Boltzmann equation cannot be solved analytically in general, but under approximations (and assumptions) can be greatly simplified. Assuming that the quantum statistical effects are negligible (which holds for most cases), the distribution functions follow Maxwell-Boltzmann statistics and we can ignore the Bose enhancement and Fermi blocking effects, which simplifies the Boltzmann equation to

$$\begin{aligned} s\frac{dY_i}{dt} = g_i \int \frac{d^3\vec{p}}{(2\pi)^3} I_i^{(\text{coll})} = & g_i \sum_{X,Y} \int \frac{d^3\vec{p}}{(2\pi)^3 2E} d\Pi_X \, d\Pi_Y \, (2\pi)^4 \delta^{(4)}(p + \sum p_X - \sum p_Y) \times \\ & \left[\langle |M_{Y \to i+X}|^2 \rangle \left(\prod_Y f_Y \right) - \langle |M_{i+X \to Y}|^2 \rangle f_i \left(\prod_X f_X \right) \right] . \end{aligned} \tag{1.91}$$

For specific processes, we can further simplify this Boltzmann equation to a more useful form.

The Boltzmann Equation for $1 \leftrightarrow 2$ Processes

Lets assume that we would like to find the evolution of the distribution function of a particle ψ that interacts only with plasma particles, B, through processes $B \leftrightarrow \psi\psi$, with $|M_{B \to \psi\psi}|^2 = |M_{\psi\psi \to B}|^2 = |M|^2$. The Boltzmann equation for Y_ψ, then, is

$$\begin{aligned} s\frac{dY_\psi}{dt} \ = \ & \int \frac{g_B d^3\vec{p}_B}{(2\pi)^3 2E_B} \prod_{i=1,2} \left(\frac{g_\psi d^3\vec{k}_i}{(2\pi)^3 2E_i} \right) (2\pi)^4 \delta^{(4)}(p - k_1 - k_2) \times \\ & \langle |M|^2 \rangle \ \left(f_B^{eq}(E_B) - f_\psi(E_1) f_\psi(E_2) \right) \ , \end{aligned} \tag{1.92}$$

where $\vec{k}_i$ are the momenta of the ψ particles, $f_B^{eq}(E_B) = e^{-E_B/T}$ the equilibrium distribution function for vanishing chemical potential[11] of B.

The Boltzmann equation can be further simplified by assuming that the distribution function of ψ is of the form

[11] In general, chemical potentials are unimportant in cosmology as explained in [31, 32].

$$f_\psi(E_{1,2}) = A(T)e^{-E_{1,2}/T} \,, \tag{1.93}$$

with $A(T)$ a function of the plasma temperature. Since $A(T)$ does not depend on the particle energy, it can be expressed in terms of the number density (1.65) of ψ as

$$A(T) = \frac{n_\psi}{n_\psi^{eq}} \,, \tag{1.94}$$

which leads to

$$f_\psi(E_1) f_\psi(E_2) = f_B^{eq}(E_B) \left(\frac{n_\psi}{n_\psi^{eq}}\right)^2 \,. \tag{1.95}$$

Also from the definition of the decay rate [13]

$$\frac{2}{g_B} m_B \Gamma_{B\to\psi\psi} = \frac{d^3\vec{k}_1}{(2\pi)^3 2E_1} \frac{d^3\vec{k}_2}{(2\pi)^3 2E_2} (2\pi)^4 \delta^{(4)}(p - k_1 - k_2) \langle |M|^2 \rangle \,, \tag{1.96}$$

the Boltzmann equation becomes

$$\begin{aligned} s\frac{dY_\psi}{dt} =& 2g_\psi^2 \; M_B \; \Gamma_{\psi\to B_1 B_2} \left[1 - \left(\frac{n_\psi}{n_\psi^{eq}}\right)^2\right] \int \frac{d^3\vec{p}_B}{(2\pi)^3 2E_B} \; e^{-E_B/T} = \\ =& \frac{g_\psi^2}{2\pi^2} \; M_B^2 \; T \; \Gamma_{B\to\psi\psi} \; K_1\left(\frac{M_B}{T}\right) \left[1 - \left(\frac{Y_\psi}{Y_\psi^{eq}}\right)^2\right] \,, \end{aligned} \tag{1.97}$$

where $K_1\left(\frac{M_B}{T}\right)$ is the first modified Bessel function of the second kind. Since we have assumed that the entropy is conserved (*i.e.* $T \sim 1/a$), the Boltzmann equation can be expressed as

$$\frac{dY_\psi}{dT} = -\frac{g_\psi^2}{2\pi^2} \frac{M_B^2 \, \Gamma_{B\to\psi\psi}}{Hs} K_1\left(\frac{M_B}{T}\right) \left[1 - \left(\frac{Y_\psi}{Y_\psi^{eq}}\right)^2\right] . \tag{1.98}$$

The Boltzmann Equation for $2 \leftrightarrow 2$ Processes

Consider a particle ψ that interacts only with plasma particles, $B_{1,2}$, through processes $\psi\psi \leftrightarrow B_1 B_2$, with $|M_{\psi\psi\to B_1\, B_2}|^2 = |M_{B_1\, B_2\to\psi\psi}|^2 = |M|^2$. Similarly to the previous case the Boltzmann equation is

$$\begin{aligned} \frac{dY_\psi}{dT} =& -\frac{1}{HsT} \int \prod_{i=1,2} \frac{g_\psi d^3\vec{p}_{\psi i}}{(2\pi)^3 2E_{\psi i}} \frac{g_i d^3\vec{k}_i}{(2\pi)^3 2E_i} \\ & (2\pi)^4 \delta^{(4)}(p_{\psi 1} + p_{\psi 2} - k_1 - k_2) \langle |M|^2 \rangle f_\psi^{eq}(E_{\psi 1}) f_\psi^{eq}(E_{\psi 2}) \left[1 - \left(\frac{Y_\psi}{Y_\psi^{eq}}\right)^2\right] \,, \end{aligned} \tag{1.99}$$

where $\vec{k}_i$ (E_i) is the momentum (energy) of B_i, $\vec{p}_{\psi i}$ ($E_{\psi i}$) is the momentum (energy) of the ψ-pair.

We define the thermal average of the total annihilation cross-section , multiplied by the relative velocity of the incoming ψ pair

$$\langle \sigma_{\psi\psi\to B_1 B_2} v \rangle \equiv \frac{1}{n_\psi^{eq\,2}} \int \prod_{i=1,2} \frac{d^3\vec{p}_{\psi i}}{(2\pi)^3} \sigma_{\psi\psi\to B_1 B_2}\, v\, f_{\psi 1}^{eq} f_{\psi 2}^{eq} \,, \tag{1.100}$$

with [13]

$$\begin{aligned} \sigma_{\psi\psi\to B_1 B_2}\, v =& \frac{g_\psi^2}{4E_{\psi 1}E_{\psi 2}} \int \prod_{i=1,2} \frac{g_i d^3\vec{k}_i}{(2\pi)^3} (2\pi)^4 \delta^{(4)}(p_{\psi 1} + p_{\psi 2} - k_1 - k_2) \langle |M|^2 \rangle = \\ =& \frac{g_\psi^2}{4E_{\psi 1}E_{\psi 2}} \int d\Omega^{(\mathrm{CM})} \frac{|\vec{p}_\psi^{\,(\mathrm{CM})}|}{(2\pi)^2 4E_\psi^{(\mathrm{CM})}} \langle |M|^2 \rangle \,, \end{aligned} \tag{1.101}$$

where the superscript (CM) indicates the center of mass of the two annihilating ψ particles. The Boltzmann equation, then, obtains the final form

$$\frac{dY_\psi}{dT} = -\frac{1}{Y_\psi^{eq} T} \frac{n_\psi^{eq} \langle \sigma_{\psi\psi\to B_1 B_2} v \rangle}{H} \left[1 - \left(\frac{Y_\psi}{Y_\psi^{eq}} \right)^2 \right] \,. \tag{1.102}$$

1.3 Dark Matter

1.3.1 Why Dark Matter?

Historically, evidence for the existence of dark matter were discovered by measurements of the velocities of galaxies in the Coma cluster [39] in the early 1930's. This study showed that in order for the galaxies to be bounded in this cluster, the total mass should be about two orders of magnitude larger that the luminous mass. Later, measurements of the velocity distributions of stars in spiral galaxies, showed that, away from the galactic center the rotational velocities reach a (approximately) constant value (*e.g.* [40]). However, standard gravitational calculations, applied for the luminous matter, showed that these velocities should decrease. Therefore, either our understanding of gravity is incorrect (at large scales) or there exists non-luminous matter in the Universe. The case is similar with various gravitational measurements (such as [41–43]) indicate that DM is the main mass component of galaxies with a halo structure. Today, direct evidence of the existence of DM come from the co-called "Bullet Cluster" [44], which is a system of two sub-clusters that collided sometime in the past. Measurements of the X-ray emission of the hot gas (left behind by the collision), show that the luminous mass of this system is spatially separated from the mass as measured by weak gravitational lensing. This shows conclusively that DM is responsible for the missing mass of the Universe[12]. The latest measurements by the *Planck collaboration* [29] of the CMB show that the relic abundance of DM is

$$\Omega_{DM} h^2 = 0.1186 \pm 0.0020 \,. \tag{1.103}$$

[12]This does not exclude the possibility that General Relativity might need corrections.

1.3.2 General Remarks on Dark Matter

In order to explain the observed DM content of the Universe, usually we assume that there is a particle with the following attributes:

- *Electrically Neutral.* The only known interaction between DM and the SM particles is gravitational. If there is an interaction between DM and the photon, it should be suppressed, since until today no evidence of irregular light emission has been detected. For example, measurements of the monochromatic photon flux from the center of our galaxy([45, 46]), limit the annihilation cross section times the relative velocity of the DM particles for processes $DM\ DM \to \gamma\gamma$ to $\sim 10^{-28}\text{cm}^{-3}\text{s}^{-1}$, for photon energy at 100 GeV. In general, the upper limit of the electric charge of the DM particle is [47]: $\frac{Q_{DM}}{e} < 10^{-14}\frac{m_{DM}}{\text{GeV}}$, with Q_{DM} the charge of the DM particle and m_{DM} its mass. However, usually the DM particle is assumed to interact with the SM particles through other interactions, in order to explain the origin of its current density. The most common are weak and Yukawa interactions, which open the possibility of detection in various experiments (DM-nucleon experiments, colliders, etc.).
- *Stable.* Since DM exists, we assume that the corresponding particle is stable (or has a lifetime larger than the age of the Universe). From the particle physics point of view, this is ensured by a symmetry. Usually we assume that the Dark Sector particles are odd under a Z_2 parity, while the SM particles are even. Therefore the lightest Dark Sector particle remains stable, since the Dark Sector particles cannot decay to SM ones.
- *Cold/Warm and non-relativistic today.* The DM usually is classified by its behaviour at the time the galactic scale perturbations enter the horizon, which happens at temperature of a few keV. Hot DM is relativistic, Cold DM is non-relativistic, and Warm DM starts to behave as non-relativistic at this temperature. In order for the structure of the Universe to be as observed today, DM is necessary. Hot DM does not reproduce current observational status. Cold or Warm DM allow for the Universe to be formed as it is today. The current lower limit [48] for the mass of the DM particle is $\sim \mathcal{O}(1 - 10\text{keV})$. This fact also points out to that DM is non-relativistic today, since its momentum decreases with the expansion of the Universe (see 1.48).
- *Non-baryonic.* If DM was baryonic, one would expect that it would radiate, thus contributing to the baryonic mass as measured from CMB anisotropies. Also, as for the known baryons, baryonic DM would be concentrated near the center of galaxies and also form a disc around them. However, as we have already mentioned, DM seems to form spherical halos around galaxies, which also show that DM is non-baryonic (see ref. [49]).

1.3.3 Dark Matter Production Mechanisms

The Freeze-out Mechanism

The conventional way to produce non-relativistic (cold) DM relic particle abundance, is the so called "freeze-out mechanism" [50, 51]. Although this mechanism is well reviewed in the literature [31, 32, 52–56], it would be helpful to outline the main steps here, since it is the production mechanism of the models studied in chapters 3 and 4 .

In the early Universe, when the temperature was much higher than the mass of the

would-be DM particles (χ), these particles were in equilibrium, which means that it was equally possible to create and destroy pairs of them due to the Z_2-symmetry. As temperature of the Universe was dropping, the thermal production of DM pairs became inefficient. Thus, χ pairs started to annihilate into lighter SM particles. As the number of these would-be DM particles was dropping, it became increasingly rare for them to interact with each other and annihilate. This yielded an almost constant number of χ's, which corresponds to DM relic density observed today.

Assuming that χ is the lighter particle of the dark sector, one can evaluate the relic density accurately[13] by solving the corresponding Boltzmann eq. (1.102), which can be expressed as

$$\frac{dn_\chi}{dt} + 3Hn_\chi = -\langle\sigma v\rangle \left[n_\chi^2 - \left(n_\chi^{eq}\right)^2\right] , \tag{1.104}$$

Also, since we are interested in non-relativistic particles, n_χ^{eq} is given by eq. (1.79).

The thermal average of the total annihilation cross section of χ-pairs to all allowed particles (k, l), multiplied by the relative velocity of the incoming particles, is usually expanded as

$$\langle\sigma v\rangle = \sum_{k,l} \langle\sigma_{\chi\chi\to k,l} v\rangle \;=\; a + b\,\langle v^2\rangle \;+\; ... \tag{1.105}$$

It should be noted, that the second term on the r.h.s. of eq. (1.104) is responsible for creating χ-pairs, while the first term for annihilating them. According to our description above, at high temperatures, much higher than m_χ, the r.h.s of eq. (1.104) vanishes. This results to a constant particle number density since

$$\frac{dn_\chi}{dt} + 3Hn_\chi \;=\; \frac{1}{\alpha^3}\frac{d(\alpha^3 n_\chi)}{dt} = 0 . \tag{1.106}$$

For lower temperatures than m_χ, the term $\langle\sigma v\rangle \left(n_\chi^{eq}\right)^2$ in eq. (1.104) should vanish, since the χ-pairs are not produced effectively (n_χ^{eq} is exponentially suppressed as shown in eq. (1.79)). Then the Boltzmann equation can be approximated as

$$\frac{dn_\chi}{dt} \approx -\left(\langle\sigma v\rangle\; n_\chi + 3H\right) n_\chi . \tag{1.107}$$

The *freeze-out* temperature, T_{FO}, is defined as the temperature at which the annihilation rate becomes comparable to the expansion rate of the Universe

$$\langle\sigma v\rangle\; n_\chi \approx H . \tag{1.108}$$

The freeze-out temperature can be evaluated iteratively, through[14]

$$x_{FO} = \log\left[c(c+2)\sqrt{\frac{45}{8}}\frac{m_\chi M_{Pl}\left(a + 6b/x_{FO}\right)}{2\pi^3 g_{\star S}^{1/2} x_{FO}^{1/2}}\right] , \tag{1.109}$$

where $x_{FO} \equiv m_\chi/T_{FO}$. The parameter c is usually chosen $c \sim 0.5$, to get into agreement with precise numerical solutions of the Boltzmann equation. Furthermore, $g_{\star S}$ counts the relativistic degrees of freedom of the Standard Model at $T_{FO} = m_\chi/x_{FO}$. Generally, from numerical calculations (see for example [32, 54]), it turns out that $x_{FO} \simeq 25$ (see Fig. 1.2).

[13] Extensive discussion on the solution of the Boltzmann equation including coannihilation effects can be found in [57].

[14] The freeze-out temperature can be calculated approximately from eq. (1.108) for $n_\chi = n_\chi^{eq}$.

Since after the freeze-out the number of particles remains constant, the yield also remains constant (as long as the entropy is conserved). Then, by calculating the freeze-out temperature, we find the present yield

$$Y_\chi(T_0) \approx Y_\chi^{eq}(T = T_{FO}) \,, \tag{1.110}$$

which results to the present relic abundance[15] for χ [57]

$$\Omega_\chi h^2 \;\approx 2.8 \times 10^8 \frac{m_\chi}{GeV} Y_\chi(T_0) \approx \; \frac{1.07 \times 10^9 \;\; \text{GeV}^{-1}}{M_{Pl}} \; \frac{x_{FO}}{g_{\star S}^{1/2}(a + 3\, b\, x_{FO}^{-1})} \,. \tag{1.111}$$

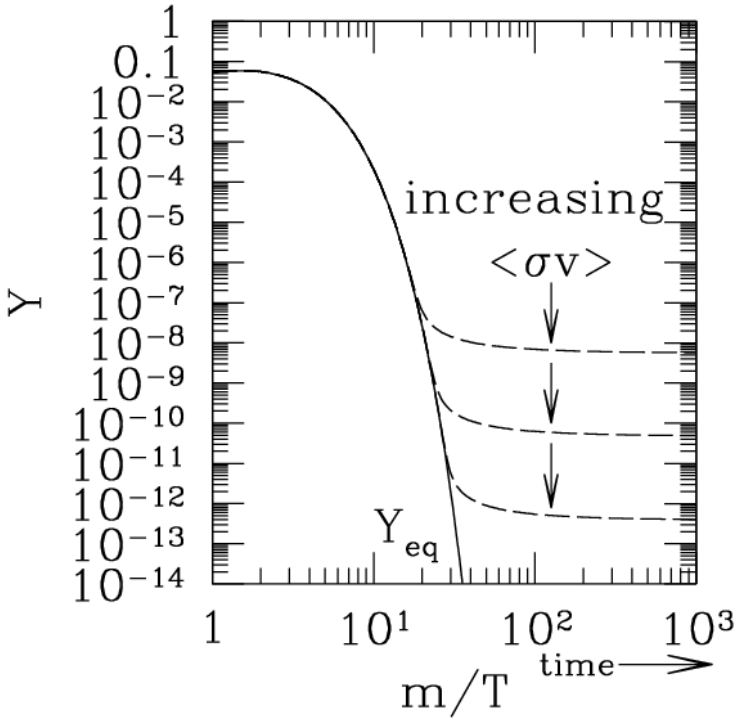

Figure 1.2: *Typical evolution of Y during the freeze-out. Note that the freeze-out occurs at $x \approx 20 - 30$, while the corresponding values of $Y(x = x_{FO})$ span several orders of magnitude. Figure obtained from ref. [55].*

The typical evolution of the Y_χ is shown in Fig. 1.2. It is apparent that as the cross section increases the Y_χ becomes smaller, therefore Ω_χ decreases (this can be seen from eq. (1.111)). Also, due to the logarithmic dependence of x_{FO} on the cross section (1.109), larger values of the cross section do not greatly affect the freeze-out temperature.

An interesting implication of eq. (1.111) arises from the unitarity bound of the annihilation cross section[16](see ref. [58]), where in order to obtain $\Omega_\chi h^2 \sim 0.1$, the mass of DM particles, produced via freeze-out, has an upper limit:

[15] Usually, near mass thresholds (an resonances), we use $\Omega_\chi h^2 \;\approx \frac{1.07\times10^9 \;\; \text{GeV}^{-1}}{M_{Pl}} \; \frac{x_{FO}}{g_{\star S}^{1/2}\langle\sigma v\rangle}$, where $\langle\sigma v\rangle$ is given in eq. (1.100).

[16] The cross section, roughly, satisfies $\langle\sigma v\rangle \lesssim \frac{4\pi}{m_\chi^2}$.

$$m_\chi \lesssim 10^5 \text{GeV} \, . \tag{1.112}$$

If other particles are almost degenerate with the χ, then there could be extra contributions (coannihilation effects) to the total annihilation cross-section due to them. Thus, the annihilation cross section is modified in order to incorporate these coannihilation effects [59]. Following [54, 59], this change in the cross section is

$$\sum_{k,l} \sigma_{\chi\chi\to k,l} \to \sigma_{eff} = \sum_{k,l} \sum_{i,j} \sigma_{i,j\to k,l} \, \frac{g_i g_j}{g_{eff}^2(x)} (1+\Delta_i)^{3/2} \, (1+\Delta_j)^{3/2} \, e^{-x(\Delta_i+\Delta_j)} \, , \tag{1.113}$$

where indices i, j run over all the co-annihilating particles with $\Delta_i = \dfrac{m_i - m_\chi}{m_\chi} \lesssim 0.1$ and $g_{eff}(x)$ is defined as

$$g_{eff}(x) \equiv \sum_i g_i \, (1+\Delta_i)^{3/2} \, e^{-x\Delta_i} \, . \tag{1.114}$$

We note that in the case where the DM particle decouples while being relativistic, which can happen if the interactions become small due to a decoupled mediator, eq. (1.111) cannot be applied. For a relativistic particle the number density is given by eq. (1.74), which gives a yield today

$$Y_\chi(T_0) \approx Y_\chi(T_{FO}) \sim \frac{2}{45 \; g_{\star S}} \, . \tag{1.115}$$

This results to a relic abundance of

$$\Omega_\chi h^2 \sim \frac{m_\chi}{g_{\star S} \text{ eV}} \, . \tag{1.116}$$

Since $g_{\star S} \lesssim 100$, even the lowest allowed DM mass $\mathcal{O}$(keV) would give a relic abundance much greater than the observed one. This shows that neutrinos, with [60] $\sum m_\nu \lesssim 0.1$ eV, cannot account for the DM content of the Universe.

The Freeze-in Mechanism

Another way to produce DM is the "freeze-in mechanism" described in ref. [61]. The key assumption is that the DM particles, χ, were absent in the early Universe ($Y_\chi \approx 0$) and produced later from the annihilation and decay of plasma particles, $B_{1,2}$. The corresponding Boltzmann equation for $2 \to 2$ processes is given in eq. (1.102). Following ref. [62], the Boltzmann equation can be expressed as

$$\begin{aligned} \frac{dY_\chi}{dT} \approx & - \frac{1}{Hs} \frac{1}{1024\pi^5} \int_{-1}^{1} dcos\theta \int_{\hat{s}_{min}}^{\infty} d\hat{s} K_1\left(\frac{\hat{s}}{T}\right) |M_{B_1 B_2 \to \chi\chi}|^2 \\ & \frac{\sqrt{\hat{s} - 4m_\chi^2}\sqrt{\hat{s} - (M_{B_1} + M_{B_2})^2}\sqrt{\hat{s} - (M_{B_1} - M_{B_2})^2}}{\hat{s}} \, , \end{aligned} \tag{1.117}$$

where $|M_{B_1 B_2 \to \chi\chi}|^2$ is the matrix element squared summed over all internal degrees of freedom , θ is the angle between the momenta of an initial and final state particle, $\hat{s}$ is the center of mass energy squared (Mandelstam $\hat{s}-$variable), $\hat{s}_{min} = (M_{B_1} + M_{B_2})^2$, $M_{B_{1,2}}$ are the masses of the bath particles. Furthermore, assuming that the interactions between the

χ's and plasma particles are described by non-renormalizable dimension$-(4+n)$ operators, the matrix element squared is

$$|M_{B_1 B_2 \to \chi\chi}|^2 \sim \frac{\hat{s}^n}{\Lambda^{2n}} \,, \tag{1.118}$$

where Λ is the cutoff energy scale of the interactions. Ignoring all masses the Boltzmann equation becomes

$$\frac{dY_\chi}{dT} \sim -\frac{4^{n+1} n!(n+1)!}{1.66\,1024\,\pi^7} \frac{45}{g_{\star S}^{3/2}} \frac{M_{Pl} T^{2n-2}}{\Lambda^{2n}} \,. \tag{1.119}$$

It is worth pointing out that this holds for $n \geq 1$, which means that the yield would be dominated by the production rate at high temperatures for any non-renormalizable operator. This high temperature contribution comes from the temperature where the plasma particles reached equilibrium, conventionally referred as the reheating temperature of the Universe (T_{RH})[17]. Therefore, integrating eq. (1.119) from T_{RH} up to $T_0 \approx 0$, and setting $g_{\star S} = g_{\star S}(T = T_{RH})$, the present yield becomes

$$Y_\chi(T_0) \sim \frac{4^{n+1} n!(n+1)!}{1.66\,1024\,\pi^7} \frac{45}{(2n-1) g_{\star S}^{3/2}(T_{RH})} \frac{M_{Pl} T_{RH}^{2n-1}}{\Lambda^{2n}} \,. \tag{1.120}$$

The Boltzmann equation for DM production via a decay of a heavier bath particle ($B \to \chi\chi$) is given in eq. (1.98). Assuming that the initial number density of χ is negligible, the Boltzmann equation becomes

$$\frac{dY_\chi}{dT} \approx -\frac{g_\chi^2}{2\pi^2} \frac{M_B^2 \Gamma_{B\to\chi\chi}}{Hs} K_1\left(\frac{M_B}{T}\right) \,. \tag{1.121}$$

Then we integrate over T to obtain the yield today. It should be noted that this integral is dominated from the contribution at[18] $T \sim \frac{M_{bath}}{5}$, which is the temperature where the production of χ reaches its maximum value, or *freeze-in* temperature (T_{FI}). Thus setting $g_{\star S} = g_{\star S}(T = T_{FI})$, the yield at $T = T_0$ is

$$Y_\chi(T_0) \sim \frac{3}{8} \frac{45}{1.66\,1024\,\pi^3} \frac{1}{g_{\star S}(T_{FI})^{3/2}} \frac{M_{Pl}\,\Gamma_{B\to\chi\chi}}{M_B^2} \,. \tag{1.122}$$

Having solved the Boltzmann equation for $1 \to 2$ and $2 \to 2$ processes, the corresponding relic abundance is given by [57]

$$\Omega_\chi h^2 \approx 2.8 \times 10^8 \frac{m_\chi}{GeV} Y_\chi(T_0) \,. \tag{1.123}$$

Both $1 \to 2$ and $2 \to 2$ processes are going to be important in the model we examine in Chapter 5.

[17] Note that Λ has to be well bellow this temperature, otherwise the corresponding effective field theory would not hold.

[18] Note that this temperature is larger than the expected freeze-out temperature of the bath particle $T_{FO} \sim \frac{M_{Bath}}{20}$. This allows us to approximate their distribution with the equilibrium one.

1.3.4 Dark Matter Candidates

As we have seen, there are various independent evidence for the existence of dark matter. Therefore, one natural question arises: *What is the particle nature of dark matter?* There is a great number of studies trying to answer this question. Some popular particle DM candidates include the QCD *axion* [63–65], *Fuzzy* DM [66], *gravitino* [67], *strongly interacting massive particle* (SIMP) [68], *weakly interacting slim particle* (WISP) [69], *weakly interacting massive particle* (WIMP) [70], *super heavy weakly interacting massive particle* (WIMPzilla) [71], etc.

WIMPs

The WIMP is one of the most well studied particle class of DM. WIMPs are particles which are neutral, stable, with masses usually from $\mathcal{O}$(GeV) up to $\mathcal{O}$(10 TeV). In most cases WIMPs interact via weak interactions (or interactions with similar strength) with the known particles, which makes them phenomenologically attractive, since they may be within reach of current searches (including the LHC).

Consider a DM particle with a mass around the EW scale ($m_{DM} \sim 100$ GeV), which is non-relativistic at its freeze-out temperature. From eq. (1.111), in order to get the observed $\Omega_{DM}h^2 \sim 0.1$, the required cross-section is of order 10^{-8} GeV^{-2}, which is a typical EW cross section. This shows that the EW scale is connected, for no apparent reason, to a cosmological particle abundance. This property is called [54] the "WIMP miracle", hence WIMPs became very attractive DM candidates. WIMPs usually appear in models beyond the SM, such as MSSM [52, 72], Kaluza-Klein [73, 74], GUTs [75], etc. However, the phenomenological analysis of such complete models is difficult and case specific. One way to study more general properties of DM is to analyse simplified models or effective field theories (EFT).

In simplified models, one introduces a relatively small number of particles (Dark Sector) and the relevant (renormalizable) interactions between the Dark Sector and the SM. Such simple models include Higgs portal [76,77], Minimal Dark Matter [78], singlet-doublet [79, 80], and more (see ref. [81] for more simplified models in the context of LHC searches). The simplified "Doublet-Triplet Fermionic Dark Matter" model [82] is studied in Chapter 3.

A more general approach is to introduce higher dimensional non-renormalizable operators between the Dark Sector and the SM. This is the EFT approach [83–87]. The general feature of this approach is the assumption that the Dark Sector is the low-energy limit of a UV-complete model. The effects of the heavy degrees of freedom (heavy particles) of all possible UV-complete models are encoded in a set of non-renormalizable operators, with coupling parameters (Wilson coefficients) suppressed by the inverse of a cutoff energy scale. We perform a detailed phenomenological analysis of the bi-doublet EFT DM [88], in Chapter 4.

Light Dark Matter

As mentioned, WIMPs are well-motivated and attractive candidates. However, there is no observation of a WIMP in dedicated experimental searches. Therefore, we have to explore other possibilities. One possible explanation for the lack of WIMP signal, is the light dark matter (LDM) scenario, where the mass of the dark matter particle is well bellow the EW scale. For example, light dark matter candidates are *sterile neutrinos* [89, 90] with

masses around $\mathcal{O}(10\,\text{keV})$. Other LDM models include *light scalar* DM [91], *milli-charged* DM [92], *dark photons* [93], etc. In Chapter 5 we study an LDM model, based on ref. [94], with a radiatively induced sub-GeV mass.

1.3.5 Dark Matter Searches

Direct Detection

Since DM form a halo around galaxies, it is expected that as the Earth moves in the Milky Way some of the DM particles would interact with known matter. The basic idea behind DM direct detection experiments is that DM particles can be observed by elastic scattering with nuclei, such that the recoil energy of the nuclei can be measured. Current experimental efforts include CDMS [95], SuperCDMS [96] PandaX [97], DarkSide [98], XENON [99], and LUX [100].

Qualitatively, the event rate per unit detector mass is [52]

$$R \approx \frac{n_{DM}\ \sigma}{m_N} \langle v \rangle \ , \tag{1.124}$$

where $\langle v \rangle$ is the average velocity of the DM particles relative to the Earth, m_N is the mass of the target nucleus, σ is the cross section for the elastic $DM\ N \to DM\ N$ scattering, n_{DM} is the number density of DM particles.

The elastic cross section, can be decomposed into a zero momentum transfer cross section (σ_0), which contains the particle physics input and depends on the DM-proton and DM-neutron interactions, and a nuclear form factor $F(q)$ encoding the momentum (q) dependence. Furthermore, σ_0 can be broken down to spin-independent and spin-dependent parts [101].[19] In general, the spin-independent part of cross section increases with the mass of the target nucleus (which is proportional to the number of nucleons), while the spin-dependent is proportional to a total spin factor (not the number of nucleons). Therefore, the spin-independent interactions dominate over the spin-dependent ones in heavy target experiments.[20]

Currently, the limits on the spin-independent cross section are set by LUX [100] and XENON [105] (see Fig. 1.3). The future sensitivity of the XENON experiment is expected to lower the current bound on the spin-independent cross section by about two orders of magnitude [106] (or observe a DM particle).

It is worth pointing out that in an elastic scattering between a DM particle and a target (T), the maximum recoil energy of the target is

$$E_{max} = 2\frac{m_{DM}^2}{(m_{DM}+m_T)^2} m_T v^2 \ , \tag{1.125}$$

where m_T is the mass of the target and $v \sim 10^{-3}$ the local velocity of the DM particles. Most detectors have a threshold at $\mathcal{O}(keV)$, therefore only particles with $m_{DM} \gtrsim 1\text{GeV}$ can be detected in DM-nucleus direct detection experiments, which makes them ideal for WIMP searches. However, for smaller DM masses (sub-GeV), DM-electron scattering may deposit a detectable amount of energy [108, 109]. Results from XENON [110], show that

[19] For discussions and examples of the calculation of these cross sections see refs. [52, 78, 102, 103].

[20] This can bee seen in the latest results from LUX, where the spin-independent [100] cross section is limited to $\lesssim 10^{-46}\text{cm}^2$, while the spin-dependent [104] is $\lesssim 10^{-41}\text{cm}^2$ (for DM mass at 100GeV).

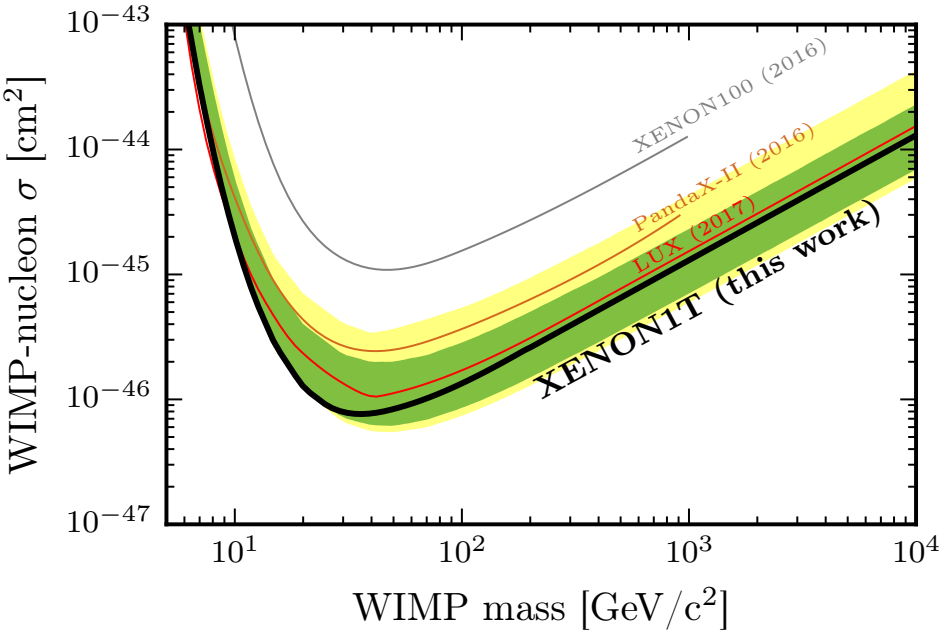

Figure 1.3: *Bounds on spin-independent WIMP-nucleon cross section as a function of the WIMP mass. The black curve shows the results from XENON1T [105]. The other curves correspond to limits from LUX [100] (red), PandaX-II [97] (brown) and XENON100 [107] (gray). The green (yellow) band shows the 1σ (2σ) sensitivity. Figure obtained from ref. [105].*

the bound of the elastic DM-electron cross section is at 10^{-38}cm^2 for a DM mass around 100 MeV.

We calculate the spin-independent cross section, in the context of EW scale WIMPs, is Chapters 3 and 4. Also, in Chapters 2 and 5, we show that for a frozen-in sub-GeV DM particle, the DM-electron cross section is extremely suppressed.

Indirect Detection

Apart from interactions with the SM particles, DM particles can interact with each other resulting to SM particles via pair annihilation processes $DM\ DM \to SM\ SM$. The resulting SM particles, then, can contribute to photon, neutrino and antiparticle fluxes measured by various telescopes and detectors. Collectively, these experiments are referred to as indirect-detection experiments. Although, these searches are extensively reviewed in the literature [52,56,111–116], it is useful for what follows to briefly discuss some of them.

1. *Gamma-rays.* Annihilation (or decay) of DM particles can lead to gamma-ray flux either in the form of continuous or monochromatic photons. Gamma-ray telescopes searching for DM include Fermi-LAT [46, 117, 118], H.E.S.S. [119, 120], VERITAS [121] and HAWC [122,123].

Continuous gamma-rays are the result of annihilation of DM to SM particles, which then emit photons with various energies. The potential astrophysical regions for DM annihilation are regions with a large DM concentration. One such region is the Galactic Center (GC), which unfortunately is not fully understood (see for example refs. [124–126]), therefore continuous gamma-ray signals may not be connected to DM. However, there

are DM dense regions in the form of Dwarf spheroidal galaxies (dSphs), which have low baryonic density, *i.e.* low background, thus providing us with more reliable limits on the $DM\ DM \to SM\ SM$ rates. However, usually the bounds on the cross sections provided by dSphs, are comparable to the cross sections needed to obtain the observed DM relic abundance (see, for example, Chapter 4).

Monochromatic gamma-rays are the product of pair annihilation (or decays) of DM particles directly to at least one photon, *i.e.* $DM\ DM \to \gamma\ X$, where X can be γ, Z or a Higgs boson. The resulting energy of the photon is $E_\gamma = m_{DM}\left(1 - \frac{m_X^2}{4m_{DM}^2}\right)$, therefore a signal of monochromatic photons could lead to a direct measurement of the mass of the DM particle. In Chapter 4, we have calculated such cross sections and discussed relevant bounds, in the context of an EFT.

2. *Solar Neutrino Flux.* Another interesting indirect signal could come from solar neutrino flux as measured by telescopes, such as IceCube [127, 128], ANTARES [129] and Super-Kamiokande [130]. As the Sun moves in the Milky Way, DM particles scatter off the Sun's nuclei (*e.g.* hydrogen). Then, depending on the resulting DM velocity, some of these DM particles are captured by the Sun, where they start to annihilate into SM particles. This results to a potentially observable contribution to the neutrino flux as measured by neutrino telescopes on Earth [131, 132]. After some time the DM capture and annihilation processes reach equilibrium [132–134]. This results in neutrino production rates, proportional to the DM-nucleon cross section [132, 133]. Therefore, such searches are complementary to the direct detection experiments. We briefly discuss the implications of solar neutrino flux to an EFT, in Chapter 4.

3. *Antiparticles.* Products of the $DM\ DM \to SM\ SM$ annihilations can be particle-antiparticle pairs. Although charged particles are everywhere, antiparticles are much less frequent. Therefore an excess on antiparticle (*e.g.* positrons) fluxes may help identify the DM particle. Currently there seems to be a positron excess from AMS [135] and PAMELA [136], but its origin is also explained by other astrophysical sources [137–141]. Therefore, such searches do not give any conclusive results for dark matter (for the time being).

Collider Searches

There are dedicated DM searches at the LHC, usually through searches that involve missing energy in the final state [142–146]. The most common of these include the mono-Z, mono-W, mono-photon and mono-jet searches, collectively referred to as mono-X searches. One example is the mono-jet channel, where one jet is produced alongside DM particles (usually a pair), which are registered as missing energy. Although such missing energy searches would only be an indirect hint of DM, combined LHC and astrophysical searches can provide enough information for the nature of the DM particle. We extensively discuss LHC searches in chapters 3 and 4. Furthermore, in Chapter 4, we examine the validity of EFTs in LHC searches.

Apart from the various dedicated DM searches, there are other indirect, potentially observable effects. For example, the so-called oblique corrections [147–149] can be affected by the presence of heavy particles in loop diagrams. Furthermore, processes such as $h \to \gamma\gamma$ and $h \to \gamma Z$ can indicate the presence of heavy charged (Dark Sector) particles through deviations from the SM expected value [150, 151]. Such indirect effects are calculated in chapters 3 and 4.

2 A Warming up Example

In the previous chapter we discussed the evidence for the existence of dark matter, probably in the form of particles. Also, we described DM production mechanisms, used to explain the DM abundance we observe today. In this chapter, we will study the simplest fermionic DM model, which is the *Singlet Dark Matter* model [152], which consists only of a Majorana fermion gauge singlet, S. If we assume that S is odd under a Z_2-symmetry while the SM particles are even, this particle is a DM candidate. However, under this assumption, there are no renormalizable ($d = 4$) interactions with the SM particles. Therefore, in the lowest order approximation, it interacts only with the Higgs-boson at the $d = 5$ level. Assuming also CP-invariance (real parameters), the dark sector Lagrangian is

$$\mathcal{L}_{\rm DM} = -\frac{1}{2\Lambda} H^\dagger H S S - \frac{1}{2} m_S S S + \text{H.c.} \,, \tag{2.1}$$

where Λ is the cut-off scale of the EFT and m_S is a mass parameter. After symmetry breaking, the above Lagrangian, in the unitary gauge, reads

$$\mathcal{L}_{\rm DM} = -\frac{1}{4\Lambda} h h S S - \frac{v}{\sqrt{2}\Lambda} h S S - \frac{1}{2} M_S S S + \text{H.c.} \,, \tag{2.2}$$

where $M_S = m_S + \dfrac{v^2}{\Lambda}$ is the mass of S.

As we discussed in the introduction, two possible ways to produce the DM relic abundance are the freeze-out and the freeze-in mechanism. We distinguish two possibilities, $M_S \leq 1$ GeV ("light DM") and $M_S > 10$ GeV ("WIMP"),[1] which serves as a first, "hands-on", calculation of the relic abundance, using these two mechanisms. In Section 2.1 we employ the freeze-in mechanism to calculate $\Omega_S h^2$, for the sub-GeV case. Furthermore, since this case is similar to the analysis presented in Chapter 5, we are going to examine carefully the production of the singlets in the early Universe. Then, in Section 2.2, we examine the second case ($M_S > 10$ GeV), and we calculate the relic abundance for S via the freeze-out mechanism.

2.1 Freeze-in

Before moving on to the calculation of the relic abundance, it would be helpful to discuss the reason that the freeze-out mechanism fails to produce the DM relic abundance for light DM particles.

Since the mass of the S-particle is well below $m_h/2$, the Higgs boson would decay to a pair of these particles, which would then contribute to the decay of the Higgs boson to invisible final states. The current bound on the branching ratio for this decay is [153]

$$BR(h \to \text{inv.}) < 0.28 \,. \tag{2.3}$$

[1] It will be apparent (see Fig 2.5) that the freeze-out mechanism can produce the observed relic abundance only for $M_S \gtrsim 50$ GeV. Furthermore, if we use the freeze-in mechanism the S-particle may be non-relativistic at its freeze-in, which makes the calculations more involved.

In terms of the EFT at hand, this bound translates to

$$\Lambda \gtrsim 10^4 \text{ GeV} . \tag{2.4}$$

This bound means that interactions between the S-particle and the SM particles are suppressed. Therefore, if we assume that the singlets were initially in equilibrium, we expect that their freeze-out temperature would be comparable to the decoupling temperature of the Higgs-boson, *i.e.* well above their mass. Thus, their relic abundance would be

$$\Omega_S h^2 \sim \frac{M_S}{g_{\star S} \text{ eV}} , \tag{2.5}$$

which, as discussed in Section 1.3.3, overcloses the Universe for $M_S > \mathcal{O}(10 \text{ keV})$.

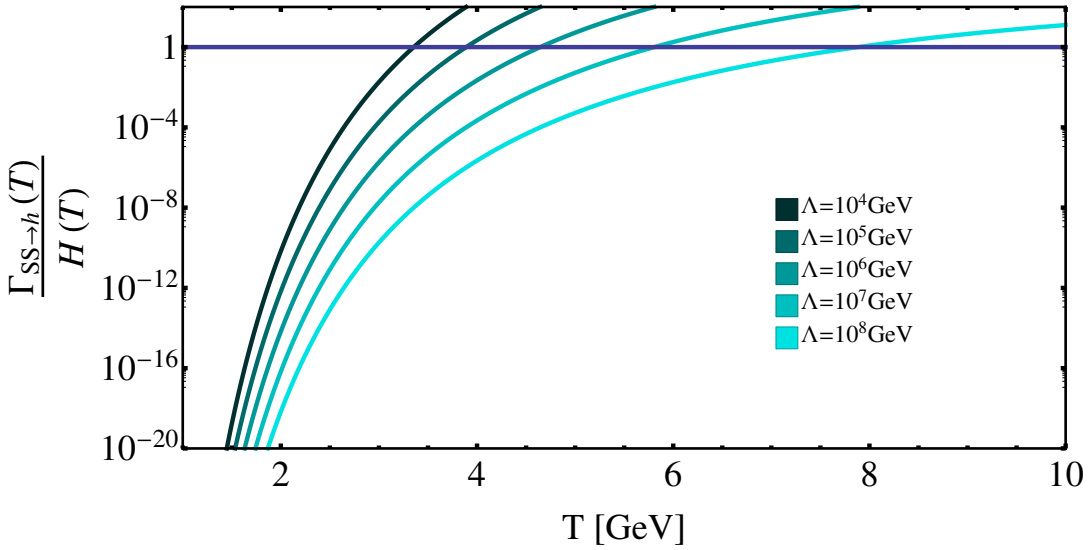

Figure 2.1: *Annihilation rate over the Hubble parameter as a function of the plasma temperature for different values of the cut off. The horizontal line shows the freeze-out temperature, i.e.* $\Gamma_{SS\to h} = H$.

In Fig. 2.1 we show the ratio of the (dominant) annihilation rate, $\Gamma_{SS\to h} = \langle \sigma_{SS\to h} \rangle \, n_S^{eq}$, over the Hubble parameter as a function of the plasma temperature for various values of the cut-off energy, assuming that the Higgs-boson remains in equilibrium below $T = 10$ GeV.[2] It is apparent that, even for the lowest possible cut-off ($\Lambda \gtrsim 10^4$ GeV), the freeze-out would happen at $T \gtrsim 3$ GeV. Consequently, for masses $M_S \lesssim 1$ GeV, the singlets would be relativistic at their freeze-out. If we take into account that the Higgs decouples at higher temperatures (*i.e.* $n_H \ll n_H^{eq}$), the S-particles would also decouple at higher temperatures. Therefore, for this light DM case, the freeze-out mechanism cannot produce the observed relic abundance. One possible solution to this problem is to assume that the singlets were absent and out of thermal equilibrium in the early Universe, and they were produced later from the plasma, *i.e.* employ the freeze-in mechanism, the observed relic abundance can be obtained.

[2]The Higgs boson decays, and at such temperatures is absent. However, assuming that it is in thermal equilibrium below $T = 10$ GeV, gives us a lower bound of the freeze-out temperature of S-particles.

Calculation of the Relic Abundance

The calculation of the yield is discussed in Section 1.3.3. However, this case is somewhat more involved, since there are both annihilation and decay production channels operating at different temperatures. These channels are[3]

$$\begin{aligned} h \to SS,\ ZZ \to SS,\ W^+W^- \to SS,\ t\bar{t} \to SS,\ hh \to SS \quad &\text{for } T < T_C\ , \\ H^\dagger H \to SS \quad &\text{for } T \geq T_C\ , \end{aligned}$$

where $T_C \approx 130$ GeV is the critical temperature [154] of EW symmetry breaking. Following the discussion of Section 1.3.3, the Boltzmann equation in terms of Y_S, before symmetry breaking, is

$$\frac{dY_S}{dT} \approx -\frac{1}{Hs}\frac{1}{1024\pi^5}\int_{-1}^{1} dcos\theta \int_{4M_H^2}^{\infty} d\hat{s}\ K_1\left(\frac{\sqrt{\hat{s}}}{T}\right)\sqrt{\hat{s}-4M_H^2}|M_{H^\dagger H\to SS}|^2\ , \tag{2.6}$$

where we take into account the thermal mass of the Higgs, with $M_H^2 \approx m_h^2 + \frac{T^2}{2}$, and

$$|M_{H^\dagger H\to SS}|^2 = \frac{4\hat{s}}{\Lambda^2}\ . \tag{2.7}$$

After symmetry breaking ($T < T_C$), the Boltzmann equation obtains the following form:

$$\begin{aligned} -Hs\frac{dY_S}{dT} \approx &\frac{1}{1024\pi^5}\int_{-1}^{1} dcos\theta\Bigg[\\ &\frac{1}{2}\int_{4m_h^2}^{\infty} d\hat{s}\ K_1\left(\frac{\sqrt{\hat{s}}}{T}\right)\sqrt{\hat{s}-4m_h^2}|M_{hh\to SS}|^2 + \\ &\frac{1}{2}\int_{4m_Z^2}^{\infty} d\hat{s}\ K_1\left(\frac{\sqrt{\hat{s}}}{T}\right)\sqrt{\hat{s}-4m_Z^2}|M_{ZZ\to SS}|^2 + \\ &\int_{4m_W^2}^{\infty} d\hat{s}\ K_1\left(\frac{\sqrt{\hat{s}}}{T}\right)\sqrt{\hat{s}-4m_W^2}|M_{W^+W^-\to SS}|^2 + \\ &\int_{4m_t^2}^{\infty} d\hat{s}\ K_1\left(\frac{\sqrt{\hat{s}}}{T}\right)\sqrt{\hat{s}-4m_t^2}|M_{t\bar{t}\to SS}|^2\Bigg] + \frac{m_h^3}{8\pi^3}\frac{v^2}{\Lambda^2}\ K_1\left(-\frac{m_h}{T}\right), \end{aligned} \tag{2.8}$$

where the last term comes from the annihilation process $h \to SS$, and the various matrix elements are

$$\begin{aligned} |M_{t\bar{t}\to SS}|^2 &= \frac{12m_t^2}{\Lambda^2}\frac{\hat{s}(\hat{s}-4m_t^2)}{(\hat{s}-m_h^2)^2}\ ,\ |M_{hh\to SS}|^2 = \frac{2\hat{s}^3}{\Lambda^2(\hat{s}-m_h^2)^2}\ , \\ |M_{VV\to SS}|^2 &= \left(\frac{2m_V^2}{\Lambda(\hat{s}-m_V^2)}\right)^2 2\hat{s}\left(3+\frac{\hat{s}(\hat{s}-4m_V^2)}{4m_V^4}\right)\ , \end{aligned} \tag{2.9}$$

[3] The contribution of the decay $h \to SS$ dominates the production of the singlets (as we will also see in Fig. 2.2), so we do not include the light quark and lepton production channels, $l\bar{l} \to SS$ and $q\bar{q} \to SS$. However, we include the top-quark contribution because of its large Yukawa coupling.

with $V = Z$ and W. We note, that the thermal corrections to the masses are not numerically significant for $T < T_C$, so we use the masses at $T = 0$, to obtain the numerical values for the Y_S.

In order to calculate the yield today, we integrate eq. (2.6) from[4] $T_{\rm RH}$ up to T_C, and eq. (2.8) from T_C to the temperature where the production of S-particles stops ($T \approx 10$ GeV).[5] Since the latter is independent of the reheating temperature, the integrals can be calculated numerically. The result for the yield, for $T < T_C$, is

$$Y_S(T < T_C) \approx \frac{6.6 \times 10^{16}\ \text{GeV}^2}{\Lambda^2}\ . \tag{2.10}$$

The contribution to Y_S before symmetry breaking is more complicated, since the corresponding integral is more involved. However, if we assume that $T_{\rm RH} \gg T_C$, we can obtain the approximate analytical result

$$Y_S(T \gtrsim T_C) \approx \frac{10^{13}\ \text{GeV}\, T_{\rm RH}}{\Lambda^2} \qquad \text{for} \qquad T_{\rm RH} \gg T_C\ . \tag{2.11}$$

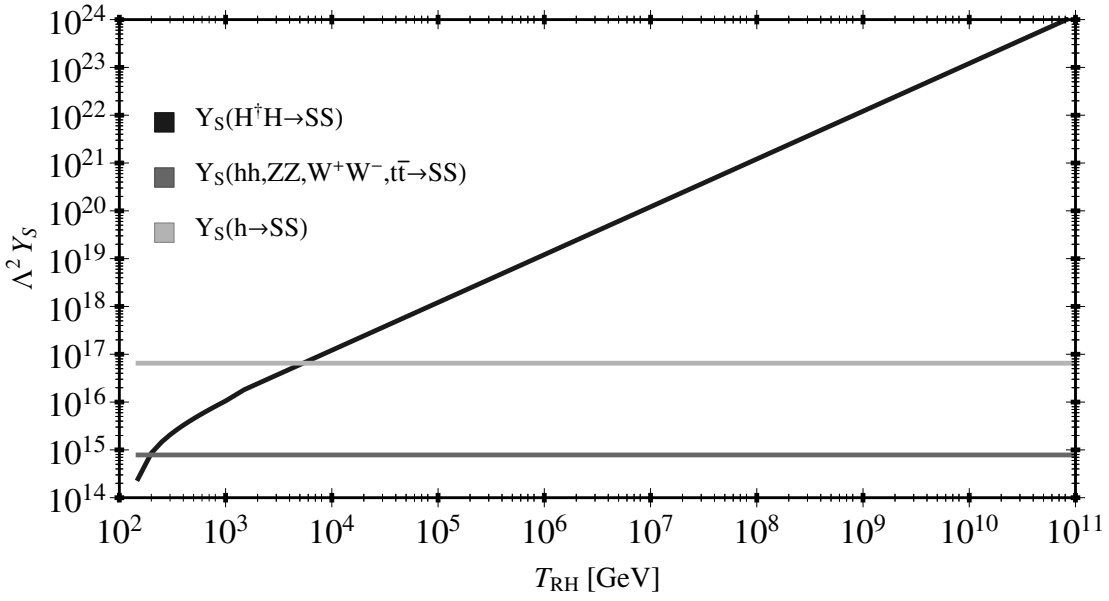

Figure 2.2: *The various contributions to Y_S as a function of $T_{\rm RH}$. Observe that the decay of the higgs boson to SS is more efficient than the combined hh, ZZ, W^+W^- and $t\bar{t} \to SS$.*

In Fig. 2.2, we show the contributions of the various channels to Y_S, as a function of the reheating temperature. Note, that the approximate result (2.11) is accurate for $T_{\rm RH} \gtrsim 400$ GeV. Also, it is worth pointing out that the dominant contribution in eq. (2.8)

[4] We assume the $T_{\rm RH} \gtrsim T_C$, to allow for low-scale baryogenesis (*e.g.* [155–158], see also discussion in Section 5.1).

[5] A particle starts to decouple when the temperature becomes comparable to its mass. After that it starts to decay into lighter particles, until its number density approximately vanishes. For the top-quark, and the Higgs and gauge bosons, this happens at $T \approx 10$ GeV (qualitatively this can be sees in Fig. 1.1). Therefore, the production of S-particles stops around this temperature.

comes from the decay of the Higgs boson to a pair of S-particles. This will be an important simplification in the analysis of Chapter 5.

Finally, from eqs. (2.10), (2.11) and (1.123), the relic abundance obtains the form

$$\Omega h^2 \approx 0.12 \times \left(\frac{M_S}{10^{-5}\ \text{GeV}}\right)\left(\frac{4.5\times 10^{10}\ \text{GeV}}{\Lambda}\right)^2\left(1+\frac{T_{\text{RH}}}{10^4\ \text{GeV}}\right)\ , \tag{2.12}$$

for $T_{\text{RH}} \gg T_C$. We observe that for $T_{\text{RH}} \gtrsim 10^4$ GeV the S production is completely dominated by the production $T = T_{\text{RH}}$. For $\Omega h^2 \approx 0.12$, we can solve (2.12) and find the relation between Λ, M_S and T_{RH}:

$$\Lambda^2 \approx (4.5\times 10^4\ \text{GeV})^2 \times \left(\frac{M_S}{10^{-5}\ \text{GeV}}\right)\left(1+\frac{T_{\text{RH}}}{10^4\ \text{GeV}}\right)\ . \tag{2.13}$$

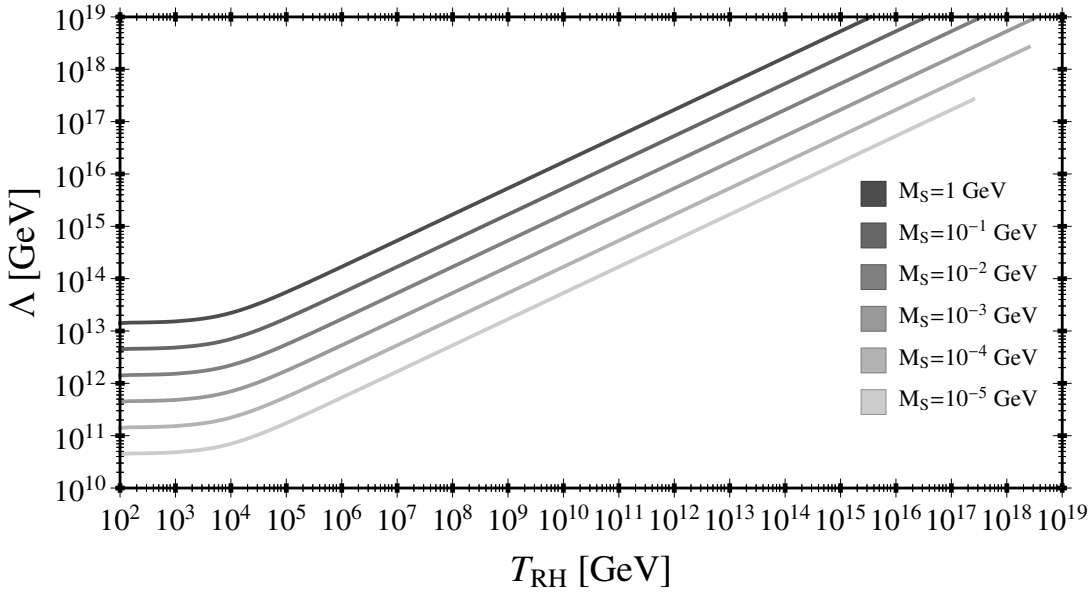

Figure 2.3: *The cut-off Λ as a function of T_{RH} that gives the observed relic abundance for the singlets, for $M_S = 10$ keV -1 GeV.*

The exact numerical calculation of eqs. (2.6) and (2.8) is also performed, and the result for various values of M_S is shown in Fig.2.3. It is apparent that the observed relic abundance can be obtained for a sub-GeV DM particle, provided a cut-off[6] $\Lambda \approx 10^{11}$ GeV up to the Planck scale, for every value of the reheating temperature ($T_{\text{RH}} \gtrsim T_C$). Moreover, as we noted previously, it is evident that the production of the S-particles at $T \approx T_{\text{RH}}$ becomes significant at and above $T \approx 10^4$ GeV (see also Fig.2.2). Finally, we should note that the above calculation holds only for $\Lambda > T_{\text{RH}}$, otherwise, the EFT framework would break down.[7]

[6] This is a general result of frozen-in DM, *i.e.* extremely suppressed interactions [77].

[7] This is the reason why the curve for $M_S = 10^{-5}GeV$ ($M_S = 10^{-4}GeV$) stops at $\Lambda \sim 10^{17}$ GeV ($\Lambda \sim 10^{18}$ GeV).

Sanity Check

The calculation of the yield is valid only if the dark matter particles remain out of equilibrium, throughout their production epoch. Thus, we should make sure that Y_S is well below its equilibrium value before it freezes-in. For the case of interest, where $\Omega h^2 \approx 0.12$, the yield today should be 1.123

$$Y_S(T > T_{FI}) \sim 4.3 \times 10^{-10} \frac{GeV}{M_S} \,. \tag{2.14}$$

Therefore, as long as we consider masses larger than $\sim 10^{-7}$ GeV, the S-particles seem unable to reach equilibrium. This can also be seen by following the evolution of $\frac{Y_S}{Y_S^{eq}}$ throughout the production of the S-particles. This can be done, by solving the Boltzmann equation including the annihilation term. Assuming there are no particle thresholds ($g_{\star S} = const.$), from eqs. (1.98), (1.102) and (1.74), the corresponding Boltamann equation is

$$\frac{dx}{dT} = -\frac{n_S^{eq}}{HT} < \sigma v > \left(1 - x^2\right) \,, \tag{2.15}$$

where $x \equiv \frac{n_S}{n_S^{eq}}$, and

$$\begin{aligned} \langle \sigma v \rangle \approx & \frac{7}{128\pi\Lambda^2} \,, & \text{for } T \gtrsim T_C \,, \\ \langle \sigma v \rangle \approx & \frac{\pi\, v^2}{32\,\Lambda^2} \frac{m_h^3}{T^5} K_1\left(\frac{m_H}{T}\right) \,, & \text{for } T < T_C \,, \end{aligned} \tag{2.16}$$

which can be solved analytically. The solution is

$$x = \frac{n_S}{n_S^{eq}} = -\tanh\left[\int_{T_{\rm RH}}^{T} dT' \frac{n^{eq}(T')}{H(T')T'} < \sigma v > (T')\right] . \tag{2.17}$$

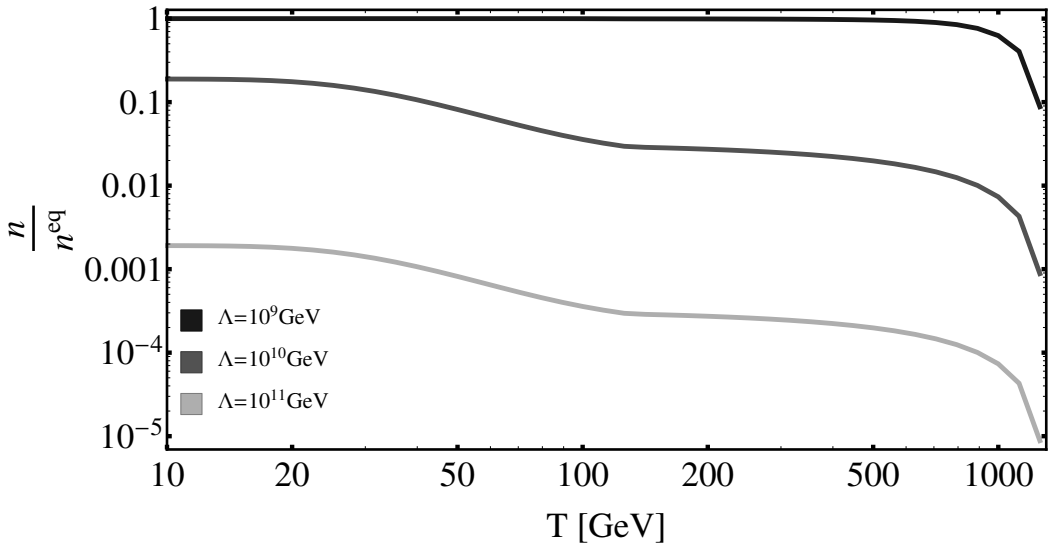

Figure 2.4: *The dependence of* $\frac{n_S}{n_S^{eq}} = \frac{Y_S}{Y_S^{eq}}$ *on the temperature, for various values of* Λ *and* $T_{\rm RH} \approx 10^3$ GeV. *The mass of the singlet is irrelevant as long as* $T \gg M_S$.

In Fig.2.4, we show $\frac{n_S}{n_S^{eq}} = \frac{Y_S}{Y_S^{eq}}$ as a function of the temperature, for $T = T_{\rm RH} \approx 10^3$ GeV–10 GeV (where the production of S-particles stops), and various values of Λ. For $\Lambda = 10^9$ GeV, the DM particles reach equilibrium almost immediately after their production begins. For larger values of the cut-off energy, n_S does not reach its equilibrium value, and since at low temperatures ($T \lesssim 10$ GeV) the annihilation rate $\Gamma_{SS\to h}$ is well below the expansion rate of the Universe (see Fig. 2.1), we do not expect the equilibration of the S-particles. Therefore, since the lowest possible value of the cut-off (see Fig. 2.3) is $\Lambda \approx 10^{11}$ GeV, we conclude that our initial assumption holds.[8]

Direct Detection

As mentioned in Section 1.3.5, direct detection experiments for such light DM particles focus on their interactions with electrons. The cross section for the process $S\,e \to S\,e$ is

$$\bar{\sigma}_{Se} \;\approx\; \frac{1}{4\pi}\frac{1}{\Lambda^2}\left(\frac{m_e}{m_h}\right)^4 . \tag{2.18}$$

Even for the lowest allowed cut-off energy ($\Lambda \approx 10^{11}$ GeV), becomes $\bar{\sigma}_{Se} \sim 10^{-72}$ cm^2, while the current experimental reach is $\bar{\sigma}_{Se}^{\rm exp} \simeq 10^{-38}$ cm^2. Therefore, this singlet DM scenario is allowed. However, the question of the origin of the small DM mass arises. We are going to answer this question in Chapter 5.

2.2 Freeze-out

The case where the S-particles were initially in thermal equilibrium is quite straightforward. The relic abundance is given in eq. (1.111), so we only need to calculate the coefficients a and b of the expansion of the total annihilation cross section (1.105). The possible annihilation channels are:[9]

$$S\,S \to W^+\,W^-,\; S\,S \to Z\,Z,\; S\,S \to h\,h,\; S\,S \to b\,\bar{b} \;\text{ and }\; S\,S \to t\,\bar{t}.$$

For every channel, the a-terms of the expansion (1.105) vanish, while the b-terms are

$$b_h = \frac{1}{4\pi}\frac{1}{\Lambda^2}\frac{M_S^4}{\left(m_h^2 - 4M_S^2\right)^2}\sqrt{1-\frac{m_h^2}{M_S^2}}\,, \tag{2.19a}$$

$$b_V = \frac{1}{S_V}\frac{1}{8\pi}\frac{1}{\Lambda^2}\frac{\left(4M_S^4 - 4M_S^2\,m_V^2 + 3m_V^2\right)}{\left(m_h^2 - 4M_S^2\right)^2}\sqrt{1-\frac{m_V^2}{M_S^2}}\,, \tag{2.19b}$$

$$b_f = \frac{3}{4\pi}\frac{1}{\Lambda^2}\frac{m_f^2\,M_S^2}{\left(m_h^2 - 4M_S^2\right)^2 + \Gamma_h^2 m_h^2}\left(1-\frac{m_f^2}{M_S^2}\right)^{3/2}\,, \tag{2.19c}$$

where V denotes W and Z gauge bosons in the final states, with $S_W = 1$ and $S_Z = 2$, and f denotes the fermionic final states b and t. We also included the total decay width of the

[8] For larger values of the reheating temperature, the singlets can reach equilibrium for $\Lambda \sim 10^{11}$ GeV. However, since $\Lambda \sim \sqrt{T_{\rm RH}}$ [see eq. (2.13)], larger values of $T_{\rm RH}$ correspond to larger values of Λ. Therefore our assumption that the S-particles remain out of equilibrium always holds.

[9] We ignore the light quark and lepton contributions, since they are suppressed due to their small masses.

Higgs, Γ_h, in the denominator of b_f, to take into account the on-shell production of the Higgs boson in the process $S\,S \to b\,\bar{b}$. The relic abundance, then, is given in eq. (1.111) and the freeze-out temperature can be calculated by eq. (1.109).

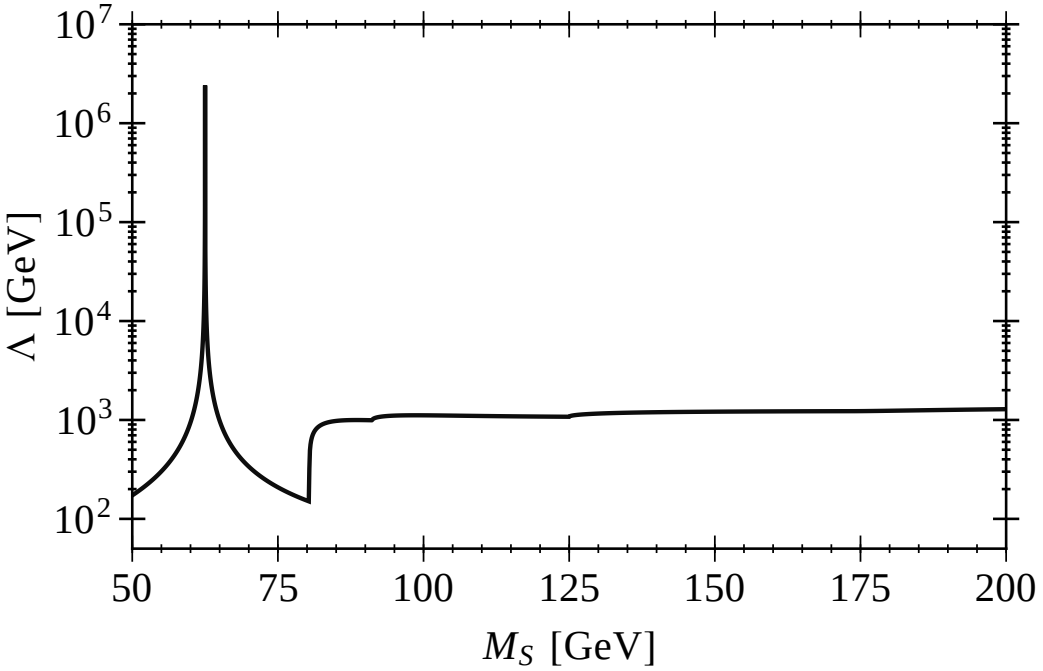

Figure 2.5: M_S *versus* Λ *that give us* $\Omega_S h^2 \approx 0.12$.

We solve for $\Omega_S h^2 \approx 0.12$, which gives the relation between Λ and M_S shown in Fig. 2.5. Observe that for $M_S > m_W$, the cut-off is at $\mathcal{O}(1\text{ TeV})$. In fact, this is the case, even for DM mass above 200 GeV. This happens because the cross section remains almost constant at large masses. Of course, this violates unitarity [14, 147], which indicates that the EFT breaks down for energies above Λ. Moreover, for $M_S \lesssim m_W$, the cut-off becomes very small[10] (with one exception, see below), since there are no available annihilation channels. Furthermore, there is a sharp peak of $\Lambda \approx 10^6$ GeV at $M_S \approx m_h/2$, corresponding to the on-shell production of the Higgs-boson. As we have already mentioned (Chapter 1, footnote 15), near particle thresholds and resonances, a more accurate estimate for the relic abundance is given by

$$\Omega_S h^2 \;\approx \frac{1.07 \times 10^9 \;\text{GeV}^{-1}}{M_{Pl}} \, \frac{x_{FO}}{g_{\star S}^{1/2} \, \langle \sigma v \rangle} \, . \tag{2.20}$$

This can modify our result for the cut-off near the on-shell production of the Higgs, by an order of magnitude [152]. However, for the purpose of this introductory example, a more careful calculation is not needed.

[10] Bellow $M_S \approx 50$ GeV, the value of the cut-off becomes comparable to M_S, so we do not show this region.

Direct Detection

In Section 1.3.5, we explained that the direct detection experiments for WIMPs focus on the DM-nucleon cross section, which is decomposed in spin-independent and spin-dependent parts. In our case, since the only interaction is via the Higgs boson, the S-nucleon cross section is purely spin-independent. In the limit that the S-particle is much heavier than nucleon, this cross section is [159]

$$\sigma_{SI} = 8 \times 10^{-45} \left(\frac{\sqrt{2}}{0.1} \frac{v}{\Lambda} \right)^2 \text{ cm}^2 \,. \tag{2.21}$$

The current bound on this cross section for the DM mass we show in Fig. 2.5, is about [100, 105] 10^{-46} GeV (see Fig. 1.3), which translates to

$$\Lambda \gtrsim 2 \times 10^4 \text{ GeV} \,. \tag{2.22}$$

It is apparent that this only holds near the on-shell production of the Higgs, which is an extreme case of parameter fine tuning.[11] One possible way to avoid such fine tuning, is to assume that there are also other particles with masses near the mass of S. Then, one has to study other simplified models, *e.g.* singlet-multiplet fermionic dark matter [79, 80, 160]. Then, apart from the renormalizable Yukawa interaction, the DM particle is allowed to be a mixture of the singlet and other neutral components of a multiplet. This opens-up new annihilation channels, which change entirely the phenomenology of the singlet DM scenario. In chapters 3 and 4, we examine other ways to reduce parameter fine tuning, by exploiting some (custodial) symmetric limits of fermionic DM models.

[11] This is the case even for the more accurate result of ref. [152].

3 Doublet-Triplet Fermionic Dark Matter

We extend the Standard Model (SM) by adding a pair of fermionic $SU(2)$-doublets with opposite hypercharge and a fermionic $SU(2)$-triplet with zero hypercharge. We impose a discrete Z_2-symmetry that distinguishes the SM fermions from the new ones. Then, gauge invariance allows for two renormalizable Yukawa couplings between the new fermions and the SM Higgs field, as well as for direct masses for the doublet (M_D) and the triplet (M_T). After electroweak symmetry breaking, this model contains, in addition to SM particles, two charged Dirac fermions and a set of three neutral Majorana fermions, the lightest of which contributes to dark matter. We consider a case where the lightest neutral fermion is an equal admixture of the two doublets with mass M_D close to the Z-boson mass. This state remains stable under radiative corrections thanks to a custodial $SU(2)$-symmetry and is consistent with the experimental data from oblique electroweak corrections. Moreover, the amplitudes relevant to spin-dependent or independent nucleus-DM particle scattering cross section *both* vanish at tree level. They arise at one loop at a level that may be observed in near future DM direct detection experiments. For Yukawa couplings comparable to the top-quark, the DM particle relic abundance is consistent with observation, not relying on co-annihilation or resonant effects and has a mass at the electroweak scale. Furthermore, the heavier fermions decay to the DM particle and to electroweak gauge bosons making this model easily testable at the LHC. In the regime of interest, the charged fermions suppress the Higgs decays to diphoton by 45-75% relative to SM prediction. This chapter is based on ref. [82].

3.1 Introduction

Motivated by astrophysical observations that suggest the existence of dark matter [115], we would like to propose a model with a fermionic WIMP (χ_1^0) whose mass and couplings are directly associated to electroweak scale providing the universe with the right thermal relic density abundance, not "tuned" by co-annihilation or resonance effects. Today, as opposed to five years ago, attempts of this sort immediately face difficulties due to strong experimental bounds [161,162][1] from direct searches on nucleus recoiling energy in WIMP-nucleus scattering processes [101]. As a result, Z- and Higgs- boson couplings to χ_1^0-pairs are strongly constrained and usually come into conflict with values of couplings required from the observed [164] DM relic abundance. We therefore seek for a model at which, at least at tree level, these couplings vanish by a symmetry and at the same time the observed relic density is reproduced. We then discuss further consequences of this idea at Large Hadron Collider (LHC).

We consider a minimal model which realises this situation, hence, in addition to Standard Model (SM) particles, we add a pair of Weyl-fermion doublets $\bar{\mathbf{D}}_\mathbf{1} \sim (\mathbf{1^c}, \mathbf{2})_{-\mathbf{1}}$ and

[1] There are of course tantalising hints from DAMA, CoGeNT, CRESST-II and CDMS-Si experiments but these face stringent constraints from recent null result experiments like XENON100 and LUX making puzzling any theoretical interpretation of them all. For a recent review, see ref. [163].

$\bar{\mathbf{D}}_\mathbf{2} \sim (\mathbf{1^c}, \mathbf{2})_{+\mathbf{1}}$ with opposite hypercharges, and a Weyl-fermion triplet $\mathbf{T} \sim (\mathbf{1^c}, \mathbf{3})_\mathbf{0}$ with zero hypercharge. The new Yukawa interactions allowed by gauge invariance and renormalizability are given by[2]

$$\mathcal{L}_{\rm Yuk} \supset Y_1\, \mathbf{T}\, \mathbf{H}\, \tau\, \bar{\mathbf{D}}_\mathbf{1} + Y_2\, \mathbf{T}\, \mathbf{H}^\dagger\, \tau\, \bar{\mathbf{D}}_\mathbf{2} - M_D\, \bar{\mathbf{D}}_\mathbf{1}\, \bar{\mathbf{D}}_\mathbf{2} - \frac{1}{2}\, M_T\, \mathbf{T}\, \mathbf{T}\,, \tag{3.1}$$

with τ being the Pauli matrices. A Z_2-discrete parity symmetry has been employed to guarantee that the new fermions interact always in pairs. Clearly, $\mathcal{L}_{\rm Yuk}$ is invariant under the interchange symmetry $\mathbf{H} \leftrightarrow \mathbf{H}^\dagger$ and $\bar{\mathbf{D}}_\mathbf{1} \leftrightarrow \bar{\mathbf{D}}_\mathbf{2}$ when $Y_1 = Y_2 \equiv Y$. Then, it is very easy to see that in this limit, one eigenvalue with mass M_D, of the neutral (3×3) mixing mass matrix, decouples from the two heavier ones and the latter is degenerate with the two eigenvalues of the (2×2) charged fermion mass matrix. At tree level approximation, except for the lightest neutral fermion (χ_1^0), all other masses are controlled by the Yukawa coupling Y. The state with $m_{\chi_1^0} = M_D$ is our DM candidate particle. This particle state contains an equal admixture of the two doublets but has *no* triplet component,

$$|\chi_1^0\rangle = 0 \cdot |\mathbf{T}\rangle + \frac{1}{\sqrt{2}}\, |\bar{\mathbf{D}}_\mathbf{1}\rangle + \frac{1}{\sqrt{2}}\, |\bar{\mathbf{D}}_\mathbf{2}\rangle\,. \tag{3.2}$$

Because the neutral component of the triplet does not participate in $|\chi_1^0\rangle$, the latter does not couple to the Higgs boson at tree level. It does not couple to the Z-gauge boson neither because of its equal admixture of neutral particles with opposite weak isospin. The situation here is analogous to the custodial symmetry [165] imposed in strongly coupled EW scenarios, where the "custodian" new particles are inserted in a similar way to protect certain quark-gauge boson couplings to obtain large radiative corrections [166–169].

The couplings $h\chi_1^0\chi_1^0$ and $Z\chi_1^0\chi_1^0$ vanish at tree level, and as a result there are no s-channel amplitudes contributing to the annihilation cross section. However, there are off-diagonal interactions such as e.g., $Z\chi_1^0\chi_2^0$ which render the t, u-channel amplitudes non-zero but yet suppressed enough to obtain the right relic density Ω_χ for $M_D \approx 100$ GeV and $Y \approx 1$. Roughly speaking, the spectrum of the model where this happens is shown schematically in Fig. 3.1. Typically, the lightest stable new particle ($m_{\chi_1^0} \approx 110$ GeV) is in the vicinity of the EW scale while all other neutral and charged fermions are above $m \equiv Yv$ which is taken around the top quark mass. The splitting of the charged fermions is also controlled by the triplet mass (M_T). Therefore, the parameters of the model are just three: M_D, M_T and m.

Naively, one may think that this model is similar to the "wino-higgsino" sector of the MSSM [170] or it is an extended variant of the singlet-doublet DM model of refs. [75,79,171, 172]. Another obvious question is, why does one want to introduce several new fermions, since a single one (for example the triplet, as in minimal DM [78] models) suffices? The answer to these questions arise from our wish to construct a model with WIMP mass *at the EW scale*, and hides inside the model building details, namely:

1. The off-diagonal entries of the "chargino" or "neutralino" mass matrix contain general Yukawa couplings (Y_1 and Y_2) that can be enhanced as opposed to the fixed-value gauge couplings of the MSSM. Evenmore, they can be equal here *i.e.,* $Y_1 = Y_2 \equiv Y \sim g$, satisfying a custodial symmetry, a realisation which is only phenomenologically allowed in the so called Split-SUSY scenarios [173, 174]. Therefore, this fermionic doublet-triplet DM sector generalises the corresponding DM sector of the Minimal Supersymmetric Standard Model (MSSM).

[2] All gauge group indices are suppressed in this equation. Its detailed form is given below in eq. (3.9).

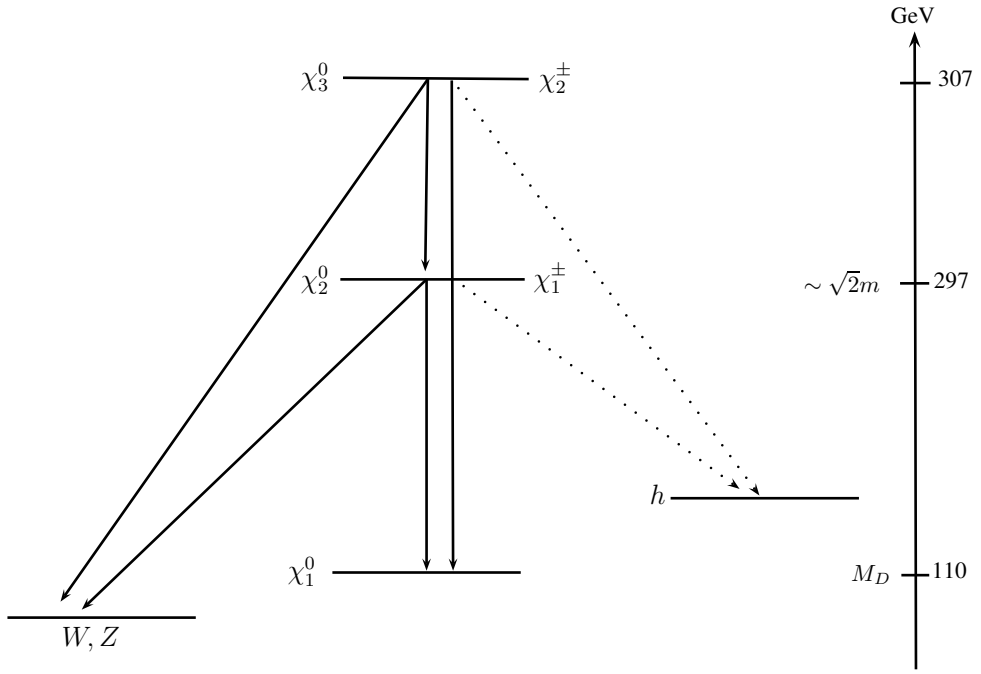

Figure 3.1: *A sketch for the mass spectrum and decays of the new physical doublet and triplet fermions. The lightest neutral particle, χ_1^0 is an equal admixture of the two doublets and has mass M_D. Particles χ_2^0 (χ_3^0) and $\chi_1^\pm$ ($\chi_2^\pm$) are mass degenerate. For the spectrum masses written to the right we have chosen $M_D = 110$ GeV, $M_T = 100$ GeV and $m = Yv = 200$ GeV. It provides the correct relic density abundance for dark matter [see Section 3.4] and is currently about ~ 10 times less sensitive to current direct detection searches [see Section 3.5].*

2. In the region where the common Yukawa coupling is comparable, say, to the top Yukawa coupling there are heavy charged leptons decaying to the lightest new fermion χ_1^0. This mass pattern, shown in Fig. 3.1, is different from the singlet-doublet DM model (at least from the minimal version) where the lightest neutral particle is, up to radiative corrections, degenerate with the charged particle a situation which is highly constrained from long lived charged particle searches at LHC [175].
3. In the limit of equal Yukawa couplings (Y) in eq. (3.1), there is a custodial $SU(2)$-symmetry that guaranties vanishing couplings at tree level between the lightest neutral particle and the Z-boson ($Z\chi_1^0\chi_1^0$) and also to the Higgs-boson ($h\chi_1^0\chi_1^0$). This is a certain "pass" for this model, at least to leading order, from the current strong direct detection experimental contraints [161, 162, 176]. Moreover, as we shall see below, $h\chi_1^0\chi_1^0$-coupling arises radiatively at one-loop order providing us with certain model predictions. Note that "blind spots" of this kind have been studied in ref. [159] for Split-SUSY and in ref. [177] for the singlet-doublet and singlet-triplet fermionic DM models.
4. Similar to the case here, the dominant annihilation channel in the higgsino DM-phase of MSSM [178], is into gauge bosons. But in the higgsino case and due to smallness of the gauge coupling, the lightest charged and neutral fermion states are degenerate so co-annihilation effects [59] are very important. It turns out that, that for higgsino

mass $\mu \sim 100$ GeV the cross section $< \sigma v > \approx \frac{g^4}{16\pi\mu^2}$ is large which results in Ω_{DM} that is too low unless μ is in the TeV range. In the doublet-triplet fermonic DM model we consider here, the lightest neutral state decouples from the heavy ones, and in the limit of large $m = Yv$ the difference in mass between the lightest neutral fermion and the lightest charged or the second lightest neutral one is normally of the order of 100 GeV (see Fig. 3.1 for an example). The annihilation cross section now goes through the t, u-channels and, relative to higgsino case, is suppressed by a factor $(m_\chi/m_{\chi_j})^4 \sim 10 - 100$ where m_{χ_j} are the heavy fermion masses $(\chi^0_{2,3}, \chi^\pm_{1,2})$, allowing a WIMP mass, m_χ, naturally of the order of 10-100 GeV.[3]

5. Our attempt here is to find a DM candidate particle consistent with the astrophysical and collider data but with mass around the electroweak scale. Vector-like gauge multiplets that are engaged here have also been used to construct minimal DM Models (MDM) in Ref. [78]. It has been found that the masses M_D or M_T should lie in the few-TeV region. In our scenario, it is the chiral (Dirac) mass terms in eq. (3.1) that play the most important role. The latter are constrained from perturbativity to be several hundreds of GeV while the lower vector-like masses, M_D and M_T, are protected by an accidental symmetry. Finally, the production and decay phenomenology of the new fermions is very distinct from the ones in MDM models and it is relatively easy to be tested with current and near future LHC data.

Within this framework of Doublet-Triplet Fermionic DM model that we describe in Section 3.2, and in particular in the region where the custodial symmetry is applied, we discuss and check constraints that include:

- An estimate of oblique corrections to electroweak observables (S, T, U parameters) [Section 3.3].
- DM thermal relic density calculation at tree level [Section 3.4].
- Direct DM detection prospects through nucleus-DM particle scattering at 1-loop [Section 3.5]
- Decay rate of the Higgs boson to two photons ($h \to \gamma\gamma$) [Section 3.6]
- Vacuum stability and perturbativity [Section 3.7]
- LHC signatures, production and decays of the new fermions[Section 3.8].

Our conclusions and various ways to extend this work are discussed in Section 3.9. An appendix with the explicit one-loop corrections to the $h\chi^0_1\chi^0_1$-vertex is given. Beyond the articles we have already mentioned, there is a reach literature regarding minimal DM extensions of the SM. A partial list is given in refs. [152, 179–198].

3.2 Model Details

As a result of what we have already mentioned in the introduction, we scan chiral fermion matter extensions of the SM gauge group according to the following, rather obvious, assumptions for the new set of fermions:

1. they must have vectorial electromagnetic interactions,
2. they must be colour singlets with integer charges,
3. their interactions must be gauge (and gravitational) anomaly free,

[3] In this study, we are only interested in DM mass of the order of the electroweak scale.

4. their masses are obtained after $SU(2)_L \times U(1)_Y$ gauge symmetry breaking, with only the SM Higgs doublet, and if gauge symmetry allows, directly, and
5. there is a parity symmetry, Z_2, under which the SM fermions transform as $+1$ while the new fermions as -1.

The most minimal model, not containing pure singlet fields,[4] consists of three fields arranged in colour singlets and representations of $SU(2)_L$, with quantum numbers denoted as $(\mathbf{1^c}, \mathbf{2I+1})^{\mathbf{Y}}_{\mathbf{L,R}}$, where $\mathbf{I}$ is the weak $SU(2)_L$ isospin and Y is the hypercharge related to the electric charge by $Q = I_3 + \frac{Y}{2}$. These new fields are[5]:

$$\mathbf{T} \sim (\mathbf{1^c}, \mathbf{3})^{\mathbf{0}}_{\mathbf{L}} \,, \qquad \mathbf{D_1} \sim (\mathbf{1^c}, \mathbf{2})^{\mathbf{+1}}_{\mathbf{R}} \,, \qquad \mathbf{D_2} \sim (\mathbf{1^c}, \mathbf{2})^{\mathbf{-1}}_{\mathbf{R}} \,. \tag{3.3}$$

One can easily check that this is a gauge and gravitational anomaly free set of chiral fermions. They sit in adjacent representations of $SU(2)_L$ with weak isospin difference $\Delta I = \frac{1}{2}$. This matches with the only spinless field of the SM, the Higgs field, with gauge labels $\mathbf{H} \sim (\mathbf{1^c}, \mathbf{2})_{\mathbf{+1}}$.

It is convenient to represent all fermions, *i.e.* SM quarks and leptons plus new fermions that belong to the DM sector, with two component, left handed, Weyl fields [28], namely[6]

$$\text{SM quarks}: \qquad \mathbf{Q} = \begin{pmatrix} u \\ d \end{pmatrix} \sim (\mathbf{3^c}, \mathbf{2})_{\mathbf{+1/3}} \,, \quad \bar{\mathbf{u}} \sim (\mathbf{3^c}, \mathbf{1})_{\mathbf{-4/3}} \,, \quad \bar{\mathbf{d}} \sim (\mathbf{3^c}, \mathbf{1})_{\mathbf{+2/3}} \,, \tag{3.4}$$

$$\text{SM leptons}: \qquad \mathbf{L} = \begin{pmatrix} \nu \\ e \end{pmatrix} \sim (\mathbf{1^c}, \mathbf{2})_{\mathbf{-1}} \,, \quad \bar{\nu} \sim (\mathbf{1^c}, \mathbf{1})_{\mathbf{0}} \,, \quad \bar{\mathbf{e}} \sim (\mathbf{1^c}, \mathbf{1})_{\mathbf{+2}} \,, \tag{3.5}$$

$$\text{DM fermions}: \qquad \mathbf{T} = \begin{pmatrix} T_1 \\ T_2 \\ T_3 \end{pmatrix} \sim (\mathbf{1^c}, \mathbf{3})_{\mathbf{0}} \,,$$

$$\bar{\mathbf{D}}_{\mathbf{1}} = \begin{pmatrix} \bar{D}_1^1 \\ \bar{D}_1^2 \end{pmatrix} \sim (\mathbf{1^c}, \mathbf{2})_{\mathbf{-1}} \,, \quad \bar{\mathbf{D}}_{\mathbf{2}} = \begin{pmatrix} \bar{D}_2^1 \\ \bar{D}_2^2 \end{pmatrix} \sim (\mathbf{1^c}, \mathbf{2})_{\mathbf{+1}} \quad . \tag{3.6}$$

SM fermions come in three copies of (3.4) and (3.5) sets of fields. We have added a left-handed antineutrino Weyl field in the SM field content in order to account for light neutrino masses via the seesaw mechanism. Although there may be interesting links between the neutrino and DM sector fields we shall scarcely refer to neutrinos in this work. We assume only one copy of the DM-sector fields in (3.6). Of course, we could also add more singlet fermions either in the SM or in the DM-sector but our intention is to keep the model as minimal as possible.

Physical masses are obtained from the gauge invariant form of Yukawa interactions. Under the assumption-5 above, the whole Yukawa Lagrangian of the model is

$$\mathscr{L}_{\text{Yuk}} = \mathscr{L}^{\text{SM}}_{\text{Yuk}} \; + \; \mathscr{L}^{\text{DM}}_{\text{Yuk}} \,, \tag{3.7}$$

[4] However, see comments below.

[5] As it was shown in ref. [199], the doublet-triplet fermionic dark matter model can be embedded in an $SO(10)$ GUT.

[6] The bar symbol over the Weyl fields is part of their names.

where the SM part reads (flavour indices are suppressed):

$$\mathscr{L}_{\rm Yuk}^{\rm SM} = Y_u \epsilon^{ab} H_a Q_b \bar{u} - Y_d H^{\dagger\, a} Q_a \bar{d} - Y_e H^{\dagger\, a} L_a \bar{e}$$
$$+ Y_\nu \epsilon^{ab} H_a L_b \bar{\nu} - \frac{1}{2} M_N \bar{\nu}\bar{\nu} + \text{H.c.}\,, \tag{3.8}$$

and the available DM-sector interactions are

$$\mathscr{L}_{\rm Yuk}^{\rm DM} = Y_1\, \epsilon^{ab}\, T^A\, H_a\, (\tau^A)^c_b\, \bar{D}_{1\,c} \;-\; Y_2\, T^A\, H^{\dagger\, a}\, (\tau^A)^c_a\, \bar{D}_{2\,c}$$
$$- M_D\, \epsilon^{ab} \bar{D}_{1\,a} \bar{D}_{2\,b} \;-\; \frac{1}{2} M_T\, T^A T^A \;+\; \text{H.c.}\,. \tag{3.9}$$

By choosing appropriate field redefinitions and without loss of generality we can make the parameters Y_1, Y_2, and M_T real and positive, while leaving M_D to be a general complex parameter. This is the only source of CP-violation[7] arising from the DM-sector in this model. If not stated otherwise, we consider real M_D values in our numerical results. The parity symmetry assumption-5 removes the following renormalizable operators:

$$H^\dagger\, \bar{D}_2\, \bar{\nu}\,, \quad H\, \bar{D}_1\, \bar{\nu}\,, \quad L\, \bar{D}_2\,, \quad H\, T\, L \quad \text{and} \quad H^\dagger\, \bar{D}_1\, \bar{e}\,. \tag{3.10}$$

Note that apart from the first two, the rest will not be allowed under the custodial symmetry. Finally, we assume that possible non-renormalizable operators that are allowed by the discrete symmetry are Planck scale suppressed and do not play any particular role in what follows.

3.2.1 The spectrum

Since there is no-mixing between the mass terms of the SM fermions and the DM sector ones, we solely concentrate on the non-SM Yukawa interactions of eq. (3.9). After electroweak symmetry breaking and the shift of the neutral component of the only Higgs field, $H^0 = v + h/\sqrt{2}$, we obtain the following mass terms

$$\mathscr{L}_{\rm Y\,(mass)}^{\rm DM} = -\begin{pmatrix}\tau_1 & \bar{D}_2^1\end{pmatrix}^T \mathcal{M}_C \begin{pmatrix}\tau_3 \\ \bar{D}_1^2\end{pmatrix} - \frac{1}{2}\begin{pmatrix}\tau_2 & \bar{D}_1^1 & \bar{D}_2^2\end{pmatrix}^T \mathcal{M}_N \begin{pmatrix}\tau_2 \\ \bar{D}_1^1 \\ \bar{D}_2^2\end{pmatrix} \;+\; \text{H.c.}$$
$$= -\sum_{i=1}^{2} m_{\chi_i^\pm} \chi_i^-\, \chi_i^+ \;-\; \frac{1}{2}\sum_{i=1}^{3} m_{\chi_i^0} \chi_i^0 \chi_i^0 \;+\; \text{H.c.}\,, \tag{3.11}$$

where $\tau_1 \equiv (T_1 - iT_2)/\sqrt{2}$, $\tau_3 \equiv (T_1 + iT_2)/\sqrt{2}$ and $\tau_2 \equiv T_3$. The charged ($\mathcal{M}_C$) and the neutral ($\mathcal{M}_N$) fermion mass matrices in eq. (3.11) are given by

$$\mathcal{M}_C = \begin{pmatrix} M_T & \sqrt{2}\, m_1 \\ \sqrt{2}\, m_2 & -M_D \end{pmatrix}\,, \qquad \mathcal{M}_N = \begin{pmatrix} M_T & m_1 & -m_2 \\ m_1 & 0 & M_D \\ -m_2 & M_D & 0 \end{pmatrix}\,, \tag{3.12}$$

[7] Electron and Neutron EDMs will arise first at two-loop level. Similarly for the anomalous magnetic moments of SM leptons. See relevant discussion in ref. [200].

where $m_{1,2} \equiv Y_{1,2}\, v$. Matrices $\mathcal{M}_C$ and $\mathcal{M}_N$ are diagonalized following the singular value decomposition and the Takagi factorisation theorems [201] into $m_{\chi^\pm} = (2 \times 2)$ and $m_{\chi^0} = (3 \times 3)$ diagonal matrices,

$$U_L^T\, \mathcal{M}_C\, U_R = m_{\chi^\pm}\ , \quad O^T\, \mathcal{M}_N\, O = m_{\chi^0}\ , \tag{3.13}$$

respectively, after rotating the current eigenstate fields into their mass eigenstates $\chi_i^\pm, \chi_i^0$ with unitary matrices, U_L, U_R and O, as

$$\begin{pmatrix} \tau_3 \\ \bar{D}_1^2 \end{pmatrix} = U_R \begin{pmatrix} \chi_1^- \\ \chi_2^- \end{pmatrix}\ , \quad \begin{pmatrix} \tau_1 \\ \bar{D}_2^1 \end{pmatrix} = U_L \begin{pmatrix} \chi_1^+ \\ \chi_2^+ \end{pmatrix}\ , \qquad \begin{pmatrix} \tau_2 \\ \bar{D}_1^1 \\ \bar{D}_2^2 \end{pmatrix} = O \begin{pmatrix} \chi_1^0 \\ \chi_2^0 \\ \chi_3^0 \end{pmatrix}\ . \tag{3.14}$$

Therefore the spectrum of this model contains, apart from the SM masses for quarks and leptons, two additional charged Dirac fermions and three neutral Majorana particles. It is the lightest Majorana particle χ_1^0 with mass $m_{\chi_1^0}$, that, perhaps, supplies the universe with cold dark matter.

It is crucial for what follows and also enlightening, to discuss the decoupling of the M_D-eigenvalue from the particle spectrum. First, $\mathcal{M}_N$, is a real symmetric matrix, under the assumption of real M_D. Then, consider the following unitary matrix Σ, having as columns orthonormal vectors,

$$\Sigma = \frac{1}{\sqrt{2}} \begin{pmatrix} \sqrt{2} & 0 & 0 \\ 0 & 1 & 1 \\ 0 & -1 & 1 \end{pmatrix}\ , \tag{3.15}$$

which by a similarity transformation, brings the lower right 2×2 sub-block of $\mathcal{M}_N$ into a diagonal form,

$$\mathcal{M}'_N\ = \Sigma^\dagger\, \mathcal{M}_N\, \Sigma = \begin{pmatrix} M_T & (m_1+m_2)/\sqrt{2} & (m_1-m_2)/\sqrt{2} \\ (m_1+m_2)/\sqrt{2} & -M_D & 0 \\ (m_1-m_2)/\sqrt{2} & 0 & M_D \end{pmatrix}\ . \tag{3.16}$$

Note that since Σ is unitary matrix, the eigenvalues of $\mathcal{M}_N$ and $\mathcal{M}'_N$ are equal. We therefore obtain, that for $m_1 = m_2$ the charged fermion mass matrix $\mathcal{M}_C$ becomes the upper-left sub-block of the $\mathcal{M}'_N$ in eq. (3.16). Therefore the eigenvalue, M_D, decouples from the neutral fermion mass matrix *i.e.* it is independent of any mixing and therefore any v.e.v, while the rest of eigenvalues of both matrices, $\mathcal{M}_C$ and $\mathcal{M}_N$, are one to one degenerate.

3.2.2 The interactions

We now turn to the interactions between the new fermions and the SM gauge-bosons or the SM Higgs-boson. The latter can be read from eq. (3.9) after rotating fields by exploiting the relations in (3.14). After a little bit of algebra we obtain[8]

$$\mathscr{L}^{\rm DM}_{\rm Y(int)} = -Y^{h\chi_i^-\chi_j^+}\, h\, \chi_i^-\, \chi_j^+\ -\ \frac{1}{2}\, Y^{h\chi_i^0\chi_j^0}\, h\, \chi_i^0\, \chi_j^0\ +\ \text{H.c.}\ , \tag{3.17}$$

[8] We use Weyl notation for fermions [28] throughout.

where

$$Y^{h\chi_i^-\chi_j^+} \equiv \frac{1}{v}\left(m_1\, U_{R\,2i}\, U_{L\,1j} + m_2\, U_{R\,1i}\, U_{L\,2j}\right) \ , \tag{3.18}$$

$$Y^{h\chi_i^0\chi_j^0} \equiv \frac{O_{1i}}{\sqrt{2}\,v}\ \left(m_1\, O_{2j} - m_2\, O_{3j}\right)\ +\ (i \leftrightarrow j)\ . \tag{3.19}$$

For completeness and especially for loop calculations, we append here the interactions between Goldstone bosons and the new fermions:

$$\begin{aligned}\mathscr{L}_{\mathrm{G}\chi\chi} = &-\frac{i\,O_{1i}}{\sqrt{2}v}\left(m_1\, O_{2j} + m_2\, O_{3j}\right) G^0\chi_i^0\chi_j^0 - \frac{i}{v}\left(m_1\, U_{R\,2i}\, U_{L\,1j} - m_2\, U_{R\,1i}\, U_{L\,2j}\right) G^0\chi_i^-\chi_j^+ \\ &+ \frac{m_1}{v}(\sqrt{2}\, U_{R\,1i}\, O_{2j} - U_{R\,2i}\, O_{1j})\, G^+\chi_i^-\chi_j^0 - \frac{m_2}{v}\left(\sqrt{2}\, U_{L\,1i}\, O_{3j} + U_{L\,2i}\, O_{1j}\right) G^-\chi_i^+\chi_j^0 \\ &+ \text{H.c}\ .\end{aligned} \tag{3.20}$$

Interactions among the new fermions and gauge bosons arise from the respective fermion kinetic terms. Interactions between $\chi^\pm$ and the photon are purely vectorial,

$$\mathscr{L}^{\gamma-\chi^\pm}_{\mathrm{KIN(int)}} = -(+e)\,(\chi_i^+)^\dagger\bar\sigma^\mu\chi_i^+\ A_\mu - (-e)\,(\chi_i^-)^\dagger\bar\sigma^\mu\chi_i^-\ A_\mu\ , \tag{3.21}$$

where A_μ is the photon field and $(-e)$ the electron electric charge. The Z-gauge boson couplings to both charged and neutral fermions can be read from[9],

$$\mathscr{L}^{Z-\chi}_{\mathrm{KIN(int)}} = \frac{g}{c_W}O'^{\,L}_{ij}(\chi_i^+)^\dagger\bar\sigma^\mu\chi_j^+ Z_\mu - \frac{g}{c_W}O'^{\,R}_{ij}(\chi_j^-)^\dagger\bar\sigma^\mu\chi_i^- Z_\mu + \frac{g}{c_W}O''^{\,L}_{ij}(\chi_i^0)^\dagger\bar\sigma^\mu\chi_j^0 Z_\mu\ , \tag{3.22}$$

where

$$O'^{\,L}_{ij} = -U^*_{L1i}\, U_{L1j} - \frac{1}{2}\, U^*_{L2i}\, U_{L2j} + s_W^2\delta_{ij}\ , \tag{3.23}$$

$$O'^{\,R}_{ij} = -U_{R1i}\, U^*_{R1j} - \frac{1}{2}\, U_{R2i}\, U^*_{R2j} + s_W^2\delta_{ij}\ , \tag{3.24}$$

$$O''^{\,L}_{ij} = \frac{1}{2}\ \left(O^*_{3i}\, O_{3j} - O^*_{2i}\, O_{2j}\right)\ , \tag{3.25}$$

with s_W, c_W the sin and cos of the weak mixing angle and g the $SU(2)_L$ gauge coupling. Finally, interactions between χ's and W-bosons are described by the terms

$$\begin{aligned}\mathscr{L}^{W^\pm-\chi^0-\chi^\mp}_{\mathrm{KIN(int)}} \ =\ & g\, O^L_{ij}\,(\chi_i^0)^\dagger\ \bar\sigma^\mu\ \chi_j^+\, W_\mu^- - g\, O^R_{ij}\,(\chi_j^-)^\dagger\ \bar\sigma^\mu\ \chi_i^0\, W_\mu^- \\ &+ g\, O^{L*}_{ij}\,(\chi_j^+)^\dagger\ \bar\sigma^\mu\ \chi_i^0\, W_\mu^+ - g\, O^{R*}_{ij}\,(\chi_i^0)^\dagger\ \bar\sigma^\mu\ \chi_j^-\, W_\mu^+\ ,\end{aligned} \tag{3.26}$$

where the mixing matrices O^L and O^R are given by

$$O^L_{ij} = O^*_{1i}\, U_{L1j}\ -\ \frac{1}{\sqrt{2}}\, O^*_{3i}\, U_{L2j}\ , \tag{3.27a}$$

$$O^R_{ij} = O_{1i}\, U^*_{R1j}\ +\ \frac{1}{\sqrt{2}}\, O_{2i}\, U^*_{R2j}\ . \tag{3.27b}$$

[9] Our notation resembles closely the one in Appendix E of ref. [28] *i.e.* $U \to U_L^\dagger$, $V \to U_R^\dagger$ and $N \to O^\dagger$.

We open a parenthesis here to discuss a comparison with MSSM: mass matrices for neutral and charged fermion in eq. (3.12) remind those of neutralinos and charginos in the MSSM. It is of course trivially understood why this happens: the doublet and the triplet fields possess the same gauge quantum numbers as the higgsino and wino fields, respectively. However, there are two crucial differences: first there is no restriction to add a bino singlet and therefore the minimal $\mathcal{M}_N$ is a 3×3, instead of 4×4, simpler matrix and second, and more important, the off-diagonal entries in $\mathcal{M}_N$ and $\mathcal{M}_C$, are not proportional to gauge couplings but to, Yukawa couplings, Y_1 and Y_2. The latter entries ($\sim Yv$) can be substantially bigger than the corresponding ones ($\sim gv$) in the neutralino mass matrix of MSSM. Furthermore, since $\tan\beta = 1$ is not, in general, a phenomenologically viable case in MSSM, there should always be a factor of hierarchy between the off diagonal entries. This is not necessarily the case here. In fact, the $\tan\beta = 1$ "blind spot" [159], is a point in parameter space protected by a custodial symmetry.

3.2.3 A custodial symmetry

It is well known that the Higgs sector in the SM obeys, in addition to the standard electroweak gauge symmetry, a custodial $SU(2)_R$ global symmetry. This symmetry is broken explicitly by the hypercharge gauge coupling g', and by the difference between the top- and bottom-quark Yukawa couplings. Similarly, the fermionic DM sector, described by eq. (3.9), obeys also such a symmetry if $Y_1 = Y_2 \equiv Y$. More explicitly, eq. (3.9) can be written in a $SU(2)_L \times SU(2)_R \times U(1)_X$ invariant form as

$$\mathscr{L}_{\rm Yuk}^{\rm DM} = -Y\,T^A\,\mathscr{H}^{x,a}\,(\tau^A)^b_a\,\bar{\mathscr{D}}_{x,b} - \frac{1}{2}\,M_D\,\epsilon^{xy}\,\epsilon^{ab}\,\bar{\mathscr{D}}_{x,a}\,\bar{\mathscr{D}}_{y,b} - \frac{1}{2}\,M_T\,T^A\,T^A \;+\; \text{H.c.}\,, \tag{3.28}$$

where x, y denote $SU(2)_R$ group indices and

$$\mathscr{H}^{x,a} = \begin{pmatrix} H^a \\ H^{\dagger\,a} \end{pmatrix}\,, \qquad \bar{\mathscr{D}}_{x,a} = \begin{pmatrix} \bar{D}_{1a} \\ \bar{D}_{2a} \end{pmatrix}\,, \tag{3.29}$$

with $H^a = \epsilon^{ab}H_b$. This extra global symmetry stands for the rotations between $H \leftrightarrow H^\dagger$ and $\bar{D}_1 \leftrightarrow \bar{D}_2$. Although this symmetry is broken by the hypercharge gauge symmetry, it is natural to study interactions among extra fermions $(\bar{\mathscr{D}}, T)$ and SM-bosons under the assumption that $SU(2)_R$ is approximately preserved in the DM sector, that is,

$$Y_1 \;=\; Y_2 \;\Rightarrow\; m_1 \;=\; m_2\,. \tag{3.30}$$

In addition, eq. (3.29) is invariant under a global $U(1)_X$ fermion number symmetry, under which only $\bar{\mathscr{D}}$ and T fields are charged with $[\bar{\mathscr{D}}] = [D_1] = [D_2] = -[T] = 1$. In that case M_D and M_T are not allowed. We therefore conclude that the limit where $Y \equiv Y_1 = Y_2$ and $M_D = M_T \to 0$ is radiatively stable and this fact motivates us to study it in more detail. Note again that, both $SU(2)_R$ and $U(1)_X$ symmetries are broken explicitly by hypercharge symmetry.

3.2.4 Lightest Neutral fermion interactions under the symmetry

Let's introduce the mass difference, $\Delta m \equiv m_1 - m_2$, between the chiral masses (or between Yukawa couplings, Y_1 and Y_2, if you wish). If $SU(2)_R$ symmetry is approximately

preserved, *i.e.* eq. (3.30) approximately holds, Δm must be treated as perturbation compared to m_1 or m_2 masses, which collectively denoted by $m = m_1$, *i.e.* $\Delta m \ll m$. We can then write the neutral fermion mass matrix in a suggestive perturbative form

$$\mathcal{M}_N \;=\; \mathcal{M}_N^{(0)} + Q \,, \tag{3.31}$$

where

$$\mathcal{M}_N^{(0)} = \begin{pmatrix} M_T & m & -m \\ m & 0 & M_D \\ -m & M_D & 0 \end{pmatrix} \,, \qquad Q = \begin{pmatrix} 0 & 0 & \Delta m \\ 0 & 0 & 0 \\ \Delta m & 0 & 0 \end{pmatrix} \,. \tag{3.32}$$

The zeroth order eigenvalues of $\mathcal{M}_N^{(0)}$ read

$$m_{\chi_1^0} = M_D \,, \tag{3.33a}$$

$$m_{\chi_2^0} = \frac{1}{2}\left[M_T - M_D - \sqrt{8m^2 + (M_T + M_D)^2}\right] \,, \tag{3.33b}$$

$$m_{\chi_3^0} = \frac{1}{2}\left[M_T - M_D + \sqrt{8m^2 + (M_T + M_D)^2}\right] \,, \tag{3.33c}$$

and the corresponding eigenvectors are

$$|1\rangle^{(0)} = \frac{1}{\sqrt{2}}\begin{pmatrix} 0 \\ 1 \\ 1 \end{pmatrix} \,, \quad |2\rangle^{(0)} = \frac{-1}{\sqrt{2+a^2}}\begin{pmatrix} a \\ 1 \\ -1 \end{pmatrix} \,, \quad |3\rangle^{(0)} = \frac{1}{\sqrt{2+a^2}}\begin{pmatrix} \sqrt{2} \\ -\frac{a}{\sqrt{2}} \\ \frac{a}{\sqrt{2}} \end{pmatrix} \,, \tag{3.34}$$

where the parameter a is given by

$$a = \frac{m_{\chi_1^0} + m_{\chi_2^0}}{m} \,. \tag{3.35}$$

The parameter a, varies in the interval $[-\sqrt{2}, 0]$ for positive M_D. A little examination of the eigenvalues show that unless, $M_D \gg M_T > 0$ where the Lightest Particle (LP) becomes the triplet, in the rest of the parameter space the LP is a "very well tempered" mixed doublet fermion, $|\chi_1^0\rangle = \frac{1}{\sqrt{2}}(|\bar{D}_1^1\rangle + |\bar{D}_2^2\rangle)$, with mass $m_{\chi_1^0} = M_D$.[10] The DM particle (χ_1^0) has then vanishing coupling to the Higgs boson because in eq. (3.19) it is $O_{11} = 0$. Note that, every neutral fermion has always vanishing diagonal couplings to Z-gauge boson, $|O_{2i}| = |O_{3i}|$, since the two doublets, $\bar{D}_1$ and $\bar{D}_2$ couple to Z with opposite weak isospin. It is therefore worth examining how eigenvalues and eigenvectors are corrected after switching on to $\Delta m \neq 0$.

Obviously, in order to find how χ_1^0 couples to Z or h non-trivially, *i.e.* to find the couplings $Y^{h\chi_1^0\chi_1^0}$ and $g^{Z\chi_1^0\chi_1^0} = gO''^{L}_{11}/c_W$ in eqs. (3.19) and (3.25), respectively, we need to know the $O(\Delta m)$ corrections, in the eigenvector O_{i1}. The corrected eigenvector, $|1\rangle = |1\rangle^{(0)} + |1\rangle^{(1)} + O[(\Delta m)^2]$, which is nothing else but the first column of the matrix O in eq. (3.13) is found to be,

$$O_{i1} = |1\rangle = \frac{1}{\sqrt{2}}\begin{pmatrix} x\,\Delta m \\ 1 + y\,\Delta m \\ 1 - y\,\Delta m \end{pmatrix} + O[(\Delta m)^2] \,, \tag{3.36}$$

[10] It is easy to show that since ${}^{(0)}\langle 1|Q|1\rangle^{(0)} = 0$, there is no correction, up to $(\Delta m)^2$, on $m_{\chi_1^0} = M_D$ LP mass.

where

$$x \equiv \frac{1}{(2+a^2)}\left[\frac{a^2}{m_{\chi_1^0}-m_{\chi_2^0}}+\frac{2}{m_{\chi_1^0}-m_{\chi_3^0}}\right], \tag{3.37}$$

$$y \equiv \frac{a}{(2+a^2)}\left[\frac{1}{m_{\chi_1^0}-m_{\chi_2^0}}-\frac{1}{m_{\chi_1^0}-m_{\chi_3^0}}\right]. \tag{3.38}$$

Simple substitution of eq. (3.36) into eqs. (3.19) and (3.25) gives

$$Y^{h\chi_1^0\chi_1^0} = \frac{(\Delta m)^2}{\sqrt{2}v}\, x\,(1+2my) + \mathrm{O}[(\Delta m)^2/m^2]\,, \tag{3.39}$$

$$g^{Z\chi_1^0\chi_1^0} \equiv \frac{g}{c_W}O''^{L}_{11} = -\frac{g}{c_W}\, y\,\Delta m + \mathrm{O}[(\Delta m)^2/m^2]\,. \tag{3.40}$$

Obviously, for sufficiently small mass difference Δm, the Spin-Independent (SI) coupling ($Y^{h\chi_1^0\chi_1^0}$) is suppressed by $(\Delta m)^2/m^2$ while the Spin-Dependent (SD) one ($g^{Z\chi_1^0\chi_1^0}$) is suppressed by $\Delta m/m$ relative to their values away from the $SU(2)_R$-symmetric limit. This maybe the reason why we have not detected DM-nucleon interactions so far. A question arises immediately about the stability of Δm under radiative corrections. A quick RGE analysis [202, 203] shows that the β-function for Δm at 1-loop is

$$\frac{d\Delta m}{d\ln(Q)} \;=\; \frac{\Delta m}{16\pi^2}\left[\frac{29}{4}Y^2+3Y_t^2-\frac{9}{20}g_1^2-\frac{33}{4}g_2^2\right], \tag{3.41}$$

where Y_t is the top-Yukawa coupling, $Y \equiv Y_1 \simeq Y_2$, and $g_{1,2}$ the hypercharge and weak gauge couplings, respectively. Eq. (3.41) means that Δm is only multiplicatively renormalized. Therefore, setting Δm to zero at tree level stays zero at 1-loop and possibly at higher orders[11] because this is a parameter point protected by the global symmetry. From eqs. (3.39) and (3.40) we conclude that for $\Delta m = 0$, only finite (threshold) and calculable quantum corrections will affect the couplings $Y^{h\chi_1^0\chi_1^0}$ and $g^{Z\chi_1^0\chi_1^0}$ which are relevant to Direct DM searches. We confirm this consequence with a direct calculation of $\delta Y^{h\chi_1^0\chi_1^0}$ in Section 3.5 and in Appendix A.

Note that x vanishes in the limit $M_D \to 0$ while $(1+2my)$ vanishes at both $M_D \to 0$ and $M_D \to M_T$ limits. However, eq. (3.39) is not accurate since $(\Delta m)^2/m^2$-terms are missing in our perturbative expansion. It turns out that the $M_D \to M_T$ limit is violated by those and higher terms, but the limit $M_D \to 0$ is protected because of the $U(1)_X$-symmetry that we discussed in Section 3.2.3. In contrast, eq. (3.40) is within 1% of its exact numerical outcome. It is also worth noticing that in the case where the Majorana masses are dominant, $M_D, M_T \gg m$, then $y \to 0$ and therefore $g^{Z\chi_1^0\chi_1^0} \to 0$, up to higher order terms.

It will be useful for the discussion, especially on the relic density, to show the mass difference between the next-to-lightest ($|m_{\chi_2^0}|$) and the lightest ($|m_{\chi_1^0}|$) neutral fermion states. This is depicted as contour lines in Fig. 3.2(a,b) on the $M_D - M_T$ plane (left plot) and on the $M_D - m$ plane with $M_T = M_D$ (right plot). Note that M_D coincides with the LP mass *i.e.* $M_D = m_{\chi_1^0}$, everywhere in these graphs. For $m = 200$ GeV, the mass difference is nowhere smaller than approximately 80 GeV, and typically, it is as large as the parameter m with the maximum value at $M_D = M_T$. Subsequently, in Fig. 3.2b, we

[11] We confirm that this result remains unchanged at two-loop level.

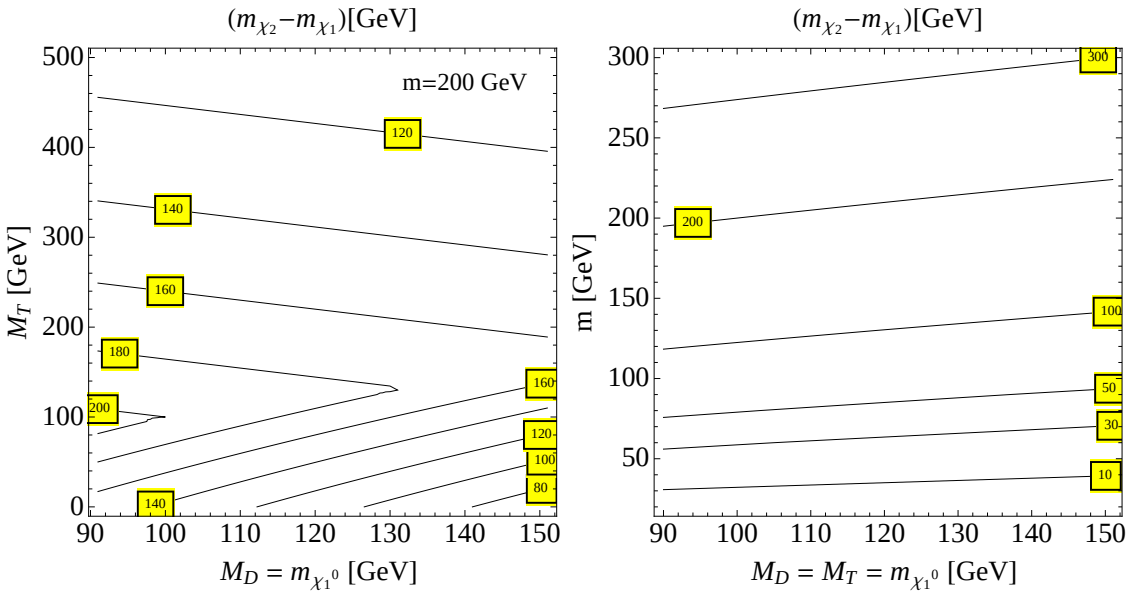

(a) (b)

Figure 3.2: *The mass difference, $|m_{\chi_2^0}|-|m_{\chi_1^0}|$, between the next-to-lightest and the lightest neutral particle state in the Doublet-Triplet Fermionic DM model on (a) M_D vs. M_T with $m = 200$ GeV, and (b) on M_D vs. m with $M_T = M_D$, plane. For both plots and for the rest to come, it is always, $m_{\chi_1^0} = M_D$.*

plot the maximum values of the mass difference on $M_D - m$ plane. Alternatively, it is easy to read from Fig. 3.2, the parameter a defined in eq. (3.35), because for the M_D values taken throughout, it is $a = -(|m_{\chi_2^0}| - |m_{\chi_1^0}|)/m$. For instance, in the plots shown, this parameter varies, approximately, in the region, $a \in [-1, -0.3]$.

3.2.5 Analytical expressions for the new interactions under the symmetry

As we have already discussed in Section 3.2.1, in the symmetric $SU(2)_R$ limit of (3.30), two of the eigenvalues from the charged fermion mass matrix are degenerate respectively with those of the neutral fermion masses given in eqs. (3.33b) and (3.33c),

$$m_{\chi_1^\pm} = m_{\chi_2^0} \,, \quad m_{\chi_2^\pm} = m_{\chi_3^0} \,. \tag{3.42}$$

In addition, it is useful for further reference to present analytical expressions for all new interactions appear in the model. All these new interactions can be simply written in matrix forms containing (at most) one parameter, the real parameter a of eq. (3.35). For example, rotation matrices defined in eq. (3.13) read

$$U = U_L = U_R = \frac{1}{\sqrt{2+a^2}} \begin{pmatrix} a & -\sqrt{2} \\ \sqrt{2} & a \end{pmatrix} \,,$$
$$O = \begin{pmatrix} 0 & -\frac{a}{\sqrt{2+a^2}} & \frac{\sqrt{2}}{\sqrt{2+a^2}} \\ \frac{1}{\sqrt{2}} & -\frac{1}{\sqrt{2+a^2}} & -\frac{a}{\sqrt{2}\sqrt{2+a^2}} \\ \frac{1}{\sqrt{2}} & \frac{1}{\sqrt{2+a^2}} & \frac{a}{\sqrt{2}\sqrt{2+a^2}} \end{pmatrix} \,. \tag{3.43}$$

The couplings between χ_1^0, W and $\chi^\pm$ given in eq. (3.27) become explicitly:

$$O_{1j}^L = -O_{1j}^{R\,*} ,$$
$$O^L = \begin{pmatrix} -\frac{1}{\sqrt{2}\sqrt{2+a^2}} & -\frac{a}{2\sqrt{2+a^2}} \\ -\frac{1+a^2}{2+a^2} & \frac{a}{\sqrt{2}(2+a^2)} \\ \frac{a}{\sqrt{2}(2+a^2)} & -\frac{4+a^2}{4+2a^2} \end{pmatrix} , \qquad O^R = \begin{pmatrix} \frac{1}{\sqrt{2}\sqrt{2+a^2}} & \frac{a}{2\sqrt{2+a^2}} \\ -\frac{1+a^2}{2+a^2} & \frac{a}{\sqrt{2}(2+a^2)} \\ \frac{a}{\sqrt{2}(2+a^2)} & -\frac{4+a^2}{4+2a^2} \end{pmatrix} , \tag{3.44}$$

while those in eqs. (3.23), (3.24) and (3.25),

$$O'^{\,L(R)} = \begin{pmatrix} \frac{-1-a^2+\left(2+a^2\right)s_W^2}{2+a^2} & \frac{a}{\sqrt{2}(2+a^2)} \\ \frac{a}{\sqrt{2}(2+a^2)} & -\frac{4+a^2-2\left(2+a^2\right)s_W^2}{2(2+a^2)} \end{pmatrix} ,$$
$$O''^{\,L} = \begin{pmatrix} 0 & \frac{1}{\sqrt{2}\sqrt{2+a^2}} & \frac{a}{2\sqrt{2+a^2}} \\ \frac{1}{\sqrt{2}\sqrt{2+a^2}} & 0 & 0 \\ \frac{a}{2\sqrt{2+a^2}} & 0 & 0 \end{pmatrix} . \tag{3.45}$$

Finally, the Higgs couplings to neutral and charged fermions in eqs. (3.19) and (3.18) are respectively:

$$Y^{h\chi^0\chi^0} = \frac{m}{v}\begin{pmatrix} 0 & 0 & 0 \\ 0 & \frac{2\sqrt{2}a}{(2+a^2)} & \frac{\left(-2+a^2\right)}{(2+a^2)} \\ 0 & \frac{\left(-2+a^2\right)}{(2+a^2)} & -\frac{2\sqrt{2}a}{(2+a^2)} \end{pmatrix} , \qquad Y^{h\chi^-\chi^+} = \frac{m}{v}\begin{pmatrix} \frac{2\sqrt{2}a}{(2+a^2)} & \frac{\left(-2+a^2\right)}{(2+a^2)} \\ \frac{\left(-2+a^2\right)}{(2+a^2)} & -\frac{2\sqrt{2}a}{(2+a^2)} \end{pmatrix} , \tag{3.46}$$

while those to Goldstone bosons given in eq. (3.20), can now be simply written as

$$Y^{G^0\chi^0\chi^0} = \frac{im}{v}\begin{pmatrix} 0 & -\frac{a}{\sqrt{2+a^2}} & \frac{\sqrt{2}}{\sqrt{2+a^2}} \\ -\frac{a}{\sqrt{2+a^2}} & 0 & 0 \\ \frac{\sqrt{2}}{\sqrt{2+a^2}} & 0 & 0 \end{pmatrix} , \qquad Y^{G^0\chi^-\chi^+} = \frac{im}{v}\begin{pmatrix} 0 & -1 \\ 1 & 0 \end{pmatrix} \forall a , \tag{3.47}$$

and

$$Y^{G^+\chi^-\chi^0} = \frac{m}{v}\begin{pmatrix} \frac{a}{\sqrt{2+a^2}} & 0 & -1 \\ -\frac{\sqrt{2}}{\sqrt{2+a^2}} & 1 & 0 \end{pmatrix} , \qquad Y^{G^-\chi^+\chi^0} = \frac{m}{v}\begin{pmatrix} -\frac{a}{\sqrt{2+a^2}} & 0 & -1 \\ \frac{\sqrt{2}}{\sqrt{2+a^2}} & 1 & 0 \end{pmatrix} . \tag{3.48}$$

Depending on whether the chiral mass m or the vectorial masses M_D and M_T are dominant, and for $M_D > 0$, there are two extreme limits for the model at hand

$$\text{“Majorana dominance”} : M_T \approx M_D \gg m \Rightarrow a \approx 0 , \quad m^2_{\chi_1^0} \approx m^2_{\chi_2^0} \approx M_D^2 , \quad m^2_{\chi_3^0} \approx M_T^2 . \tag{3.49}$$

$$\text{“Dirac dominance”} : M_T \approx M_D \ll m \Rightarrow a \approx -\sqrt{2} , \quad m^2_{\chi_2^0} \approx m^2_{\chi_3^0} \approx M_D^2 + 2m^2 . \tag{3.50}$$

The “Majorana dominance” limit corresponds more or less to the “higgsino-wino” scenario of the MSSM where the first two neutral particle masses are degenerate, while the “Dirac dominance” limit is the imprint of a large Yukawa coupling in eq. (3.9). It is the latter

case that in addition to $SU(2)_R$-symmetry, it is protected by the global $U(1)_X$ symmetry. For example, plugging in $a = -\sqrt{2}$ into eq. (3.46), we immediately see that the Higgs couplings to new fermions become diagonal resulting in a vanishing, as long as $M_D \to 0$, one loop corrections to the $h-\chi_1^0-\chi_1^0$ vertex, as we qualitatively confirmed in Section 3.2.4 below eq. (3.39), and as we shall see below in Section 3.5.

3.2.6 Composition of the lightest Neutral Fermion

As we showed in eqs. (3.33) and (3.34), in the symmetric limit $m_1 = m_2$, the neutral fermion mass matrix $\mathcal{M}_N$, can be diagonalized analytically into three mass eigenstates

$$|\chi_i^0\rangle \;=\; O_{i1}\,|1\rangle + O_{i2}\,|2\rangle + O_{i3}\,|3\rangle \;. \tag{3.51}$$

Following conventional MSSM nomenclature [52], lets define the "Doublet" composition of the χ_i^0 as

$$F_D^i = |O_{i2}|^2 + |O_{i3}|^2 \;. \tag{3.52}$$

Then we say that a state of χ_i^0 is (D)oublet-like if $F_D^i > 0.99$, it is (T)riplet like if $F_D^i < 0.01$ and it is (M)ixed state if $0.01 < F_D^i < 0.99$.

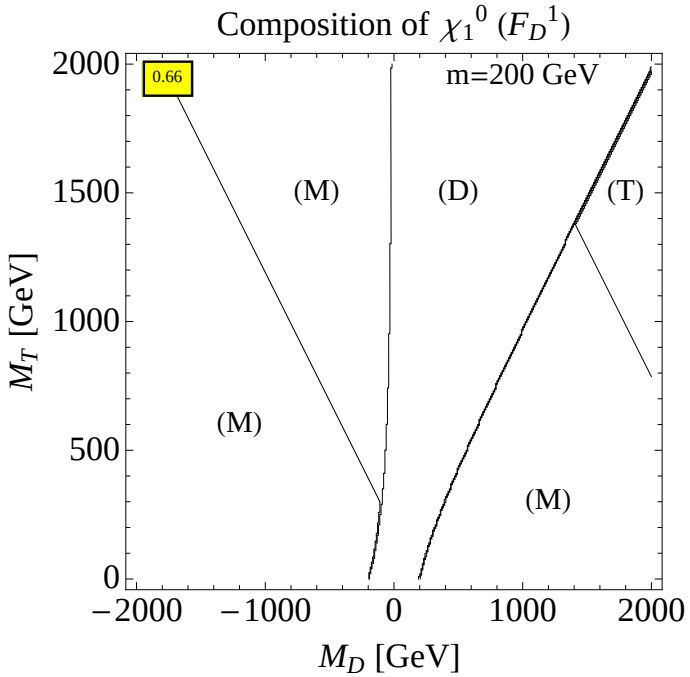

Figure 3.3: *The composition of the WIMP in terms of (D)oublet, (T)riplet and (M)ixed states following the definition given in the paragraph below eq. (3.52), on a M_D vs. M_T plane and for fixed (common) Yukawa coupling, $Y = m/v \simeq 200/174 \simeq 1.15$.*

In Fig. 3.3 we present the composition of the DM candidate particle χ_1^0 on a M_D vs. M_T plane for fixed mass, $m = 200GeV$. Both Z and Higgs-boson couplings to pairs of χ_1^0's vanish at tree level only in the region denoted by (D) (for Doublet) where M_D is (most of the time) positive and equal to, or less, than M_T. It is mostly in this region we are focusing on in this study, because in this region the model evades, without further tweaks, direct DM detection experimental bounds. Note also that for light $M_D = \chi_1^0 \lesssim 150$ GeV $<< m$,

the WIMP composition satisfies (D) condition for every value of M_T. For negative values of M_D, χ_1^0 is a pure doublet only in the region $|M_D| \leq m$ but shrinks down to unacceptably small M_D for large values of M_T; otherwise it is a mixed state everywhere in Fig. 3.3. For large $M_D \gg M_T$, the χ_1^0-composition consists of mainly a triplet.

Note that when the lightest state is pure (D)oublet the heavier states are exactly an equal admixture of doublets and the triplet *i.e.* $F_D^{2,3} = 0.5$.

3.3 Estimate of Electroweak Corrections

In the limit of large Yukawa couplings, $Y = Y_1 = Y_2 \simeq 1$, we generally expect large contributions from the new fermions, $\chi^0, \chi^\pm$, to (Z, W)-gauge boson self-energy one-loop diagrams. In this section we investigate constraints on the doublet-triplet fermion model parameter space, $\{M_D, M_T, m\}$, from the oblique electroweak parameters S, T and U [147].

Due to Z_2-parity symmetry, at one-loop level, there is no mixing between the extra fermions, $\chi^0, \chi^\pm$, and the SM leptons. Therefore corrections to electroweak precision observables involving light fermions arise only from gauge bosons vacuum polarisation Feynman diagrams *i.e.* there are only oblique electroweak corrections. In order to estimate these corrections it is convenient to calculate the S, T and U parameters, in the limit where $m_{\chi^0}, m_{\chi^\pm} \gtrsim m_Z$. This is true when the doublet mass M_D, is greater than m_Z and m is much greater than m_Z (see Fig. 3.2). We shall not consider the case of a light dark matter particle, $m_{\chi_1^0} \lesssim m_Z$.

Following closely the notation by Peskin and Takeuchi in ref. [147], we write,

$$\alpha\, S \equiv 4e^2\, \frac{d}{dp^2} \left[\Pi_{33}(p^2) - \Pi_{3Q}(p^2)\right]\Big|_{p^2=0} , \tag{3.53a}$$

$$\alpha\, T \equiv \frac{e^2}{s_W^2 c_W^2 m_Z^2}\, \left[\Pi_{11}(0) - \Pi_{33}(0)\right] , \tag{3.53b}$$

$$\alpha\, U \equiv 4e^2\, \frac{d}{dp^2} \left[\Pi_{11}(p^2) - \Pi_{33}(p^2)\right]\Big|_{p^2=0} , \tag{3.53c}$$

where $\alpha = e^2/4\pi$. In numerics we use input parameters from ref. [204], the bare value at lowest order $s_W^2 = g'^2/(g'^2 + g^2) \simeq 0.2312$ and the Z-pole mass $m_Z = 91.1874$ GeV. We calculate corrections arising only from the extra fermions, $\chi^0_{i=1..3}, \chi^\pm_{i=1..2}$, to the $g^{\mu\nu}$ part of the gauge boson self energy amplitudes, $\Pi_{IJ} \equiv \Pi_{IJ}(p^2)$, where I and J may be photon (γ), W or Z,

$$\Pi_{\gamma\gamma} = e^2\, \Pi_{QQ} , \tag{3.54a}$$

$$\Pi_{Z\gamma} = \frac{e^2}{c_W s_W}\, \left(\Pi_{3Q} - s^2 \Pi_{QQ}\right) , \tag{3.54b}$$

$$\Pi_{ZZ} = \frac{e^2}{c_W^2 s_W^2}\, \left(\Pi_{33} - 2s^2 \Pi_{3Q} + s^4 \Pi_{QQ}\right) , \tag{3.54c}$$

$$\Pi_{WW} = \frac{e^2}{s_W^2}\, \Pi_{11} , \tag{3.54d}$$

where $s_W = \sin\theta_W, c_W = \cos\theta_W$. We find,

$$\Pi_{QQ} = -\frac{p^2}{8\pi^2}\sum_{i=1}^{2}\left[\frac{2}{3}E - 4\,b_2(p^2, m^2_{\chi_i^\pm}, m^2_{\chi_i^\pm})\right] , \tag{3.55a}$$

$$\Pi_{3Q} = \frac{p^2}{16\pi^2}\sum_{i=1}^{2}(Z^L_{ii} + Z^R_{ii})\left[\frac{2}{3}E - 4\,b_2(p^2, m^2_{\chi_i^\pm}, m^2_{\chi_i^\pm})\right] , \tag{3.55b}$$

$$\Pi_{11} = \frac{1}{16\pi^2}\sum_{i=1}^{3}\sum_{j=1}^{2}\Bigg[(|O^L_{ij}|^2 + |O^R_{ij}|^2)G(p^2, m^2_{\chi_i^0}, m^2_{\chi_j^\pm}) - \\ - 2\Re e(O^{L\,*}_{ij}O^R_{ij})m_{\chi_i^0}m_{\chi_j^\pm}I(p^2, m^2_{\chi_i^0}, m^2_{\chi_j^\pm})\Bigg] , \tag{3.55c}$$

$$\Pi_{33} = \frac{1}{16\pi^2}\sum_{i,j=1}^{2}\left[(Z^L_{ij}Z^L_{ji} + Z^R_{ij}Z^R_{ji})G(p^2, m^2_{\chi_i^\pm}, m^2_{\chi_j^\pm}) - 2Z^L_{ij}Z^R_{ji}m_{\chi_i^\pm}m_{\chi_j^\pm}I(p^2, m^2_{\chi_i^\pm}, m^2_{\chi_j^\pm})\right] \\ + \frac{1}{16\pi^2}\sum_{i,j=1}^{3}\left[O''^L_{ij}O''^L_{ji}\,G(p^2, m^2_{\chi_i^0}, m^2_{\chi_j^0}) + (O''^L_{ij})^2\,m_{\chi_i^0}m_{\chi_j^0}\,I(p^2, m^2_{\chi_i^0}, m^2_{\chi_j^0})\right] , \tag{3.55d}$$

where $Z^{L(R)}_{ij} \equiv O'^{L(R)}_{ij} - s^2_W\delta_{ij}$. In addition, $E \equiv \frac{2}{\epsilon} - \gamma + \log 4\pi - \log Q^2$ is the infinite part of loop diagrams. The various one-loop functions in eqs. (3.55) are given by

$$G(p^2, x, y) = -\frac{2}{3}p^2\,E + (x+y)\,E + 4\,p^2\,b_2(p^2, x, y) - 2\left[y\,b_1(p^2, x, y) + x\,b_1(p^2, y, x)\right] , \tag{3.56}$$

$$I(p^2, x, y) = 2\,E - 2\,b_0(p^2, x, y) , \tag{3.57}$$

$$b_0(p^2, x, y) = \int_0^1 dt \log\frac{\Delta}{Q^2} , \quad b_1(p^2, x, y) = \int_0^1 dt\,t\,\log\frac{\Delta}{Q^2} , \tag{3.58}$$

$$b_2(p^2, x, y) = \int_0^1 dt\,t\,(1-t)\,\log\frac{\Delta}{Q^2} , \quad \Delta = ty + (1-t)x - t(1-t)\,p^2 - i\epsilon . \tag{3.59}$$

There are numerous useful identities,

$$b_0(p^2, x, y) = b_0(p^2, y, x) , \quad b_2(p^2, x, y) = b_2(p^2, y, x) , \tag{3.60}$$

$$G(p^2, x, y) = G(p^2, y, x) , \quad I(p^2, x, y) = I(p^2, y, x) , \tag{3.61}$$

$$b_1(p^2, x, y) = b_0(p^2, y, x) - b_1(p^2, y, x) , \quad b_1(p^2, x, x) = \frac{b_0(p^2, x, x)}{2} , \tag{3.62}$$

that will help us to simplify our expressions below.

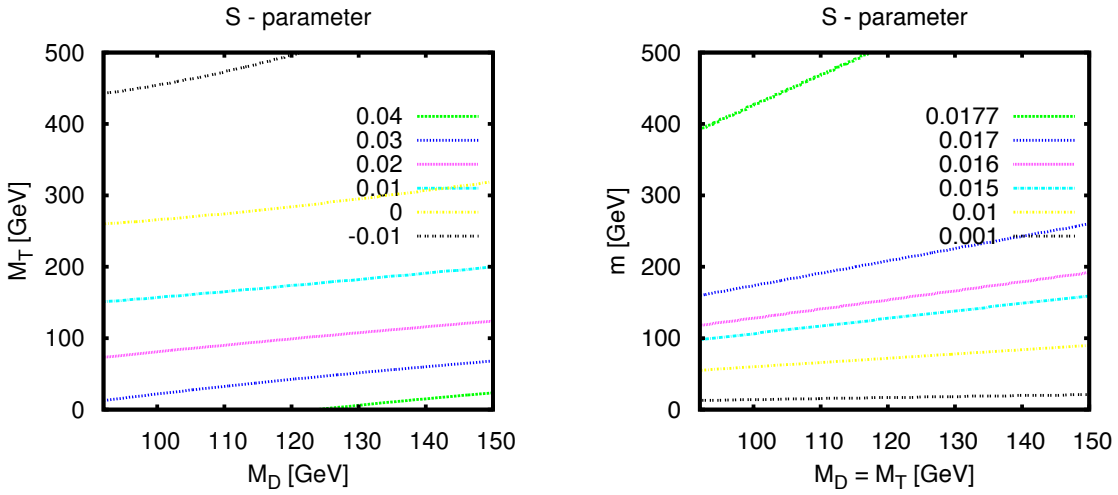

Figure 3.4: *Contour plots of the S-parameter on the M_D vs. M_T plane (left) for $m = 200GeV$ and on M_D vs. m plane (right) for $M_T = M_D$.*

Furthermore, in the exact $SU(2)_R$ limit where $m_1 = m_2$, there is no isospin breaking in $\bar{D}$-components and therefore $T = 0$, while the S-parameter receives non-zero, non-decoupled, contributions due to the enlarged particle number of the $SU(2)$-sector. Specifically, in the limit where $M_D = M_T \ll m = m_1 = m_2$, there is a light neutral fermion ($m_{\chi_1^0}$) and heavy degenerate other four (two neutral and two charged) fermions, with squared mass x, resulting in

$$\Pi'_{3Q}(0) \approx \frac{1}{16\pi^2}\left[-2E + 2\ln(\frac{x}{Q^2})\right], \tag{3.63a}$$

$$\Pi'_{33}(0) = \Pi'_{11}(0) \approx \frac{1}{16\pi^2}\left[-2E + 2\ln(\frac{x}{Q^2}) + \frac{1}{18}\right], \tag{3.63b}$$

$$\Pi_{33}(0) = \Pi_{11}(0) \approx \frac{1}{16\pi^2}\left[\frac{3x}{2}E - \frac{3x}{2}\ln(\frac{x}{Q^2}) + \frac{x}{4}\right]. \tag{3.63c}$$

Plugging in eqs. (3.63) into eqs. (3.53) we arrive at the approximate values expressions

$$S \approx \frac{1}{18\pi}, \quad T \approx U \approx 0\,. \tag{3.64}$$

This result is also confirmed numerically in Fig. 3.4 where we draw contours of the S-parameter on M_D vs. M_T plane (left plot) and on M_D vs. m plane (right plot). As it is shown, for large m we obtain $S \to 1/18\pi \simeq 0.0177$ while for $m \to 0$ we obtain $S \to 0$, as expected because in this case only vector-like masses will exist in $\mathscr{L}_{\rm Yuk}^{\rm DM}$ of eq. (3.9), that make no contribution to parameter S. Experimentally, we know [204] that when the U-parameter is zero, the parameters S and T which fit the electroweak data are constrained to be [12]

$$S = 0.04 \pm 0.09\,, \tag{3.65a}$$

$$T = 0.07 \pm 0.08\,. \tag{3.65b}$$

[12] **Note added**: Updated constraints [60] for the S and T parameters (with fixed $U = 0$), show a 1.5 σ deviation for the T-parameter. However, relaxing $U = 0$, vanishing T is well within limits.

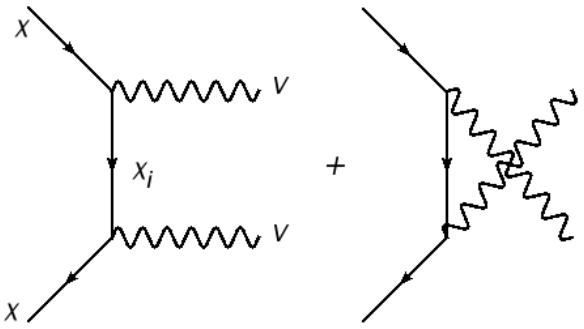

Figure 3.5: *Lower level Feynman diagrams contributing to annihilation cross section for the process* $\chi + \chi \to V + V$ *for* $V = W, Z$.

Predictions for the S-parameter shown in Fig. 3.4a,b comfortably fall within the bound of (3.65a). In addition, even though it is not shown, the T, U-parameters are always negligibly small[13].

3.4 The Thermal Relic Dark Matter Abundance

As we have seen, $V\chi_1^0\chi_1^0$ with $V = W, Z$ and $h\chi_1^0\chi_1^0$ are forbidden at tree level if χ_1^0 is a pure doublet *i.e.* $m_{\chi_1^0} = M_D$, in the exact $SU(2)_R$-limit. Therefore, the annihilation cross section for the lightest neutral fermion results solely from the following $t-$ and $u-$channel tree level Feynman diagrams, shown in Fig. 3.5, with neutral or charged fermion exchange, collectively shown as χ_i, with axial-vector interactions

$$\chi_1^0 \ + \ \chi_1^0 \to W^+ \ + \ W^- \ , \tag{3.66a}$$

$$\chi_1^0 \ + \ \chi_1^0 \to Z \ + \ Z \ . \tag{3.66b}$$

All other processes vanish at tree level. This can easily be understood by looking at the matrix forms of O''^L and $Y^{h\chi^0\chi^0}$ in eqs. (3.45) and (3.46). Before presenting our results for the annihilation cross section it is helpful to (order of magnitude) estimate the thermal dark matter relic density for χ_1^0s. Consequently, by expanding the total cross section as in eq. (1.105) and keeping only the zero-relative-velocity a-terms we find (for $M_D = M_T$):

$$a_W = \frac{g^4\,\beta_W^3}{32\pi}\,\frac{m_\chi^2}{(m_\chi^2 + m_{\chi_j}^2 - m_W^2)^2} \ \xrightarrow[m \gg M_D]{m_{\chi_j} \gg m_\chi} \ \frac{g^4\,\beta_W^3}{32\pi}\left(\frac{m_\chi}{m_{\chi_j}}\right)^4 \frac{1}{m_\chi^2} \ , \tag{3.67a}$$

$$a_Z = \frac{g^4\,\beta_Z^3}{64\pi\,c_W^4}\,\frac{m_\chi^2}{(m_\chi^2 + m_{\chi_j}^2 - m_W^2)^2} \ \xrightarrow[m \gg M_D]{m_{\chi_j} \gg m_\chi} \ \frac{g^4\,\beta_Z^3}{64\pi\,c_W^4}\left(\frac{m_\chi}{m_{\chi_j}}\right)^4 \frac{1}{m_\chi^2} \ , \tag{3.67b}$$

where $g \approx 0.65$ is the electroweak coupling, $\beta_V = \sqrt{1 - m_V^2/m_\chi^2}$ for $V = W, Z$, and in order to simplify notation, we take $m_\chi \equiv m_{\chi_1^0}$ to denote the DM particle mass and $m_{\chi_j} \equiv m_{\chi_j^0} = m_{\chi_{j-1}^\pm} \geq m_\chi$ for $j = 2, 3$ [see eq. (3.42)] the heavier neutral and charged fermions of the DM-sector. In the case where $M_D = M_T$, the heavier fermions are degenerate with mass, $m_{\chi_j}^2 = 2m^2 + M_D^2$, and the mass spectrum pattern is similar to the one shown in

[13] This result has been also confirmed by ref. [205]. Furthermore, it was found that T increases quickly beyond the $SU(2)_R$ symmetric limit, *i.e.* as Y_1 deviates from Y_2.

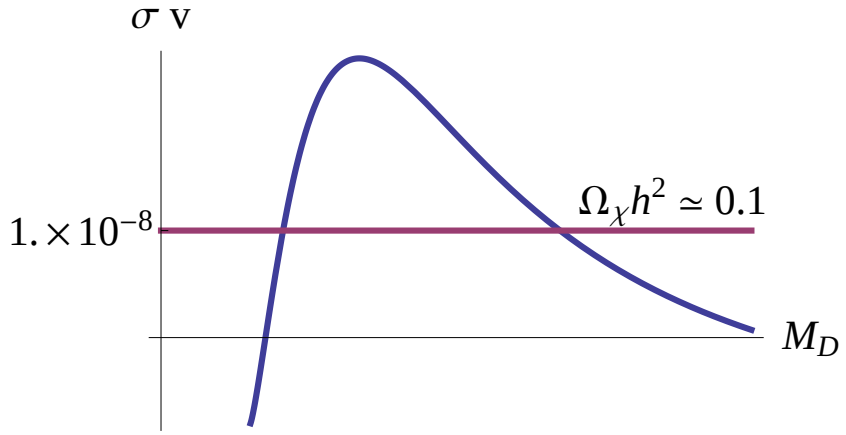

Figure 3.6: *Sketch of the resulting annihilation cross section.*

Fig. 3.1. Following this pattern in eq. (3.67) we have taken the limit of $m \gg M_D$ or alternatively, $m_{\chi_j} \gg m_\chi$.

Obviously, eqs. (3.67a) and (3.67b) viewed as functions of M_D, exhibit a maximum extremum since both a's vanish in the limits of $M_D \to 0$ and $M_D \to \infty$ and, in addition, they are positive definite. The maximum cross section is obtained approximately at $M_D \approx \sqrt{2}m$. The situation is clearly sketched in Fig. 3.6. Once again, we assume that particle-χ is a cold thermal relic, and that its mass is about few tens bigger than its freeze-out temperature (see relevant discussion in Section 1.3.3). Then, the relic abundance (1.111) is

$$\Omega_\chi\, h^2 \sim 0.1\, \frac{10^{-8}\ \text{GeV}^{-2}}{\sigma v}\ . \tag{3.68}$$

Therefore, if the correct cross section, $\sigma v \approx 10^{-8}$ GeV^{-2}, that produces the right relic density, $\Omega_\chi\, h^2 \sim 0.1$, happens to be below the maximum of σv in Fig. 3.6 then there are two of its points crossing the observed relic density: one for low M_D and one for high M_D with the single crossing point being at $M_D \approx \sqrt{2}m$. The mass spectrum of new fermions with high M_D exhibits nearly degeneracy in the first two states *i.e.* $m_\chi = m_{\chi_2} \simeq M_D$. This shares similarities with the MSSM (or more precisely with the Split SUSY with $\tan\beta = 1$ "wino-higgsino" scenario) for higgsino dark matter which is well studied and we are not going to pursue further here. The other case, on the other hand, with low $M_D \lesssim m$, exhibits a mass hierarchy between the DM candidate particle (χ) and all the rest (χ_j) particles. It is the suppression factor (m_χ/m_{χ_j}) to the fourth power in eqs. (3.67a) and (3.67b) that prohibits the cross section from taking on very large values. It is therefore evident that this low M_D scenario can provide the SM with a DM candidate particle with mass M_D that lies "naturally" at the EW scale as this suggested by the observation $\sigma \approx 10^{-8}$ GeV^{-2}, and is accompanied by heavy fermions, few to several times heavier (depending on the value of m) than M_D.

Before proceeding further, it is worth looking back at Fig. 3.2, the mass difference between the first two neutral states. For $m \gtrsim 100GeV$ the mass difference is always more than 50% than the lightest mass m_χ. This in turn suggests that *no significant* contributions to $\Omega_\chi h^2$ are anticipated from co-annihilation effects [59].

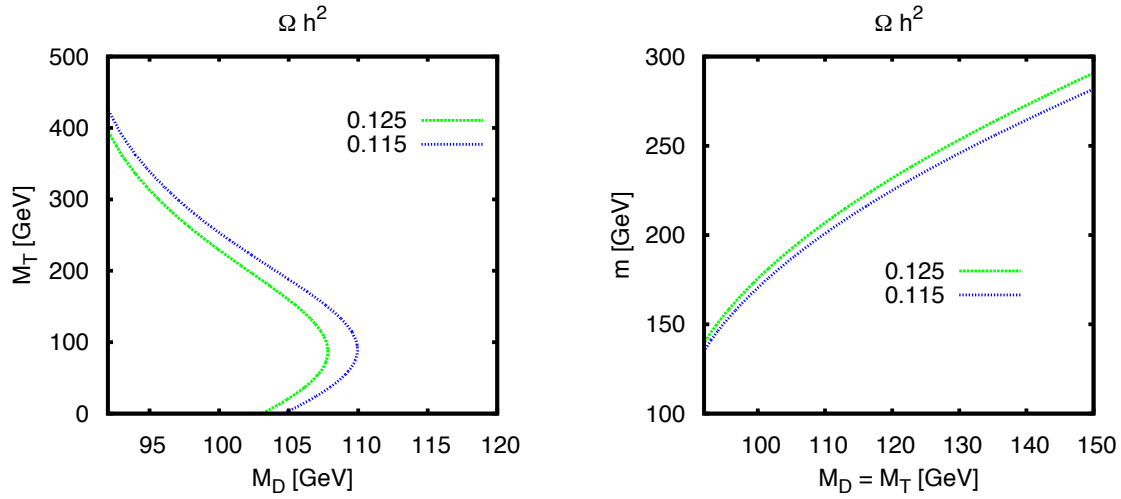

Figure 3.7: *(Left) Contour plots on the plane M_D vs M_T for the observed relic density $\Omega_\chi h^2$ [see eq. (3.69)] of the lightest neutral fermion with $m = 200$ GeV. (Right) The same on M_D vs. m plane for $M_D = M_T$. Recall that for both plots it is $m_\chi = M_D$.*

In the end, we have calculated the today's relic density of the neutral, stable, and therefore, DM-candidate particle χ. Our calculation is a tree level one; see however comments below. Within the context of the (spatially flat) six-parameters standard cosmological model, *Planck* experiment [164][14] reports a density for cold, non-baryonic, dark matter, that is

$$\Omega_{DM}\, h^2 = 0.1199 \pm 0.0027\ . \tag{3.69}$$

The 2-σ value is satisfied only in the area between the two lines in both plots in Fig. 3.7. This happens for rather low $m_\chi = M_D$ in the region $92 \lesssim m_{\chi_1^0} \lesssim 110$ GeV and for $M_T \lesssim 420$ GeV on the $M_D - M_T$ plane with fixed $m = 200$ GeV, in Fig. 3.7a.[15] We also observe that the result for $\Omega_\chi h^2$ is not very sensitive to the triplet mass, M_T. Even vanishing M_T-values are in accordance with the observed $\Omega_\chi h^2$, with mass values m_χ laying nearby the EW scale. (If M_D is in the region $m_W < M_D < m_Z$, and if we neglect three body decays, then the cross section becomes about half the one for $M_D > m_Z$. This means that Ωh^2 is doubled and therefore larger M_T (about twice as large) masses may be consistent with the observed Ωh^2 values in eq. (3.69).

We also consider the effect on $\Omega_\chi h^2$ from varying m and M_D, with $M_D = M_T$, in Fig. 3.7b. Obviously, the lower the m is the lower the M_D should be. For $m_\chi \simeq 91$ GeV the correct density is obtained for $m \simeq 140$ GeV. As we move to heavier values *i.e.* $m \approx 300$ GeV, M_D (which is equal to m_χ), is required to be heavier, but not much heavier, than M_Z. However, as we shall discuss in Section 3.7, those heavy values of m are not accepted by the vacuum stability constraint without modifying the model.

[14] **Note added**: Although the Planck collaboration has updated the results [29] [see eq. (1.103)], the observed DM relic abundance remains almost unchanged.

[15] We have not considered the case $M_D < M_Z$ as this would require further three body decay analysis which is beyond the scope of this analysis.

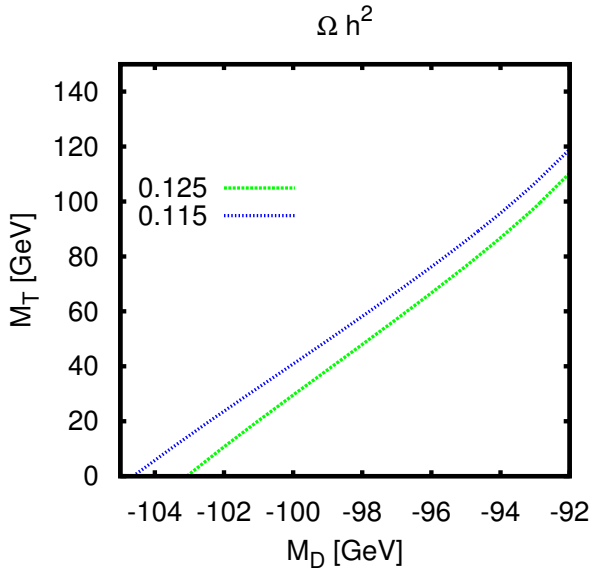

Figure 3.8: *Same as Fig. 3.7a but for negative values of M_D.*

Consistent $\Omega_\chi h^2$ with observation is also achieved for negative values of M_D in the same region as for positive M_D as it is shown in Fig. 3.8. (This is the small area for negative M_D shown in Fig. 3.3 where χ_1^0 is Doublet). The M_T values where this happens are limited in the mass region smaller than about 120 GeV. The EW S parameter in this region is slightly moved upwards but is still consistent with eq. (3.65a). However, as we shall see below, the $M_D < 0$ region suffers from huge suppression relative to SM in the $h \to \gamma\gamma$ decay rate.

One loop corrections to the annihilation cross section contribute only to the b_V-parameter *i.e.* they are p-wave suppressed, if $m_\chi \lesssim (m_Z + m_h)/2$. Our estimate, using the crude formula of eq. (3.76) below, shows that one loop induced b_V-terms are, numerically, about 10 times smaller than the tree level ones. However, if the above limit is not hold, then (s-wave) a-terms are coming into the final $\sigma_{Ann}v$. These terms could be of the same order as for the tree level b-terms and, in principle, for a precise $\Omega_\chi h^2$ prediction, they have to be included in the calculation.

We therefore conclude that, DM particle mass around the EW scale is possible and this requires large couplings of the heavy fermions to the Higgs boson *i.e.* large $m = Yv$ with $Y \approx 1$, and secondarily, relatively low values of triplet mass *i.e.*, $M_T \simeq M_D$. This scenario can be hinted or completely excluded at the LHC because the couplings of the heavy new fermions (both neutral and charged) to the Higgs and gauge bosons are, in general, not suppressed in the symmetry limit [see discussion in Section 3.8].

3.5 Direct DM Detection

Following the notation of Drees and Nojiri in ref. [206], the Higgs boson mediated part of the effective Lagrangian for light quark (u, d, s) - WIMP (*i.e.* the neutral fermion χ_1^0)

interaction is given by

$$\mathcal{L}_{\rm scalar} = f_q^{(h)}\, \bar{\chi}_1^0 \chi_1^0\, \bar{q} q \ . \tag{3.70}$$

Note that in this model there are no tensor contributions (at 1-loop level) since χ_1^0 does not interact directly with coloured particles (as opposed to supersymmetric neutralino for example). The next step is to form the nucleonic matrix elements for the $\bar{q}q$ operator in eq. (3.70) and we write

$$\langle n|m_q \bar{q} q|n\rangle = m_n f_{Tq}^{(n)} \ , \tag{3.71}$$

where $m_n = 0.94$ GeV, is the nucleon mass. The form factors $f_{Tq}^{(n)}$ are obtained within chiral perturbation theory and the experimental measurements of pion-nucleon interaction term, and they are subject to significant uncertainties. $f_{Tq}^{(n)}$ for $q = u, d$ [207] are generically small by, say, a factor of $O(10)$ compared to $f_{Ts} = 0.14$ obtained from ref. [208] value which we adopt into our numerical findings here. However, bear in mind that f_{Ts} is subject to large theoretical errors [52, 207]. For instance, the average value quoted from lattice calculations [209] is 0.043 ± 0.011, which is smaller by a factor of three from the one obtained from chiral perturbation theory. This will result in, at least, a factor of $\mathcal{O}(10)$ reduction in the WIMP-nucleon cross section results, presented in Fig. 3.9, below.

The Higgs boson couples to quarks and then to gluons through the one-loop triangle diagram. Subsequently, the gluons (G) couple to the heavy quark current through the heavy quarks ($Q = c, b, t$) in loop. The analogous ($q \to Q$) matrix element in eq. (3.70) for $m_Q \bar{Q} Q$ can be replaced by the trace anomaly operator $-(\alpha_s/12\pi) G \cdot G$ to obtain

$$\langle n|m_Q \bar{Q} Q|n\rangle = \frac{2}{27} m_n \left[1 - \sum_{q=u,d,s} f_{Tq}^n\right] \equiv \frac{2}{27} m_n f_{TG} \ . \tag{3.72}$$

We are ready now to write down the effective couplings of χ_1^0 to nucleons ($n = p, n$):

$$\frac{f_n}{m_n} = \sum_q \frac{f_q^{(h)}}{m_q} f_{Tq}^{(n)} \ + \ \frac{2}{27} \sum_Q \frac{f_Q^{(h)}}{m_Q} f_{TG} \ . \tag{3.73}$$

Note that the bigger the f_{Ts} is, the bigger the f_n becomes. Also note that $f_q^{(h)} \propto m_q$. Furthermore, for $f_{Ts} \simeq 0.14$ the second term in eq. (3.73), which is formally a two loop contribution to f_n, is about a factor of two smaller than the first one. Under the above assumption for the f_{Ts} dominance we obtain $f_p = f_n$. In this case, the Spin Independent (SI) elastic scattering cross section at zero momentum transfer, of the WIMP χ_1^0 scattering off a given target nucleus with mass m_N in terms of the coupling f_p is

$$\sigma_{0(\rm scalar)} = \frac{4}{\pi} \frac{m_{\chi_1^0}^2 m_N^4}{(m_{\chi_1^0} + m_N)^2} \left(\frac{f_p}{m_n}\right)^2 \ . \tag{3.74}$$

The perturbative dynamics of the model is contained in the factor f_p and therefore, from eq. (3.73), in $f_q^{(h)}$ and $f_Q^{(h)}$. In this particular model the form factor $f_q^{(h)}$ reads,

$$\frac{f_q^{(h)}}{m_q} \ = \ \frac{g\, [\Re e(Y^{h\chi_1^0\chi_1^0}) - \delta Y^{h\chi_1^0\chi_1^0}]}{4\, m_W\, m_h^2} \ . \tag{3.75}$$

The Higgs coupling to lightest neutral fermions is given in eq. (3.19). In particular, under the custodial symmetry consideration we adopt here, it is obvious from eq. (3.46),

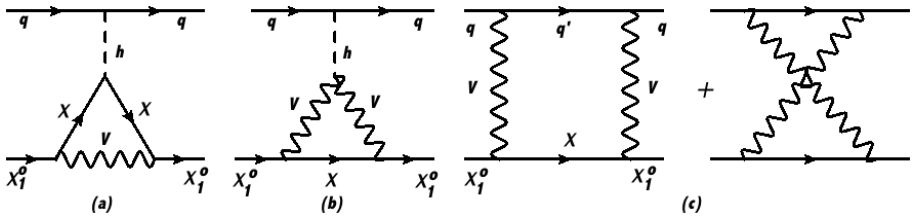

Figure 3.9: *Feynman diagrams (in unitary gauge) related to spin independent (SI) elastic cross section $\chi_1^0 + q \to \chi_1^0 + q$ where $q = u, d, s$ – light quarks. Particle V represents W or Z and χ represents $\chi^{\pm}_{i=1..2}$ or $\chi^0_{i=1..3}$, respectively. One loop self energy corrections are absent in the particular scenario we have chosen.*

that $Y^{h\chi_1^0\chi_1^0} = 0$, at tree level. Generic one-loop corrections will be proportional to, $g^2Y/4\pi \approx 0.03$, which can easily fall in the experimental exclusion region from current direct experimental DM searches for large $Y \sim 1$ coupling (see for instance eq.(3) in ref. [159]). We therefore need to calculate the one loop corrections, $\delta Y^{h\chi_1^0\chi_1^0} \equiv \delta Y$ to the $h\chi_1^0\chi_1^0$-vertex.

There is a fairly quick way to get an order of magnitude reliable calculation of δY through the Low Energy Higgs Theorem (LEHT) [150, 210–212]. Application of LEHT in the region of our interest *i.e.* , $m_{\chi_1^0} \approx m_W \approx m_h \ll m_{\chi_i^\pm}$ or $M_D \approx M_T \approx m_W \ll m$, and considering only Goldstone boson contributions to χ_1^0 one-loop self energy diagrams, results in

$$\delta Y \;=\; \frac{\partial}{\partial v}\delta M_D(v) \;\approx\; \frac{Y^3}{4\pi^2}\,\frac{M_D\, m}{M_D^2 + 2m^2}\,, \quad M_D \approx M_T \approx m_W \approx m_h \ll m\,. \tag{3.76}$$

Let's inspect eq. (3.76). First, the middle term explains trivially why the Higgs coupling is zero at tree level: the lightest eigenvalue of the neutral mass matrix is M_D which is independent on any vacuum expectation value. Then because at one loop, the χ_1^0 self-energies involve only the heavy fermion masses (both charged and neutral) which depend on the v.e.v through $m = Yv$ or through m_W, m_Z in the propagators of $\chi_i^\pm, \chi^0_{i=2,3}$ and W, Z respectively, the one loop correction δY *does not* in general vanish. Second, the third term of the equality eq. (3.76) shows that the effect increases by the third power of the Yukawa coupling Y [recall eq. (3.28)] and vanishes when $M_D \to 0$ [the $U(1)_X$ symmetry limit]. As for the numerical approximation, eq. (3.76) is always less than 20% of the exact calculation (see below) even though we have completely neglected the non-Goldstone diagrams that are proportional to gauge couplings. It is however a crude approximation which is only relevant when the new heavy fermions are far heavier than the Z, W, h-bosons as well as from the lightest neutral fermion.

In Appendix A, we calculate the exact one-loop amplitude for the vertex $h - \chi_1^0 - \chi_1^0$ with physical external χ_1^0 particles at a zero Higgs-boson momentum transfer. A similar calculation has been carried out in ref. [102] for the MSSM and in ref. [103] for minimal DM models. However, due to peculiarities of this model that have been stressed out in the introduction with respect to the aforementioned models, a general calculation is needed. The one-loop corrected vertex amplitude arises from (a) and (b) diagrams[16] depicted in Fig. 3.9 involving vector bosons (W or Z) and new charged ($\chi^\pm_{i=1,2}$) or neutral ($\chi^0_{i=1..3}$)

[16]Note that, Eq. (3.46) implies that there are no self energy contributions to - $i\,\delta Y$ - at one-loop.

fermions, as

$$i\,\delta Y = \sum_{j=(a),(b)} \left(i\,\delta Y_j^{\chi^\pm} + i\,\delta Y_j^{\chi^0}\right) . \tag{3.77}$$

Detailed forms, not resorting to CP-conservation, for δY's are given in Appendix A. We have proven both analytically and numerically that when the external particles χ_1^0 are on-shell, infinities cancel in the sum of the two vertex diagrams in Fig. 3.9a,b without the need of any renormalization prescription, and the resulting amplitude - $i\,\delta Y$ - is finite and renormalization scale invariant.

We have also carried out the one-loop calculation of the box diagrams in Fig. 3.9c. The effective operators for box diagrams consist of scalar, $f_q^{(\rm box)}$ [like the f_q in eq. (3.70)] and twist operators, $g_q^{(1)}$ and $g_q^{(2)}$ written explicitly for example in ref. [206]. In the parameter space of our interest where $M_D \ll m$, the $f_q^{(\rm box)}$ contributions to $f_q^{(h)}$ in eq. (3.73), are in general two orders of magnitude smaller than the vertex ones arising from Fig. 3.9(a,b), and they are only important in the case where the latter cancel out among each other. Moreover, it has recently been shown in refs. [213–215] that, the full two-loop[17] gluonic contributions are relevant for a correct order of magnitude estimate of the cross section in the heavy WIMP mass limit, especially when adopting the "lattice" value for f_{T_s}. We are not aware, however, of any study dealing with those corrections and WIMP mass around the electroweak scale which is the case of our interest. Such a calculation is quite involved and is beyond the scope of the present work.

In Fig. 3.10 we present our numerical results for the SI nucleon-WIMP cross section. The current LUX [162] (XENON100 [161]) experimental bounds for a 100 GeV WIMP mass is [18] $\sigma_0^{(SI)} \lesssim 1(2) \times 10^{-45}$ cm^2 at 90% C.L.

From the left panel of Fig. 3.10 we observe that in the region where $M_T \ll M_D \ll m$ the cross section is by one to two orders of magnitude smaller than the current experimental bound. More specifically, in the region where we obtain the right relic density [see Fig. 3.7a] the prediction for the $\sigma_0^{(SI)}$ is about to be observed only for large values of M_T ($M_T \approx$ 500 GeV), while it is by an order of magnitude smaller for low values of M_T ($M_T \lesssim$ 100 GeV). There is a region, around $M_T \approx 25$ GeV, where box corrections, that arise from the diagram in Fig. 3.9c, on scalar and twist-2 operators become important because the vertex corrections mutually cancel out. However, in this region the cross section becomes two to four orders of magnitude smaller than the current experimental sensitivity. We also remark that $\sigma_0^{(SI)}$ reaches a maximum value, indicated by the closed contour line in the upper left corner of Fig. 3.10a, and then starts decreasing for larger M_T and M_D values, a situation that looks like following the Appelquist-Carazzone decoupling theorem [217]. However, even at very large masses, M_D and M_T, not shown in Fig. 3.10, there is a constant piece of δY, and hence of $\sigma_0^{(SI)}$, that does not decouple. This can be traced respectively in the second and the first terms of integrals I_4^V, and I_5^V of eq. (A.7), in the limit $M_D = M_T \to \infty$. This non-decoupling can also been seen in the heavy particle, effective field theory analysis of ref. [213] and also in refs. [78, 103]. We have also checked numerically that $\sigma_0^{(SI)}$ vanishes at $M_D \to 0$ as expected from eq. (3.76) and from the $U(1)_X$ global symmetry.[19]

[17] The next to leading order in α_S calculation has been carried out for the Wino DM scenario in ref. [216].

[18] **Note added**: The current bound ([100] and [105]) for a DM mass at 100 GeV is $\sigma_0^{(SI)} \lesssim 10^{-46}$ cm^2 (see Fig. 1.3). From Fig 3.10, it is apparent that $M_D \gtrsim M_T$ is favoured, for $m \approx 200$ GeV.

[19] Because only $\bar{D}_{1,2}$ are charged under $U(1)_X$ (not the Higgs boson), and χ_1^0 is a linear combination of only $\bar{D}$'s.

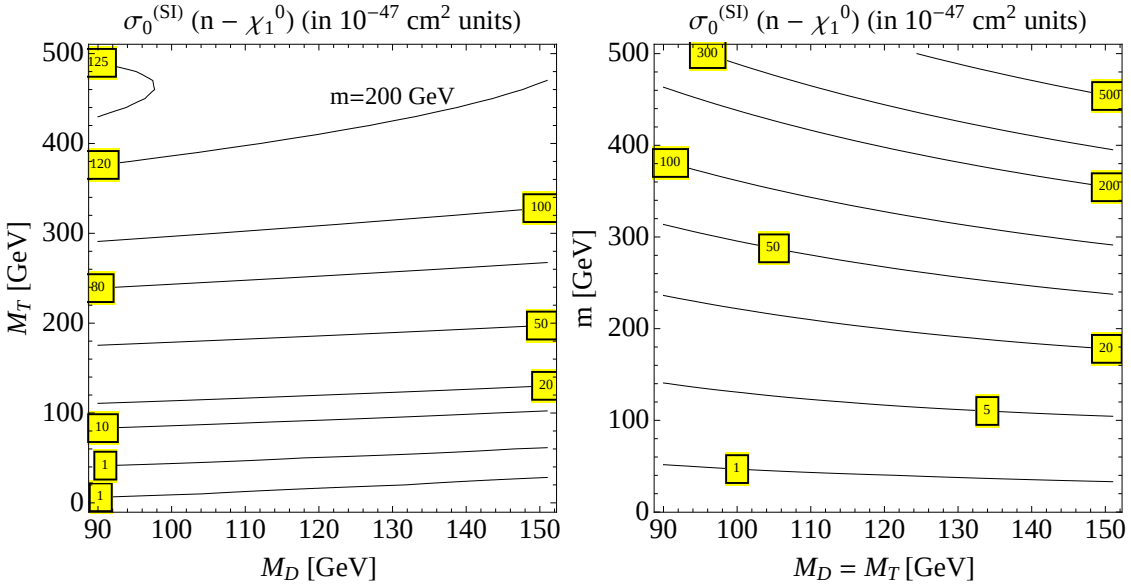

Figure 3.10: *Results (in boxed labels) for the Spin-Independent (SI) scattering cross section for the nucleon - WIMP (n-χ_1^0) in units of* 10^{-47} cm^2 *on a* M_D *vs.* M_T *plane for fixed parameter* $m = Yv = 200$ GeV *(left) and on* M_D *vs.* m *plane for fixed* $M_T = M_D$ GeV *(right).*

In Fig. 3.10b, we also plot predictions for the Doublet-Triplet Fermionic model on SI cross section $\sigma_0^{(SI)}$ on M_D vs. m plane for $M_T = M_D$. As we recall from eq. (3.76), the cross section increases with m (or Y) as $m^2 \propto Y^2$. It becomes within current experimental sensitivity reach for $m \gtrsim 400$ GeV while for low $m \approx 100$ GeV, $\sigma_0^{(SI)}$ is about 100 times smaller. Besides, for heavy M_D and m (upper right corner), $\sigma_0^{(SI)}$ becomes excluded by current searches although vacuum stability bounds hit first. If we compare with the corresponding plot for the relic density in Fig. 3.7b, we see that the observed $\Omega_\chi h^2$ is allowed by current experimental searches on $\sigma_0^{(SI)}$ but it will certainly be under scrutiny in the forthcoming experiments [163].

Finally, for negative values of M_D consistent with the observed density depicted in Fig. 3.8, it turns out that $\sigma_0^{(SI)}$ is by a factor of about ~ 10 bigger than the corresponding parameter space for $M_D > 0$ given in Fig. 3.10a. In fact, the region of 1-loop cancellations happened for $M_T \approx 20$ GeV, do not take place for $M_D < 0$. However, within errors discussed at the beginning of this section, this is still consistent with current experimental bounds.

3.6 Higgs boson decays to two photons

In the Doublet-Triplet Fermionic model there are two pairs of electromagnetically charged fermions and antifermions, namely, $\chi_1^\pm, \chi_2^\pm$. They have electromagnetic interactions with charge $Q = \pm 1$ and interactions with the Higgs boson, $Y^{h\chi^-\chi^+}$, given in general by eqs. (3.17) and (3.18), or in particular, in the symmetry limit, by eq. (3.46). These latter interactions are of similar size as of the top-quark-antiquark pairs with the Higgs boson *i.e.* $Y \sim 1$. Hence, we expect a substantial modification of the decay rate, $\Gamma(h \to \gamma\gamma)$

relative to the SM one[20] $\Gamma(h \to \gamma\gamma)_{SM}$, through the famous triangle graph [150],

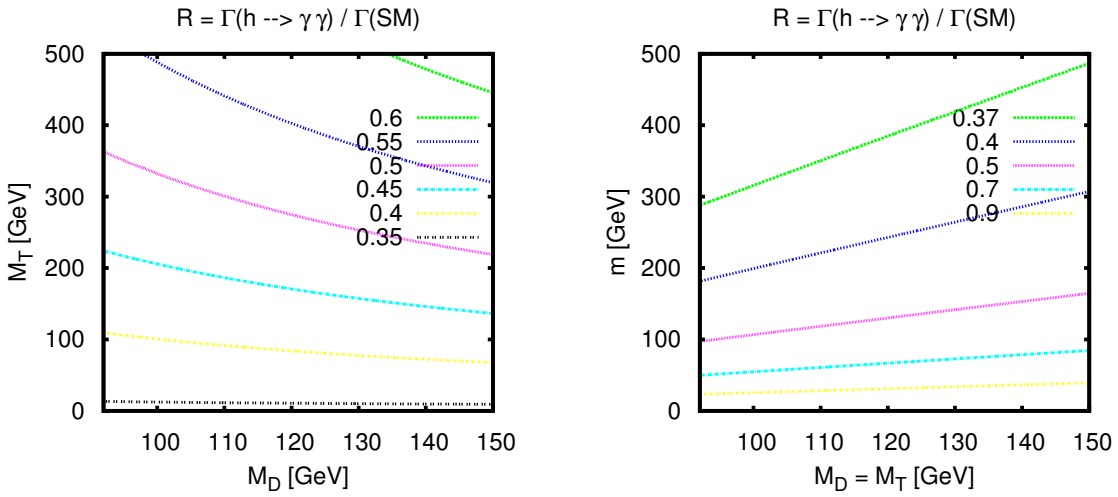

(a) (b)

Figure 3.11: *Contour lines for the ratio, $R = \Gamma(h \to \gamma\gamma)/\Gamma(h \to \gamma\gamma)_{\rm SM}$, for the decay rate of Higgs boson decays into two photons over the SM prediction on (a) M_D vs. M_T plane with $m = 200$ GeV and (b) on M_D vs. m plane with $M_T = M_D$.*

involving W-gauge bosons, the top-quark (t) and the new fermions $\chi_i^\pm$. Under the assumption of real M_D, $Y^{h\chi_i^-\chi_i^+}$ is also real, and we obtain:

$$R \equiv \frac{\Gamma(h \to \gamma\gamma)}{\Gamma(h \to \gamma\gamma)_{(\rm SM)}} = \left| 1 + \frac{1}{A_{\rm SM}} \sum_{i=\chi_1^\pm,\chi_2^\pm} \sqrt{2}\, \frac{Y^{h\chi_i^-\chi_i^+}\, v}{m_{\chi_i^+}}\, A_{1/2}(\tau_i) \right|^2 , \tag{3.78}$$

where $A_{\rm SM} \simeq -6.5$ for $m_h = 125$ GeV, is the SM result dominated by the W-loop [218], with $\tau_i = m_h^2/4m_i^2$ and $A_{1/2}$ is the well known function given for example in ref. [151].[21] The $\chi_i^\pm$-fermion contribution ($Q = 1, N_c = 1$), is also positive because the ratio, $\frac{Y^{h\chi_i^-\chi_i^+}}{m_{\chi_i^+}}$, is always positive when $m_{\chi_1^0} = M_D$, as can be seen by inspecting eqs. (3.46), (3.50) and (3.33). After using the simplified (by symmetry) eq. (3.46) with $a \approx -\sqrt{2}$, we approximately obtain

$$\sum_i \frac{\sqrt{2}\, m}{m_{\chi_i^+}}\, A_{1/2}(\tau_{\chi_i^+}) \approx +\frac{8}{3} , \tag{3.79}$$

which means that $\Gamma(h \to \gamma\gamma)$ is smaller than the SM expectation. But how much smaller? In Fig. 3.11 we plot contours of the ratio $R \equiv \Gamma(h \to \gamma\gamma)/\Gamma(h \to \gamma\gamma)_{(\rm SM)}$ on (M_D vs. M_T)-plane for $m = 200$ GeV (Fig 3.11a) and M_D vs. m-plane for ($M_T = M_D$) (Fig 3.11b).

[20] The Higgs boson production cross section is the same with the SM because the new fermions are uncoloured.

[21] The Higgs-fermion vertex is parametrized here as $\mathcal{L} \supset -Y\, h\, \bar{f}\, f + \text{h.c.}$ and therefore for the top-quark Yukawa we obtain $Y_i \to Y_t/\sqrt{2}$ from eq. (3.8) while for the new charged fermions $Y_i \to Y^{h\chi_i^-\chi_i^+}$ from eqs. (3.17) and (3.18).

Our numerical results plotted in Fig. 3.11 are exact at one-loop. We observe that the new charged fermions render the ratio less than unity

$$R \lesssim 1 \,, \tag{3.80}$$

everywhere in the parameter space considered. Let's look at this in a more detail. The contribution of fermions $\chi_i^\pm$ in eq. (3.78), depends on the quantity[22]

$$\sim \frac{2\,m^2}{2\,m^2 + M_D\,M_T} \,, \tag{3.81}$$

which is always positive for $M_D, M_T > 0$ *i.e.* it adds to the top-quark contribution and subtracts from the large and negative W-boson one resulting in a suppressed R-ratio. If instead we choose $M_D < 0$, then for $|M_D M_T| > \sqrt{2}|m|$, one can obtain $R \gtrsim 1$, a situation which is explored in ref. [203]. As can be seen from Fig. 3.3 however, in this case the DM candidate particle (χ_1^0) is not a pure doublet. It is instead a mixed state. (In fact the states $|1\rangle$ and $|2\rangle$ are interchanged in eq. (3.34)). As a consequence, there is a non-zero (and generically large) $h\chi_1^0\chi_1^0$-coupling already present at tree level, and, bear in mind fine tuning, it is excluded by direct DM search bounds.

By comparing areas with the observed relic density in Figs.3.7(a,b) we see that, the results for $0.35 \lesssim R \lesssim 0.5$ shown in Figs. 3.11(a,b) are within 1σ-error compatible with current central values of CMS measurements [220] (0.78 ± 0.27) but are highly "disfavoured" by those from ATLAS [24] ones, $1.65 \pm 0.24(stat)^{+0.25}_{-0.18}(syst)$. The forthcoming second LHC run will be decidable in favour or against this outcomes here.[23]

Fig. 3.11(a) or eq. (3.81), shows also that when M_T becomes heavy the ratio R approaches the current CMS central value. This happens because one of the two charged fermion eigenvalues becomes very heavy, $m_{\chi_2^+} \approx M_T$, and therefore it is decoupled from the ratio. As we discussed in Section 3.4, large $M_T \sim 1$ TeV values, may be consistent with the observed $\Omega_\chi h^2$ for $m_W < M_D < m_Z$. We have found that even in this case, R is always smaller than 0.65.

If we assume that $M_D < 0$ and χ_1^0 pure doublet as shown in Fig. 3.3, then it is always $R < 1$. In fact, using the input values from Fig. 3.8 for the correct relic density, the suppression of R is even higher, $0.25 \lesssim R \lesssim 0.35$. Alternatively, if we assume that M_D is a general complex parameter, then the coupling, $Y^{h\chi_1^-\chi_1^+}$, is complex too. In this case one has to add the CP-odd Higgs contribution into eq. (3.78) which is always positive definite. For large phases relatively large M_T the ratio R may be greater than one, however, again the direct detection bounds are violated by a factor of more than 10-1000.

Of course, if we increase M_D, the parameter space may be compatible with the observed relic density seen in the right side of "heavy" M_D-branch in Fig. 3.6. However, following our motivation for "*only* EW scale DM" we do not discuss this region further which is anyhow very well known from MSSM studies.

We therefore conclude that in the doublet triplet fermionic model *thermal DM relic abundance for low DM particle mass $m_{\chi_1^0} \approx M_Z$, consistent with observation [164] and with direct DM searches [161, 162] leads to a substantial suppression (45-75%) for the rate $\Gamma(h \to \gamma\gamma)$ relative to the SM expectation.*

[22] This quantity is obtained also by using the low energy Higgs theorem as in ref. [219] for the singlet-doublet DM-case.

[23] **Note added**: The latest results from ATLAS and CMS measurements, show that the $h \to \gamma\gamma$ branching ratio is close to the SM prediction with [221] $R(h \to \gamma\gamma) = 1.14^{+0.19}_{-0.18}$ (at 1σ).

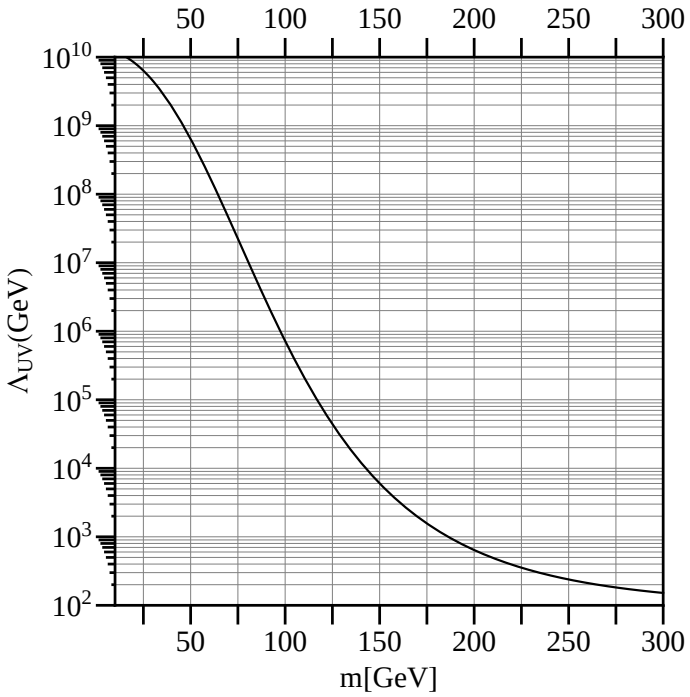

Figure 3.12: *The vacuum stability plot:* Λ_{UV} *against* $m = Yv$.

We have also calculated the ratio R for the Higgs boson decay into $Z\gamma$. The results are similar to the case of $R(h \to \gamma\gamma)$. In particular, in the parameter space explored in Fig. 3.11(a), we observe exactly the same shape of lines with a ratio slightly shifted upwards in the region, $0.4 \lesssim R(h \to Z\gamma) \lesssim 0.7$. This suppression is due to the same reason discussed in the paragraph below eq. (3.81).

3.7 Vacuum Stability

The stability of the Standard Model vacuum is an important issue, so we need to find an energy scale (Λ_{UV}) where new physics is needed, in order to make the vacuum stable or metastable (unstable with lifetime larger than the age of the universe). To make an estimate about the Λ_{UV} of the theory, one needs to calculate the tunnelling rate between the false and the true vacuum and impose that the SM vacuum has survived until today[24]. Following ref. [223], we can see that the bound for the Higgs self coupling, λ, becomes[25]:

$$\lambda(\Lambda_{UV}) = \frac{4\pi^2}{3\ \ln\left(\dfrac{H_0}{\Lambda_{UV}}\right)}, \tag{3.82}$$

where Λ_{UV} is the cut-off scale and H_0 is the Hubble constant $H_0 = 1.5 \times 10^{-42}$ GeV. In order to impose the contstraint (3.82), we also need to find the running parameter λ by solving the renormalization group equations. The one-loop beta functions for the model at hand are given in ref. [202, 203, 224][26], and we solve this set of differential equations

[24]The probability of the tunnelling has been calculated at tree level in ref. [222].
[25]This bound can also be found in ref. [203].
[26]We need to make the substitutions $\tilde{g}_{2d} \to -Y_1$ and $\tilde{g}_{2u} \to -Y_2$ because of different conventions with ref. [202].

using as initial input parameters:

$$\alpha_3(M_Z) = 0.1184\,, \quad \alpha_2(M_Z) = 0.0337\,, \quad \alpha_1(M_Z) = 0.0168\,, \tag{3.83}$$

$$\lambda(M_Z) = 0.1303\,, \quad y_t(M_Z) = 0.9948\,, \quad M_Z = 91.1876\ \text{GeV}. \tag{3.84}$$

The result for the cut-off scale as a function of $m = Yv$ is given in Fig. 3.12. As we can see, $\Lambda_{UV} \approx 600$ GeV for $m \approx 200$ GeV which is quite small while $\Lambda_{UV} \approx 20$ TeV for $m \approx 130$ GeV. The result for Λ_{UV} in Fig. 3.12 is only approximate. Threshold effects, from the physical masses of the doublet, triplet and even the top-quark, together with comparable two-loop corrections to β-functions, which can be found for example in refs. [202, 224], are missing in Fig. 3.12. These effects may change the outcome for Λ_{UV} by a factor of two or so but they will not change the conclusion, that extra new physics is required already nearby the TeV-scale for $m \approx 200$ GeV. The form of new physics will probably be in terms of new scalar fields since extra new fermions will make Λ_{UV} even smaller. These scalars may be well within reach at the second run of the LHC [203] but it is our assumption here that they do not intervene with the DM sector.

As far as the (1-loop) perturbativity of the Yukawa couplings $Y \sim 1.2$ (for $m = 200$) and Y_t, is concerned, these exceed the value 4π at around the respective scales, 10^9 and 10^{10} GeV. Given the modifications of the model that must be performed at $\Lambda_{UV} \sim$ TeV scale, the perturbativity bound is of secondary importance here.

3.8 Heavy fermion production and decays at LHC

The unknown new fermions that have been introduced into this model to accompany the DM mechanism can be searched for at the LHC in a similar fashion as for charginos and neutralinos of the MSSM. Multilepton final states associated with missing energy may arise in three different ways from the decays of new fermion pairs: $\chi_i^+\chi_j^-$, $\chi_i^\pm\chi_j^0$, and $\chi_i^0\chi_j^0$.

3.8.1 Production

A recent study at LHC [225, 226] has presented upper limits in the signal production cross sections for charginos and neutralinos, in the process

$$p \ + \ p \ \to \ W^* \ \to \ \chi_1^+ \ + \ \chi_2^0\,, \tag{3.85}$$

which is mediated by the W-gauge boson. One can use Fig. 9b from ref. [225] to set limits to the cross section and therefore to constrain the parameter space. This figure fits perfectly into our study since it assumes a) 100% branching ratio for the χ_1^+ and χ_2^0 decays as it is the case here [see Section 3.8.2 below] b) degenerate masses for χ_1^+ and χ_2^0 as it is exactly the case here as shown in eq. (3.42). The production cross section has been calculated in ref. [227] also including next to leading order QCD corrections. The parton-level, tree level, result is

$$\frac{d\hat{\sigma}}{d\hat{t}}(u + d^\dagger \to W^* \to \chi_i^+ + \chi_j^0) \ = \ \frac{1}{16\pi\hat{s}^2}\left(\frac{1}{3\cdot 4}\sum_{\text{spins}}|\mathcal{M}|^2\right)\,, \tag{3.86}$$

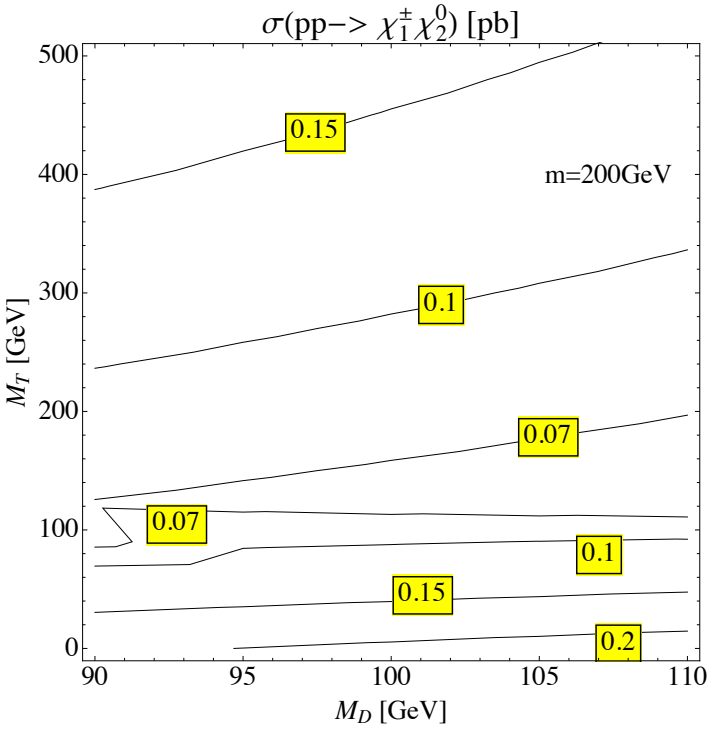

Figure 3.13: *Contours of the production cross section for the new fermions, $\sigma(pp \to \chi_1^\pm \chi_2^0)$ [in pb], on M_D vs. M_T plane, at LHC with $\sqrt{s} = 8$ TeV.*

where the factors 1/3 and 1/4 arise from colour and spin average of initial states, $\hat{s}, \hat{t}, \hat{u}$ are the Mandelstam variables at the parton level, and

$$\sum_{\text{spins}} |\mathcal{M}|^2 = |c_1|^2(\hat{u}-m^2_{\chi_i^+})(\hat{u}-m^2_{\chi_j^0})+|c_2|^2(\hat{t}-m^2_{\chi_i^+})(\hat{t}-m^2_{\chi_j^0})+2\Re e[c_1 c_2^*]m_{\chi_i^+}m_{\chi_j^0}\,\hat{s}\ , \quad (3.87)$$

with the coefficients c_i being

$$c_1 = -\frac{\sqrt{2}\,g^2}{\hat{s}-m_W^2}\,O_{ji}^{L\,*}\ , \qquad c_2 = -\frac{\sqrt{2}\,g^2}{\hat{s}-m_W^2}\,O_{ji}^{R\,*}\ .$$

We let the indices $i = 1, 2$ and $j = 1, 2, 3$ free as there is a situation of a complete mass degeneracy between the heavy neutral and charged fermions when $M_D = M_T$. Our result in eqs. (3.86) and (3.87) are in agreement with refs. [28, 227].

By convoluting eq. (3.86) with the proton's pdfs and integrating over phase space we obtain in Fig. 3.13, the production cross section for $\sigma(pp \to \chi_1^\pm \chi_2^0)$ [in pb]. In the region with correct DM relic density, we obtain typical values varying in the interval $(0.07 - 0.2)$ pb for $\sqrt{s} = 8$ TeV. This is about 1400-4000 events at LHC before any experimental cuts assuming 20 fb^{-1} of accumulated luminosity. This is within current sensitivity search and analysis has been performed by ATLAS [225] and CMS [226] for simplified supersymmetric models. Looking for example in Fig. 9b in ATLAS [225], for the same parameter space as in our Fig. 3.13, the observed upper limit on the signal cross section varies in the interval (0.14-1.2) pb. In the region where $M_D = M_T$, all heavy fermions are mass degenerate. In this case the total cross section is the sum of all possible production modes $\chi_{1,2}^\pm \chi_{2,3}^0$, and the total cross section is about 0.15 pb which is on the spot of current LHC sensitivity (0.14 pb) [225].

3.8.2 Decays

Just by looking at a typical spectrum of the model in Fig. 3.1, we see that the heavy fermions can decay on-shell to two final states with a gauge boson and the lightest neutral stable particle. Therefore, the lightest charged and the next to lightest neutral fermions decay like

$$\chi_1^\pm \;\to\; \chi_1^0 \;+\; W^\pm \,, \tag{3.88a}$$

$$\chi_2^0 \;\to\; \chi_1^0 \;+\; Z \,. \tag{3.88b}$$

In our case where χ_1^0 is a "well tempered doublet" there are no-off diagonal couplings to the Higgs boson, like for example $h\chi_1^0\chi_2^0$. Therefore, particles $\chi_1^\pm$ and χ_2^0 decay purely to final states following (3.88a) and (3.88b) with 100% branching fractions. The signature at hadron colliders is the well known from SUSY searches, trileptons plus missing energy.

Analytically we find the decay widths [28, 228]:

$$\begin{aligned}
\Gamma(\chi_i^+ \to \chi_j^0 + W^+) &= \frac{g^2\, m_{\chi_i^+}}{32\pi}\, \lambda^{1/2}(1, r_W, r_j) \left\{ (|O_{ji}^L|^2 + |O_{ji}^R|^2) \left[1 + r_j - 2r_W + \frac{(1-r_j)^2}{r_W} \right] \right. \\
&\qquad \left. - 12\, \sqrt{r_j}\, \Re e(O_{ji}^{L\,*} O_{ji}^R) \right\} , \\
\Gamma(\chi_i^0 \to \chi_j^0 + Z) &= \frac{g^2\, m_{\chi_i^0}}{16\pi c_W^2}\, \lambda^{1/2}(1, r_Z, r_j) \left\{ |O''^L_{ij}|^2 \left[1 + r_j^0 - 2r_Z + \frac{(1-r_j^0)^2}{r_Z} \right] \right. \\
&\qquad \left. + 6\, \sqrt{r_j^0}\, \Re e[(O''^L_{ij})^2] \right\} ,
\end{aligned} \tag{3.89}$$

where

$$r_W \equiv m_W^2/m_{\chi_i^+}^2 \,, \quad r_Z \equiv m_Z^2/m_{\chi_i^0}^2 \,, \quad r_j \equiv m_{\chi_j^0}^2/m_{\chi_i^+}^2 \,, \quad r_j^0 \equiv m_{\chi_j^0}^2/m_{\chi_i^0}^2 \tag{3.90a}$$

$$\lambda(x,y,z) \equiv x^2 + y^2 + z^2 - 2xy - 2xz - 2yz \,. \tag{3.90b}$$

Numerical results for the decay widths for the processes (3.88a) and (3.88b) in the area of interest are depicted in Fig. 3.14(a) and (b), respectively.

Both decay widths behave similarly. In the area $M_D \approx M_T \approx 100$ GeV we observe maximum values $\Gamma \approx 3$ GeV. As M_T increases or decreases, the widths get smaller than 1 GeV. This is easily understood if we look back at the mass difference $|m_{\chi_2^0}| - |m_{\chi_1^0}|$ in Fig. 3.2(a) and recall that for the parameter considered in Fig. 3.14, it is $m_{\chi_1^0} = M_D$ and $m_{\chi_2^0} = m_{\chi_1^\pm}$.

For heavier charged fermions, new decay channels include

$$\chi_2^+ \to \chi_1^+ + Z \,, \tag{3.91a}$$

$$\chi_2^+ \to \chi_1^+ + h \,, \tag{3.91b}$$

that are mostly kinematically allowed in the low $M_D \approx 100$ GeV but high $M_T \gtrsim 220$ GeV regime. For the heavier neutral particles, if kinematically allowed they would decay to W, Z-gauge bosons and/or the Higgs boson, through

$$\chi_3^0 \to \chi_1^\pm + W^\mp \,, \tag{3.92a}$$

$$\chi_3^0 \to \chi_2^0 + Z \,, \tag{3.92b}$$

$$\chi_3^0 \to \chi_2^0 + h \,. \tag{3.92c}$$

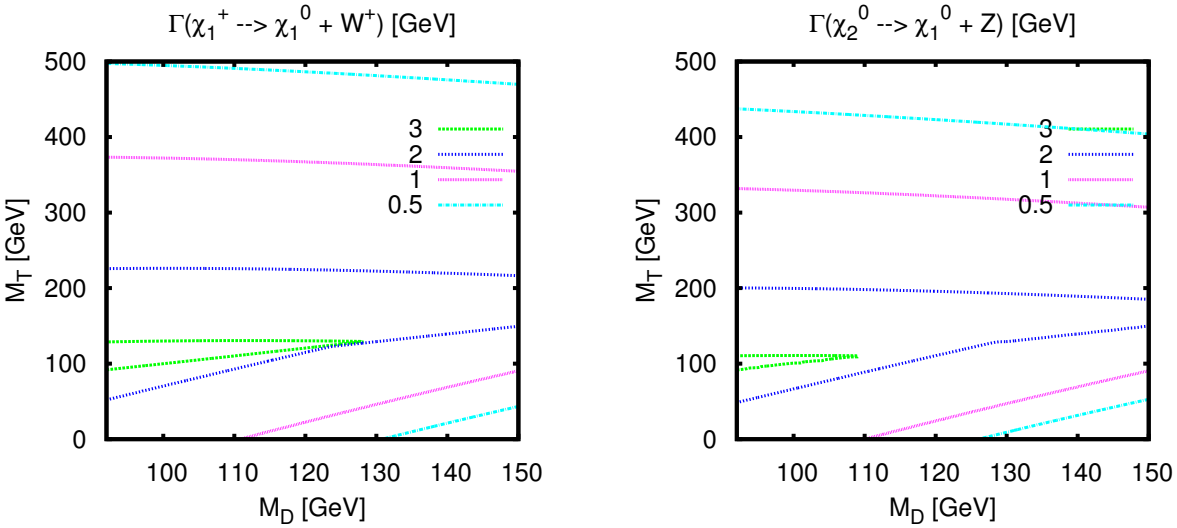

Figure 3.14: *Contour plots for the decay rates [in GeV] for the processes* $\chi_1^+ \to \chi_1^0 + W^+$ *(left) and* $\chi_2^0 \to \chi_1^0 + Z$ *(right). We assume* $m = 200$ GeV.

3.9 Conclusions

Our motivation for writing this paper was to import a simple DM sector in the SM with particles in the vicinity of the electroweak scale responsible for the observed DM relic abundance, preferably not relying on co-annihilations or resonant effects, and capable of escaping current detection from nucleon-recoil experiments. Meanwhile, we studied consequences of this model in EW observables and Higgs boson decays ($h \to \gamma\gamma, Z\gamma$) and other possible signatures at LHC.

This SM extension consists of two fermionic $SU(2)_L$-doublets with opposite hypercharges and a fermionic $SU(2)_L$-triplet with zero hypercharge. The new interaction Lagrangian is given in eq. (3.9), and contains both Yukawa trilinear terms together with explicit mass terms for the doublets and triplet fields. Under the assumption of a certain global $SU(2)_R$-symmetry, discussed in Section 3.2.3, that rotates H to $H^\dagger$ and $\bar{D}_1$ to $\bar{D}_2$, the two Yukawa couplings become equal with certain consequences that capture our interest throughout this work. After electroweak symmetry breaking this sector widens the SM with two charged Dirac fermions and three neutral Majorana fermions, the lightest (χ_1^0) of which plays the role of the DM particle. Under the symmetry assumption and for Yukawa couplings comparable to top-quark, the lightest neutral particle (χ_1^0) may have mass equal to the vector-like mass of the doublets, M_D, and its field composition contains only an equal amount of the two doublets [see Fig. 3.3]. As a result, the couplings of the Higgs and the Z-bosons to the lightest neutral fermion pair vanish at tree level.

Within this framework we observe in Fig. 3.7, that $\Omega_\chi h^2$, is in accordance with observation [eq. (3.69)] provided that the parameters of the model, M_D, M_T and m, lie naturally at the EW scale *i.e.* without the need for resonant or co-annihilation effects. Moreover, the χ_1^0-nucleon SI cross section (which appears at one-loop), at the time of publication of this analysis, was around 1-100 times smaller than the experimental sensitivity from LUX

and XENON as it is shown in Fig. 3.10. However, latest results are able to exclude the region of the parameter space where $M_D \lesssim M_T$ (for $m = 200$ GeV). In addition, we find that the oblique electroweak parameters S, T and U are all compatible with EW data fits as it is shown in Fig. 3.4, a result which is partly a consequence of the global symmetry exploited.

We also look for direct implications at the LHC. We find that the existence of the extra charged fermions reduces substantially the ratios of the Higgs decay to di-photon and to $Z\gamma$ w.r.t the SM. At the time of publication of this work, this was a certain prediction of this scenario. For very large Yukawa coupling, this reduction maybe of up to 65% relative to the SM expectation (which is excluded as we discuss below) as we obtain from Fig. 3.11. Furthermore, the production and decays of the new charged/neutral fermion states, is within current and forthcoming LHC reach. Decay rates for some of these states are shown in Fig. 3.14.

We should notice here that the minimality of the Higgs sector together with the Z_2-parity symmetry preserves the appearance of new flavour changing or CP-violating effects beyond those of the SM, for up to two-loop order (for a nice discussion of effects on EDMs from the charged fermions, see ref. [200]).

On top of collider/astrophysical constraints, we made an estimate of the consequences of the new states to vacuum stability of the model. The 1-loop result for the UV cut-off scale, above which the model needs some completion, is given in Fig. 3.12. We see that for the parameter space of interest, new physics, probably in the form of new, supersymmetric, scalars is needed already nearby the TeV or multi-TeV scale to cancel fermionic contributions in the quartic Higgs coupling. For example, this solution may take the form of an MSSM extension with $\bar{D}_{1,2}$ and T superfield (extensions with a triplet superfield have been explored in ref. [229]).

Note added: In summary, in this work we basically studied the synergy between $\Omega_\chi h^2, \sigma_0^{SI}$, and $R(h \to \gamma\gamma)$, in a simple fermionic DM model. The original findings of this analysis can be summarized in the following:

If $R(h \to \gamma\gamma)$ was found to be suppressed, then charged fermion states could be discovered at the second run of LHC compatible with $\Omega_\chi h^2$ with $m_\chi \approx m_Z$. If instead $R(h \to \gamma\gamma)$ was found to be enhanced, then the DM particle would be heavy, $m_\chi \sim 1$ TeV, or otherwise excluded by direct DM detection bounds. If $R \sim 1$, then one would have to go to large M_T values where, however, $\Omega_\chi h^2$ is only barely compatible with $m_\chi \approx m_Z$.

As it turns out, latest results from LHC show that the branching ratio of $h \to \gamma\gamma$ is close to the SM prediction (see footnote 23). Furthermore, direct detection experiments seem to favour small values of M_T for $m \approx 200$ GeV. Therefore, the $m_{\chi_1^0} \approx m_Z$ realization of the Doublet-Triplet Fermionic DM model is excluded (or new physics has to be introduced), which is also noted in subsequent studies of this model.

Following our publication of the Doublet-Triplet Fermionic DM model, a more general analysis was performed in ref. [230] for $Y_1, |Y_2| \in [0, 1.5]$, $arg(Y_2) \in [0, \pi]$ and $M_D, M_T \in [0, 400]$ GeV. There, it was found that although the observed relic abundance can be obtained, the $h \to \gamma\gamma$ branching ratio is always suppressed, with $R(h \to \gamma\gamma) \lesssim 0.8$ in the entire parameter space. In a more recent analysis [231], this result was once again confirmed. In addition, it was shown that the observed relic abundance can be obtained for a DM mass above 1 TeV, relying on strong coannihilation effects due to the radiative mass splitting between the DM and the lightest charged fermion. However, this region was not further explored since it cannot be probed at the LHC.

The Doublet-Triplet Fermionic Dark Matter model was also studied in the case of an extended scalar sector in ref. [232], where, an $SU(2)_L$-doublet scalar is added along with an $SU(2)_L$-triplet scalar. It was shown that the lightest fermion can be the DM particle either near the EW scale or the TeV scale. In the heavy DM scenario, the coannihilation effects are strong, resulting to lowest DM mass at ~ 1 TeV for the pure fermion doublet DM and ~ 2.8 TeV for the pure triplet case. The more appealing EW region for fermion DM was extensively analysed. As it was shown, the correct relic abundance can be obtained for large Yukawa coupling (in the custodial limit) and DM mass $m_{\chi_1^0} \sim 80$ GeV, while avoiding relevant direct and indirect detection bounds. Moreover, it was shown that the charged scalars can affect $R(h \to \gamma\gamma)$ to be within the LHC limits, with scalar masses above the DM mass (up to ~ 300 GeV) and moderate couplings between the Higgs and the new scalars ensuring perturbativity and vacuum stability (at tree level). It was also argued that the new heavy scalars are not going to affect the potential LHC signal (discussed in Section 3.8). Therefore, based on the analysis of ref. [231] regarding future LHC reach, the Doublet-Triplet Fermionic Dark Matter model may still be detectable in the 300 fb^{-1} phase of the LHC.

Apart from studying possible extensions of this model, this work can be extended in several ways as for example, to investigate the role of CP-violating phases of M_D on baryogenesis. Also, indirect DM searches, e.g. photon flux due to $\chi_1^0\chi_1^0 \to \gamma\gamma$, could be also an interesting avenue. We postpone all these interesting phenomena for future study.

4 Effective Theory for Electroweak Doublet Dark Matter

In the previous chapter we studied the Doublet-Triplet Fermionic Dark Matter model. We showed that the DM content of the Universe can be explained by a relatively simple model. Furthermore, by imposing a global (custodial) symmetry in the Yukawa sector, we found that the DM particle can have a mass at the electroweak scale, without coannihilations or resonant effects, *i.e.* fine tuning. Moreover, this imposed symmetry is responsible for the vanishing of the DM-Higgs interaction at tree-level, which helps avoid the bounds from direct-detection experiments. However, from the LHC results regarding the branching ratio of the Higgs boson to two photons, became evident that this model needs completion. The need for completion of this model was further indicated by studying the stability of the SM vacuum. We showed that in order for the SM vacuum to be stable, heavy particles have to be introduced, probably near the TeV scale. In general, the number of possible completions of this model is practically infinite. One possible completion would be the extension of the scalar sector, which can be done by adding heavy scalar weak singlets, doublets, etc. Another possibility may be the extension of the gauge sector, which again can be realized in a number of different ways. However, regarding the dark matter phenomenology around the electroweak scale, the exact nature of the heavy degrees of freedom is not important. This is because, the particle content well above the electroweak scale, can be simply integrated out. Therefore, we do not have to find the correct completion(s), we only have to study an effective field theory (EFT) based on the particle content of the doublet-triplet model. This would allow us to study all possible completions in a model-independent way, with a minimal Dark Sector.

In this chapter, we perform a detailed study of an effective field theory which includes the Standard Model particle content extended by a pair of Weyl fermionic SU(2)-doublets with opposite hypercharges. A discrete symmetry guarantees that a linear combination of the doublet components is stable and can act as a candidate particle for dark matter. The dark sector fermions interact with the Higgs and gauge bosons through renormalizable $d = 4$ operators, and non-renormalizable $d = 5$ operators that appear after integrating out extra degrees of freedom above the TeV scale. We study collider, cosmological and astrophysical probes for this effective theory of dark matter. We find that a WIMP with a mass nearby the electroweak scale, and thus observable at LHC, is consistent with collider and astrophysical data only when fairly large magnetic dipole moment transition operators with the gauge bosons exist, together with moderate Yukawa interactions. In this chapter we present the analysis of ref. [88].

4.1 Introduction and Motivation

There is convincing evidence for the existence of dark matter from observation of gravitational effects at astrophysical and cosmological scales but not yet confirmed at Earth's colliders, where interactions between the hypothetical DM particle (WIMP) is probed through

its interactions with the Standard Model particles (for recent reviews see [56,111,115,233]). Out of all energy density in the universe, approximately 25% seems to consist of DM, probably in the form of WIMPs, with its relic density today with respect to the critical density, to be precisely known by the Planck collaboration [164,234] [see eq. (3.69)].[1] Out of many WIMP candidates one of the most studied is the lightest higgsino particle [178, 235], a fermion which is a linear combination of the neutral components of the $SU(2)_L$-bi-doublet superpartners of the Minimal Supersymmetric Standard Model (MSSM) scalar Higgs doublets. A higgsino WIMP fulfilling the constraint of eq. (3.69), which concurrently escapes the direct DM search bounds, must be heavier than the TeV scale, and therefore difficult to be reached at the Large Hadron Collider (LHC).

In this work, we shall consider a "higgsino like" DM sector of the Standard Model (SM) gauge structure, with mass *as close to the electroweak scale as possible,* supplied also by related effective operators of dimension less than or equal to five. Since $SU(2)_L$ fermionic doublets are not singlets under the SM gauge group, there are important interactions already at the renormalizable level, providing annihilation processes of WIMP to SM particles or interactions between the WIMP and the nucleons. Other, what we call "Earth" detectable effects, include contributions to the Electroweak (EW) parameters, to the Higgs boson decay into diphotons, and to other LHC processes, like mono-jets, mono-Z, etc. [145].

Apart from MSSM and its variants, there are many simple models for DM that contain bi-doublets,[2] in their low energy spectrum. For instance, there are models with $SU(2)_L$ doublets+singlet(s) [75, 79, 80, 171, 172, 219, 230, 236] or doublets+triplet [82, 231]. For EW scale DM at work in most of these models, the need of low energy cut off, of the order of 1 TeV, is sometimes unavoidable.[3] In addition, recent attempts to investigate low energy DM-models arising from Grand Unified Theories (e.g., from an SO(10) GUT), seem to incorporate bi-doublets, often in association with other particles, in their low energy particle content [199, 237, 238]. This low energy content, may also be part of a non-GUT extension of the Standard Model, as for instance a subgoup of SO(10), such as the left-right symmetric model [239]. There are also Effective Field Theory (EFT) approaches with the SM+χ, or simply SM_χ, where χ is the SM-singlet, up to dimension six effective operators [85, 240]. One should remark however, that a light singlet fermionic dark matter is not favoured by SO(10)–GUT constructions consistent with a unification and intermediate symmetry breaking scale at the TeV scale [237, 241].

Motivated by all the above we would like to study the phenomenology of a SM with $SU(2)_L$-bi-doublets with electroweak mass. In terms of physical masses, this model contains a charged Dirac fermion and two Majorana (or Pseudo-Dirac) neutral fermions with their masses splitted with mass differences in the vicinity of tens of GeV due to the presence of $d = 5$ non-renormalizable operators. We study the implications of all the related to dark matter $d = 5$ operators for the relic abundance, for direct as well as indirect searches. A general study of Majorana fermionic dark matter based on SM-extensions of the bi-doublets has been discussed in ref. [242]. Our EFT can be viewed as a decoupling limit of all extra fermion states but not those arising from the $SU(2)_L$ bi-doublet system.

[1] **Note added**: The updated results from the Planck collaboration [29] show a slightly different value for the DM relic abundance [see eq. (1.103)] .

[2] By the name "bi-doublets" we mean two Weyl fermion $SU(2)_L$-doublets with opposite hypercharge.

[3] It has been shown in ref. [82] that for EW scale DM particle mass one needs relatively large Yukawa couplings between the extra vector-like fermions and the Higgs boson. These lead in turn to vacuum instabilities of the Higgs potential [203], that arise already at the TeV scale, depending on the largeness of the Yukawa couplings and the particle content of the model.

The EFT at hand, generalizes the phenomenology of Standard Models with additional $SU(2)_L$ multiplets, sometimes called Minimal Dark Matter models [78,152,243]. The most basic of these models is just a Dirac mass term, *c.f.* eq. (4.1), for the bi-doublet fermion multiplet. However, without the imposition of a symmetry the WIMP will not be stable (although higher spin SU(2)-reps will be "accidentally" stable). We discuss in the next section available symmetries that not only protect the WIMP for decaying, like a Z_2 or lepton number, but also forbid potentially dangerous couplings to the Z-boson like charge conjugation or custodial symmetry.

A similar to our EFT, has been studied in ref. [86] for higgsino DM scenario in high scale supersymmetry breaking, using a mass splitting of $\mathcal{O}(\lesssim 1$ GeV) originated through $d = 5$ Yukawa interactions and radiative corrections. For higgsino mass parameter $\lesssim \mathcal{O}(1)$ TeV, the parameter space is constrained from direct detection and Electric Dipole Moment searches. The EFT employed here is complementary to ref. [86]. We assume that the cut-off scale is of order $\Lambda = \mathcal{O}(1$ TeV) and for this reason, we introduce a complete set of $d = 5$ operators, *i.e.* Yukawa and dipole transition operators. We later use all these operators to calculate different observables and constrain the parameter space accordingly. Furthermore, the Yukawa couplings are not restricted by supersymmetry. This, in turn, allows us to focus on larger mass differences and therefore different phenomenology.

As we show in this work, a viable WIMP with mass nearby the electroweak scale acquires fairly large non-zero magnetic dipole moments. Magnetic dipole interacting DM has already been studied in refs. [87, 244, 245], a scenario called Magnetic Inelastic Dark Matter (MiDM). In MiDM, the WIMP (χ) is supplemented by a "excited WIMP state", ($\chi^\star$), with $m_{\chi^\star} - m_\chi = \mathcal{O}(100)$ KeV. A consequence of this, is a large nucleus-WIMP cross section, comparable to experimental limits for inelastic nucleus-WIMP scattering. Moreover, in ref. [87], a connection between direct detection and Gamma-ray line signals pointed out, for such small mass splitting. Our work is more general than this scenario, simply because the fermions we introduce are doublets under the $SU(2)_L$. Apart from this, we focus on relatively large mass difference, of order $\mathcal{O}(1 - 10)$ GeV, between the two neutral fermion states. These facts lead to qualitatively different phenomenology. In particular, the direct detection scattering, in our case, is elastic. Also, due to a symmetry the lightest fermion does not interact directly with Z-boson and the dominant annihilation channels in the early universe are different. Although the EFT studied here is more general from the one suggested previously in the literature, the dipole moments that are responsible for the observed DM relic abundance, provide also enough monochromatic photon flux from the center of our galaxy, to bound considerably (but not to exclude) the parameter space of the model. It is therefore understood that our model could provide an explanation for a possible signal in the near future.

The outline of this chapter is the following: in Section 4.2 we describe the effective theory and associated possible accidental symmetries and in Appendix B we list the effective $d = 5$ and $d = 6$ operators, that may be present in this extension of the SM. In Section 4.3 we describe the interactions and the mass spectrum. Consequently, in Section 4.4 various collider and direct DM detection constraints are analysed. In addition, in Section 4.5 the DM relic density is calculated, and we study the corresponding cosmological constraints. Moreover, we discuss the phenomenology of possible indirect signals for DM searches, from gamma-rays, and briefly, from neutrino fluxes. In Section 4.6 we study possible signals of this model at LHC at 8 and 13 TeV. Finally, in Section 4.7 we summarise our findings.

4.2 Symmetries and the effective theory

In the SM particle content we add a fermionic bi-doublet, that is a pair of Weyl fermion $SU(2)$-doublets with opposite hypercharges, $\mathbf{D_1}$, that transform under $(SU(3), SU(2)_L)_Y$ like $(\mathbf{1^c}, \mathbf{2})_{-\mathbf{1}}$ and $\mathbf{D_2}$, that transform as $(\mathbf{1^c}, \mathbf{2})_{+\mathbf{1}}$.[4] The doublet $\mathbf{D_2}$ has exactly the same gauge quantum numbers as the SM Higgs field $\mathbf{H}$, while $\mathbf{D}_1$ carries the quantum numbers of the SM lepton doublet but not necessarily sharing lepton number. Then the model under study includes gauge invariant kinetic terms like[5] $D^{\dagger\, xa}\bar{\sigma}^\mu \mathscr{D}_\mu D_{xa}$, with $(x = 1, 2)$ the number of doublets and $(a = 1, 2)$ their $SU(2)_L$-quantum numbers. These fields have renormalizable couplings with the SM electroweak gauge bosons through $\mathscr{D}_\mu$, the covariant derivative for the SM gauge group $SU(2)_L \times U(1)_Y$.

4.2.1 Custodial symmetry

In addition to gauge invariant kinetic term, an invariant Dirac-type mass term for the bi-doublets is

$$\mathscr{L}_{\rm DM} \supset -M_D\, \epsilon^{ab} D_{1\,a} D_{2\,b} + \text{H.c.} = -M_D\, \det \mathcal{D} + \text{H.c.}\,, \tag{4.1}$$

where ϵ^{ab} is the antisymmetric tensor, with $\epsilon^{12} = -\epsilon^{21} = 1$ and, for later notational use, we define $D_{1a} \equiv (D_1^0, D_1^-)^T$, $D_{2a} \equiv (D_2^+, D_2^0)^T$. In order to make things clearer below, in the second equality of eq. (4.1) we used the definition of the determinant to write the matrix

$$\mathcal{D}_{xa} = \begin{pmatrix} D_{1a} & D_{2a} \end{pmatrix} = \begin{pmatrix} D_1^0 & D_2^+ \\ D_1^- & D_2^0 \end{pmatrix}. \tag{4.2}$$

Written in this form it is now transparent that $\mathcal{D}$ is invariant not only under the $SU(2)_L$ but also under another $SU(2)$, say $SU(2)_R$. The transformation rule under $SU(2)_L \times SU(2)_R$ with corresponding unitary matrices U_L and U_R is

$$\mathcal{D} \to U_L\, \mathcal{D}\, U_R\,, \tag{4.3}$$

where U_L acts on the rows and U_R acts on the columns of $\mathcal{D}$, respectively. On the other hand, it is well known [165] that, the SM Higgs sector is also invariant under a global $SU(2)_R$ symmetry. In this case we can write the Higgs field in $(\mathbf{2}, \mathbf{2})$ form of $SU(2)_L \times SU(2)_R$ as

$$\mathcal{H}_{ax} = \begin{pmatrix} H_a^* & H_a \end{pmatrix} = \begin{pmatrix} -\Phi^{0*} & \Phi^+ \\ \Phi^- & \Phi^0 \end{pmatrix}. \tag{4.4}$$

Similarly, the Higgs field is invariant under $SU(2)_L \times SU(2)_R$ with a transformation law $\mathcal{H} \to U_L\, \mathcal{H}\, U_R$. Obviously, we can now write down a $SU(2)_L \times SU(2)_R$ non-renormalizable $d = 5$ Yukawa operator as

$$\mathscr{L} \supset \frac{y}{\Lambda} [\mathrm{Tr}(\mathcal{H}^\dagger \mathcal{D})]^2 + \text{H.c.} \tag{4.5}$$

where Λ is the scale of masses that are being integrated out. EW symmetry breaking breaks $SU(2)_L \times SU(2)_R$ down to its diagonal subgroup, $SU(2)_{L+R}$. The latter symmetry is the well known *custodial* symmetry [165]. Most pronouncedly it is broken by the difference in magnitude between the top and bottom Yukawa couplings and by the $U(1)_Y$ gauge symmetry but, importantly, keeps radiative EW corrections under control. One of our study benchmarks below arises from eq. (4.5).

[4] Note that $\mathbf{D_{1,2}}$ correspond to $\bar{\mathbf{D}}_{\mathbf{1,2}}$ of Chapter 3.

[5] Throughout this chapter, we adopt the convenient two-component Weyl spinor notation of ref. [28].

4.2.2 Charge conjugation symmetry

The new $\mathbf{D_1}$- and $\mathbf{D_2}$-fermion fields form a pseudo-real representation of SU(2). In order to make the presentation transparent, we redefine the Weyl fields as

$$\xi^b = \epsilon^{ab}\, D_{1a}\ , \qquad \eta_b = D_{2b}\ , \tag{4.6}$$

where we can easily arrive at a Dirac fermion field Lagrangian written in terms of the two, two-component Weyl spinor fields, ξ and η, as

$$\mathscr{L}_{\rm DM} \ = \ i\xi_a^\dagger \bar\sigma^\mu \mathscr{D}_\mu \xi^a + i\eta^{\dagger a} \bar\sigma^\mu \mathscr{D}_\mu \eta_a - M_D\,(\eta_a \xi^a + \eta^{a\dagger}\xi_a^\dagger)\ . \tag{4.7}$$

The bi-doublets-mass term, M_D, can be taken real and positive. In eq. (4.7), we have suppressed all spinor indices, but have left the gauge group indices intact to show our covariant notation (to be used below). Now, it is well known that the Lagrangian (4.7), beyond $SU(2)_L$-symmetry, accommodates a $O(2)$-symmetry which, apart from making the usual phase invariance transformation $SO(2) \sim U(1)$ group $\xi \to e^{-i\theta}\xi$ and $\eta \to e^{i\theta}\eta$, it contains a discrete symmetry under which

$$C^{-1}\,\eta_a\, C \ = \ \xi^a\ . \tag{4.8}$$

This discrete symmetry is a *charge conjugation symmetry (c.c.)*, associated to the charge conjugation operator C with $C^2 = (C^{-1})^2 = I$. This symmetry simply exchanges the two Weyl fields $\xi \leftrightarrow \eta$ or to a "free" notation, $D_1 \leftrightarrow D_2$. There is a similar symmetry in the Higgs sector, where another explicit bi-doublet mass term exists, that of the Higgs field. Then the corresponding charge conjugation symmetry for the Higgs field, which leaves invariant the kinetic terms as well as the Higgs potential in the Standard Model, reads accordingly as,

$$C^{-1}\, H_a\, C \ = \ H^{\dagger\, a}\ , \tag{4.9}$$

where H_a is the SM Higgs doublet, $H_a \equiv (\Phi^+, \Phi^0)^T$. What basically c.c. symmetry does, is to exchange the columns of matrices $\mathcal{D}$ and $\mathcal{H}$ in eqs. (4.2) and (4.4), respectively. For the Higgs field, charge conjugation becomes somewhat trivial for the following reason. In order to read physical masses we have to expand the Lagrangian in terms of fields that vanish at the minimum. There are many $SU(2)_L \times U(1)_Y$ equivalent Higgs representations, but the most known is the so-called Kibble parametrization [246],

$$\mathbf{H} \ = \ \mathbf{U}\,\mathbf{H_0} \ = \ \mathbf{U} \begin{pmatrix} 0 \\ v + \frac{h}{\sqrt{2}} \end{pmatrix}\ , \tag{4.10}$$

where $\mathbf{U}$ is any 2×2 unitary matrix describing a unitary gauge transformation, v is the vacuum expectation value [*c.f.* eq. (4.18)], and h is the *real*-valued Higgs field. The matrix $\mathbf{U}$ is absorbed in gauge boson, lepton, quark field redefinitions, *and, in particular* model at hand, in the dark sector fields ξ and η (or D_1 and D_2). Therefore, c.c. symmetry, (4.9), has no effect on $\mathbf{H_0}$. On the other hand, the discrete c.c. symmetry in (4.8), acts in a non-trivial way in the dark sector of the model after EW symmetry breaking. We will *assume* that this is a symmetry of the Lagrangian and examine implications from this hypothesis.

4.2.3 The discrete Z_2-symmetry

Unfortunately, the c.c. or the custodial symmetries alone can not account for the stability of DM lightest particle and an extra discrete Z_2-symmetry that distinguishes SM-particles from DM-particles is needed. To "throw away" dangerous $d = 4$ operators that are responsible for WIMP decay, like $D_1 H^\dagger \bar{e}$ or higher [see Appendix B for assignments and in particular eq. (B.4)], it could be enough to impose a lepton number symmetry for example. It is safer however, to impose an external Z_2-discrete symmetry under which the SM fermions are odd while the dark matter fermions and the Higgs boson are even eigenstates. Such a discrete symmetry, or equivalently, its variant known from MSSM as R-parity, is preserved in SO(10) with the Higgs field in a **126** representation [247] and are common in Grand Unified Theories (GUTs) with low mass dark matter particles [199, 237, 238, 248]. We shall therefore assume such a Z_2-symmetry in what follows.

4.2.4 Symmetric limits used in the analysis

Our model, is based on an effective theory described by the following Lagrangian:

$$\mathscr{L} = \mathscr{L}_{\rm SM} + \mathscr{L}_{\rm DM} + \mathscr{L}^{d=5}_{\rm SM+DM} \,. \tag{4.11}$$

$\mathscr{L}_{\rm SM}$ is the SM renormalizable Lagrangian, $\mathscr{L}_{\rm DM}$ is the DM sector renormalizable Lagrangian given by eq. (4.7) and $\mathscr{L}^{d=5}_{\rm SM+DM}$ is the Lagrangian that contains the dimension-5 operators relevant to DM interactions. We assume that higher dimensional operators ($d \geq 6$) are suppressed and throughout this work we are focusing on up-to $d = 5$ effective operators. For the sake of completeness, however, in Appendix B we construct all relevant operators for both dimensionalities $d = 5$ and $d = 6$.

We show below that by using the c.c. symmetry of eq. (4.8), or the custodial symmetry or just the $U(1)$ phase symmetry we can arrive at four distinct choices in the parameter space. Moreover, this is very convenient for the phenomenological study that follows. First, $\mathscr{L}^{d=5}_{\rm SM+DM}$ contains effective operators that after spontaneous EW symmetry breaking split the masses of the neutral particles from their original common mass M_D. The most general, linearly independent set of operators, is

$$\begin{aligned} -\mathscr{L}^{d=5}_{\rm SM+DM} \supset & \quad \frac{y_1}{2\Lambda}\,(H_a\xi^a)\,(H_b\xi^b) \;+\; \frac{y_2}{2\Lambda}\,(H^{\dagger\,a}\eta_a)\,(H^{\dagger\,b}\eta_b) \;-\; \frac{y_{12}}{\Lambda}\,(H_a\xi^a)\,(H^{\dagger\,b}\eta_b) \\ & + \;\; \frac{\xi_{12}}{\Lambda}\,(\xi^a\eta_a)\,(H^{\dagger\,b}H_b) \;+\; \text{H.c.}\,, \end{aligned} \tag{4.12}$$

where Λ is the cut-off of the effective, SM+bi-doublet, theory.[6] If the c.c. symmetry (4.8) is imposed the last two terms of eq. (4.12) are unaffected, but the first two terms must be the same. This means that under c.c. symmetry the relation

$$y_1 \;=\; y_2 \;\equiv\; y\,, \tag{4.13}$$

holds. We always follow this symmetry condition in the analytical expressions as well in the numerical results throughout this work. Even more, one can write the independent c.c. symmetry invariant $d = 5$ operators

$$y\,(H_a\xi^a - H^{\dagger a}\eta_a)^2 \quad \text{or} \qquad y\,(H_a\xi^a + H^{\dagger a}\eta_a)^2\,, \tag{4.14}$$

[6] In eq. (B.1) we give examples of what sort of heavy particle mass the Λ might be.

in addition to the operators multiplying y_{12} and ξ_{12} in eq. (4.12). Based on symmetries discussed above, there are additional restrictions on Yukawa couplings

$$(1)\ y = y_{12}\ , \qquad (2)\ y = -y_{12}\ , \qquad (3)\ y_{12} = 0\ , \qquad (4)\ y = y_{12} = 0\ , \quad \forall y\ , \quad \forall \xi_{12}\ . \tag{4.15}$$

Cases (1) and (2) above, may correspond to the $SU(2)_L \times SU(2)_R$ symmetry limit of eq. (4.5). Case (3) is not really supported by any symmetry consideration, in fact it violates the custodial symmetry, and is only adopted here for covering the mass spectrum phenomenology (*c.f.* Fig. 4.1). In choosing the benchmark for case (4) we are motivated by the following: in a full gauge invariant theory, y_{12} and ξ_{12} may have certain relations with y. For example, in the fermionic doublet-triplet DM model of ref. [82] one finds $\xi_{12} = -2y = 2y_{12}$ after decoupling the heavy triplet in the custodial limit. If the continuous $U(1)$-phase symmetry is employed (or if the two $SU(2)_R$ symmetries for $\mathcal{D}$ and $\mathcal{H}$ are different) then $y = 0$ for all y_{12} and ξ_{12}. In this case there are two, mass degenerate, Dirac fermions in the spectrum: one neutral and one charged. This completes our study benchmark points which are mostly based upon the underlying global symmetries of the model rather on a random choice of the model parameters.

There are also $d = 5$ magnetic and electric dipole operators related to the dark sector particles. A detailed form of these operators is given in Appendix B. In this work we shall focus on the magnetic dipole operators

$$-\mathscr{L}^{d=5}_{\rm SM+DM} \supset \frac{d_\gamma}{\Lambda}\, \xi^a\, \sigma^{\mu\nu}\, \eta_a\, B_{\mu\nu} \ + \ \frac{d_W}{\Lambda}\, \xi^b\, \sigma^{\mu\nu}\, (\tau^A)_b{}^c\, \eta_c\, W^A_{\mu\nu} \ + \ \text{H.c.}\ , \tag{4.16}$$

where $B_{\mu\nu}$ and $W^A_{\mu\nu}$ are the $U(1)_Y$ and $SU(2)_L$ field strength tensors respectively and τ^A the Pauli matrices with $A = 1, 2, 3$ and $\sigma^{\mu\nu} \equiv \frac{i}{4}(\sigma^\mu \bar\sigma^\nu - \sigma^\nu \bar\sigma^\mu)$. These operators are invariant under (4.8) since $C^{-1}\, \xi \sigma^{\mu\nu} \eta\, C = \eta \sigma^{\mu\nu} \xi = -\xi \sigma^{\mu\nu} \eta$, $C^{-1} W^A_{\mu\nu} C = (-1)^{2-A} W^A_{\mu\nu}$ (no sum in A) and $C^{-1} B_{\mu\nu} C = -B_{\mu\nu}$. We shall see below that both moments d_γ and d_W, play an important role in achieving the correct relic density.

As promised earlier in this section, the new, beyond the SM parameters needed to describe the dark sector are the following six:

$$M_D\ , \quad \Lambda\ , \quad y\ , \quad \xi_{12}\ , \quad d_\gamma\ , \quad d_W\ . \tag{4.17}$$

Throughout, we assume them all to be real. More importantly, we *assume* that the mass M_D is around or below the EW-scale, that is of the order of $\mathcal{O}(100)$ GeV. The mass scale Λ for extra scalars and fermions, are far above the EW scale, possibly at the TeV-scale. As a result, we assume that this EFT contains three (but two distinct) mass scales,

$$M_D \simeq v \simeq 174\ \text{GeV}\ , \qquad \Lambda \simeq \mathcal{O}(1)\ \text{TeV}\ . \tag{4.18}$$

4.3 Phenomenology

4.3.1 Mass Spectrum

After electroweak symmetry breaking and the shift of the neutral component of the Higgs field $H_0 = (0, v + h/\sqrt{2})^T$, in eqs. (4.7) and (4.12), we obtain

$$\mathscr{L}^{\rm DM}_{\rm (mass)} = -m_{\chi^\pm}\, \chi^-\, \chi^+ \ - \ \frac{1}{2} \sum_{i=1}^{2} m_{\chi^0_i}\, \chi^0_i \chi^0_i \ + \ \text{H.c.}\ , \tag{4.19}$$

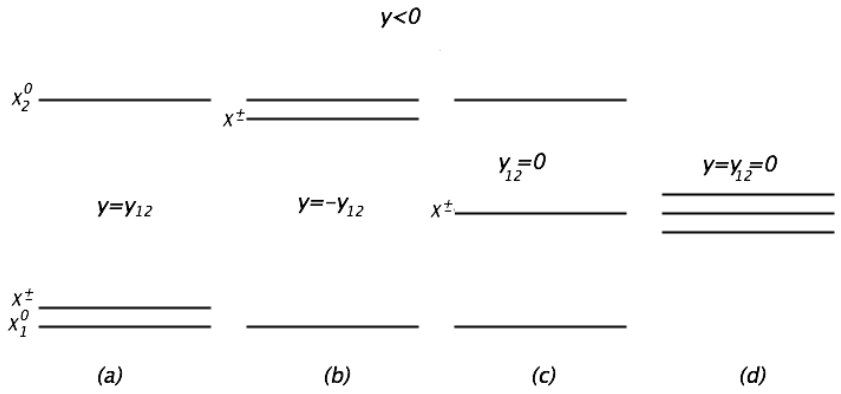

Figure 4.1: *Mass hierarchies of the dark fermions χ_1^0, $\chi^\pm$ and χ_2^0 (bottom to top) for $y < 0$, following the c.c. symmetry of eq. (4.15) for the cases (a) $y = y_{12}$, (b) $y = -y_{12}$, (c) $y_{12} = 0$ and (d) $y = y_{12} = 0$. The mass spectrum for $y > 0$ is obtained from this figure by exchanging $\chi_1^0 \leftrightarrow \chi_2^0$.*

where, under the c.c. symmetry restrictions (4.13), the physical fields are two neutral Majorana fermions (χ_1^0, χ_2^0) and one pair of Dirac charged fermions $(\chi^\pm)$

$$\chi_1^0 = \frac{1}{\sqrt{2}}\,(D_1^0 + D_2^0)\,, \quad \chi_2^0 = -\frac{i}{\sqrt{2}}\,(D_1^0 - D_2^0)\,, \tag{4.20a}$$

$$\chi^+ = i\,D_2^+\,, \qquad \chi^- = i\,D_1^-\,, \tag{4.20b}$$

with masses,

$$m_{\chi^\pm} \;=\; M_D \;+\; \xi_{12}\,\omega\,, \tag{4.21a}$$

$$m_{\chi_1^0} \;=\; m_{\chi^\pm} \;+\; \omega\,(y - y_{12})\,, \qquad \omega \equiv \frac{v^2}{\Lambda}\,, \tag{4.21b}$$

$$m_{\chi_2^0} \;=\; m_{\chi^\pm} \;-\; \omega\,(y + y_{12})\,. \tag{4.21c}$$

Without loss of generality, our natural choice for field redefinitions is such that $M_D > 0$. Under the c.c. symmetry the state χ_1^0 is even, while the states $\chi_2^0, \chi^\pm$ are odd, *i.e.*

$$C^{-1}\,\chi_1^0\,C = +\chi_1^0\,, \qquad C^{-1}\,\chi_2^0\,C = -\chi_2^0\,, \tag{4.22}$$

$$C^{-1}\,\chi^+\,C = -\chi^-\,, \qquad C^{-1}\,\chi^-\,C = -\chi^+\,. \tag{4.23}$$

However, in general and far from custodial symmetry limits, only χ^+ and χ^- are particle-antiparticle states with common mass, $m_{\chi^\pm}$.

In what follows, we sort the masses so that the lightest particle is χ_1^0. Also, we assume $M_D + \xi_{12}\,\omega > 0$, for otherwise the contribution from $d = 5$ operators to the masses, *i.e.* the term $\xi_{12}\,\omega$ would be unnaturally large, in order to satisfy the LEP bound [249–251] $m_{\chi^\pm} \gtrsim 100$ GeV. There are two equivalent set of mass spectra: one with $y \leq 0$ where $m_{\chi_1^0} \leq m_{\chi_2^0}$ and the other $y \geq 0$ where $m_{\chi_2^0} \leq m_{\chi_1^0}$. In Fig. 4.1, we show the spectrum for the $y \leq 0$ case. The mass spectrum for $y > 0$ is exactly the same after exchanging $\chi_1^0 \leftrightarrow \chi_2^0$. We note that the mass hierarchies between $\chi^\pm$, χ_1^0 and χ_2^0 displayed in Fig. 4.1 do not depend on M_D and ξ_{12}, although their central mass values are all shifted uniformly upon their variation. Therefore, following eq. (4.15), we distinguish four mass spectra:

(a) $y = y_{12} < 0$: the lightest neutral DM fermion χ_1^0 is almost degenerate with the charged one $\chi^\pm$ (see Fig. 4.1a) with

$$m_{\chi_1^0} = m_{\chi^\pm} \ , \quad m_{\chi_2^0} = m_{\chi^\pm} + 2\omega|y| \ . \tag{4.24}$$

(b) $y = -y_{12} < 0$: the heavy neutral fermion χ_2^0 is degenerate with the charged fermion $\chi^\pm$ (Fig. 4.1b) with

$$m_{\chi_1^0} = m_{\chi^\pm} - 2\omega|y| \ , \quad m_{\chi_2^0} = m_{\chi^\pm} \ . \tag{4.25}$$

(c) $y_{12} = 0 \ , \forall y < 0$: all χ_1^0 and χ_2^0 are split from $\chi^\pm$ by an equal amount $\omega|y|$ with (Fig. 4.1c)

$$m_{\chi_1^0} = m_{\chi^\pm} - \omega|y| \ , \quad m_{\chi_2^0} = m_{\chi^\pm} + \omega|y| \ . \tag{4.26}$$

(d) $y_{12} = y = 0$: all four particles and antiparticles are degenerate in mass (Fig. 4.1d)

$$m_{\chi_1^0} = m_{\chi^\pm} = m_{\chi_2^0} \ . \tag{4.27}$$

This case describes two Dirac fields: one neutral and one charged. It can be viewed as a limit of case (c) when $y \to 0$. All these mass relations have been derived at tree level. However, it is known that these mass differences are altered by a finite piece of $\mathcal{O}(100$ – 1000 MeV), when radiative corrections are taken into account [252]. Even in the custodial symmetry limit, these corrections should be proportional to the $U(1)_Y$ gauge coupling. They are small compared to $\omega|y|$ contributions to the masses from the $d = 5$ operators when the scale Λ is low, e.g., $\mathcal{O}(1)$ TeV. As a result, the mass hierarchies depicted in Fig. 4.1 will survive beyond tree level in all cases apart from case (d).

4.3.2 Dark Matter Particle Interactions

Our notation follows closely that of ref. [82]. We calculate the Higgs interactions with the extra fermions from eq. (4.12). We find,

$$\begin{aligned} \mathscr{L}^{\rm DM}_{\rm Y(int)} = & - Y^{h\chi^-\chi^+}\, h\, \chi^-\, \chi^+ \ - \ \frac{1}{2}\, Y^{h\chi_i^0\chi_j^0}\, h\, \chi_i^0\, \chi_j^0 \\ & - \ \frac{1}{2}\, Y^{hh\chi^-\chi^+}\, h\, h\, \chi^-\, \chi^+ - \ \frac{1}{4}\, Y^{hh\chi_i^0\chi_j^0}\, h\, h\, \chi_i^0\, \chi_j^0 \ + \ \text{H.c.} \ , \end{aligned} \tag{4.28}$$

where

$$Y^{h\chi^-\chi^+} = \sqrt{2}\, \xi_{12}\, \frac{\omega}{v}, \qquad Y^{hh\chi^-\chi^+} = \xi_{12}\, \frac{\omega}{v^2}, \tag{4.29a}$$

$$Y^{h\chi_1^0\chi_1^0} = \frac{\sqrt{2}\,\omega}{v}\, (\xi_{12} + y - y_{12}), \qquad Y^{hh\chi_1^0\chi_1^0} = \frac{\omega}{v^2}\, (\xi_{12} + y - y_{12}), \tag{4.29b}$$

$$Y^{h\chi_2^0\chi_2^0} = \frac{\sqrt{2}\,\omega}{v}\, (\xi_{12} - y - y_{12}), \qquad Y^{hh\chi_2^0\chi_2^0} = \frac{\omega}{v^2}\, (\xi_{12} - y - y_{12}), \tag{4.29c}$$

$$Y^{h\chi_1^0\chi_2^0} = 0, \qquad Y^{hh\chi_1^0\chi_2^0} = 0. \tag{4.29d}$$

The 4-point $h^2\chi^2$ vertices are proportional to 3-point $h\chi^2$ vertices. Interestingly enough, off-diagonal couplings to h in (4.29d), vanish identically due to the c.c. symmetry of eqs. (4.22) and (4.23), using that $C^{-1}\, h\, C = h$.

Since D_1 and D_2 carry $SU(2)_L \times U(1)_Y$ quantum numbers, there are renormalizable interactions involving gauge bosons and the dark fermions, $\chi^0_{1,2}$ and $\chi^\pm$. For instance, the interaction between $\chi^\pm$ and the photon reads

$$\mathscr{L}^{\gamma-\chi^\pm}_{\rm KIN(int)} = -(+e)\,(\chi^+)^\dagger \bar\sigma^\mu \chi^+\, A_\mu - (-e)\,(\chi^-)^\dagger \bar\sigma^\mu \chi^-\, A_\mu\ , \tag{4.30}$$

where A_μ is the photon field and $(-e)$ the electron electric charge. Similarly, the Z-gauge boson couplings to charged and neutral dark fermions are

$$\mathscr{L}^{Z-\chi}_{\rm KIN(int)} = \frac{g}{c_W} O'^{\,L} (\chi^+)^\dagger \bar\sigma^\mu \chi^+ Z_\mu - \frac{g}{c_W} O'^{\,R} (\chi^-)^\dagger \bar\sigma^\mu \chi^- Z_\mu + \frac{g}{c_W} O''^{\,L}_{ij} (\chi^0_i)^\dagger \bar\sigma^\mu \chi^0_j Z_\mu\ , \tag{4.31}$$

where

$$O'^{\,L} = O'^{\,R} = -\frac{1}{2}(1 - 2s^2_W)\ , \tag{4.32a}$$

$$O''^{\,L}_{ij} = \frac{1}{2}\ (O^*_{2i}\, O_{2j} - O^*_{1i}\, O_{1j})\ , \tag{4.32b}$$

$$O = \frac{1}{\sqrt{2}} \begin{pmatrix} 1 & i \\ 1 & -i \end{pmatrix}\ , \qquad O''^{\,L} = -\frac{i}{2} \begin{pmatrix} 0 & 1 \\ -1 & 0 \end{pmatrix}\ . \tag{4.32c}$$

With s_W (c_W) we denote the $\sin\theta_W$ ($\cos\theta_W$) of the weak mixing angle and with g the $SU(2)_L$ gauge coupling. The coupling $Z\,\chi^0_i\,\chi^0_j$ is non-zero only for $i \neq j$ due to the c.c. symmetry with $C^{-1} Z_\mu C = -Z_\mu$. The $O''^{\,L}$ is an antisymmetric matrix due to the Majorana nature of χ^0_i fermions and the hermiticity of the Lagrangian.

Interactions between χ's and W–bosons are described by the following terms

$$\begin{aligned} \mathscr{L}^{W^\pm-\chi^0-\chi^\mp}_{\rm KIN(int)} \ &= \ g\, O^L_i\, (\chi^0_i)^\dagger\, \bar\sigma^\mu\, \chi^+\, W^-_\mu - g\, O^R_i\, (\chi^-)^\dagger\, \bar\sigma^\mu\, \chi^0_i\, W^-_\mu \\ &\quad + g\, O^{L*}_i\, (\chi^+)^\dagger\, \bar\sigma^\mu\, \chi^0_i\, W^+_\mu - g\, O^{R*}_i\, (\chi^0_i)^\dagger\, \bar\sigma^\mu\, \chi^-\, W^+_\mu\ , \end{aligned} \tag{4.33}$$

where the mixing column matrices O^L and O^R are given by

$$O^L_i = \ \frac{i}{\sqrt{2}}\, O^*_{2i} = \frac{1}{2} \begin{pmatrix} i \\ -1 \end{pmatrix}\ , O^R_i = \frac{i}{\sqrt{2}}\, O_{1i} = \frac{1}{2} \begin{pmatrix} i \\ -1 \end{pmatrix}\ , \tag{4.34}$$

with the identity $O^R_i = O^L_i$ being again a consequence of the c.c. symmetry. Using the same matrices we can write the three-point dipole interactions of eq. (B.5) in the diagonal basis [7]

$$\begin{aligned} \mathscr{L}^{\rm 3-point}_{\rm dipole} \ &= -\frac{\omega}{v^2}\,(d_\gamma\, s_W \ + \ d_W\, c_W)\, O''^{L}_{ij}\, \chi^0_i\, \sigma_{\mu\nu}\, \chi^0_j\, F^{\mu\nu}_Z \\ &\quad - \frac{\omega}{v^2}\,(d_\gamma\, s_W \ - \ d_W\, c_W)\, \chi^-\, \sigma_{\mu\nu}\, \chi^+\, F^{\mu\nu}_Z \\ &\quad + \frac{\omega}{v^2}\,(d_\gamma\, c_W \ - \ d_W\, s_W)\, O''^{L}_{ij}\, \chi^0_i\, \sigma_{\mu\nu}\, \chi^0_j\, F^{\mu\nu}_\gamma \\ &\quad + \ \frac{\omega}{v^2}\,(d_\gamma\, c_W \ + \ d_W\, s_W)\, \chi^-\, \sigma_{\mu\nu}\, \chi^+\, F^{\mu\nu}_\gamma \\ &\quad - 2\frac{\omega}{v^2}\, d_W\, O^{R\,*}_i\, \chi^-\, \sigma_{\mu\nu}\, \chi^0_i\, F^{\mu\nu}_{W^+} \\ &\quad + \ 2\frac{\omega}{v^2}\, d_W\, O^L_i\, \chi^+\, \sigma_{\mu\nu}\, \chi^0_i\, F^{\mu\nu}_{W^-} \ + \ \text{H.c.}\ , \end{aligned} \tag{4.35}$$

[7] We are not concerned here about CP-violating phenomena and we set $e_{\gamma,W} = 0$.

where $F_V^{\mu\nu} = \partial^\mu V^\nu - \partial^\nu V^\mu$, $V = Z, A$ and $W^\pm$. Interestingly enough, EFT dipole $d = 5$ operators, generate photon interactions with the neutral dark particles, with a coupling that vanishes in the limit $d_\gamma c_W \simeq d_W s_W$. There is also an alignment of couplings in eq. (4.35) with the those in eqs. (4.31) and (4.33), that is important for achieving a "natural" cancellation of two different contributions in the cross section for $\chi_1^0\chi_1^0 \to VV$, where V can be Z,W or γ. Moreover, the four-point interactions involving dipole operators are

$$\begin{aligned}\mathscr{L}^{4-\text{point}}_{\text{dipole}} =& -2\,i\,g\,\frac{\omega}{v^2}\,d_W\,O''^L_{ij}\,\chi_i^0\,\sigma_{\mu\nu}\,\chi_j^0\,W^{+\mu}\,W^{-\nu} + 2\,i\,g\,\frac{\omega}{v^2}\,d_W\,\chi^-\,\sigma_{\mu\nu}\,\chi^+\,W^{+\mu}\,W^{-\nu}\\ &+ 4\,i\,g\,\frac{\omega}{v^2}\,d_W c_W\,O_i^{R*}\,\chi^-\,\sigma_{\mu\nu}\,\chi_i^0\,W^{+\mu}Z^\nu \;+\; 4\,i\,g\,\frac{\omega}{v^2}\,d_W c_W\,O_i^L\,\chi^+\,\sigma_{\mu\nu}\,\chi_i^0\,W^{-\mu}Z^\nu\\ &+ 4\,i\,g\,\frac{\omega}{v^2}\,d_W s_W\,O_i^{R*}\,\chi^-\,\sigma_{\mu\nu}\,\chi_i^0\,W^{+\mu}A^\nu \;+\; 4\,i\,g\,\frac{\omega}{v^2}\,d_W s_W\,O_i^L\,\chi^+\,\sigma_{\mu\nu}\,\chi_i^0\,W^{-\mu}A^\nu\\ &+\;\text{H.c.}\end{aligned} \tag{4.36}$$

In Section 4.5, we will see that these EFT dipole interactions are important for making the annihilation and coannihilation cross section of the WIMP dark matter particle χ_1^0, compatible with the measurement (3.69) for the DM relic density.

4.4 "Earth" constraints in the Dark Sector

In this section we study constraints imposed on the parameter space, from WIMP(χ_1^0)-nucleon scattering experiments searching directly for DM, from direct and oblique LEP electroweak observables and from the LHC data for the Higgs boson decay to two photons.

4.4.1 Nucleon-WIMP direct detection experimental bounds

In the limit that the DM particle χ_1^0 is much heavier than nucleon, the spin independent (SI) and spin dependent (SD) cross sections are given by [159]

$$\sigma_{\text{SI}} = 8\times10^{-45}\,\text{cm}^2\left(\frac{Y^{h\chi_1^0\chi_1^0}}{0.1}\right)^2, \qquad \sigma_{\text{SD}} = 3\times10^{-39}\,\text{cm}^2\left(\frac{g^{Z\chi_1^0\chi_1^0}}{0.1}\right)^2. \tag{4.37}$$

From the interactions in eq. (4.31), we see that $g^{Z\chi_1^0\chi_1^0} = 0$ at tree level and therefore $\sigma_{\text{SD}} \approx 0$. For the SI cross section the current bound from LUX [253, 254] is $\sigma_{\text{SI}} \simeq \{1-3.5\}\times10^{-45}$ cm^2, for $m_{\text{DM}} \simeq \{100-500\}$ GeV, respectively.[8] This gives

$$|Y^{h\chi_1^0\chi_1^0}| \;\lesssim\; \{0.04, 0.06\}\,, \tag{4.38}$$

which through the r.h.s. of eq. (4.29b) yields a constraint for the combination $\xi_{12}+y-y_{12}$. The one-loop contributions have been calculated in refs. [82, 231]. We have worked out the formula given in Appendix A, for zero Yukawa couplings and $M_D \gg M_{W,Z}$, and we find

$$\delta Y^{h\chi_1^0\chi_1^0} = \left(\frac{3g}{8\pi}\right)^2\frac{\sqrt{2}M_Z}{v}\,\frac{M_D - M_Z}{M_D} \simeq 4\times10^{-3}\,. \tag{4.39}$$

[8] **Note added**: The updated bounds from LUX [100] and XENON [105] for this mass range is $\sigma_{\text{SI}} \simeq \{1-6\}\times10^{-46}$ cm^2 (see Fig. 1.3). Therefore, it is expected that $|Y^{h\chi_1^0\chi_1^0}|$ would be shifted towards smaller values (by a factor of ~ 3), resulting to a more restricted parameter space.

This is an order of magnitude smaller[9] than the current[10] LUX bound in eq. (4.38). In the limit $M_D \to \infty$, the model exhibits a non-decoupling behaviour, as expected from the EFT analysis of refs. [78, 103, 213]. On the other hand, for $M_D \to 0$ the one-loop contribution vanishes.

Based upon eqs. (4.29b) and (4.38) we obtain the inequality

$$|\xi_{12} + y - y_{12}| \;\leq\; \frac{1}{\sqrt{2}} \left(\frac{\Lambda}{v}\right) Y^{\rm bound}(m_{\chi_1^0}) \,, \tag{4.40}$$

where $Y^{\rm bound}(m_{\chi_1^0})$ is the bound of eq. (4.38). Eq. (4.40) sets strong bounds on the couplings ξ_{12} and/or y. Relevant to the cases depicted in Fig. 4.1 we obtain, for $\Lambda = 1$ TeV and $m_{\chi_1^0} \sim 100$ GeV the following constraints:

$$\begin{aligned}
&({\rm a,d}): \quad -0.16 \lesssim\; \xi_{12} \;\lesssim 0.16 \,, \\
&({\rm b}): \quad -\frac{16 + 200\, y}{100} \lesssim\; \xi_{12} \;\lesssim \frac{16 - 200\, y}{100} \,, \\
&({\rm c}): \quad -\frac{16 + 100\, y}{100} \lesssim\; \xi_{12} \;\lesssim \frac{16 - 100\, y}{100} \,.
\end{aligned} \tag{4.41}$$

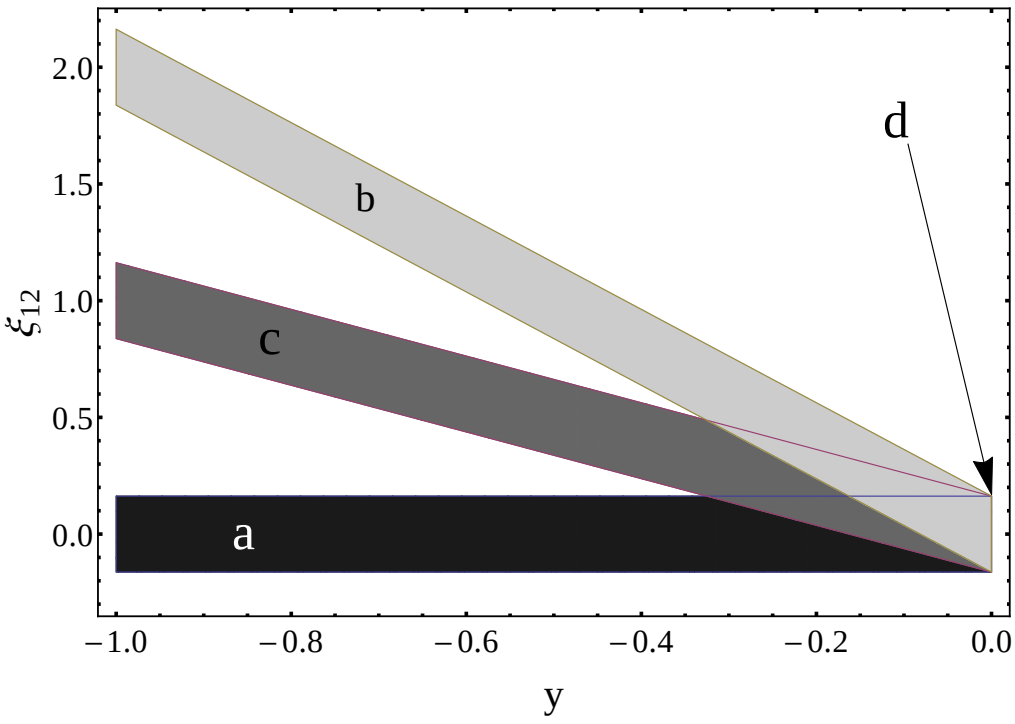

Figure 4.2: *Yukawa couplings y vs. ξ_{12} compatible with the bound of eq. (4.38) related to the LUX DM detection experiment, for the four cases of the mass spectrum and $\Lambda = 1$ TeV.*

[9] It is shown in ref. [216] that for next to leading order corrections in α_s, the SI cross section is even smaller.

[10] **Note added**: With the updated limits, the one-loop correction seems to be about 3–7 times below current sensitivity.

Therefore, *for $y \sim -1$, the parameter ξ_{12} is always positive* with a small variation band of about 10% w.r.t. the $|y|$ value due to the LUX bound. An example for the case (c) is shown in Fig. 4.2. For even bigger values of $|y|$, we obtain, ξ_{12} as big as $|y|$ for case (c) or as big as $2|y|$ in case (b). The band of the allowed values for ξ_{12}, e.g., the shaded area in Fig. 4.2, expands if we increase Λ.

Apparently, from eq. (4.21), if $y = 0$ we get $m_{\chi_1^0} = m_{\chi_2^0}$. In addition, if dipole operators of eq. (4.35) are present, severe bounds on d_γ and d_W can be set based on contribution to WIMP-nucleon cross section from $\gamma\,, Z$-exchange graphs [255–257]. In our case these bounds are avoided because we choose always $m_{\chi_2^0} - m_{\chi_1^0} \gtrsim 2$ GeV [244].

It is worth repeating here, that ξ_{12} is in principle positive everywhere for the cases (b,c), which means that essentially the charged particle $\chi^\pm$ is behaving as an extra lepton circulating in the $h \to \gamma\gamma$ loop decay process. Therefore, we expect that $R_{h\to\gamma\gamma}$ will be in general smaller than in the SM.

4.4.2 LEP bounds

Next we examine constrains from LEP, that although have been derived particularly for the MSSM, they can easily be adapted to this model. From Fig. 4.1 we observe that always, the next-to-lightest particle is the charged dark fermion $\chi^\pm$ with mass $m_{\chi^\pm} = M_D + \xi_{12}\,\omega$ that, as explained before, is assumed to be positive.

Depending on the mass difference between the lightest neutral particle $m_{\chi_1^0}$ and the charged one $m_{\chi^\pm}$, the bound on $m_{\chi^\pm}$ varies within ~ 90 GeV to ~ 100 GeV [249–251]. We will use the most conservative choice

$$m_{\chi^\pm} \;\gtrsim\; 100 \text{ GeV}\,, \tag{4.42}$$

which in terms of ξ_{12}, ω and M_D becomes:

$$\xi_{12} \;\gtrsim\; \frac{100 - M_D}{\omega}, \quad \forall\, y_{12}\,. \tag{4.43}$$

As we have seen, the bound from direct detection experiments implies a positive value on ξ_{12} for the cases (b,c). Thus, the LEP bound (4.43) is always satisfied if $M_D \gtrsim 100$ GeV. In the case where $M_D \lesssim 100$ GeV one may evade the LEP bound with a large positive ξ_{12}. For example, for $\Lambda = 1$ TeV and $M_D = 50$ GeV, we need, $\xi_{12} \gtrsim 1.7$. Interestingly, this may be compatible with (4.41) only in cases (b) and (c) with $\Lambda = 1$ TeV and certain values of y.

4.4.3 $h \to \gamma\gamma$

For the model under study, the ratio $R_{h\to\gamma\gamma} \equiv \frac{\Gamma(h\to\gamma\gamma)}{\Gamma(h\to\gamma\gamma)_{(\mathrm{SM})}}$ is given by [82] [see eq. (3.78)]. The ratio R is currently under experimental scrutiny at LHC. The current[11] combined value is $R_{h\to\gamma\gamma} = 1.15^{+0.28}_{-0.25}$ [258]. Note that the gluon fusion channel $gg \to h$, involved in the Higgs boson production at LHC, is not affected in the context of this model, since $\chi_i^0, \chi^\pm$ are uncoloured particles. In principle, there are $d = 6$ operators, such as $H^\dagger H\, G_{\mu\nu}\, G^{\mu\nu}$, but we assume that these are quite suppressed in comparison to the SM

[11] **Note added**: The updated result [221] is $R_{h\to\gamma\gamma} = 1.14^{+0.19}_{-0.18}$. From Fig 4.3, it seems that the minimum and maximum allowed values of ξ_{12} are slightly affected. As a result, y is restricted to be somewhat smaller (see Fig. 4.4), but our final results remain mostly unaffected.

contribution. An analogous operator exists in the case of $h \to \gamma\gamma$, just replacing $G^{\mu\nu}$ with the photon field strength tensor, $F^{\mu\nu}$ when integrated out heavy (of order bigger than Λ) particles. These operators arise at loop level and are suppressed by the scale Λ. Therefore, for the process $h \to \gamma\gamma$, the effect is dominated by the SM charged particles and the new $\chi^{\pm}$ circulating in the triangle diagram.

Below we study the ratio R in two complementary regions for M_D: a) $M_D \lesssim 100$ GeV and b) $M_D \gtrsim 100$ GeV.

- $\mathbf{M_D \lesssim 100}$ GeV

From eq. (4.29a) we expect that ξ_{12} would be restricted to small values from the loop induced $h \to \gamma\gamma$ bound, where we should also expect that, for M_D below 100 GeV, the bound from LEP will be important as we explained previously in Section 4.4.2.

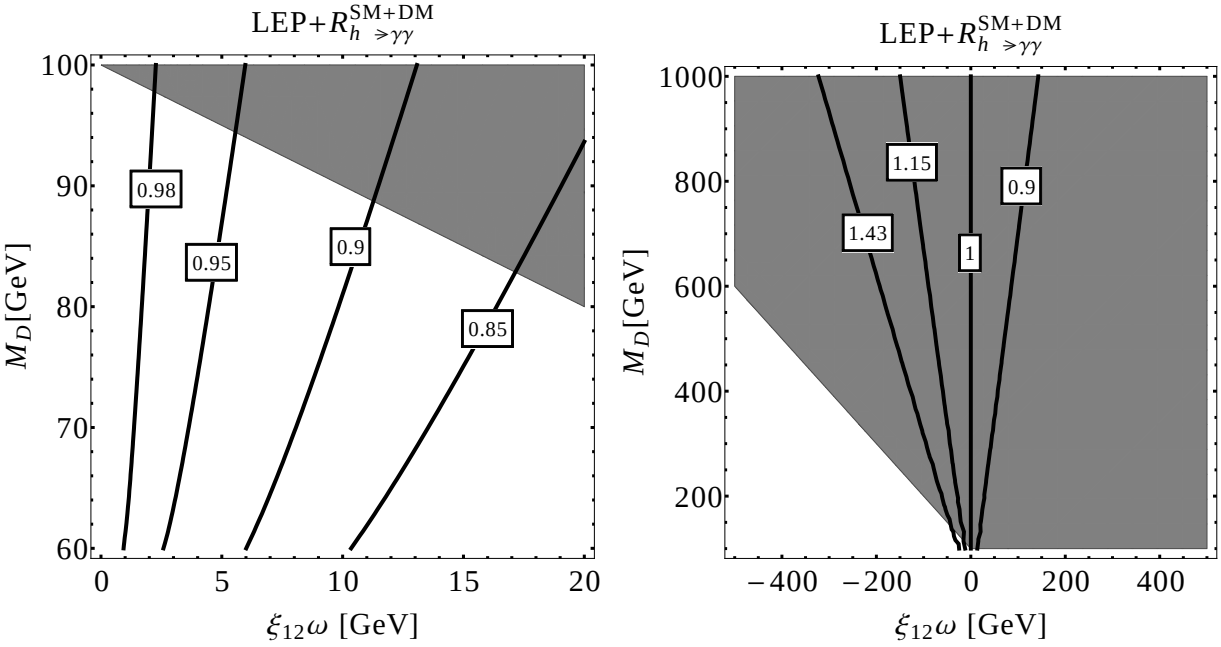

Figure 4.3: *Combination of the constraints from negative LEP "chargino" searches applied to $\chi^{\pm}$ and the ratio $R_{h\to\gamma\gamma}$ from LHC (Run I), for (a) $M_D \lesssim 100$ GeV and (b) $M_D \gtrsim 100$ GeV. The shaded region is compatible to the LEP $\chi^{\pm}$ bound, while the contours show the values of $R_{h\to\gamma\gamma}$ from eq. (3.78) on $\xi_{12}\,\omega - M_D$ plane.*

When $M_D \lesssim 100$ GeV, ξ_{12} should always be positive or zero in order to satisfy the LEP bound (4.43). Then the charged fermion behaves as an extra lepton and lowers the ratio R. This is clear from eqs. (4.29a) and (3.78). In addition, one can easily observe that, since LEP restricts $m_{\chi^{\pm}}$ to be above 100 GeV, the function $A_{1/2}(\tau = m_h^2/4m_{\chi^{\pm}})$ lies within the interval $\sim 1.5 - 1.3$. These observations lead us to another improved bound between ξ_{12}, ω and M_D, for the combined constraints from LEP and $R_{h\to\gamma\gamma}$:

$$100 - M_D \;\lesssim\; \xi_{12}\,\omega \;\lesssim\; 0.1\,M_D\,, \qquad \forall\, y_{12}. \tag{4.44}$$

Therefore, if $M_D \lesssim 100$ GeV, we obtain a minimum allowed value for M_D, which is around 90 GeV, as illustrated in Fig. 4.3(a). As a consequence, the case $M_D \lesssim 100$ GeV is disfavoured.

- $\mathbf{M_D \gtrsim 100}$ GeV

If $\xi_{12} > 0$, then eq. (4.44) still holds. The only difference from the previous case arises from eq. (4.43), which now allows ξ_{12} to be also negative. Consequently, for $\xi_{12} < 0$, the $R_{h\to\gamma\gamma}$ can be greater than unity and we obtain

$$\xi_{12}\,\omega \;\gtrsim\; -0.3\,M_D\,, \quad \text{or} \quad \xi_{12}\,\omega \;\gtrsim\; 100 - M_D\,, \quad \forall y_{12} \text{ and } \xi < 0. \tag{4.45}$$

Therefore, the combined result for $M_D \gtrsim 100$ GeV is:

$$-\,0.3\,M_D \;\lesssim\; \xi_{12}\,\omega \;\lesssim\; 0.1\,M_D \quad \text{and} \quad \xi_{12}\,\omega \;\gtrsim\; 100 - M_D\,, \quad \forall y_{12}. \tag{4.46}$$

This inequality is illustrated in Fig. 4.3(b). We notice that eq. (4.46) results in a very weak bound for $\xi_{12} < 0$ compared to the constraints from direct detection experiments, as can be seen in Fig. 4.2. Eq. (4.46) may nicely be combined in terms of the physical charged fermion mass $m_{\chi^\pm}$ and the "doublet" mass M_D as

$$0.7\,M_D \;\lesssim\; m_{\chi^\pm} \;\lesssim\; 1.1\,M_D\,. \tag{4.47}$$

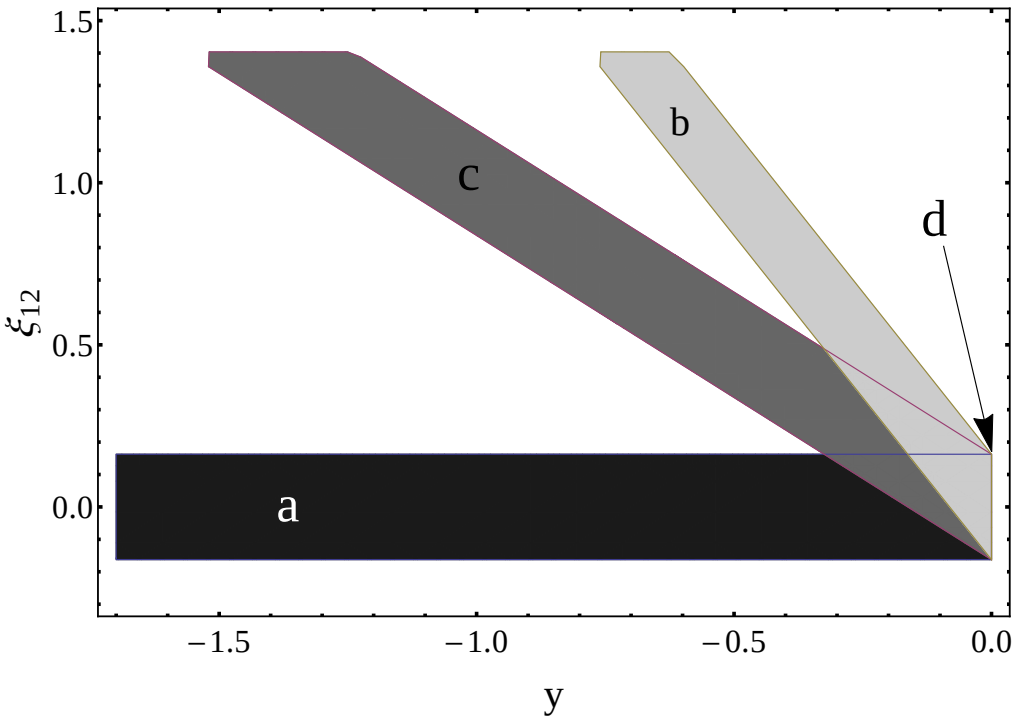

Figure 4.4: *y vs. ξ_{12} regions allowed by combining LEP, $R_{h\to\gamma\gamma}$ and DM direct detection constraints, for $\Lambda = 1$ TeV and $M_D = 300$ GeV for the four cases studied. Notice that case (d) is the intersection of the three other cases.*

Before moving on to the calculation of the relic density, we summarize the phenomenological constraints imposed to this model by LEP $\chi^\pm$ searches, the $h \to \gamma\gamma$ decay and the

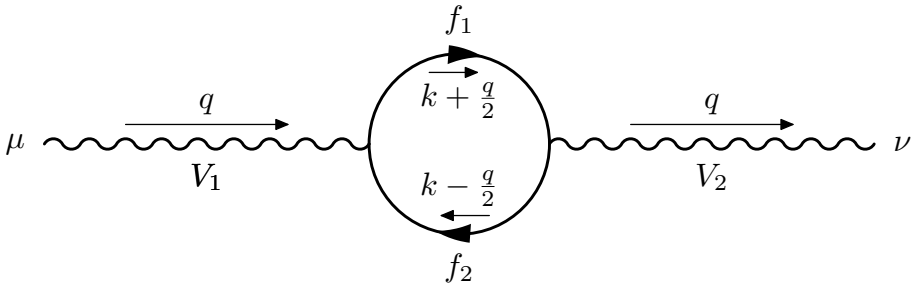

Figure 4.5: *The Feynman diagram contributing to the oblique parameters. $V_{1,2}$ represent the gauge bosons Z, W, or γ, while $f_{1,2}$ are $\chi^0_{1,2}$ and/or $\chi^{\pm}$.*

direct DM detection experiments. As can be seen from Fig. 4.4, these constraints confine the parameters y and ξ_{12} in small regions for given M_D and the cut-off of the theory. As discussed previously, M_D is always $\gtrsim 90$ GeV which is independent of the cut off. A general comment is that the bound imposed by the direct detection experiments in eq. (4.38) binds y and ξ_{12} together (and also forces ξ_{12} to be mostly positive).

4.4.4 Electroweak oblique corrections

In general, when one adds new matter into the SM particle content, with non-trivial gauge quantum numbers, severe bounds arise from the so-called oblique electroweak corrections. These loop corrections to electroweak precision observables are commonly parametrised by three parameters, S, T and U, introduced long ago in refs. [147, 259]. Even though the new matter fields $\mathbf{D_1}$ and $\mathbf{D_2}$ have common, vectorlike, mass M_D from eq. (4.1), there are mass splittings amongst the two doublets as well amongst their components themselves. These mass splittings arise from $d = 5$ operators in eq. (4.12) as discussed in the previous section.

In order to calculate the S, T and U parameters in the EFT at hand, we need to calculate vacuum polarization diagrams like the one depicted in Fig. 4.5, for all relevant interactions arisen from $d = 4$ and $d = 5$ operators given in Section 4.3.2. The general form of this diagram is

$$
\begin{aligned}
i\,\Pi^{\mu\nu}_{V_1V_2} = \int d^dk\mu^\epsilon \frac{(-1)}{(2\pi)^d} \frac{1}{\left[(k+\frac{q}{2})^2 - m_1^2\right]\left[(k-\frac{q}{2})^2 - m_2^2\right]} \times \\
\mathrm{Tr}\left[\left(a_{21}\gamma^\mu + \frac{b_{21}}{4\Lambda}[\not{q}, \gamma^\mu]\right)\left(\not{k} + \frac{\not{q}}{2} + m_1\right)\left(a_{12}\gamma^\nu - \frac{b_{12}}{4\Lambda}[\not{q}, \gamma^\nu]\right)\left(\not{k} - \frac{\not{q}}{2} + m_2\right)\right],
\end{aligned}
\tag{4.48}
$$

where μ is the renormalization scale, $\epsilon \equiv 4 - d$, $a_{12,21}$ and $b_{12,21}$ are the gauge and the dipole couplings for every possible $\{f_{1,2}\ ,\ V_{1,2}\}$ combination, where $V_{1,2}$ can be the gauge bosons Z, W, or γ and $f_{1,2}$ are $\chi^0_{1,2}$ and/or $\chi^{\pm}$.

If we express the fermion masses circulating in the loop as $m_{1,2} = M_D + c_{1,2}\, v^2/\Lambda$ and expand eq. (4.48) up to the order $\mathcal{O}(\Lambda^{-1})$ [12], the term proportional to $g^{\mu\nu}$ and its

[12] By doing so, one avoids the introduction of involved $d = 6$ operators. Their inclusion would lead to weak bounds on the corresponding Wilson coefficients (a related discussion can be found in ref. [260]).

derivative w.r.t. q^2 at $q^2 = 0$, read as

$$\Pi_{V_1V_2}(q^2=0) = \epsilon\,\frac{a_{12}a_{21}}{8\pi^2\Lambda}(c_1+c_2)v^2\;M_D\;\log\left(\frac{M_D^2}{\mu^2}\right)\xrightarrow{\epsilon\to 0}0\,, \tag{4.49a}$$

$$\begin{aligned}\frac{d}{dq^2}\Pi_{V_1V_2}(q^2=0) &= \frac{a_{12}a_{21}}{12\pi^2}\left[\log\left(\frac{M_D^2}{\mu^2}\right)+\frac{2}{\epsilon}-\gamma+\log(4\pi)\right]\\ &+\frac{1}{48\pi^2\,\Lambda M_D}\Bigg\{6M_D^2\,(a_{21}b_{12}+a_{12}b_{21})\left[\log\left(\frac{M_D^2}{\mu^2}\right)+\frac{2}{\epsilon}-\gamma+\log(4\pi)\right]\\ &\qquad+4a_{12}a_{21}(c_1+c_2)v^2\Bigg\}\,.\end{aligned} \tag{4.49b}$$

Using these equations and substituting for every combination of $\{f_{1,2}, V_{1,2}\}$, the a_{12}, a_{21}, b_{12}, b_{21} and c_1, c_2 in the expressions for the parameters S, T, and U [147], with the interactions given in Section 4.3.2, one obtains up to terms of $\mathcal{O}(1/\Lambda^2)$, that

$$S = -\frac{2}{3\pi}\,\frac{v^2\,y_{12}}{\Lambda\,M_D}\,,\qquad T=0\,,\qquad U=0\,. \tag{4.50}$$

These results have been checked independently using the analytical expressions of ref. [82] [see eq. (3.63)] and interactions from Section 4.3.2 keeping terms up to $1/\Lambda$. In addition, they have been verified numerically by taking the decoupling limit of the fermion triplet mass $M_T \gg M_D$ in ref. [82].

The parameter S measures the size of the new fermion sector *i.e.* the number of the extra $SU(2)_L$ irreducible representations that have been added in the model. In general, the contribution of degenerate fermions to the S-parameter is

$$S \sim \sum_{\text{new fermions}} (T^3_{(R)} - T^3_{(L)})\,, \tag{4.51}$$

where $T^3_{(L,R)}$ is the isospin of the left- and right-handed fermions. So, in a case similar to ours, where the fermions are nearly degenerate, the S-parameter takes the form

$$S \sim \sum_{\text{new fermions}} (T^3_{(R)} - T^3_{(L)}) + f(m_{\chi_1^0}, m_{\chi_2^0}, m_{\chi^+})\,, \tag{4.52}$$

where $f(m_{\chi_1^0}, m_{\chi_2^0}, m_{\chi^+})$ is a function that vanishes if the three masses are equal. Therefore, in our case, the $S-$parameter for two vector-like doublets would arise only from the mass differences, which means that S-parameter is proportional to the Yukawa couplings [13]. After performing the calculation, it turns out that

$$f(m_{\chi_1^0}, m_{\chi_2^0}, m_{\chi^+}) \propto \frac{\Delta m_{1^+} + \Delta m_{2^+}}{M_D}\,, \tag{4.53}$$

where $\Delta m_{i^+} \equiv m_{\chi_i^0} - m_{\chi^\pm}$. This is proportional to y_{12}, as can been seen in eq. (4.50). Furthermore, no magnetic dipole parameters d_γ or d_W are involved in S-parameter in (4.50) up to $\mathcal{O}(1/\Lambda^2)$, as also expected from dimensional arguments.

[13] The coupling ξ_{12} is just a universal shift to M_D and thus it does not contribute to the mass difference. Also, as it turns out, y does not appear in $\frac{d}{dq^2}\Pi_{V_1V_2}(q^2=0)$ (for every V_1 and V_2 combination). Only y_{12} contributes to the oblique EW parameters at the approximation in $1/\Lambda$.

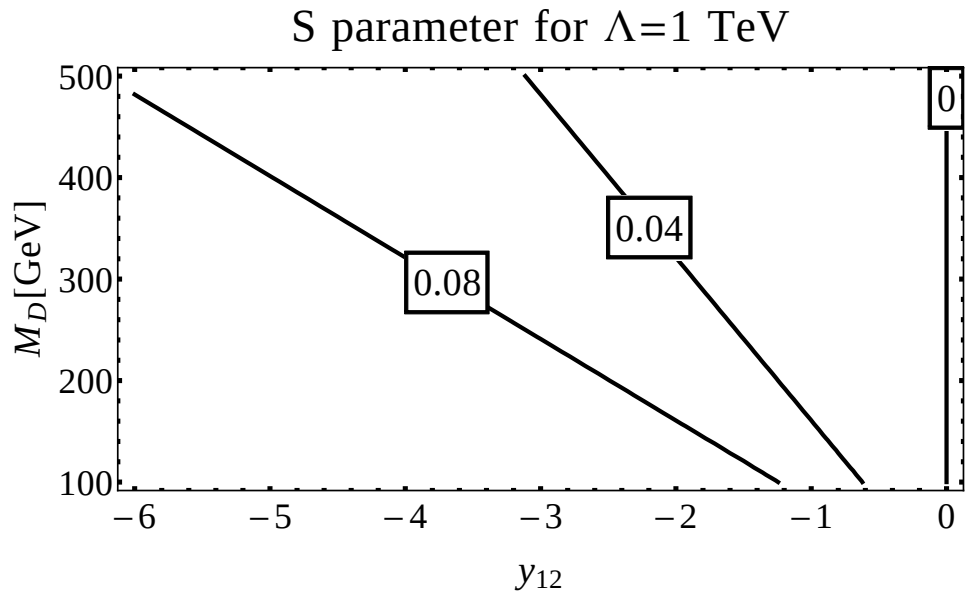

Figure 4.6: *Contours of the S-parameter on $y_{12} - M_D$ plane for $\Lambda = 1$ TeV.*

The $U-$parameter, on the other hand, measures the size of the isospin breaking contribution from the new fermions. So, it should be suppressed due to the c.c. (or custodial) symmetry (which limits the isospin breaking) and the fact that we are keeping only terms up to $1/\Lambda$. Up to this order, the parameter T is zero too, because $\Pi_{V_1V_2}(q^2 = 0) = 0$, a result which is independent of the symmetric limits for y_{12}. Usually, the parameters T and U are proportional to the ratio $\dfrac{\Delta m^2}{M_Z^2 \text{ or } M_D^2}$, where Δm^2 is some mass-squared difference arising from isospin breaking. In our model this should be the case when $y \neq 0$ and $y_{12} \neq 0$, which means that higher order terms could give a non-vanishing (but suppressed by terms $\propto \Lambda^{-2}$) contribution. Experimentally, S, T and U-parameters fit the electroweak data for $U = 0$ with values[14] [234]:

$$S = 0.00 \pm 0.08 \,, \qquad T = 0.05 \pm 0.07 \,. \tag{4.54}$$

In Fig. 4.6, we present a contour plot for the S-parameter obtained from eq. (4.50) as a function of y_{12} and M_D for $\Lambda = 1$ TeV. As expected, stronger (1σ) bounds from eq. (4.54) are obtained in the region $M_D \approx 100$ GeV, where it must be $|y_{12}| \lesssim 1$. On the other hand, relaxed bounds on $|y_{12}|$ are obtained for higher values of M_D and/or Λ.

Apparently the result of eq. (4.50), does not interfere with the bounds discussed before for the cases (b) and (c), since the allowed values of y_{12}, obtained from (4.54), are equivalent to those obtained by the combination of the DM direct searches, the $h \to \gamma\gamma$ decay and LEP $\chi^{\pm}$ bounds. On the contrary, in case (a) where $y = y_{12}$, the bounds on y arise only from the $S-$parameter.

[14] **Note added**: Updated constraints [60] for the S and T parameters (with fixed $U = 0$), show that the T-parameter deviates from zero at 1.5 σ. However, if we allow for non-vanishing U-parameter, $T = 0$ is allowed.

4.5 Cosmological and astrophysical constraints

In the context of this model, it is essential to calculate the DM relic density Ωh^2 of the dark fermion χ_1^0, in order to impose the cosmological constraint related to the Planck satellite measurements [234], as expressed in eq. (3.69). Assuming that χ_1^0 constitutes the DM of the universe, we are able to set severe constraints on the parameters of eq. (4.17), in conjunction to those found previously in Section 4.4. From now on we focus on benchmark cases (b) and (c) mainly because there is more freedom to move around the parameter space as compared to cases (a) and (d).

In this Section 1.3.3 we described briefly the freeze-out mechanism and discussed the solution of the Boltzmann equation. Here, we present general, analytical, predictions for $\Omega_\chi h^2$, aiming to understand its dependences, and then numerical solutions are discussed. Additionally, we study the constraints imposed by the gamma fluxes produced by DM annihilations in the galactic center (GC) [45, 46] and in various dwarf spheroidal satellite galaxies (dSph) [117]. Finally, at the end of this section, we briefly discuss neutrino fluxes from the Sun, which are constrained from IceCube experiment [127, 261].

4.5.1 A close look at the relic density

Before discussing the bounds imposed by the data on Ωh^2, it would be helpful to study the numerical values of the annihilation cross section that are used to calculate the relic abundance. As discussed in Section 4.4.3, if $M_D \gtrsim 90$ GeV, then the coupling to the Higgs boson is approximately zero. Therefore, the most important annihilation channels, assuming for the time being that coannihilation effects are irrelevant, are $\chi_1^0\chi_1^0 \to W^+W^-$, ZZ, γZ and $\gamma\gamma$. There are no final states with fermions, since their corresponding interaction vertices are absent. There are no $\chi_1^0\chi_1^0 Z/\gamma$ terms in the Lagrangian of eqs. (4.31) and (4.35), or they are restricted because of bounds by direct detection experiments $Y^{h\chi_1^0\chi_1^0} \approx 0$.

Keeping only the first term in the expansion of eq. (1.105) we obtain

$$a_{VV} = \frac{\beta_V^{3/2}\, m_{\chi_1^0}^2}{32\pi\, S_V\, v^2} \frac{\left[g^2v^4 - 4\,g\,v^2\omega\,K_V\left(m_{\chi_1^0}+m_\chi\right) + 4\,K_V^2\,\omega^2\left(2m_{\chi_1^0}m_\chi + M_V^2\right)\right]^2}{v^6\left(m_{\chi_1^0}^2 + m_\chi^2 - M_V^2\right)^2}, \tag{4.55}$$

where V denotes W and Z gauge bosons in the final states for the processes $\chi_1^0\chi_1^0 \to W^+W^-$ or $\chi_1^0\chi_1^0 \to ZZ$. Also, we abbreviate, $\beta_V \equiv 1 - M_V^2/m_{\chi_1^0}^2$, $K_W \equiv d_W$, $S_W \equiv 1$, $K_Z \equiv c_W\,(c_W d_W + s_W d_\gamma)$ and $S_Z \equiv 2\,c_W^4$. The mass m_χ denotes $m_{\chi^\pm}$ for $V = W$ and $m_{\chi_2^0}$ for $V = Z$.

For the channels γZ and $\gamma\gamma$, we find

$$a_{\gamma Z} = \frac{\beta_{\gamma Z}^3\, m_{\chi_1^0}^2}{2\pi\, c_W^2\, v^2} \frac{C_\gamma^2\,\omega^2\,\left[g\,v^2\left(m_{\chi_1^0}+m_{\chi_2^0}\right) - \omega\,K_Z\left(4m_{\chi_1^0}m_{\chi_2^0}+M_Z^2\right)\right]^2}{v^6\left[2\left(m_{\chi_1^0}^2+m_{\chi_2^0}^2\right) - M_Z^2\right]^2}, \tag{4.56a}$$

$$a_{\gamma\gamma} = \frac{m_{\chi_1^0}^4\, m_{\chi_2^0}^2\,\omega^4\, C_\gamma^4}{\pi\,(m_{\chi_1^0}^2 + m_{\chi_2^0}^2)^2\, v^8}, \tag{4.56b}$$

with $\beta_{\gamma Z} \equiv 1 - M_Z^2/4m_{\chi_1^0}^2$ and $C_\gamma \equiv (c_W d_\gamma - s_W d_W)$. These channels $\gamma\gamma$ and γZ, contribute to the monochromatic gamma fluxes from the GC. Thus, in conjunction to the

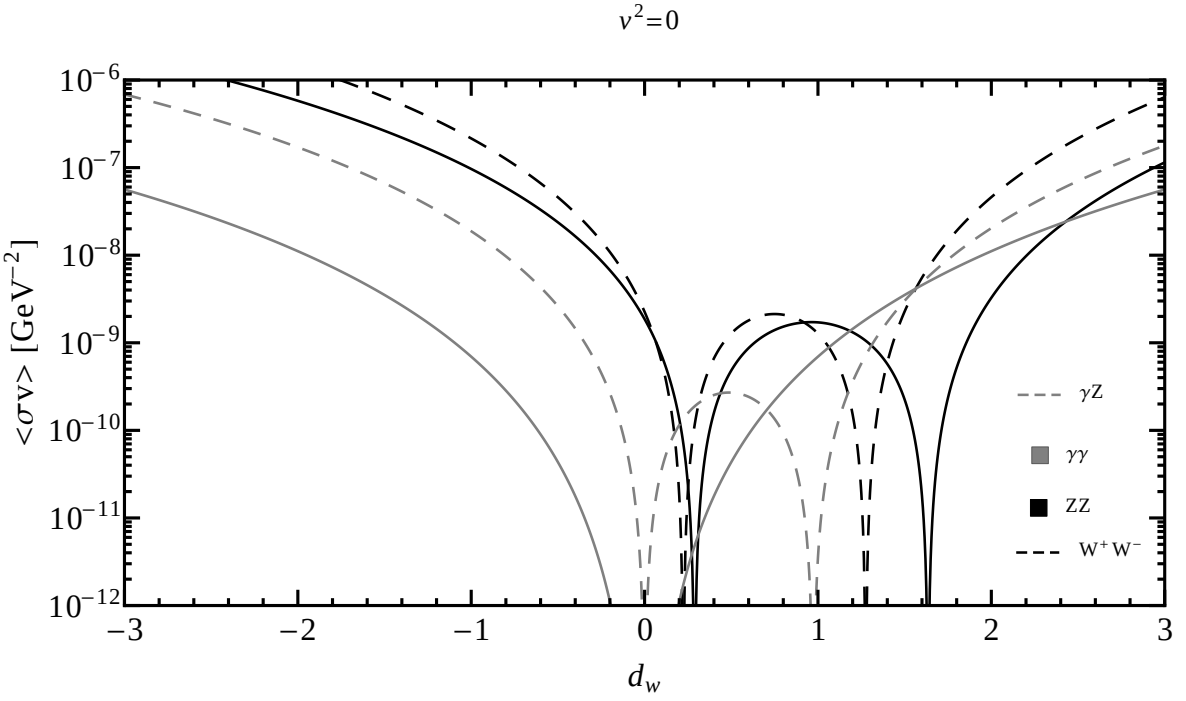

Figure 4.7: *The dependence of different annihilation channels on d_W for $M_D = 400$ GeV, $\Lambda = 1$ TeV, $y = -y_{12} = -\frac{\xi_{12}}{2} = -0.8$ and $d_\gamma = 0$. Notice that, in a certain range of d_W values, there is at least one dip for each channel cross section.*

corresponding bounds from Fermi-LAT experiment, one gets severe constraints for the coupling C_γ. Due to absence of χ_1^0 couplings to Z and γ and the nearly vanishing Higgs mediated $\hat{s}$-channel, all the above processes arise from $\hat{t}$ and $\hat{u}$ channels.

Eqs. (4.55), (4.56a) and (4.56b), contain one or more solutions with respect to d_W. This means that d_W could act as a regulator that minimizes the total annihilation cross section as the (required) low mass M_D tends to amplify it (generally the cross section scales as M_D^{-2} if we ignore magnetic dipole interactions). This minimization, will be proved essential when trying to obtain cosmologically acceptable relic abundance at the electroweak scale.

Qualitatively, concerning the minimum of the *total* annihilation cross section as a function of the dipole couplings one anticipates that each cross section should be minimized for almost the same value of d_W, in order for the *total* annihilation cross section to be at its minimum. In addition, $d_\gamma \approx \frac{s_W}{c_W} d_W$ so that C_γ is quite small. This keeps d_γ from obtaining large negative values, because a_{WW} can be minimized only for $d_W > 0$.

A numerical example is shown in Fig. 4.7. We observe that there are two minima for the annihilation cross sections to ZZ, W^+W^- and γZ and one minimum for $\gamma\gamma$. The first minimum of a_{ZZ} and a_{WW} coincides with the vanishing point of C_γ, which gives small cross sections for $\chi_1^0\chi_1^0 \to \gamma\gamma$ and γZ. On the other hand, the second minimum of a_{ZZ} and a_{WW} is in a region where the annihilation to $\gamma\gamma$ and γZ blows up. Furthermore, for negative d_W, there are no such minima and, as can be seen from Fig. 4.7, every cross section becomes quite large.

Since eq. (1.111) is an approximation which could lead to an error up to $\sim 10\%$ (as discussed in ref. [59]), the Boltzmann equation must be solved numerically. To do this we implement the $d = 4$ and $d = 5$ operators to the computer program microOMEGAs [262]

via the LanHEP [263] package[15] in order to obtain more accurate results for the relic abundance.

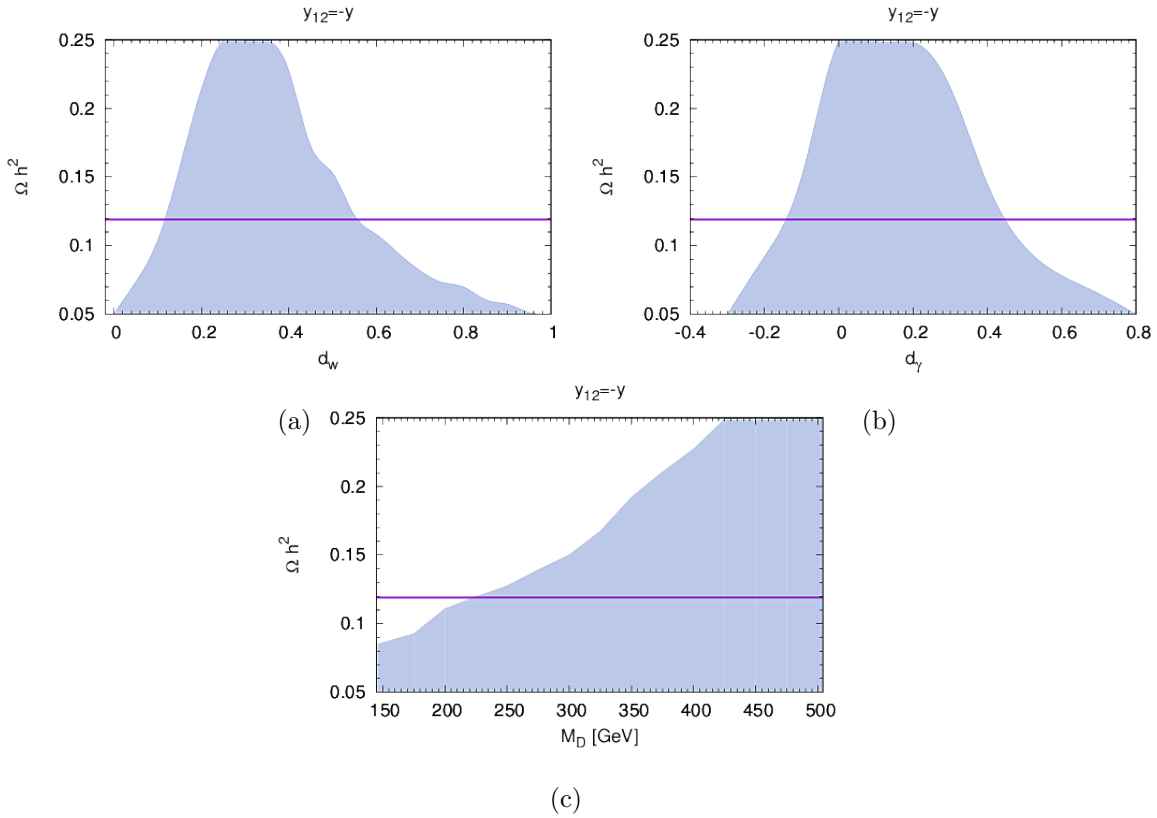

Figure 4.8: *Relic abundance dependence on the parameters* (*a*) d_W, (*b*) d_γ, *and* (*c*) M_D, *for* $\Lambda = 1$ TeV *and* $y_{12} = -y$. *The cosmologically allowed (shaded) region corresponds to the variation of the other parameters in* (4.17) *not shown in the plot. The horizontal line stands for* $\Omega h^2 = 0.12$.

In Figs. 4.8a, 4.8b and 4.8c we examine the dependence of the relic abundance Ωh^2 on the parameters, d_W, d_γ and M_D, respectively. Because all parameters in (4.17), run freely, the corresponding plots are given as shaded areas in Fig. 4.8. We remark that: *a)* The minimization effects on the various cross sections discussed before, are evident in the numerical results too. *b)* As expected, when M_D increases, Ωh^2 increases too. *c)* For acceptable Ωh^2 and M_D of a few hundred GeV, d_W must lie in the region $0.1 \lesssim d_W \lesssim 0.5$, which does not include the zero node. The dipole moment to photon d_γ should be in the region $-0.2 \lesssim d_\gamma \lesssim 0.5$, which includes the zero node. *d)* The minimization of the total annihilation cross section, is not enough to produce the observed DM density for $M_D \lesssim 200\,\text{GeV}$.

[15] More information about these packages can be found in https://lapth.cnrs.fr/micromegas/ and http://theory.sinp.msu.ru/~semenov/lanhep.html.

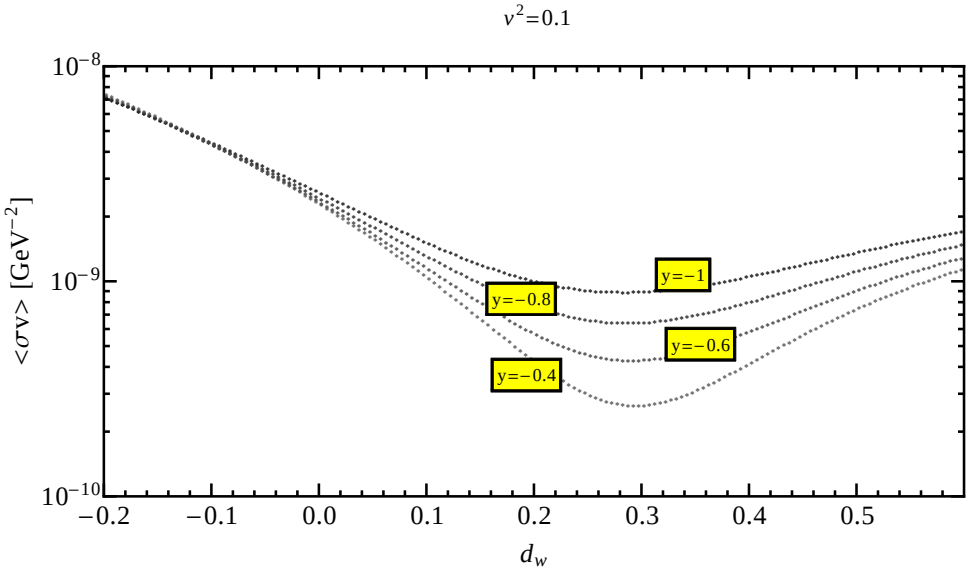

Figure 4.9: *ZZ annihilation cross section dependence on d_W for different values of $y = -y_{12} = -\frac{\xi_{12}}{2}$, $\Lambda = 1$ TeV, $M_D = 400$ GeV, $d_\gamma = 0$ and $v^2 = 0.1$. At the minimum, the values of the cross section decreases as we lower the values of $|y|$. The behaviour of the W^+W^- annihilation channel is similar.*

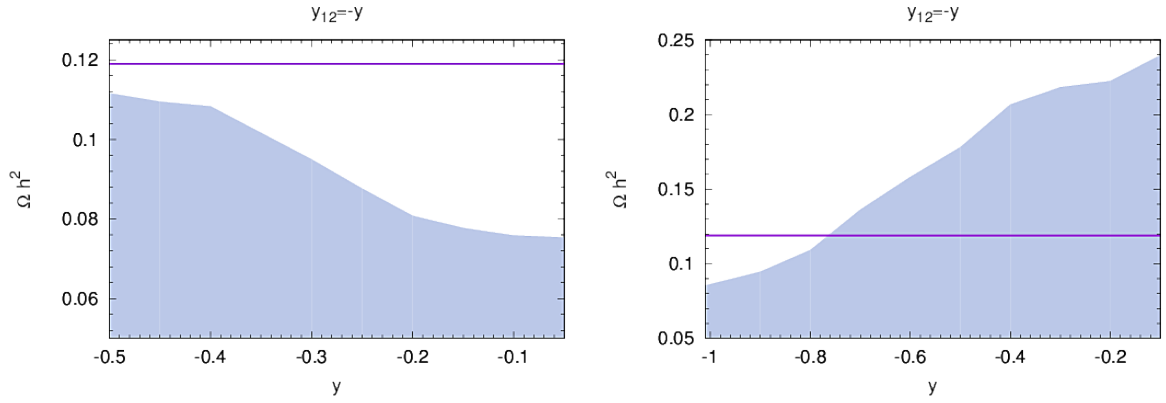

(a) (b)

Figure 4.10: *y vs. Ωh^2, for $\Lambda = 1$ TeV and (a) $M_D = 200$ GeV and (b) $M_D = 400$ GeV. Other parameters from the list (4.17) vary in the range constrained from "Earth" constraints and for $y_{12} = -y$. The dependence of the relic density on y changes for different values of M_D.*

The dependence of the relic density on the parameter y is complicated due to the following competing effects: The coannihilation channels, increase the total annihilation cross section as $|y|$ tends to zero, since the mass differences of the initial particles involved become smaller and smaller. But, as shown in Fig. 4.9, the $b-$term in the expansion of eq. (1.105), tends to decrease the value of the cross sections (around the minimum), at least for the annihilation to ZZ and W^+W^-.

Moreover, in Fig. 4.10 we study the dependence of Ωh^2 on y, for various values of the mass M_D. In the region $M_D \lesssim 260$ GeV, the relic abundance becomes smaller for

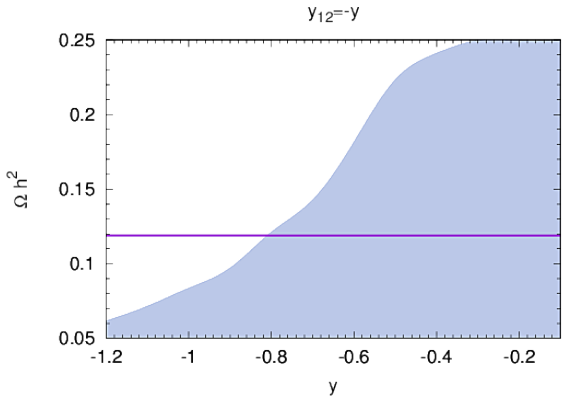

Figure 4.12: Ωh^2 *versus* y*, for* $y_{12} = -y$*,* $\Lambda = 1$ TeV *and* $M_D \leq 500$ GeV*. The shaded area and the curves are as in Fig. 4.8.*

smaller y (an example for $M_D = 200$ GeV is shown in Fig. 4.10a), which means that the coannihilation effects dominate over the $b-$term, and vice-versa for larger values of M_D (Fig.4.10b).

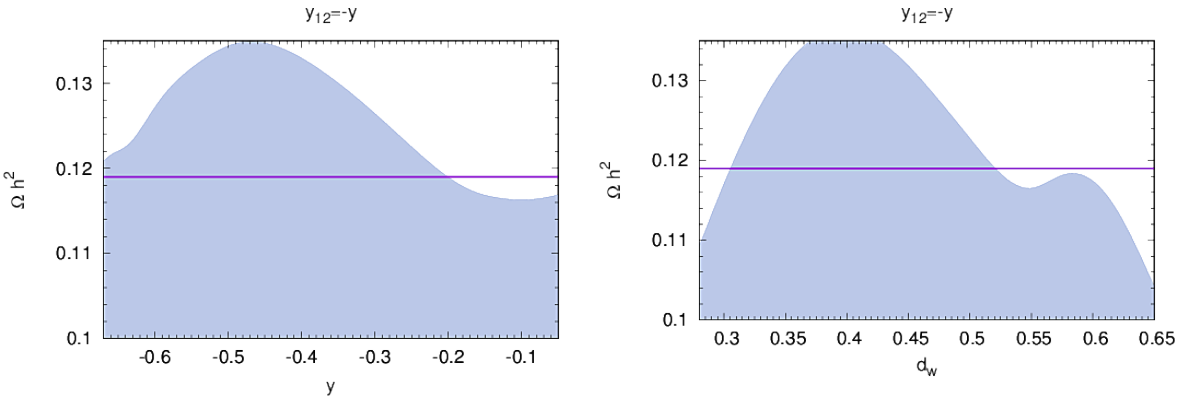

(a) (b)

Figure 4.11: *Turning point as can be seen in (a)* y *versus* Ωh^2 *and (b)* d_W *versus* Ωh^2*, for* $y_{12} = -y$*,* $\Lambda = 1$ TeV *and* $M_D = 260$ GeV*. The shaded area and the curves are as in Fig. 4.8.*

There is a small region at $M_D \approx 260$ GeV where this dependence is mixed. We call this value of M_D *"turning point"*. An example of this behavior is shown in Fig.4.11a. As we can see, the relic abundance rises until $y \sim -0.4$ and then decreases, but for $y \sim -0.06$ it starts to increase again. Also, as shown in Fig. 4.11b, we obtain two maxima for Ωh^2 with respect to d_W, as a result of this effect, since the value of d_W which minimizes the annihilation cross section depends on y.

Although y has no definite effect on Ωh^2, the relic density increases as M_D increases. Therefore, if we calculate the relic density in the allowed parameter space, the dependence of the relic on y would be dominated by its dependence for larger M_D. In Fig. 4.12, we show the dependence of Ωh^2 on y. The relic density decreases as $|y|$ becomes larger and for $|y| \gtrsim 0.9$ the DM becomes under-abundant.

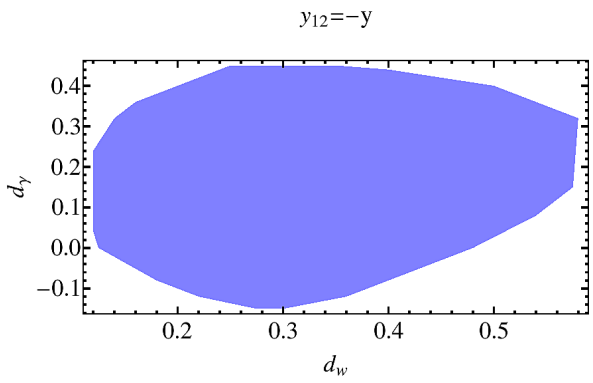

Figure 4.13: *The plane $d_W - d_\gamma$ of the parameter space that gives the observable relic abundance, for $\Lambda = 1$ TeV and $y_{12} = -y$. The same region holds also for $y_{12} = 0$. We allow variation of other parameters in* (4.17) *consistently with observational data.*

Finally, the case where $y_{12} = 0$ yields similar results with the case $y_{12} = -y$ just discussed, as can be deduced from Figs. 4.8 and 4.12. Also, for other values of the cut-off scale Λ, the parameters $d_{\gamma,W}$ and y should be rescaled in order for the ratios d_W/Λ, d_γ/Λ and y/Λ to remain unchanged.

4.5.2 Cosmological constraints due to relic density

Having studied the constraints from *LEP*, $R_{h\to\gamma\gamma}$, the direct detection DM experiments as well as the Planck satellite bound on the relic density for this effective theory, we are able delineate the cosmologically acceptable regions of the parameter space. For this reason, we perform a combined scan in the so far allowed parameter space which is also cosmologically preferred, for the cases $y_{12} = -y$ and $y_{12} = 0$ at $\Lambda = 1$ TeV. First, for $\Lambda = 1$ TeV, in Fig. 4.13 we display the part of the $d_\gamma - d_W$ plane, that is compatible to the DM relic density, varying all the other parameters, but keeping $M_D \lesssim 500$ GeV. Apparently the parameter d_W is bounded to be positive in order to explain the DM relic abundance for a WIMP mass at electroweak scale. Also, the region where d_γ is positive, is larger than the region where it is negative, a situation explained in the preceding analysis. A similar region is also found for $y_{12} = -y$ and $y_{12} = 0$.

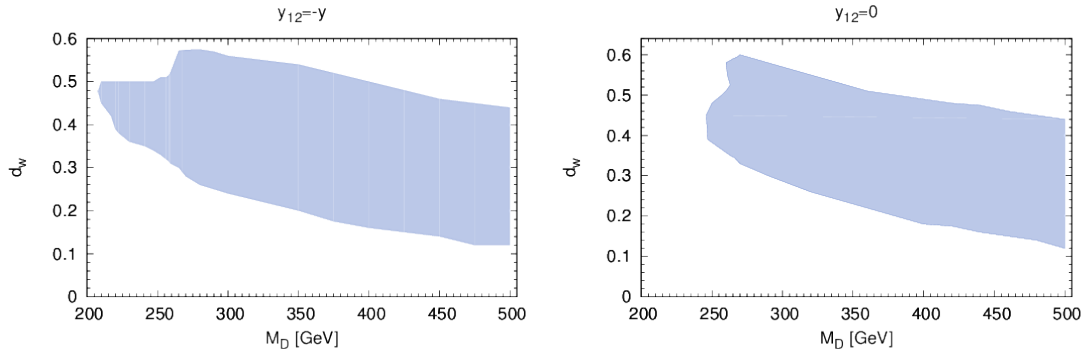

(a) M_D vs d_W, for $\Lambda = 1$ TeV and $y_{12} = -y$. (b) M_D vs d_W, for $\Lambda = 1$ TeV and $y_{12} = 0$.

Figure 4.14: *As in Fig. 4.13 but for acceptable values on the plane $M_D - d_W$.*

In Fig. 4.14 we observe that M_D vastly affects the allowed values for d_W that provide the correct relic abundance. This is due to the fact that the minimum of the total annihilation cross section depends on the mass M_D, as can be seen from eqs. (4.55), (4.56a) and (4.56b) and also from the fact that the maximum of Ωh^2 varies as M_D changes, see also Fig. 4.8c. Moreover, as M_D becomes larger, the minimization of the cross section becomes less necessary. Note that, for $y_{12} = 0$ there is a gap for d_W at $M_D \approx 260$ GeV, a result of the "turning point" discussed at the end of the previous paragraph (see Fig. 4.11b). For $y_{12} = -y$, this "turning point" is ineffective.

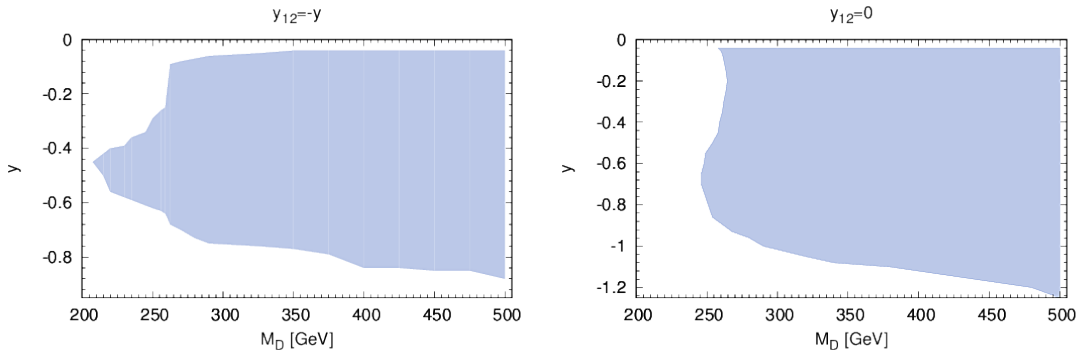

(a) M_D vs y, for $\Lambda = 1\ TeV$ and $y_{12} = -y$. (b) M_D vs y, for $\Lambda = 1$ TeV and $y_{12} = 0$.

Figure 4.15: *Values on $M_D - y$ plane that provide acceptable DM relic abundance.*

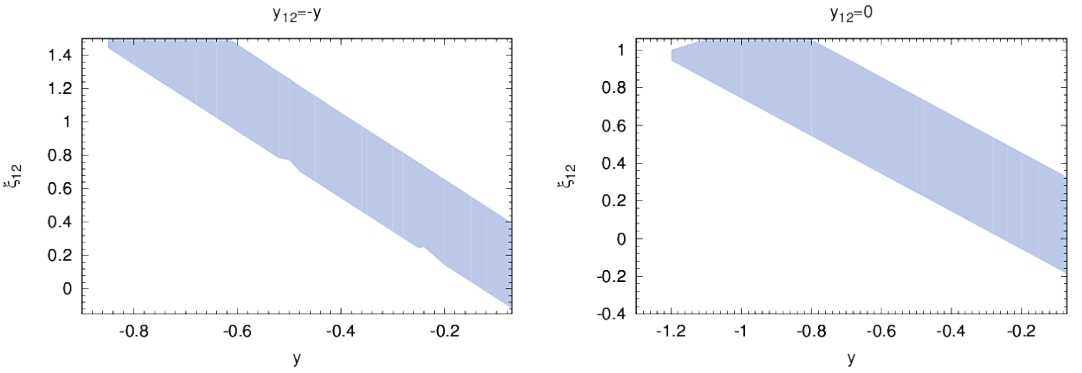

(a) y vs ξ_{12}, for $\Lambda = 1$ TeV and $y_{12} = -y$. (b) y vs ξ_{12}, for $\Lambda = 1$ TeV and $y_{12} = 0$.

Figure 4.16: *As in Fig. 4.15, but for the Yukawa parameters $y - \xi_{12}$.*

In Fig. 4.15 one can see the dependence of M_D on y, in the region where the DM density complies the current cosmological bound. We observe that for large values of M_D, for $|y| < 0.85(1.25)$ for the case $y_{12} = -y$ ($y_{12} = 0$) we obtain the desired Ωh^2. On the contrary, when $M_D \lesssim 300$ GeV in both cases for y_{12}, $|y|$ seems to be strongly dependent on M_D. This happens because the bound on $|y|$ from Earth-based experiments becomes stronger than the one from the relic abundance for smaller masses. In addition to that, since Ωh^2 tends to decrease as $|y|$ becomes smaller for $M_D \lesssim 260$ GeV, $|y|$ is also bounded from below. Furthermore, due to the "oscillation" of the relic abundance (Fig. 4.11a), at $M_D \sim 260$ GeV there is a "gap" on the allowed values of y (similar to d_W). Additionally, in Fig. 4.16, we see that ξ_{12} follows y, a remaining result from the direct detection bound

(similar to Fig. 4.2).

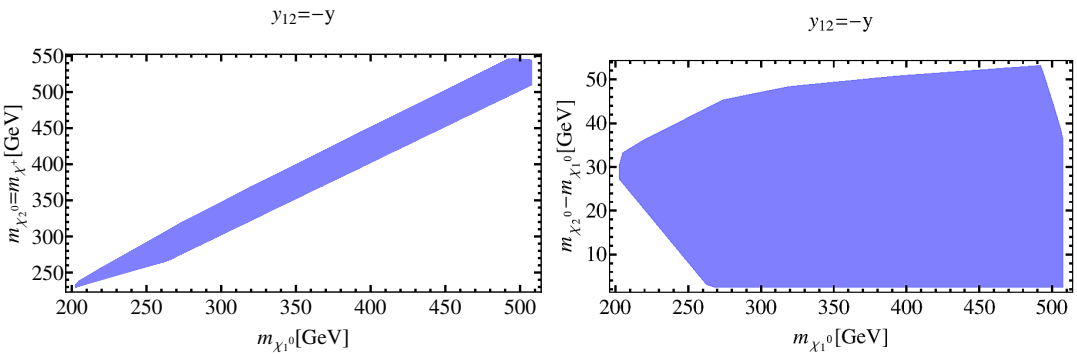

(a) (b)

Figure 4.17: *(a) The cosmologically allowed mass of the WIMP versus the mass of the heavy fermions and (b) their mass difference for $y_{12} = -y$. Similar regions can be obtained for $y_{12} = 0$.*

The Yukawa couplings and the mass parameter M_D displayed, fix the masses and their differences. For the sake of completeness, the masses and their difference from $m_{\chi_1^0}$ are shown in Fig. 4.17 for $y_{12} = -y$ (similar region holds also for $y_{12} = 0$). We observe that $m_{\chi_1^0} \gtrsim 200$ GeV, for $y_{12} = -y$, which is also what one should expect from Fig. 4.15. In addition to this, the mass difference $m_{\chi_2^0} - m_{\chi_1^0}$ is in the region $\sim 2 - 50$ GeV. Finally, we note that this mass difference takes slightly larger values ($\sim 2 - 70$ GeV) for the other case of the symmetric limit for y_{12}, while $m_{\chi^\pm} - m_{\chi_1^0}$ is always half that [see eq. (4.21)]. Accordingly, the smallest possible mass of the WIMP in this case is ~ 250 GeV (which again can be seen also from Fig. 4.15).

4.5.3 Gamma-rays

Having delineated the cosmologically acceptable regions concerning the DM abundance, we will proceed calculating other astrophysical observables, like the gamma-ray fluxes (monochromatic and continuous) originating from the Milky Way GC and dSphs.

Continuous Gamma spectrum

In our model the DM pair annihilation cross sections have been studied in Section 4.5.1. In particular, the relevant relations can be found in eq. (4.55). From refs. [117, 264] we observe that the bounds on the cross sections a_{ZZ} and a_{WW} are above the required $\sim 3 \times 10^{-26}$ cm^{3}s^{-1} (for masses above 200 GeV) which generally gives the desired relic abundance. More precisely, for $m_{\chi_1^0} \gtrsim 200$ GeV, the bound from dSphs is below $\sim 5 \times 10^{-26}$ cm^{3}s^{-1} for the annihilation $\chi_1^0\chi_1^0 \to W^+W^+$ (assuming that the branching ratio is 100%). The same bound holds the annihilation to a pair of Z-bosons, since their gamma spectra are quite similar. When applied to our model, which generally gives smaller branching ratios, these bounds should be even weaker.

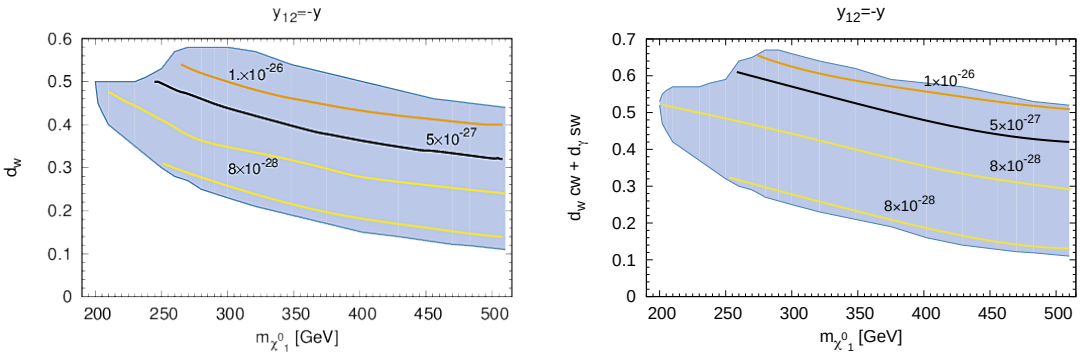

(a) (b)

Figure 4.18: *Allowed region in the parameter space from collider, DM direct detection and relic density constraints discussed in sections 4 and 5.3, respectively, as a function of the WIMP mass and the couplings d_W and K_Z/c_W. The contours show the values of the thermally averaged cross sections (a) for a_{WW} and (b) for a_{ZZ} in* $\mathrm{cm}^3\mathrm{s}^{-1}$ *for $y_{12} = -y$. Similar for $y_{12} = 0$. We take $\Lambda = 1$ TeV.*

As it is shown in Fig. 4.18, the relevant to continuous emission of photons cross sections, $\sigma_{\chi_1^0\chi_1^0 \to W^+W^-, ZZ}$ are safe with experimental bounds from continuous gamma ray spectrum discussed in this paragraph.

Constraints from Gamma-ray monochromatic spectrum

As we have seen, this effective theory relies on the various WIMPs magnetic dipole moment operators in order to give us the observed relic abundance. This could result to annihilations of pairs of WIMPs into photons which could be detectable from observations of gamma ray monochromatic spectrum originated from the GC. In this paragraph, we will calculate the cross sections for processes that could give such gamma rays [eqs. (4.56a) and (4.56b)]. As input, we use the parameter space that evade all the other, previously examined, bounds and use the results[16] from Fermi-LAT [45, 46] to set additional bounds to the parameters of this model. These bounds depend strongly on the DM halo profile[17] (and the region of interest) that one follows. Thus, we study the profile which gives the strongest bound. This comes from the $R3$ region which is optimized for the Navarro-Frenk-White NFWc($\gamma = 1.3$) profile [265] (the relevant discussion on these regions of interest is found in [45]). So, the annihilation cross section for $\chi_1^0\chi_1^0 \to \gamma\gamma$ for this region of interest is bounded to be smaller than $\sim 10^{-28}\ cm^3 s^{-1}$ for photon energy ($E_\gamma = m_{\chi_1^0}$) at 200 GeV up to $\sim 3.5 \times 10^{-28}$ for $E_\gamma \sim 450$ GeV (and if we extrapolate up to $\sim 5 \times 10^{-28}$ for $E_\gamma \sim 500$ GeV). For the process $\chi_1^0\chi_1^0 \to \gamma Z$, we need to rescale this bound by a factor of two, since there is one photon in the final state instead of two. This process results to different value of $E_\gamma = m_{\chi_1^0}\,(1 - m_Z^2/4m_{\chi_1^0}^2)$.

Fig. 4.19 illustrates that the annihilation to γZ (and less to $\gamma\gamma$), violates the Fermi-LAT bound, mainly for larger values of E_γ. Thus, the values of d_W and d_γ are constrained so that C_γ is even smaller than the cosmologically acceptable values.

[16] **Note added**: Results from H.E.S.S. (ref. [120]) are in agreement with the ones from Fermi-LAT.
[17] The bounds have up to a factor of 15 difference for different profiles and regions.

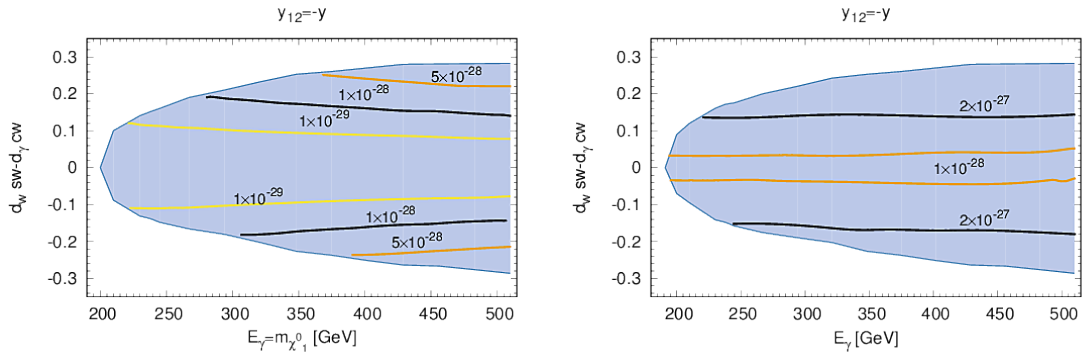

(a) (b)

Figure 4.19: *The allowed, as in Fig. 4.18, region of the parameter space, in terms of the photon energy and the coupling C_γ. The contours show the values of the thermally averaged cross sections $a_{\gamma\gamma}$ (a) and $a_{\gamma Z}$ (b) in $cm^3 s^{-1}$ for $y_{12} = -y$. Again $y_{12} = 0$ results in an almost identical plot.*

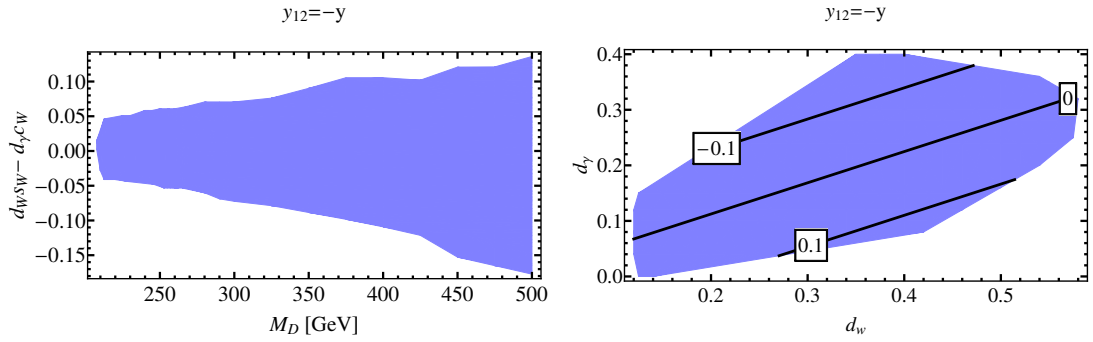

(a) (b)

Figure 4.20: *Allowed regions on a) $M_D - C_\gamma$ plane and b) $d_W - d_\gamma$ plane for $y_{12} = -y$, consistent with "Earth" constraints, the observed relic abundance and the bounds from gamma-ray monochromatic spectrum, discussed sections 4, 5.3 and 5.4.2, respectively, in the text. Almost identical regions are allowed for $y_{12} = 0$. The contour lines in (b) show the value of the $\chi_1^0\chi_2^0$-photon coupling C_γ.*

It is evident from Fig. 4.20a, that in order this model to deceive the current monochromatic gamma ray bounds from GC, we should limit the dipole couplings so they satisfy the relation $|d_W s_W - c_W d_\gamma| \lesssim 0.05$ ($\Lambda = 1$ TeV) for $M_D = 200$ GeV up to $|d_W s_W - c_W d_\gamma| \lesssim 0.15$ for $M_D = 500$ GeV. Therefore, one can delineate accordingly the parameter space on the $d_W - d_\gamma$ plane, that evades all bounds and yields the correct relic density, which is shown in Fig. 4.20b. It should be noted, that the other parameters remain unchanged as in the previous section, since they do not affect WIMP pair annihilation rates to two photons or to a photon and a Z-boson. Other values of y_{12} result to almost identical regions to these in Fig. 4.20.

Concluding this paragraph, we note that the Fermi-LAT data set upper bounds to the annihilation cross section of two WIMPs into one or two photons, relating strongly the two dipole couplings, resulting to positive values for d_γ. Therefore, the two neutral particles

of the model have an almost zero coupling to photon ($C_\gamma \approx 0$), while the other parameters are intact.

It is worth pointing out that there is a non-relativistic non-perturbative effect, known as "Sommerfeld enhancement" [266], that can boost the annihilation cross section, sometimes even, by orders of magnitude. For the bi-doublet case here, it has been calculated in the literature and the results are shown in refs. [267–269]. As it turns out, for the masses we are considering here, this effect is non-important. It becomes only sizeable for WIMP, "higgsino-like" masses greater than about 1 TeV or so.

4.5.4 Neutrino flux from the Sun

Another interesting indirect signal could come from solar neutrino flux. The cross section for neutrino production from WIMP annihilations in the Sun, can be decomposed to the spin-dependent and spin-independent WIMP-nucleon cross sections. Therefore, such experiments compete with direct detection ones. Recent results from IceCube [261], show that the spin-independent cross section bound is relaxed as compared to the one obtained from direct detection experiments [253]. On the other hand, the latest spin-dependent cross section bound from solar neutrino flux [127], is much stronger than the one derived from LUX [270] for $m_{\chi_1^0} \gtrsim 200$ GeV. In our study, the spin-independent bound from IceCube is evaded, since the constraints from LUX have been introduced from the beginning of this analysis. In addition, due to the c.c. symmetry, the spin-dependent cross section vanishes, since $\chi_1^{0\dagger}\bar{\sigma}^\mu\chi_1^0 Z_\mu$ is odd under the transformation introduced in Section 4.2. Thus, these bounds, leave the allowed parameter space unaffected[18].

4.6 LHC searches

Having found that there is a viable area in the parameter space, which produces the observed DM relic abundance of the universe while avoiding all the other experimental and observational constraints, we move on to find out whether this theory can provide us with observational effects at the LHC. First, we calculate the cross sections for some channels at $\sqrt{\hat{s}} = 8$ TeV and compare them to the current bounds from LHC (Run I) and then we do the same at Run II with $\sqrt{\hat{s}} = 13$ TeV.

In this section we are looking at the mono-Z channel for which the experimental analysis is performed by ATLAS [271], the mono-W channel where we use the results from ATLAS [272] (a weaker bound is obtained from the analysis of CMS [273]), the hadronically decaying W/Z-boson channel searched for by ATLAS [274]. DM interacting with vector bosons can be probed by dijet searches through vector boson fusion as discussed in refs. [275, 276]. The analysis has been performed by ATLAS [153][19] (which gives a somewhat stronger bound than CMS [277]). Furthermore, there are mono-jet searches from CMS [278]. Finally, there is also the mono-photon channel searches [274, 279], but in our case it is not very important due to the Fermi-LAT bound discussed previously in Section 4.5.3.

We note that, for these processes, an extensive study has been performed in ref. [145]

[18] **Note added**: There are updated results for the spin-dependent cross section in ref. [104]. However, our result still holds, since the corresponding cross section vanishes in our case.

[19] The fermions considered here, do not contribute to the invisible decays of the Higgs boson, but bounds from ref. [153] still apply for a dijet + $\not{E}_T$ final state.

with singlet Dirac DM particle and for operators with dimension $d = 7$. However, in the analysis we perform here there are differences: *a)* The set of operators is different, since we consider Yukawa, dipole and renormalizable operators. These operators produce mass splittings between the Dark-sector fermions. In addition to this, the interactions with the gauge bosons come from both 3- and 4-point terms in the Lagrangian with different Lorentz structure than the $d = 7$ ones. *b)* The parameter space in which we calculate the cross sections for these processes, respects other experimental and observational constraints. In addition, for the dijet channel and at $\sqrt{\hat{s}} = 13$ TeV, another dedicated study has been performed in ref. [280]. Again our case is different because of the inclusion of $d = 4$ and 5 operators in the calculations of the LHC cross sections, while at the same time the parameter space is also constrained by all the other bounds discussed in sections 4.4 and 4.5.

4.6.1 LHC constraints at 8 TeV

In this paragraph we calculate the cross sections for the relevant channels at 8 TeV and compare them to the current bounds from LHC. The bounds we use throughout this analysis are:

- *Mono-Z*: $pp \to \chi_1^0\chi_1^0 + (Z \to l^+l^-)$, $l = e, \mu$, with cross section $\lesssim 0.27\, fb$ [271].
- *Mono-W*: $pp \to \chi_1^0\chi_1^0 + (W \to \mu\nu_\mu)$, with cross section $\lesssim 0.54\ fb$ [272].
- *Hadronically decaying Z/W*: $pp \to \chi_1^0\chi_1^0 + (W/Z \to hadrons)$, with $\sigma_{\not{E}_T + hadrons} \lesssim 2.2\ fb$ [274].
- *Dijet*: $pp \to \chi_1^0\chi_1^0 + 2\, jets$, with $\lesssim 4.8\ fb$ [153].
- *Mono-jet*: $pp \to \chi_1^0\,(\chi_2^0 \to \chi_1^0 + \nu\bar{\nu}) + jet$ with $\sigma_{\not{E}_T + jet} \lesssim 6.1\, fb$ [278].

The cross sections for the first four channels in the allowed parameter space are shown in Fig. 4.21. It is apparent that the current bounds of LHC for these processes cannot put any further restrictions to the allowed parameter space. On top of that, as M_D becomes larger, the cross sections decrease. There are two reasons for this. First, as M_D increases, the masses increase, and, second, the dipole moments d_W and d_γ relevant for the observed relic abundance, move to smaller values as M_D becomes larger (see Fig. 4.14), which reduces the interaction strength of the WIMP to the gauge bosons.

We should point out that we only calculate the cross sections of the hard processes (before showering, jet reconstruction, etc.).[20] This means that in general, the actual cross sections should be smaller than the ones we present here, since the cuts we are able to use for the hard processes are weaker than the cuts used in the experimental analyses.

The cross section for the mono-jet channel[21] is shown in Fig. 4.22a. Again, as it can be seen, the cross section is significantly smaller than the current bound from LHC. Additionally, similar to the other channels discussed here, as M_D increases, the cross section tends to decrease. But, since this cross section depends strongly on both the dipole moments, d_γ and d_W, and the Yukawa coupling y (through the branching ratio of $\chi_2^0 \to \chi_1^0 + \nu\bar{\nu}$), the shaded area is larger than the areas in Fig. 4.21, because the available values of y do not depend strongly on M_D (see Fig. 4.15). Also, it is apparent from Figs. 4.21 and 4.22(a), that for future DM searches at the LHC (for the model we study here), the mono-jet channel seems to be the most promising, since it could result to the largest number of

[20] For the calculation we use the program CalcHEP v.3.6 of ref. [281].

[21] We approximate this cross section by $\sigma_{pp\to\chi_1^0\chi_2^0} \times \sum_{i=e,\mu,\tau} BR_{\chi_2^0\to\chi_1^0\bar{\nu}_i\nu_i}$.

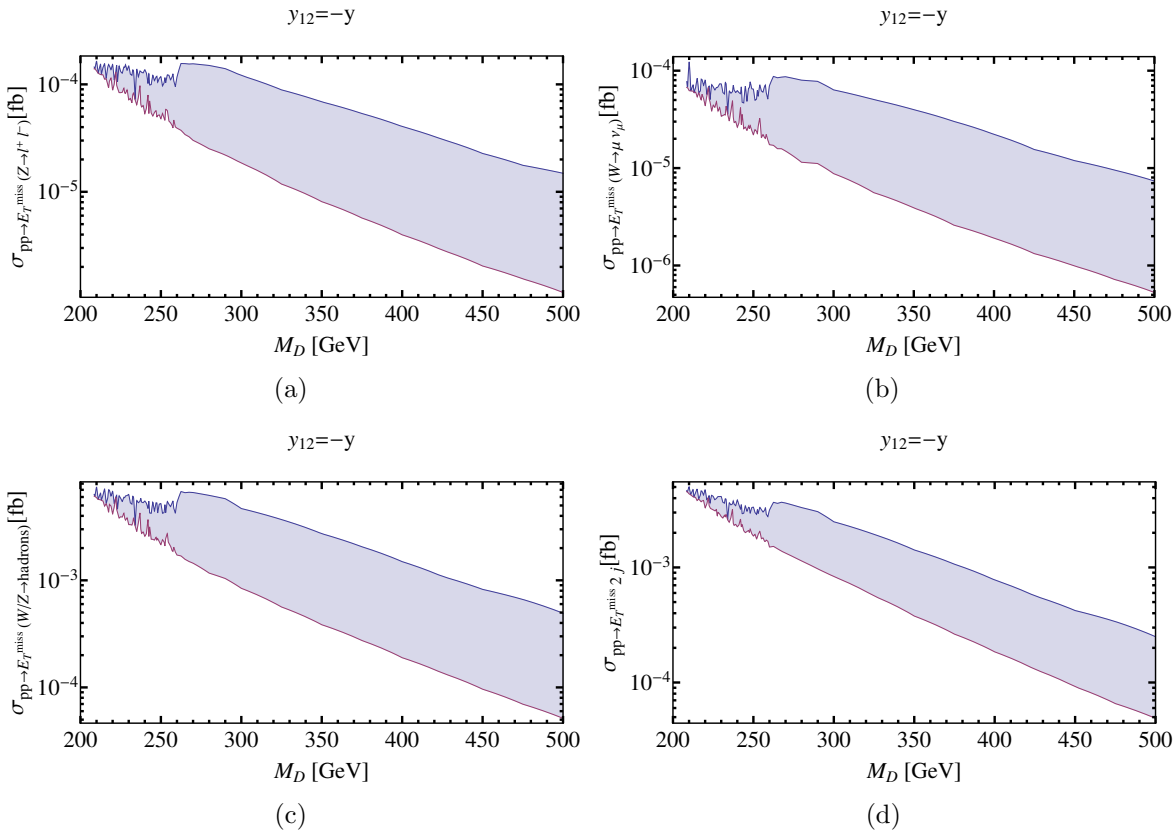

Figure 4.21: *The cross sections for the (a) mono-Z, (b) mono-W, (c) hadronically decaying Z/W and (d) the dijet processes at $\sqrt{\hat{s}} = 8$ TeV versus the doublet-mass parameter M_D, while all the other parameters run freely and for $y_{12} = -y$. The other case with $y_{12} = 0$ gives almost identical results. The "spikes" appeared is a result of varying a random selection of parameters.*

events compared to other channels discussed here.

4.6.2 Mono-jet searches at 13 TeV

For LHC (RunII) with $\sqrt{\hat{s}} = 13$ TeV, the mono-jet channel provides the biggest number of events when compared to other channels. From Fig. 4.22b, we observe that the production of a jet accompanied with missing E_T, can reach cross sections up to $\sim 2.5\, fb$ for both cases $y_{12} = 0$ and $y_{12} = -y$ and for $M_D \approx 300$ GeV. This means that the number of events that can, in principle, be observed [22] is around 250 (750) for LHC expected luminosity reach of 100 (300) fb^{-1}.

Before closing this section, we should remark issues about the validity of our calculations at such high center-of-mass energy. The validity of calculations for such theories at the LHC depends on the cut-off energy and the couplings. The energy for which the calculation of an observable becomes invalid is $\sim \Lambda/C$,[23] where C is the Wilson coefficient for the relevant operator. In our case, and for the mono-jet searches, the relevant $d = 5$ term (a

[22] Very recently, a mono-jet+photon search has been proposed in ref. [282]. Emphasised for higgsinos, this final state can often be as competitive as the monojet channel.

[23] This holds under the assumption that the couplings of the *UV complete* model are ~ 1.

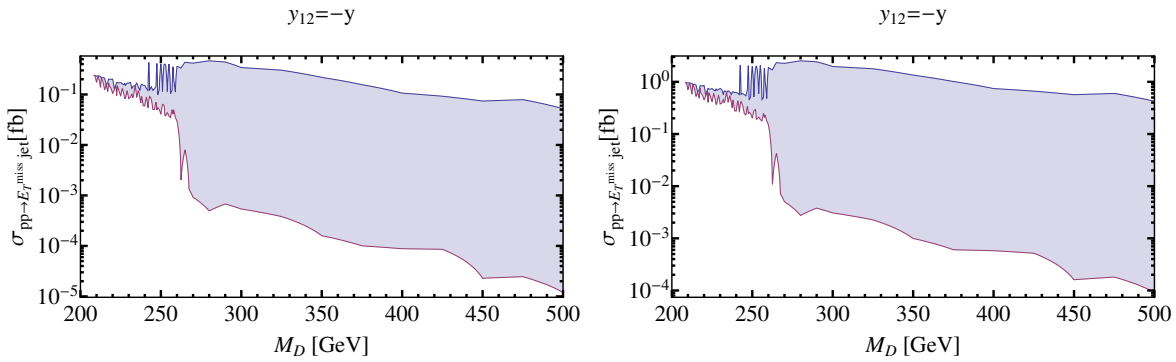

Figure 4.22: *As in Fig. 4.21 for the mono-jet channel with (a)* $\sqrt{\hat{s}} = 8$ TeV *and (b)* $\sqrt{\hat{s}} = 13$ TeV.

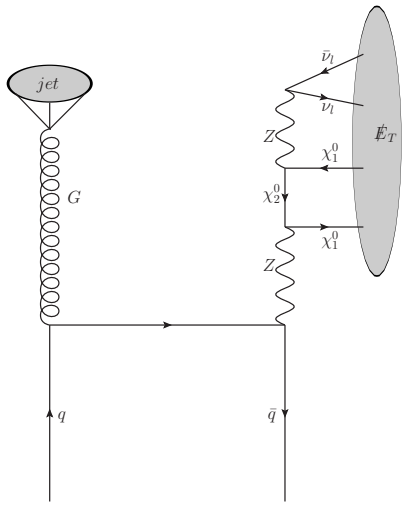

Figure 4.23: *A Feynman diagram for the mono-jet process. The time "runs" upwards.*

Feynman diagram is shown in Fig.4.23) is $C\,\chi_1^0\,\sigma_{\mu\nu}\,\chi_2^0\,F_Z^{\mu\nu}$ with $C \sim c_W d_W + s_W d_\gamma$. Thus, if the pair of $\chi_1^0\,\chi_2^0$ particles are produced with energy larger than $\sim \Lambda(c_W d_W + s_W d_\gamma)^{-1}$, the calculation is considered to be inaccurate. In order to understand this, a numerical example is given in Fig. 4.24, where the dependence of the differential cross section on the invariant mass of the dark sector particles (which measures the energy that would be transferred by the integrated out particle) is shown for $M_D = 250$ GeV, $d_W = 0.45$ and $d_\gamma = 0.25$. We observe that above ~ 2 TeV, the mono-jet differential cross section falls rapidly, and, the main contribution to the inclusive cross section, around 85% for this particular example, arises for invariant masses with $M(\chi_1^0\chi_2^0) \lesssim 2$ TeV. In addition, since $C \approx 0.5$ and $\Lambda = 1$ TeV, the energy scale where this calculation is inaccurate is $\frac{\Lambda}{C} \sim 2$ TeV, and therefore this calculation is, in principle, reliable.

Furthermore, the limit discussed above could be different, since the expansion of the *UV complete* model is generally written in powers of $\frac{\lambda}{M}$, where λ is a generic coupling (or a function of couplings) of this model and M is the mass of the particle which is integrated out. The convergence of this expansion depends on the value of $\frac{\lambda}{M}$ which is, in principle, different from $\frac{C}{\Lambda}$. An extensive discussion on the limitations of effective theories at the

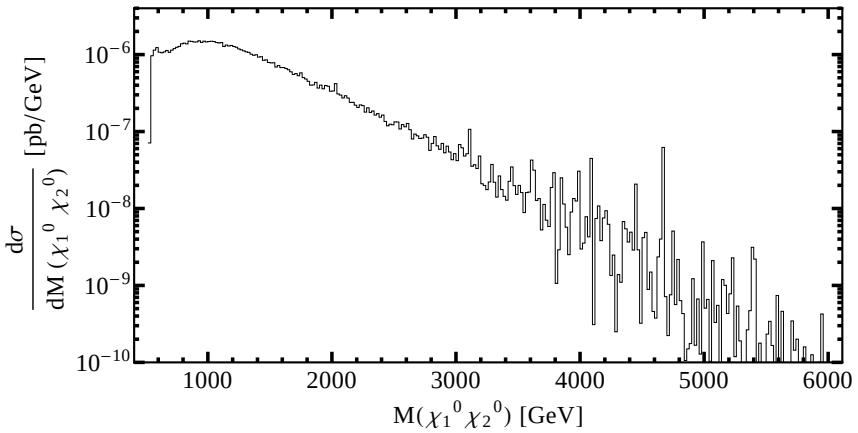

Figure 4.24: *The dependence of the mono-jet differential cross section, $d\sigma/dM(\chi_1^0\chi_2^0)$, on the invariant mass for the pair of the neutral fermions, for $\sqrt{\hat{s}} = 13$ TeV, $M_D = 250$ GeV, $d_W = 0.45$ and $d_\gamma = 0.25$.*

LHC can be found in refs. [283, 284]. Finally, as shown in ref. [285], there are cases where the decay width of the particle that is integrated out vastly affects the cross section. There are also UV independent bounds coming from unitarity, discussed in refs. [286, 287]. A detailed study of these effects is beyond the scope of this work.

4.7 Conclusions

We have introduced in the SM particle spectrum a fermionic bi-doublet: a pair of Weyl fermion $SU(2)_L$-doublets, $\mathbf{D}_1$ and $\mathbf{D}_2$, with opposite hypercharges. In addition, we assume a discrete Z_2-symmetry that distinguishes $\mathbf{D}_1$ and $\mathbf{D}_2$ from the SM fields. This anomaly free set of fermions, together with the Z_2-symmetry are quite common features in non-supersymmetric SO(10) GUT constructions for light dark matter. Light $SU(2)_L$ doublets, whose components are parts of the WIMP have been also considered countless of times in "UV-complete" non-supersymmetric or supersymmetric models (*i.e.* higgsino dark matter). Our work is related to these UV models when all other particles but the doublets have been integrated out in their low energy spectrum.

At the renormalizable level the mass spectrum consists of a electromagnetically neutral, and a charged Dirac, fermions. Under the presence of $d = 5$ operators, the neutral Dirac fermion is split into two Majorana states, the WIMP, χ_1^0, and its excited state, χ_2^0. Moreover, the $d = 5$ operators include magnetic and electric dipole transitions which are, in principle, generated by a UV-complete theory, possibly at the TeV scale. We ask here the question whether the dark matter particle χ_1^0, with mass ($m_{\chi_1^0}$), *around the EW scale*, is compatible to various collider, astrophysical and cosmological data.

In order to reduce fine tuning and extensive scans of the parameter space, in Section 4.3.1 we adopted four scenarios, a,b,c and d, based on well motivated symmetry limits of the theory such as a charge conjugation or a custodial symmetry that act on $\mathbf{D}$'s and Higgs field H. These low energy symmetries simplify enough the analytical expressions of the interactions and possibly help to construct UV-completions of the model. After collecting all relevant $d = 5$, and $d = 6$ (though the latter not used in the analysis), operators in Appendix B, we went on to investigate their implications into collider and astrophysical

processes.

In Section 4.4, we performed a constraint analysis based *(i)* on scattering WIMP-nucleus recoiling experiments, such as LUX, *(ii)* on LEP searches for new fermions, as well as *(iii)* on LHC searches for the decay $h \to \gamma\gamma$. Bounds on the model parameters (4.17) are collected in Fig. 4.4. Only in cases (b) and (c) there is still enough freedom to carry on. In the same section, we also studied contributions from the new fermion interactions into oblique electroweak S, T and U parameters. Only the S parameter is affected, and, as a consequence, only case (a) is further constrained.

Focused on the more interesting cases (b) and (c), in Section 4.5 we calculated the relic density Ωh^2 for χ_1^0. In the presence of $d = 5$ dipole operators there are destructive interference effects in the (dominant) amplitudes for WIMP annihilations (or co-annihilations) into SM vector bosons. The minima in the cross sections correspond to certain, usually non-zero, values for the coefficients of the dipole operators d_W and d_γ [see eqs. (4.56a) and (4.56b)]. Nearby these minima the relic density is found to be consistent with observation [eq. (3.69)] for $m_{\chi_1^0} \gtrsim 200$ GeV. Although continuous gamma ray spectrum constraints are harmless, constraints from monochromatic gamma ray spectrum are serious for the photon dipole coupling as it is shown in Figs. 4.19 and 4.20. The coefficient d_W has to be more than 10% a value which is non-negligible for UV models with dark matter at the EW scale. d_γ on the other hand can be tuned to zero without a problem.

Apart from possible aesthetics, the main reason in insisting for EW dark matter mass, $m_{\chi_1^0} \approx M_Z$, has to do with enhancing the possibility of observing the dark sector at the LHC (or, in any case, to be as close as visible in the Run II phase). In Section 4.6 we estimated the cross section for producing χ_1^0 at LHC with center of mass energy $\sqrt{\hat{s}} = 8$ and 13 TeV and in association with a jet (monojet) or 2 jets or a W or a Z. We found that the monojet process is the most promising with a few hundred of events at $\sqrt{\hat{s}} = 13$ TeV and with $m_{\chi_1^0} \simeq 200 - 350$ GeV (see Fig. 4.22).

5 Radiative Light Dark Matter

In previous chapters, we examined two models which predict a dark matter particle with mass at the electroweak scale. A common feature in both models was a global symmetry in the Yukawa sector, which is responsible for evading the bounds imposed by direct detection experiments without fine-tuning, since the so-called blind spots appear naturally. However, as the sensitivity of direct detection experiments increases, such bind-spots might not be able explain the lack of dark matter signal, since loop corrections to spin-independent interactions usually do not vanish. Therefore, if no DM signal is detected, the prospect of a dark matter particle with mass well bellow the electroweak scale (where the direct detection experiments are still insensitive) have to be contemplated. In this case, though, one questions arises: *What is the origin of the suppressed DM mass?* In this chapter, we propose an answer to this question. Specifically, we demonstrate that the mass of the DM particle can be generated in a natural way, along with the observed relic abundance without parameter fine tuning.

We present a Peccei–Quinn (PQ)-symmetric two-Higgs doublet model that naturally predicts a fermionic singlet dark matter in the mass range 10 keV–1 GeV. The origin of the smallness of the mass of this light singlet fermion arises predominantly at the one-loop level, upon soft or spontaneous breakdown of the PQ symmetry via a complex scalar field in a fashion similar to the so-called Dine–Fischler–Sredniki–Zhitnitsky axion model. The mass generation of this fermionic Radiative Light Dark Matter (RLDM) requires the existence of two heavy vector-like SU(2) isodoublets, which are not charged under the PQ symmetry. In this chapter show how the RLDM can be produced via the freeze-in mechanism, thus accounting for the missing matter in the Universe. Finally, we briefly discuss possible theoretical and phenomenological implications of the RLDM model for the strong CP problem and the Large Hadron Collider. This chapter is based on the work of ref. [94].

5.1 Introduction

Ongoing searches for the elusive missing matter component of the Universe, the so-called dark matter, have offered no conclusive evidence so far. From analyses of the CMB power spectrum and from pertinent astronomical studies, we now know that about one quarter of the energy budget of our Universe should be in the form of DM, and so many candidate theories have been put forward to address this well-known DM problem [115]. Among the suggested scenarios, those predicting Weakly Interactive Massive Particles (WIMPs) constitute one class of popular models that may not only account for the DM itself, but also leave their footprints in low-energy experiments, or even at high-energy colliders, such as the LHC [142]. In particular, for WIMPs near the electroweak scale, the WIMP-nucleon scattering cross section is estimated to be somewhat below 10^{-46} cm^2 as measured by LUX [100].

Projected experiments that lie not very far ahead in future will be capable of reach-

ing sensitivity in the ballpark 10^{-47}–10^{-48} cm^2 [106], and so they will be getting closer to the neutrino-nucleon background cross section, the infamous "neutrino floor," where disentangling neutrino signals from those of WIMPs will become almost an impossible task [288]. Therefore, DM models have to be constructed (or revisited) to avoid such severe constraints, *e.g.* by contemplating scenarios that either sufficiently suppress the WIMP-nucleon interaction, or move the DM mass to the sub-GeV or ultra-TeV region.

Several models have been proposed featuring a light DM in the mass range $\mathcal{O}$(keV)–$\mathcal{O}$(GeV), such as sterile neutrino DM [89, 90, 289–291], light scalar DM [91] and milli-charged DM [92], including their possible implications for future DM searches [292, 293]. However, one central problem of such models is the actual origin of the small mass for the light DM, which could be more than six orders of magnitude below the electroweak scale.

In this work we address this mass hierarchy problem, by presenting a new radiative mechanism that can predominantly account for the smallness in mass for the light DM. The so-generated Radiative Light Dark Matter (RLDM) is a fermionic singlet S and can naturally acquire a mass in the desired range: 10 keV–1 GeV. A minimal realization of this radiative mechanism requires the extension of the Standard Model (SM) by one extra scalar doublet, resulting in a Peccei–Quinn (PQ)-symmetric two-Higgs doublet model [294, 295], augmented by two fermionic heavy vector-like SU(2) isodoublets D_1 and D_2, which are not charged under the PQ symmetry. The mass of the RLDM is predominantly generated at the one-loop level, upon soft or spontaneous breakdown of the PQ symmetry via a complex scalar field, *e.g.* Σ, in close analogy to the so-called Dine–Fischler–Sredniki–Zhitnitsky (DFSZ) axion model that addresses the strong CP problem [63, 64].

We analyse the production mechanisms of the RLDM in the early Universe, and show that it can account for its missing matter component via the so-called freeze-in mechanism [61]. In fact, we illustrate how the freeze-in mechanism remains effective in the RLDM model, without the need to resort to suppressed Yukawa couplings. In this context, we investigate two possible scenarios of both theoretical and phenomenological interest. In the first scenario, we consider the breaking of the PQ scale $f_{\rm PQ}$ to be comparable to the one required for the DFSZ model to solve the strong CP problem, *i.e.* $f_{\rm PQ} \sim 10^9$ GeV. We find that such PQ scale can exist within this realization, provided an appropriate isodoublet mass M_D and reheating temperature $T_{\rm RH}$ is considered. In the second scenario, we relax the constraint of the strong CP problem on $f_{\rm PQ}$, and investigate its possible lower limit, with the only requirement that $T_{\rm RH}$ be larger than the critical temperature T_C of the SM electroweak phase transition, thus allowing for the $B+L$-violating sphaleron processes to be in thermal equilibrium. This requirement is introduced here, so as to leave open the possibility of explaining the cosmological baryon-to-photon ratio η_B via low-scale baryogenesis mechanisms, such as electroweak baryogenesis [155, 156] and resonant leptogenesis [157, 158, 296, 297]. In this second scenario, we find that the heavy Higgs bosons of the two-Higgs doublet model (2HDM) may have masses as low as a few TeV, which are well within reach of the LHC.

The layout of this chapter is as follows. In Section 5.2, we first introduce the PQ-symmetric 2HDM, augmented with a singlet fermion S and a fermionic pair of vector-like doublets $D_{1,2}$. Then, we describe the radiative mechanism for the RLDM, once the PQ symmetry is broken softly, and show that a radiative mass in the range 10 keV–1 GeV can be naturally generated. In Section 5.3, we outline the relevant Boltzmann equation for computing the relic abundance of the RLDM. Utilising the freeze-in mechanism, we present in Section 5.4 numerical estimates for the allowed parameter space of our RLDM model. Based on these results, we explore the possibility whether our model can account

	$SU(2)_L$	$U(1)_Y$	$U(1)_{\rm PQ}$	Z_2
S	1	0	-1	odd
D_1	2	-1	0	odd
D_2	2	1	0	odd
Φ_1	2	1	1	even
Φ_2	2	1	-1	even

Table 5.1: *Quantum number assignments of particles pertinent to the RLDM Model.*

for the strong CP problem within a scenario similar to the DFSZ axion model. Moreover, we investigate whether an absolute lower limit exists for the heavy Higgs-boson masses in our effective 2HDM. Indeed, we find that our RLDM model may allow for heavy Higgs bosons at the TeV scale, whose existence can be probed at the LHC. Finally, Section 5.5 summarises our conclusions and outlines possible new directions for further research.

5.2 Radiative Mechanism

In this section we present a minimal extension of the SM, in which the small mass of the light DM, in the region 10 keV–1 GeV, can have a radiative origin, generated at the one-loop level. This radiative mechanism is minimally realised within the context of a constrained 2HDM obeying a Peccei–Quinn symmetry. In addition, the model under study contains a singlet fermion S charged under the PQ symmetry and a fermionic pair of massive isodoublets $D_{1,2}$ with zero PQ charges. Finally, we delineate the parameter space for which a viable scenario of Radiative Light Dark Matter can be obtained consistent with the observed relic abundance.

5.2.1 The Model

In the 2HDM under consideration, we impose a global PQ symmetry $U(1)_{\rm PQ}$, which forbids the appearance of a bare mass term for the singlet fermion S at the tree level. This PQ symmetry will be broken softly or spontaneously which in turn triggers a radiative mass for S at the one-loop level. The fermion S is stable and receives naturally a small sub-GeV mass, leading to a RLDM scenario. On the other hand, we note that a candidate for a light DM would probably be relativistic at its freeze-out (see Section 2.1), resulting in an extremely large relic abundance (similar to [50]) for the allowed range of DM masses that are larger than about 3 keV, *e.g.* see refs. [48, 298]. Therefore, the DM should be produced out of thermal equilibrium in the early Universe. The mechanism that we will be utilising here is the so-called freeze-in mechanism [61], described in Section 1.3.3, which assumes that the DM particles were absent initially and are produced only later from the plasma.

The relevant Yukawa and potential terms of our model are given by

$$-\mathcal{L}^Y \;=\; Y_1 \epsilon^{ab} \Phi_{1a}\, D_{1b}\, S + Y_2 \Phi_2^{\dagger a}\, D_{2a}\, S \;+ M_D \epsilon^{ab} D_{1a}\, D_{2b} \;+\; \text{H.c.}\,, \tag{5.1}$$

$$\begin{aligned} V(\Phi_1,\Phi_2) \;=\; & m_{11}^2 \Phi_1^{\dagger a}\Phi_{1a} + m_{22}^2 \Phi_2^{\dagger a}\Phi_{2a} - m_{12}^2(\Phi_1^{\dagger a}\Phi_{2a} + \text{H.c}) + \frac{\lambda_1}{2}(\Phi_1^{\dagger a}\Phi_{1a})^2 \\ & +\; \frac{\lambda_2}{2}(\Phi_2^{\dagger a}\Phi_{2a})^2 + \lambda_3 \Phi_1^{\dagger a}\Phi_{1a}\Phi_2^{\dagger b}\Phi_{2b} + \lambda_4 |\Phi_1^{\dagger a}\Phi_{2\,a}|^2\,, \end{aligned} \tag{5.2}$$

where $a, b = 1, 2$ are $SU(2)_L$-group indices (with $\epsilon^{12} = -\epsilon^{21} = +1$), S is a Weyl-fermion SM singlet, $D_{1,2}$ are two Weyl-fermion $SU(2)_L$-doublets, and $\Phi_{1,2}$ are two scalar $SU(2)_L$-doublets. A complete list of the PQ and hypercharge quantum numbers of the aforementioned particles is given in Table 5.1, including a Z_2-parity which excludes the mixing of dark-sector particles with those of the SM. For simplicity, we assume that the new dark-sector interactions are CP invariant and so take their respective couplings to be real in the physical mass basis.

As can be seen from (5.2), we have assumed that the PQ symmetry is broken by the lowest dimensionally possible mass operator in the scalar potential V, namely by allowing only the dimension-2 mixing term m_{12}^2 between Φ_1 and Φ_2. This dimension-2 operator breaks softly the $U(1)_{\rm PQ}$-symmetry in the potential, but could result from spontaneous breaking of the $U(1)_{\rm PQ}$ by a scalar Σ, which acquires a VEV $\langle\Sigma\rangle \equiv f_{\rm PQ} \sim m_{12}$ (see Section 5.4). If the PQ-breaking scale $f_{\rm PQ}$ is high enough, one may neglect, to a good approximation, the potential quartic couplings $\lambda_{1,2,3,4}$, as they do not affect much the radiative mass mechanism and the DM production rates which we will be discussing in the next section.

The mass parameters m_{11}^2 and m_{22}^2 of the scalar potential V in eq. (5.2) may be eliminated in favour of the VEVs $v_{1,2}$ of the Higgs doublets $\Phi_{1,2}$, by virtue of the minimization conditions on V (for a review on 2HDMs, see [299]). These VEVs are related to the SM Higgs VEV v, through: $v^2 = v_1^2 + v_2^2$. In the kinematic region where $m_{12}^2 \gg v^2$, the mass parameters m_{11}^2 and m_{22}^2 are approximately given by

$$m_{11}^2 \;\approx\; m_{12}^2\, t_\beta \;+\; \mathcal{O}(v^2)\,, \tag{5.3}$$

$$m_{22}^2 \;\approx\; m_{12}^2\, t_\beta^{-1} \;+\; \mathcal{O}(v^2)\,, \tag{5.4}$$

where $t_\beta \equiv \tan\beta = v_2/v_1$.

5.2.2 One-Loop Radiative Mass

Having introduced the minimal model under investigation, we can now discuss the radiative mechanism responsible for the generation of a mass of dimension-3 for the singlet fermion S. We assume that $m_{12} \gtrsim 1$ TeV, such that the main contribution to the mass of the S particle comes from the diagram shown in Fig. 5.1. In addition, there will be a tree-level mass $M_S^{\rm tree}$ generated after the SM electroweak phase transition, given by $M_S^{\rm tree} \simeq Y_1 Y_2\, v^2/M_D$. Under the assumption that M_D is very large, *i.e.* $M_D \gg v$, the tree-level contribution turns out to be sub-dominant compared to the radiatively induced mass $M_S^{\rm rad}$, and hence it can be ignored for most of the parameter space. We will return to this point at the end of this section.

After evaluating the relevant one-loop self-energy graph shown in Fig. 5.1 at zero external momentum ($p \to 0$), we obtain

$$M_S^{\rm rad} \;=\; -\,2\, Y_1 Y_2\, M_D\, m_{12}^2\, I(M_D, m_{11}, m_{22})\,, \tag{5.5}$$

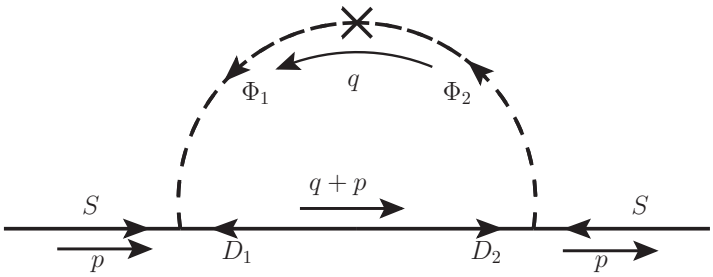

Figure 5.1: *One-loop diagram responsible for the mass generation of the singlet fermion S.*

where

$$I(M_D, m_{11}, m_{22}) \;=\; \int \frac{d^4q}{(2\pi)^4}\, \frac{1}{(q^2 - M_D^2)(q^2 - m_{11}^2)(q^2 - m_{22}^2)}\;. \tag{5.6}$$

Employing the approximate relations given in (5.3) and (5.4), the one-loop radiative mass of S is finite and may conveniently be expressed as follows:

$$M_S^{\rm rad} \;=\; \frac{2y^2}{(4\pi)^2}\, \frac{M_D}{t_\beta - t_\beta^{-1}} \left[\frac{t_\beta \ln\left(t_\beta/r^2\right)}{t_\beta - r^2} \;-\; \frac{t_\beta^{-1} \ln\left(t_\beta^{-1}/r^2\right)}{t_\beta^{-1} - r^2} \right], \tag{5.7}$$

with $y^2 \equiv Y_1 Y_2$ and $r \equiv M_D/m_{12}$. Observe that the interchange $t_\beta \leftrightarrow t_\beta^{-1}$ leaves $M_S^{\rm rad}$ unchanged. Assuming that $t_\beta = 1$ for different kinematic regimes of the ratio r, the following simplified forms for $M_S^{\rm rad}$ are obtained:

$$M_S^{\rm rad} \;\simeq\; \frac{2y^2}{(4\pi)^2}\, M_D \qquad \text{for } r \ll 1\;, \tag{5.8}$$

$$M_S^{\rm rad} \;\simeq\; \frac{y^2}{(4\pi)^2}\, M_D \qquad \text{for } r \sim 1\;, \tag{5.9}$$

$$M_S^{\rm rad} \;\simeq\; \frac{2y^2}{(4\pi)^2}\, \frac{M_D \,\ln r^2}{r^2} \qquad \text{for } r \gg 1\;. \tag{5.10}$$

Note that for $M_D \gg m_{12}$ (corresponding to $r \gg 1$), the radiative mass $M_S^{\rm rad}$ of the singlet fermion S is suppressed by the square of the hierarchy factor r. The latter allows for scenarios, for which the Yukawa couplings are of order 1, *i.e.* $y^2 = Y_1 Y_2 = \mathcal{O}(1)$, for 10 keV $\leq M_S^{\rm rad} \leq 1$ GeV. On the other hand, for $r \sim 1$ and $r \ll 1$, one needs either a low M_D of order TeV and $y \approx 0.1$, or $M_D \approx 10^8$–10^9 GeV and $y \approx 10^{-3}$–10^{-4}.

In Fig. 5.2, we display the values of the coupling parameter $y = \sqrt{Y_1 Y_2}$, as a function of M_D, which yield a radiatively induced mass $M_S^{\rm rad}$ for the singlet fermion S in the region 10 keV $\leq M_S^{\rm rad} \leq 1$ GeV, for $t_\beta = 1$ and $r = 10^{-2}$. In particular, we see that for every set of $M_S^{\rm rad}$, M_D, r, there is an acceptable range of perturbative values for y. However, if $r \gg 1$, the desirable value of y may exceed 10 according to (5.10), and our perturbative results do no longer apply. Such non-perturbative values of y are excluded from our numerical estimates for the determination of the relic abundance of S which we perform in the next section.

In a similar context, we note that a large mass for m_{11}, m_{12}, m_{22} and M_D might seem to be a huge fine tuning for generating a light sub-GeV radiative mass for S. However, we may easily convince ourselves that this is not the case. The absence of fine tuning can

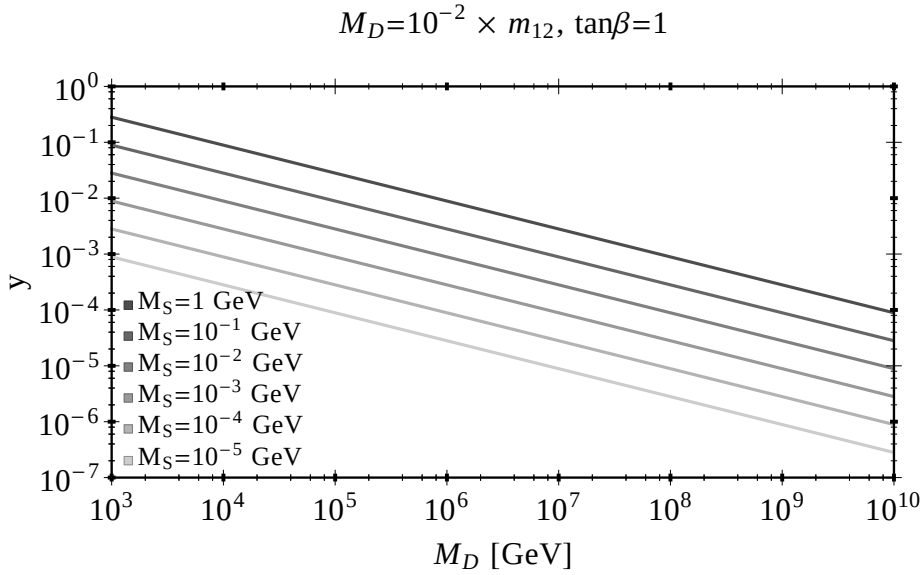

Figure 5.2: *Predicted values for* M_D *versus* $y = \sqrt{Y_1 Y_2}$ *as obtained from* (5.7)*, for* $M_S \simeq M_S^{\rm rad}$ *ranging from* 10 keV *to* 1 GeV*, after setting* $t_\beta = 1$ *and* $r = 10^{-2}$*.*

be seen in an easier way, if we rotate from the general weak basis spanned by Φ_1 and Φ_2 to the so called *Higgs basis* [299,300], H_1 and H_2, where H_1 contains the SM VEV v and H_2 has exactly no VEV. Note that in the Higgs basis, the assignment of the PQ charges to the fields H_1 and H_2 is not canonical. Moreover, in this rotated Higgs basis, one has that the new Higgs-mass parameters obey the relation: $\widetilde{m}^2_{22} \gg \widetilde{m}^2_{11}, \widetilde{m}^2_{12}$. In addition, the analogue of the diagram in Fig. 5.1 is now represented by a set of two self-energy graphs, where the fields H_1 and H_2 are circulating in the loop. The ultraviolet (UV) infinities cancel, after the contributions from these two diagrams are added. For $t_\beta = 1$ and $r = 1$, we then obtain the same result as the one stated in (5.9). Hence, we observe that a small mass for the singlet fermion S arises naturally in an SM+S effective field theory. This effective field theory results from integrating out the heavy $D_{1,2}$ and H_2 fields from (5.1) in the Higgs basis.

Besides the radiative mass $M_S^{\rm rad}$ of S which violates the PQ symmetry by two units (*cf.* Table 5.1), there will be a tree-level contribution to the mass of S after the SM electroweak phase transition. For most r values of interest here, the relative size of the two contributions can naively be estimated to be

$$\frac{M_S^{\rm tree}}{M_S^{\rm rad}} \sim \frac{8\pi^2 v^2}{M_D^2} \,. \tag{5.11}$$

Thus, for $M_D \gg \sqrt{8}\pi v \simeq 2.2$ TeV, the tree-level contribution can be safely ignored. In our numerical estimates, the tree-level mass term $M_S^{\rm tree}$ is always less than 10% of the radiative mass term $M_S^{\rm rad}$. Hence, the total mass M_S of the stable fermion S is given predominantly by the radiative mass term, implying that $M_S \simeq M_S^{\rm rad}$ to a very good approximation.

We conclude this section by commenting on the possibility of considering a radiative model alternative to the one discussed here. For instance, one may envisage a scenario that instead of the single S, one of the neutral components of the doublets $D_{1,2}$ becomes the RLDM. In this case, however, the charged component $D^\pm$ from $D_{1,2}$ will be almost

degenerate with the light sub-GeV DM particle, which is excluded experimentally. The general SM+$D_{1,2}$ effective theory has been studied in [88].

5.3 Dark Matter Abundance

In this section we first describe the relevant effective Lagrangian that governs the production of the stable fermions S in the early Universe. We then solve numerically the Boltzmann equation that determines the yield $Y_S \equiv n_S/s$ of these fermions S, where n_S is the number density of S particles and s is the entropy density of the plasma (1.77). Having thus estimated the value of Y_S, we can then use it to deduce the respective relic abundance $\Omega_S h^2$ of the S particles in the present epoch. Finally, we present approximate analytic results for $\Omega_S h^2$ and compare these with the observationally favoured value: $\Omega_{\rm DM} h^2 \simeq 0.12$.

As mentioned in the previous section, the stable fermions S will play the role of the DM, which are produced via the freeze-in mechanism [61]. The key assumption is that the DM fermions S were absent (*i.e.* their number density was suppressed) in the early Universe and were produced later from annihilations and decays of plasma particles, *e.g.* from $\Phi_{1,2}$ and $D_{1,2}$, according to the model discussed in Section 5.2. Furthermore, we will assume that $D_{1,2}$ were also absent in the early Universe, so as to avoid over-closure of the Universe, unless the Yukawa couplings $Y_{1,2}$ are taken to be extremely suppressed, such that decays of the sort $D_1^0 \to h\, S$ are made slow and inefficient. The latter results in a contrived scenario, in which obtaining a viable DM parameter space requires a good degree of fine tuning. In order for the $SU(2)_L$-doublet fermions $D_{1,2}$ to be absent, we take their bare mass M_D to be above the reheating temperature $T_{\rm RH}$ of the Universe. This simplifies considerably our analysis, as the heavy fermions $D_{1,2}$ can be integrated out.

The effective Lagrangian that determines the production rate of S particles after reheating is given by

$$-\mathcal{L}_{\rm eff}^{d=5} \;=\; \frac{1}{2\tilde{\Lambda}}\left(\Phi_1^\dagger\Phi_1 + \tilde{a}\Phi_2^\dagger\Phi_2 + \tilde{b}\Phi_1^\dagger\Phi_2 + \tilde{c}\Phi_2^\dagger\Phi_1\right) SS \;+\; \text{H.c.}\,, \tag{5.12}$$

where $\tilde{a}, \tilde{b}$ and $\tilde{c}$ denote the Wilson coefficients of the dimension-5 operators. The calculation of the relic abundance is not straightforward in this basis, since $\Phi_{1,2}$ mix and the identification of the physical fields is obscured, especially after SSB where further mixing between the scalar fields is introduced. Therefore, according to our discussion at the end of Section 5.2.2, it would be more convenient to rotate the scalars to the so-called Higgs basis [299], where only one doublet H_1 develops a VEV and is identified with the SM Higgs doublet. To further simplify calculations, and without much loss of generality, we assume that the Higgs basis is also the mass eigenstate basis. This assumption is well justified for relatively large values of m_{12}, as it leads to the so-called *alignment limit* of the 2HDM [301–305], which is favoured in the light of global analyses of experimental constraints [306, 307]. In the Higgs basis, the dimension-5 effective Lagrangian reads

$$-\mathcal{L}_{\rm eff}^{d=5} \;=\; \frac{y^2}{M_D}\frac{t_\beta}{1+t_\beta^2}\left(H_1^\dagger H_1 - H_2^\dagger H_2 - t_\beta\, H_1^\dagger H_2 + t_\beta^{-1}\, H_2^\dagger H_1\right) SS \;+\; \text{H.c.}\,, \tag{5.13}$$

where H_1 is the SM Higgs doublet and H_2 is the heavy scalar doublet with $\langle H_2\rangle = 0$.

Note that in the limit of integrated-out H_2, eq. (5.13) matches the Lagrangian (2.1),

with

$$\Lambda = \frac{M_D}{2y^2}\frac{1+t_\beta^2}{t_\beta} \,. \tag{5.14}$$

In fact, as we will see in this section, some of the results of Section 2.1 can be also applied here.

5.3.1 Boltzmann Equation for Y_S

In order to determine the relic abundance of S particles, we need to solve the Boltzmann equation for their yield Y_S [see Section 1.3.3]. Since we assume that the singlets S remained out of equilibrium throughout the history of the Universe (at least up to the phase of reheating), our only concern will then be their production. The main production channels, depending on the plasma temperature T, are the following:[1]

$$\begin{aligned} H_1^\dagger H_1,\ H_1^\dagger H_2,\ H_2^\dagger H_1 &\to SS \qquad \text{for } T_C \le T < T_{\rm RH} \,, \\ H_2^\dagger H_2 &\to SS \qquad \text{for } T < T_{\rm RH} \,, \\ h &\to SS \qquad \text{for } T < T_C \,, \end{aligned} \tag{5.15}$$

where h is the Higgs field with mass $m_h \approx 125$ GeV and $T_C \approx 130$ GeV is the critical temperature of the SM electroweak phase transition. For $T < T_C$, one has to add new channels, for instance $W^+W^- \to SS$, but their contribution to the production of the DM particles is negligible compared to $h \to SS$.

Following [61], the Boltzmann equation for the yield Y_S becomes

$$\begin{aligned} sH\frac{dY_S}{dT} \;=\; & -\frac{1}{512\pi^5}\sum_{i,j=H_1,H_2}\left[\int_{(m_i+m_j)^2}^{\infty} d\hat{s}\, P_{ij}\,|M_{ij}|^2 K_1\!\left(\frac{\sqrt{\hat{s}}}{T}\right)\right] \\ & + \left(\frac{t_\beta}{1+t_\beta^2}\right)^2 \frac{y^4}{2\pi^3}\frac{m_h^3 v^2}{M_D^2} K_1\!\left(\frac{m_h}{T}\right) , \end{aligned} \tag{5.16}$$

where T is the temperature of the plasma, H is the Hubble parameter, K_1 is the first modified Bessel function of the second kind, $P_{ij} \equiv \sqrt{\hat{s}-(m_i+m_j)^2}\sqrt{\hat{s}-(m_i-m_j)^2}/\sqrt{\hat{s}}$ is a kinematic factor, and $|M_{ij}|^2$ is the squared matrix element, summed over internal degrees of freedom, for the $2 \to 2$ annihilation processes: $H_i^\dagger H_j \to SS$. The last term on the RHS of (5.16) arises from the decay $h \to SS$, upon ignoring the mass of the S particles. Also, upon ignoring M_S, the squared matrix elements $|M_{ij}|^2$ for the various $2 \to 2$ processes are

$$\begin{aligned} |M_{H_1^\dagger H_1 \to SS}|^2 \;&=\; |M_{H_2^\dagger H_2 \to SS}|^2 \;=\; 16\left(\frac{t_\beta}{1+t_\beta^2}\right)^2 y^4 \frac{\hat{s}}{M_D^2} \,, \\ |M_{H_1^\dagger H_2 \to SS}|^2 \;&=\; |M_{H_2^\dagger H_1 \to SS}|^2 \;=\; 8\,(t_\beta^2 + t_\beta^{-2})\left(\frac{t_\beta}{1+t_\beta^2}\right)^2 y^4 \frac{\hat{s}}{M_D^2} \,. \end{aligned} \tag{5.17}$$

The solution to the Boltzmann equation is obtained by integrating (5.16) over the temperature T. The limits of integration for the various channels are the ones shown in (5.15). However, before doing that, we have to make an assumption for the critical temperature

[1] Note that for $T < T_C$, we only consider the production via $h \to SS$. This is because the other channels give negligible contribution to Y_S, as can be seen from Fig. 2.2.

and the thermal corrections to the masses of the scalar fields. In what follows, we assume that the critical temperature T_C and the thermal effects on the masses (for $T > T_C$) are similar to the pure SM Higgs sector and they are given by [154]

$$T_C \sim m_h \,, \qquad m_{H_1}^2 \approx m_h^2 + \frac{1}{2}T^2 \,, \qquad m_{H_2}^2 \approx \frac{1+t_\beta^2}{t_\beta} m_{12}^2 + \frac{1}{2}T^2 \,. \tag{5.18}$$

Under these assumptions and restricting $T_{\rm RH}$ to be above T_C, we can compute the yield Y_S at $T \approx 0$, which in turn implies the relic abundance (1.123).

5.3.2 Approximate Results for $\Omega_S h^2$

In general, the yield Y_S cannot be calculated analytically, but depending on the reheating temperature $T_{\rm RH}$, we are able to present approximate analytic results. We find that for decoupled $D_{1,2}$, *i.e.* $T_{\rm RH} > M_D$, the relic abundance $\Omega_S h^2$ derived from Y_S in (1.123) takes on the form

$$\Omega_S h^2 \approx 0.12 \times \left(\frac{M_S}{10^{-5}\,\text{GeV}}\right)\left(\frac{2\times 10^8\,\text{GeV}}{M_D}\right)^2\left(\frac{y}{4.7\times 10^{-2}}\right)^4\left[\left(\frac{t_\beta}{1+t_\beta^2}\right)^2+\left(\frac{T_{\rm RH}}{10^4\,\text{GeV}}\right)\right], \tag{5.19}$$

for $T_{\rm RH} \gg m_{12}$, and

$$\Omega_S h^2 \approx 0.12 \times \left(\frac{M_S}{10^{-3}\,\text{GeV}}\right)\left(\frac{2\times 10^5\,\text{GeV}}{M_D}\right)^2\left(\frac{y}{4.7\times 10^{-4}}\right)^4\left(\frac{t_\beta}{1+t_\beta^2}\right)^2\left[1+\left(\frac{T_{\rm RH}}{10^4\,\text{GeV}}\right)\right], \tag{5.20}$$

for $T_{\rm RH} \ll m_{12}$.[2] Equations (5.19 and 5.20) are accurate up to 1%, except for $T_{\rm RH} \sim m_{H_2}$, where the deviation from the exact result is about 20%. Note that in both the regimes of $T_{\rm RH}$, there are two contributions to $\Omega_S h^2$, given by the two terms contained in the last factors of (5.19) and (5.20). The first contribution does not depend on the reheating temperature $T_{\rm RH}$ and arises from the decay $h \to SS$, while the second one is proportional to $T_{\rm RH}$. This second contribution is a result of the decoupling of the heavy fermionic doublets $D_{1,2}$ and indicates that for $T_{\rm RH} \gtrsim 10^4$ GeV, the production of S particles is dominated by $2 \to 2$ annihilation processes given in (5.15). As discussed in [61, 62], the latter is a general result for the freeze-in production mechanism via non-renormalizable operators (see also Fig. 2.2). Finally, it is worth pointing out that $\Omega_S h^2$ is symmetric under $t_\beta \to t_\beta^{-1}$, as is the expression for M_S in (5.7).

5.4 Results

In Section 5.2.2, we have shown that the mass of the singlet S can be generated at the one-loop level, if the PQ symmetry is softly broken, and in Section 5.3 we have calculated the relic abundance of the S particles. In this section, we will be exploring the validity of the parameter space of our minimal model. To this end, one may consider the parameters,

$$T_{\rm RH} \,,\; M_D \,,\; y^2 \,,\; t_\beta \;\text{ and }\; m_{12} \,,$$

as being independent. However, we prefer to solve the mass formula $M_S^{\rm rad}$ in (5.7) for y^2 and replace it with a physical observable, the S-particle mass M_S which is taken in

[2] For $T_{\rm RH} \ll m_{12}$ the heavy scalar (H_2) is decoupled. Therefore we can obtain eq. (5.20) from eqs. (2.12) and (5.14).

our numerical estimates to be in the region: 10 keV $\leq M_S \leq$ 1 GeV. Consequently, the parameters that we allow to vary independently are

$$T_{\rm RH}\ ,\ M_D\ ,\ M_S\ ,\ t_\beta\ \ \text{and}\ \ m_{12}\ . \tag{5.21}$$

We perform a scan over this parameter space, while imposing the perturbativity constraint on the Yukawa couplings: $Y_{1,2} < \sqrt{4\pi}$. In this way, we find the values of these parameters that satisfy the observed DM relic abundance [29] [see eq. (1.103)]

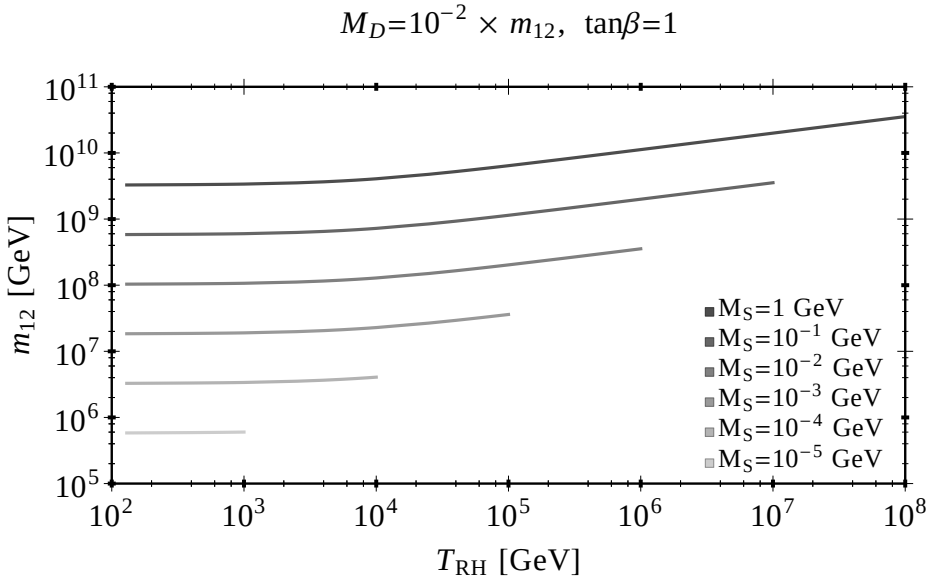

Figure 5.3: $T_{\rm RH}$ *versus* m_{12} *for* $r = M_D/m_{12} = 10^{-2}$, $t_\beta = 1$ *and several RLDM masses* M_S.

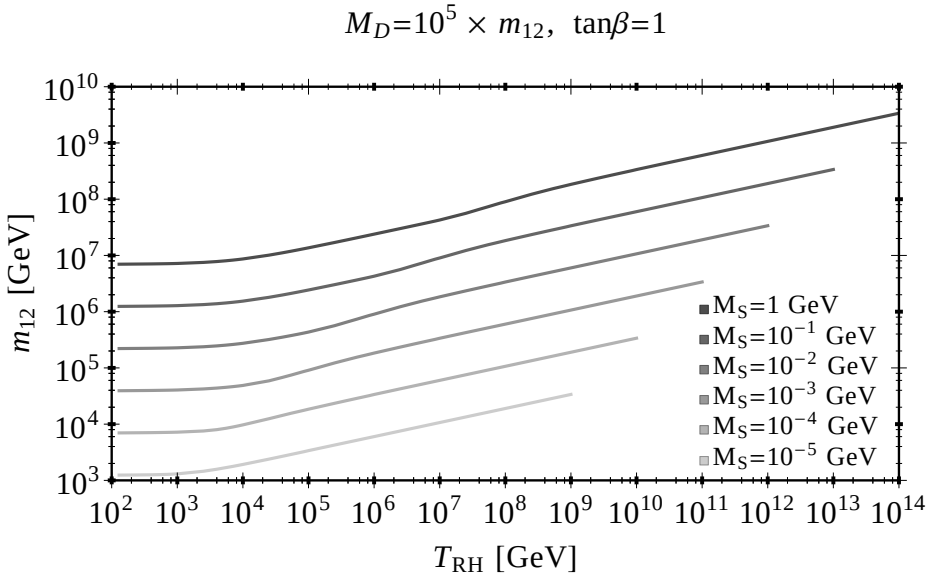

Figure 5.4: *The same as in Figure 5.4, but for* $r = M_D/m_{12} = 10^5$.

In Fig. 5.3 we present contour lines on the $T_{\rm RH}$–m_{12} plane for discrete values of the S-particle mass M_S in the region: 1 keV $\leq M_S \leq$ 1 GeV, for $t_\beta = 1$ and $r = 10^{-2}$, which

give the DM relic abundance (1.103). For $m_{12} \simeq 10^{10}$ GeV, the reheating temperature $T_{\rm RH}$ can vary between the critical temperature $T_C \simeq 130$ GeV and 10^8 GeV. This upper bound on $T_{\rm RH}$ may be as high as 10^{14} GeV, if the parameter $r = M_D/m_{12}$ is increased to the value $r = 10^5$, as depicted in Fig. 5.4. Yet, at the same time, m_{12} increases by one order of magnitude or so. On the other hand, for $m_{12} \simeq 1 - 10$ TeV, an acceptable DM relic abundance is reached only for large r and for $M_S \simeq 1$ keV, as can be seen from Fig. 5.4. Most remarkably, we notice that the predicted values for $\Omega_S h^2$ are compatible with the observed DM relic abundance $\Omega_{\rm DM} h^2$, for a wide range of values for the parameters m_{12}, M_D and $T_{\rm RH}$. Interestingly enough, the required Yukawa couplings $Y_{1,2}$ for a viable RLDM are sizeable, and always larger than the electron Yukawa coupling.

We recall here that we explore only regions where the fermion doublets $D_{1,2}$ are decoupled after the reheating of the Universe, *i.e.* we assume $M_D \gg T_{\rm RH}$. As a working hypothesis, we assume the decoupling condition: $M_D > 3\,T_{\rm RH}$. This condition is motivated by the fact for $T \approx M_D/3$, the $D_{1,2}$ particles become non-relativistic and, as a consequence, its number density is exponentially suppressed by a Boltzmann factor. Correspondingly, for the scenario considered in Fig. 5.3, the heavy scalar H_2 will be also decoupled, because $m_{H_2} \gg M_D$.

Furthermore, we observe that for $T_{\rm RH} \gtrsim 10^4$ GeV, m_{12} becomes linearly dependent on the reheating temperature (as Fig. 2.3), as expected from the approximate analytic expression in (5.20). We also obtain a similar behaviour in Fig. 5.4. In this case, however, the heavy scalar doublet H_2 is no longer constrained to be decoupled. As a result, there is an interface region at $T_{\rm RH} \sim m_{12}$ that lies between the two linear regimes, $T_{\rm RH} \ll m_{12}$ and $T_{\rm RH} \gg m_{12}$. At the interface region, there is a transition caused by the contribution of the heavy scalar doublet H_2 to the production of singlet fermions S [cf. (5.15)], which can reach equilibrium with the plasma when $T_{\rm RH} \gg m_{12}$.

5.4.1 Solving the Strong CP Problem

It is known that in the SM there is an explicit breaking of CP (and P) discrete symmetry due to the instanton-induced term

$$\mathcal{L}_\theta \;=\; \frac{\theta}{32\pi^2}\,{\rm Tr}(G_{\mu\nu}\widetilde{G}^{\mu\nu})\;. \tag{5.22}$$

In the above, θ is a CP-odd parameter which can be absorbed into the quark masses. However, this θ-parameter cannot be fully eliminated, since the combination: $\bar{\theta} = \theta - {\rm ArgDet}M_q$, where M_q is the quark mass matrix, becomes a physical observable. It contributes to the neutron dipole moment and experimentally, it is severely bounded to be: $|\bar{\theta}| \lesssim 10^{-11}$ [308]. The problem of why $\bar{\theta}$ is much smaller than all other CP-violating parameters, such as the well-known parameter $\varepsilon_K \sim 10^{-3}$ from the $K^0\overline{K}^0$ system, introduces another hierarchy problem in the SM known as the *strong CP problem*. A possible solution, suggested by Peccei and Quinn [294, 295], is to promote the θ-parameter into a dynamical field which naturally minimizes the energy. This dynamical field, called *the axion* [309,310], is a pseudo-Goldstone boson of the global anomalous PQ symmetry.

The SM has no global anomalous $U(1)_{\rm PQ}$-symmetry. One possible way to realise such a symmetry is to non-trivially extend its Higgs sector by adding a second Higgs doublet, resulting in the PQ-symmetric 2HDM. However, charging simply the field doublets Φ_1 and Φ_2 under the PQ symmetry as done in Table 5.1 does not lead to a healthy model. Such a model predicts a visible keV-axion with PQ-breaking scale $f_{\rm PQ} \sim 100$ GeV, which

is already excluded by the experiment. A minimal extension suggested by Dine–Fischler–Sredniki [64]–Zhitnitsky [63] (DFSZ) is to add a SM singlet Σ with charge +1 under $U(1)_{\rm PQ}$-symmetry such that the scalar potential term,

$$\lambda_\Sigma \, \Sigma^2 \, \Phi_1^\dagger \, \Phi_2 \; + \; \text{H.c.} \; \subset \; V(\Phi_1, \Phi_2, \Sigma) \; , \tag{5.23}$$

is invariant. Then, such a Σ-dependent term that occurs in the DFSZ potential $V(\Phi_1, \Phi_2, \Sigma)$ breaks the PQ symmetry spontaneously, when the electroweak singlet field Σ receives a large VEV $\langle \Sigma \rangle$ which is not necessarily tied in with that of the electroweak scale v. For this reason, in this work we have made the identification

$$\langle \Sigma \rangle \; \equiv \; f_{\rm PQ} \; \approx \; m_{12} \; , \tag{5.24}$$

with $\lambda_\Sigma \approx 1$. From experimental constraints and astrophysical considerations, the PQ-breaking scale $f_{\rm PQ}$ must be typically larger than 10^9 GeV [311]. Interestingly, within the RLDM scenario, there are values for m_{12} satisfying this constraint and at the same time are compatible with the observed $\Omega_{\rm DM}h^2$, as discussed in the previous section. An example is shown in Fig. 5.3 for $M_S = 1$ GeV and $T_{\rm RH} \ll m_{12}$. In addition, values where $m_{12} \gtrsim 10^9$ GeV can be also obtained for other hierarchies *e.g.* $r \sim 1$ and $r \gg 1$, as shown in Fig 5.4. This seems to be a rather generic feature of the RLDM realization.

Although the above is a strong indication that the DFSZ solution to the strong CP problem is consistent with the RLDM scenario, a detailed analysis of the UV-complete DSFZ-extended model lies beyond the scope of this article. In particular, for $f_{\rm PQ} \sim 10^{11}$ GeV [312], the axion becomes a sizeable DM component resulting in a two-component DM, consisting of the axion and the S particle, and so a more careful treatment will be required.

5.4.2 Detection of RLDM

We observe that for small enough reheating temperatures, $T_{\rm RH} \sim 1$ TeV, the fermion doublets $D_{1,2}$, as well as the heavy scalar doublet H_2, can lie at the TeV scale, provided that M_S is of order $\mathcal{O}(10$ keV$)$. This is shown in Figs. 5.3 and 5.4 for light M_S, where M_D and m_{12} lie in the vicinity of the TeV scale. As a result, the DM particle S can be probed indirectly by looking for its associated "partners" of the heavy Higgs doublet H_2. In general, we expect that at the LHC, the heavy sector of the 2HDM will be efficiently explored up to the TeV scale [303, 313]. For the RLDM scenario at hand, however, such exploration may be somehow challenging, when looking for charged Higgs bosons with masses larger than ~ 1 TeV for a wide range of t_β values [303, 313].

On the other hand, direct detection experiments for sub-GeV DM particles focus on their interactions with atomic electrons (see Sections 1.3.5 and 2.1). However, in the RLDM scenario, such a detection of S particles is practically unattainable, because S interacts feebly with the SM Higgs boson with a coupling proportional to $v/M_D \ll 1$ yielding a cross section for $S\,e \to S\,e$, which is highly suppressed by fourth powers of the electron-to-Higgs-mass ratio, *i.e.*

$$\bar{\sigma}_{Se} \; \approx \; \frac{y^4}{\pi} \frac{t_\beta^2}{(1+t_\beta^2)^2} \left(\frac{m_e}{m_h} \right)^4 \frac{1}{M_D^2} \; \approx \; 10^{-50} \times \frac{y^4 \, t_\beta^2}{(1+t_\beta^2)^2} \left(\frac{1 \;\text{GeV}}{M_D} \right)^2 \text{cm}^2 \; . \tag{5.25}$$

Hence, a simple estimate shows that $\bar{\sigma}_{Se}$ is much smaller than its current experimental

reach: $\bar{\sigma}_{Se}^{\rm exp} \simeq 10^{-38}\,{\rm cm}^2$.[3]

Another potentially observable effect could originate from the invisible Higgs boson decay, $h \to SS$. Current LHC analyses report the upper bound [153] given in eq. (2.3), which for the RLDM scenario translates into

$$M_D \;\gtrsim\; 10^4 \times y^2 \frac{t_\beta}{1+t_\beta^2}\ {\rm GeV}\ .$$

Note that this constraint is comfortably satisfied for the entire range of our parameter space.[4]

In summary, at least for the foreseeable future, the RLDM particle S proposed here will remain elusive. This leaves only a window for the LHC to find indirectly a second heavy Higgs doublet H_2 and/or a pair of heavy fermion doublets $D_{1,2}$.

5.5 Conclusions

Chapters 3 and 4, were dedicated to the study of EW-scale WIMPs. By carefully studying symmetric cases (charge conjugation or $SU(2)_R$ custodial), we were able to find a way to avoid the bounds imposed by direct detection experiments, without parameter fine tuning, while keeping the models as minimal as possible. In this chapter, we dropped the requirement of the EW-scale WIMP, thus avoiding current and (possibly) future experimental constraints, and focused on the case of a sub-GeV DM particle.

One central problem of most electroweak scenarios that require the existence of very light DM particles in the keV-to-GeV mass range is the actual origin of this sub-GeV scale. To address the origin of such a small scale, we have presented a novel radiative mechanism that can naturally generate a sub-GeV mass for a light singlet fermion S, which is stable and can successfully play the role of the DM.

In order to minimally realize such a Radiative Light Dark Matter, we have considered a Peccei–Quinn symmetric two-Higgs doublet model, which was extended with the addition of a singlet fermion S and a pair of massive vector-like SU(2) isodoublets $D_{1,2}$ that are not charged under the PQ symmetry. Instead, the singlet fermion S is charged under the PQ symmetry and so it has no bare mass at the tree level. However, upon soft breaking of the PQ symmetry, we have shown how the singlet fermion S receives a non-zero mass at the one-loop level. The so-generated radiative mass for the singlet fermion S lies naturally in the cosmologically allowed region of ~ 10 keV–1 GeV.

We have computed the relic abundance of the RLDM S, for different plausible heavy mass scenarios. Specifically, for all scenarios we have been studying, we have assumed that the S particles were absent in the early Universe, whilst the fermion isodoublets $D_{1,2}$ stay out of equilibrium through the entire thermal history of the Universe, because their gauge-invariant mass M_D is taken to be well above the reheating temperature $T_{\rm RH}$. Then, we have found that the observationally required relic abundance for the RLDM S can be produced via decays and annihilations of Higgs-sector particles.

[3] As shown in Section 2.1, the minimum value of Λ is obtained for $T_{\rm RH} = T_C$ (see Fig. 2.3). This corresponds to a decoupled H_2, which means that the lowest possible value of $\frac{M_D}{2y^2}\frac{1+t_\beta^2}{t_\beta}$ is equal to the lowest possible value Λ. Therefore, as in the light singlet DM of Section 2.1, the RLDM model has a maximum S-electron cross section $\bar{\sigma}_{Se} \sim 10^{-72}\ {\rm cm}^2$.

[4] Again, this can be seen from Fig. 2.3 and eq. (5.14).

We have analyzed a heavy mass scenario where the PQ-breaking scale $f_{\rm PQ}$ can reach values $\sim 10^9$ GeV as required by the Dine–Fischler–Sredniki–Zhitnitsky axion model to explain the strong CP problem. We have found that for appropriate isodoublet masses (*e.g.* in Fig. 5.3 $M_D \sim 10^{-2}\, f_{\rm PQ}$), the RLDM particle S in such a scenario can successfully account for the missing matter component of the Universe. In addition, we have investigated whether a lower mass limit exists for the heavy Higgs scalars, within the context of a viable RLDM scenario. We have found that the masses of the heavy scalars can be as low as TeV, which allows for their possible detection at the LHC in the near future.

The PQ-symmetric scenario we have studied here generates a viable RLDM at the one-loop level. However, one may envisage other extensions of the SM, in which the required small mass for the light DM could be produced at two or higher loops. For instance, if the SM is extended by two scalar triplets, a small DM mass can be generated through their mixing at the two-loop level, in a fashion similar to the Zee model. In this context, it would be interesting to explore possible models where both the tiny mass of the SM neutrinos and the small mass of the light DM have a common radiative origin and study their phenomenological implications.

6 Conclusions and Future Directions

A great number of independent astrophysical and cosmological observations, indicate that the total matter content of the Universe is dominated by an unknown component, probably in the form of electrically neutral, stable particles. However, despite the numerous direct, indirect, and collider experiments, these particles have not been identified yet. In this thesis, we studied the phenomenology of three models which contain particle dark matter candidates.

The first chapter was dedicated to the introduction of the basic formalism we used throughout this thesis. In the first part of this chapter, we reviewed the Standard Model of particle physics. Particularly, we discussed its gauge structure, particle content, and the Higgs mechanism. Next, in the second part, we introduced the basic formalism of standard cosmology and discussed the thermodynamics of the expanding Universe. In the third part of this chapter, we reviewed the evidence for the existence of dark matter. We discussed the features of the hypothetical DM particle, and demonstrated how the *freeze-out* and *freeze-in* mechanism can provide an explanation for the observed DM relic abundance. Finally, we reviewed some DM-oriented direct, indirect, and collider searches.

Next, in Chapter 2, as an introductory example, we studied the *Singlet Dark Matter* model, which consists of a fermion gauge singlet, S. Assuming that this particle does not mix with the SM fermions, we introduced the only possible S-Higgs interaction, in the form of a $d = 5$, non-renormalizable operator. Then we calculated its relic abundance in two distinct mass regions. Focusing on the sub-GeV scenario, we argued that the freeze-out mechanism cannot be applied. Then, we calculated the relic abundance for the S-particle using the freeze-in mechanism. In particular, we examined carefully the production of these particles in the early Universe, discussing also their possible equilibration, and we found the values of the parameters that the observed DM relic abundance can be obtained. Afterwards, we considered the heavier case, with DM mass above 10 GeV, and showed that the observed relic abundance can be produced via freeze-out mechanism. However, due to the direct detection bounds, we showed that only a narrow, fine-tuned region of the parameter space is allowed.

In Chapter 3, we considered the "Doublet-Triplet Fermionic Dark Matter" model, which consists of two Weyl fermionic iso-doublets, and one Majorana fermion $SU(2)_L$-triplet. Exploiting a global $SU(2)_R$ symmetry in the Yukawa sector we were able to show that the spin-independent cross section is suppressed, since it appears through loop corrections. Moreover, we showed that this model accommodates a particle with mass $\approx$ 90 GeV, which can account for the dark matter content of the Universe, provided a sizeable Yukawa coupling. Furthermore, we demonstrated how the WIMP of this model can be produced (and even detected) at the LHC. Although this model was "quite minimal" (there were only three free parameters), it showed us how various observables can cooperate towards the same goal, *i.e. a WIMP at the EW scale and detectable at the LHC*. However, due to the requirement of a sizeable Yukawa coupling, the branching ratio of $h \to \gamma\gamma$ and the stability of the SM vacuum, indicated that this model needs completion, probably near the TeV scale.

Next, in Chapter 4, we studied an EFT model, consisting of a pair of doublets (the same as in the previous work), which was motivated by the doublet-triplet case. Assuming that the cut-off energy is at $\mathcal{O}($ TeV), we performed a phenomenological analysis including all possible renormalizable and non-renormalizable operators up to $d = 5$. In this EFT, the non-renormalizable operators are responsible for the mass splitting between the components of the two doublets, the interaction between the DM particle and Higgs bosons, and dipole interactions with the gauge bosons. As in the previous work, the custodial (or charge conjugation) symmetric limit ensured the reduction of parameter fine tuning as well as the simplification of the parameter space. The main result of this analysis was that the dark matter particle can be near the electroweak scale (while evading all direct, indirect and collider constraints), only in the presence of non-vanishing dipole operators. This is a certain prediction for the pure doublet fermionic dark matter scenario, which can help pointing towards the right direction for possible UV-completions. Furthermore, the non-zero dipole operators indicate possible sizeable cross sections for the processes $DM\ DM \to \gamma\gamma$ and $DM\ DM \to \gamma Z$, which can lead to a potential indirect signal with a WIMP mass near the electroweak scale. Finally, we showed that the cross sections for the current mono-X searches at the LHC are somewhat suppressed, but the mono-jet channel seems to be within reach of the 300fb^{-1} luminosity phase of the LHC. Although it seems paradoxical to introduce an EFT motivated by a model which needs completion, we were able to follow a path which lead to new results, *i.e. if the low-energy content consists of these two doublets, and the mass of the DM particle is near the EW scale, then there are heavier particles (with masses around* 1 TeV*) which generate sizeable dipole interactions.*

In Chapters 3 and 4, we examined two cases of *well motived and natural* EW-scale WIMPs. One of the main issues we encountered was the lack of WIMP-signal, despite the increased sensitivity of direct detection experiments. In Chapter 5, we tried to explain this missing signal by assuming that the mass of the DM particle is below the GeV scale, therefore completely abandoning the WIMP hypothesis. By following the spirit of the previous chapters, *i.e. be as natural as possible*, we tried to explain the origin of the sub-GeV mass of the DM particle. In this chapter, we introduced a two-Higgs doublet model, symmetric under a global $U(1)_{PQ}$ (Peccei-Quinn) symmetry. In addition to the extended Higgs sector, we introduced two Weyl iso-doublets with opposite hypercharges (and neutral under $U(1)_{PQ}$), with mass well above the reheating temperature of the Universe. The dark matter particle is a gauge singlet charged under the Peccei-Quinn symmetry, therefore massless at tree level. Assuming that $U(1)_{PQ}$ breaks due to a two-dimensional term in the scalar potential, we showed that a mass term for the dark matter particle emerges at one-loop level. In addition, we showed that the observed relic abundance can be obtained through the freeze-in mechanism. This was a minimal model which explains, at the same time, the dark matter density of the Universe and the origin of the smallness of the mass of the dark matter particle, without the need for parameter fine tuning.

The work presented in this thesis can lead to other studies motivated by the findings of each model. In particular, the Doublet-Triplet Fermionic Dark Matter model, which belongs in the family of simplified dark matter models, shows that the electroweak-scale WIMP scenario is still viable (as the low-energy limit of a complete model). Interestingly, extensions of this model can be studied in the future, which can be motivated either phenomenologically, *e.g.* correcting the branching ratio of the Higgs decay to two photons, or theoretically, *e.g.* $SO(10)$ GUTs predicting a doublet-triplet low-energy particle content supplied by a Z_2-symmetry.

As we showed in our EFT analysis in Chapter 4, the phenomenological study of minimal

dark sectors can lead to interesting results. Generally, by only studying such low-energy sectors, some characteristics of the complete model can be identified. Therefore, the study of various EFTs can be used to classify possible completions of simple dark sectors. The EFT framework, can be used to examine, phenomenologically or theoretically, well-motivated complete models in a generalized fashion.

Certainly, the sub-GeV dark matter scenario can be realized in a natural way. However, there are still some open questions that need to be addressed. In particular, the PQ breaking scale, which is important in the RLDM, may be linked to the strong CP problem. Moreover, certain values of the PQ scale can provide with a sizeable axion relic abundance. Therefore, the investigation of the origin of the PQ scale, perhaps by embedding the RLDM in the DFSZ, can provide interesting insight. Also, since the RLDM was a "proof of concept" of natural sub-GeV dark matter models, an interesting direction for the future would be to identify other models with similar attributes.

With particle colliders, constantly pushing the limits of modern technology, ever-increasing direct detection sensitivity, and satellites able to detect the aftermath of the Big Bang, the DM particle seems to be within our reach. Theoretical research on dark matter (as well as other related topics), helps to point towards the right direction in the pursuit of a *complete particle theory*. The work presented in this thesis, may steer us closer to that goal.

7 Appendix

A One-loop Vertex

The 1-loop corrected vertex amplitude arises from (a) and (b) diagrams depicted in Fig. 3.9 involving vector bosons (W or Z) and new charged ($\chi^{\pm}_{i=1,2}$) or neutral ($\chi^0_{i=1..3}$) fermions. It can be written as,

$$i\,\delta Y = \sum_{j=(a),(b)} (i\,\delta Y_j^{\chi^{\pm}} + i\,\delta Y_j^{\chi^0})\,, \tag{A.1}$$

where

$$\begin{aligned} i\,\delta Y_{(a)}^{\chi^{\pm}} &= -g^2 \sum_{i,j=1}^{2} \Big\{ \Big(O_{1j}^R\, O_{1i}^{L*}\, Y^{h\chi_j^- \chi_i^+} \;+\; O_{1i}^R\, O_{1j}^{L*}\, Y^{h\chi_i^- \chi_j^+} \Big)\; I_1^{Wij} \\ &+ m_{\chi_i^+}\, m_{\chi_j^+} \Big(O_{1j}^R\, O_{1i}^{L*}\, Y^{h\chi_i^- \chi_j^{+}*} \;+\; O_{1i}^R\, O_{1j}^{L*}\, Y^{h\chi_j^- \chi_i^{+}*} \Big)\; I_2^{Wij} \qquad \text{(A.2a)} \\ &+ \Big[O_{1j}^L\, O_{1i}^{L*} \Big(m_{\chi_i^+}\, Y^{h\chi_i^- \chi_j^{+}*} + m_{\chi_j^+}\, Y^{h\chi_j^- \chi_i^+} \Big) \\ &+ O_{1i}^R\, O_{1j}^{R*} \Big(m_{\chi_i^+} Y^{h\chi_j^- \chi_i^{+}*} + m_{\chi_j^+} Y^{h\chi_i^- \chi_j^+} \Big) \Big]\; I_3^{Wij} \Big\}, \end{aligned}$$

$$\begin{aligned} i\,\delta Y_{(a)}^{\chi^0} &= \frac{g^2}{c_W^2} \sum_{i,j=1}^{3} \Big\{ O_{j1}^{\prime\prime L}\, O_{i1}^{\prime\prime L}\, Y^{h\chi_i^0 \chi_j^0}\, I_1^{Zij} + m_{\chi_i^0}\, m_{\chi_j^0}\; O_{i1}^{\prime\prime L}\, O_{j1}^{\prime\prime L}\, Y^{h\chi_i^0 \chi_j^{0}*}\, I_2^{Zij} \\ &- O_{1j}^{\prime\prime L}\, O_{i1}^{\prime\prime L} \Big(m_{\chi_i^0} Y^{h\chi_i^0 \chi_j^{0}*} + m_{\chi_j^0} Y^{h\chi_i^0 \chi_j^0} \Big)\; I_3^{Zij} \Big\}, \qquad \text{(A.2b)} \end{aligned}$$

$$i\,\delta Y_{(b)}^{\chi^{\pm}} = -\frac{\sqrt{2}\, g^2 m_W^2}{v} \sum_{i=1}^{2} \Big[\big(|O_{1i}^L|^2 \;+\; |O_{1i}^R|^2 \big)\; I_4^{Wi} \;+\; 2\, m_{\chi_i^+}\, O_{1i}^{L*}\, O_{1i}^R\, I_5^{Wi} \Big], \tag{A.2c}$$

$$i\,\delta Y_{(b)}^{\chi^0} = -\frac{\sqrt{2} g^2 m_Z^2}{c_W^2\, v} \sum_{i=1}^{3} \Big\{ O_{i1}^{\prime\prime L}\, O_{1i}^{\prime\prime L}\, I_4^{Zi} \;-\; m_{\chi_i^0}\, (O_{i1}^{\prime\prime L})^2\, I_5^{Zi} \Big\}\,, \tag{A.2d}$$

where the integrals, $I^V_{1\ldots5}$, are defined in terms of Passarino-Veltman (PV) functions [314] as,

$$\begin{aligned} I_1^{Vij} &= (D-1)\, m_i^2\, C_0(-p, p, m_i, m_V, m_j) - \frac{m_i^2}{m_V^2}\, B_0(0, m_i, m_j) \\ &+ (D-1)\, B_0(p, m_V, m_j) - \frac{1}{m_V^2}\, A_0(m_j)\,, \qquad \text{(A.3)} \end{aligned}$$

$$I_2^{Vij} = (D-1)\, C_0(-p, p, m_i, m_V, m_j) - \frac{1}{m_V^2}\, B_0(0, m_i, m_j), \tag{A.4}$$

$$
\begin{aligned}
I_3^{Vij} &= \left(D-2+\frac{m_i^2}{m_V^2}-\frac{m_{\chi_1^0}^2}{m_V^2}\right) m_{\chi_1^0}\left[C_{11}(-p,p,m_i,m_V,m_j)-C_{12}(-p,p,m_i,m_V,m_j)\right] \\
&+ \left(1+\frac{m_i^2}{m_V^2}-\frac{m_{\chi_1^0}^2}{m_V^2}\right) m_{\chi_1^0} C_0(-p,p,m_i,m_V,m_j) - \frac{m_{\chi_1^0}}{m_V^2} B_1(p,m_V,m_j) \\
&+ \frac{m_{\chi_1^0}}{m_V^2} B_0(0,m_i,m_j)\,, \qquad \text{(A.5)}
\end{aligned}
$$

$$
\begin{aligned}
I_4^{Vi} &= \left(2-D-\frac{m_i^2}{m_V^2}+\frac{m_{\chi_1^0}^2}{m_V^2}\right) m_{\chi_1^0}\left[C_{11}(p,-p,m_V,m_i,m_V)-C_{12}(p,-p,m_V,m_i,m_V)\right] \\
&- (D-3)\, m_{\chi_1^0} C_0(p,-p,m_V,m_i,m_V) + \frac{m_{\chi_1^0}}{m_V^4}(m_i^2-m_{\chi_1^0}^2) B_1(p,m_V,m_i) \\
&- \frac{m_{\chi_1^0}}{m_V^4} A_0(m_i)\,, \qquad \text{(A.6)}
\end{aligned}
$$

$$
I_5^{Vi} = (D-1)\, C_0(p,-p,m_V,m_i,m_V) + \frac{1}{m_V^4} A_0(m_i)\,, \qquad \text{(A.7)}
$$

where $D \equiv 4-2\,\epsilon\,\delta_{\overline{\rm MS}}$ and $\delta_{\overline{\rm MS}}=1$ for $\overline{\rm MS}$ and $\delta_{\overline{\rm MS}}=0$ for $\overline{\rm DR}$ scheme. All external particles (i.e., χ_1^0) are taken on-shell and $m_i = m_{\chi_i^0}$ for $V=Z$ and $m_i = m_{\chi_i^\pm}$ for $V=W$. Our notation for PV-functions A, B, C, follows closely the one defined in the Appendix of ref. [315]. Functions A_0, B_0, B_1 contain both infinite and finite parts while C_0, C_{11}, C_{12} - functions are purely finite. Our calculation has been done in unitary and (for a cross check) in Feynman gauge. The result for - $i\,\delta Y$ - is both renormalization scale invariant and finite.

B Non-renormalizable operators

Apart from the mass term in eq. (4.1), and the renormalizable couplings to gauge bosons discussed in Section 4.3, the "D"-doublets couple to the bosons of the theory through non-renormalizable $d=5,6$ interactions. Gauge numbers, denoted as $(SU(3)_C, SU(2)_L)_{U(1)_X}$, for the particles here are: for quarks $\mathbf{Q}\sim(\mathbf{3^c},\mathbf{2})_{\frac{1}{3}}$, $\bar{\mathbf{u}}\sim(\mathbf{3^c},\mathbf{1})_{-\frac{4}{3}}$, $\bar{\mathbf{d}}\sim(\mathbf{3^c},\mathbf{1})_{+\frac{2}{3}}$, for leptons: $\mathbf{L}\sim(\mathbf{1^c},\mathbf{2})_{-1}$, $\bar{\mathbf{e}}\sim(\mathbf{1^c},\mathbf{1})_{+2}$, for the Higgs doublet: $\mathbf{H}\sim(\mathbf{1^c},\mathbf{2})_{+1}$ and finally for the new bi-doublets: $\mathbf{D_1}\sim(\mathbf{1^c},\mathbf{2})_{-1}$ and $\mathbf{D_2}\sim(\mathbf{1^c},\mathbf{2})_{+1}$. Schematically, the possible interactions are: $ffHH$, $ff\mathscr{D}H$, $ff\mathscr{D}\mathscr{D}$, where $\mathscr{D}$ is the covariant derivative acting in both Weyl fermions f or to the Higgs fields. We arrange all Weyl fermions f to be left-handed.

We list below all relevant possible independent $d=5$ and $d=6$ operators. An analogous list has been constructed in ref. [316] but for the fermionic *singlet* extension of the SM. The complete set of $d=5,6$ Standard Model operators can be read from ref. [317].

B.1 $d=5$ non-renormalizable operators

- $ffHH$: The $d=5$ operators alter the DM mass spectrum and the Higgs-boson interactions with the dark sector obtained for $f=D_1, D_2$, when integrating out

heavy particles. Examples of possible simplified models that result into these operators, are obtained by integrating out fermion neutral singlets (S_0) and triplets (T), fermion charged singlets ($S^\pm$) and triplets ($T^\pm$), or scalar singlets, ($\Phi_{S_0}, \Phi_{S^\pm}$) and triplets, ($\Phi_{T^0}, \Phi_{T^\pm}$). In fully $SU(2)_L$-invariant form we have

$$
\begin{aligned}
-\mathscr{L}_{\rm dim=5} \supset\ & +\frac{\lambda_1^2}{2\,M_{S_0}}\,(\epsilon^{ab}H_aD_{1b})\,(\epsilon^{cd}H_cD_{1d})\ +\ \frac{\lambda_2^2}{2M_{S_0}}\,(H^{\dagger a}D_{2a})\,(H^{\dagger b}D_{2b}) \\
& +\frac{\lambda_{12}}{M_{S_0}}\,(\epsilon^{ab}H_aD_{1b})\,(H^{\dagger c}D_{2c})\ +\ \frac{\lambda'_{12}}{M_{S^\pm}}\,(\epsilon^{ab}H_aD_{2b})\,(H^{\dagger c}D_{1c}) \\
& +\frac{Y_1^2}{2\,M_T}\,[\epsilon^{ab}H_a(\tau^A)^c_bD_{1c}]\,[\epsilon^{fg}H_f(\tau^A)^h_gD_{1h}]\ +\ \frac{Y_2^2}{2\,M_T}\,[H^{\dagger a}(\tau^A)^b_aD_{2b}]\,[H^{\dagger c}(\tau^A)^d_cD_{2d}] \\
& +\frac{Y_{12}}{M_T}\,[H^{\dagger a}(\tau^A)^b_aD_{2b}]\,[\epsilon^{cd}H_c(\tau^A)^f_dD_{1f}]\ +\ \frac{Y'_{12}}{M_{T^\pm}}\,[H^{\dagger a}(\tau^A)^b_aD_{1b}]\,[\epsilon^{cd}H_c(\tau^A)^f_dD_{2f}] \\
& +\frac{\xi_{12}}{M_{\Phi_0}}\,(\epsilon^{ab}D_{1a}D_{2b})(H^{\dagger c}H_c) \\
& +\frac{k_1^2}{2\,M_{\Phi_T^\pm}}\,[\epsilon^{ab}D_{1a}(\tau^A)^c_bD_{1c}]\,[\epsilon^{fg}H_f(\tau^A)^h_gH_h]+\frac{k_2^2}{2\,M_{\Phi_T^\pm}}\,[\epsilon^{ab}D_{2a}(\tau^A)^c_bD_{2c}]\,[H^{\dagger d}(\tau^A)^f_d\epsilon_{fg}H^{\dagger g}] \\
& +\frac{k_{12}}{M_{\Phi_{T_0}}}\,[\epsilon^{ab}D_{1a}(\tau^A)^c_bD_{2c}]\,[H^{\dagger d}(\tau^A)^g_dH_g]\ +\ \frac{k'_{12}}{M_{\Phi_{T_0}}}\,[\epsilon^{ab}D_{2a}(\tau^A)^c_bD_{1c}]\,[H^{\dagger d}(\tau^A)^g_dH_g] \\
& +\ \text{H.c.}\,, \qquad\qquad (B.1)
\end{aligned}
$$

where the meaning of various mass scales is rather obvious e.g., those suppressed by $M_{S_0}, M_{S^\pm}$ and $M_{T,T^\pm}$ are derived from integrating out heavy fermionic neutral and/or charged singlets and triplets $S_0, S^\pm$ and, $T, T^\pm$ respectively, and so on.

However, not all operators in eq. (B.1) are independent; in fact most of them are not. Using a standard identity for Pauli matrices, $(\tau^A)_{ab}(\tau^A)_{cd} = 2(\delta_{ad}\delta_{bc} - \frac{1}{2}\delta_{ab}\delta_{cd})$, one can arrive at the most general form of (B.1) written as

$$
\begin{aligned}
-\mathscr{L}_{\rm dim=5} \supset\ & +\frac{y_1}{2\,\Lambda}\,(\epsilon^{ab}H_aD_{1b})\,(\epsilon^{cd}H_cD_{1d})\ +\ \frac{y_2}{2\Lambda}\,(H^{\dagger a}D_{2a})\,(H^{\dagger b}D_{2b}) \\
& +\ \frac{y_{12}}{\Lambda}\,(\epsilon^{ab}H_aD_{1b})\,(H^{\dagger c}D_{2c})\ +\ \frac{\xi_{12}}{\Lambda}\,(\epsilon^{ab}D_{1a}D_{2b})(H^{\dagger c}H_c)\ +\ \text{H.c.} \qquad\qquad (B.2)
\end{aligned}
$$

where we use a common mass scale Λ at which heavy particles are integrated out and the complex valued Yukawa couplings $y_1, y_2, y_{12}, \xi_{12}$. We should also remark that the last operator in (B.2) is somewhat trivial and it can appear in any powers of the Higgs polynomial. At EW vacuum it adds a common mass to D_1 and D_2 as in eq. (4.1) does. All operators in (B.2) give masses to neutral components of the WIMPs except from the last one that gives mass also to the charged components.

Furthermore, in this class belongs the famous Weinberg operator for neutrino masses, with $f = L$ being the SM lepton doublet

$$
\frac{y_\nu}{2\,\Lambda}\,(\epsilon^{ab}H_aL_b)\,(\epsilon^{cd}H_cL_d)\ +\ \text{H.c.} \qquad\qquad (B.3)
$$

The origin of this operator is not necessarily related to the DM sector. Note that the first three terms in eq. (B.2), can also be obtained by integrating out heavy right-handed neutrino states, $\bar{\nu} \sim (\mathbf{1^c}, \mathbf{1})_\mathbf{0}$, from renormalizable Yukawa couplings, $H^\dagger\, D_2\, \bar{\nu} + H\, D_1\, \bar{\nu} + \text{H.c.}$ as in the see-saw model for neutrino masses.

Of course there are additional terms, *e.g.* LD_2HH, but these in general, break the Z_2-discrete (or lepton number) symmetry that keeps the DM particle stable. Interestingly enough, these terms are connecting the DM particle to neutrinos, see for instance [318]. These independent operators are

$$\frac{\eta_1}{2\,\Lambda}\,(\epsilon^{ab} H_a D_{1b})\,(\epsilon^{cd} H_c L_d) \;+\; \frac{\eta_{12}}{\Lambda}\,(\epsilon^{ab} H_a L_b)\,(H^{\dagger c} D_{2c}) \\ +\; \frac{\zeta_{12}}{\Lambda}\,(\epsilon^{ab} L_a D_{2b})(H^{\dagger c} H_c) \;+\; \text{H.c.} \tag{B.4}$$

- $ff\mathscr{D}H$: In this case the fermion bilinear must be a weak doublet with hypercharge -1. The only such combination, $D_2^\dagger \bar{\sigma}^\mu \bar{e} \mathscr{D}_\mu H^\dagger + \text{H.c.}$, is not invariant under the Z_2-symmetry.
- $ff\mathscr{D}\mathscr{D}$: Under Z_2-symmetry there are three possibilities : $D_1\mathscr{D}\mathscr{D}D_2, \mathscr{D}\mathscr{D}D_1D_2$ and $\mathscr{D}D_1\mathscr{D}D_2$. After some algebra, and taking the equations of motion into account we find that these lead to dipole operators of the form

$$\frac{d_\gamma}{\Lambda}\,\epsilon^{ab} D_{1a}\,\sigma^{\mu\nu}\,D_{2b}\,B_{\mu\nu} \;+\; \frac{d_W}{\Lambda}\,\epsilon^{ab} D_{1a}\,\sigma^{\mu\nu}\,(\tau^A)_b{}^c\,D_{2c}\,W^A_{\mu\nu} + \\ \frac{i\,e_\gamma}{\Lambda}\,\epsilon^{ab} D_{1a}\,\sigma^{\mu\nu}\,D_{2b}\,\widetilde{B}_{\mu\nu} \;+\; \frac{i\,e_W}{\Lambda}\,\epsilon^{ab} D_{1a}\,\sigma^{\mu\nu}\,(\tau^A)_b{}^c\,D_{2c}\,\widetilde{W}^A_{\mu\nu} \;+\; \text{H.c.}\,, \tag{B.5}$$

where $B_{\mu\nu}$ and $W^A_{\mu\nu}$ are the $U(1)$ and $SU(2)_L$, field strength tensors, respectively, and $\widetilde{B}_{\mu\nu} \equiv \epsilon_{\mu\nu}{}^{\rho\sigma}\,B_{\rho\sigma}$. These operators are electric and magnetic dipole moments for the DM particle. They arise directly at $d = 5$ level, whereas quark and/or lepton magnetic moments arise at $d = 6$ level.

We have not found other than the above $d = 5$ independent operators.

B.2 $d = 6$ non-renormalizable operators

Focusing only in interactions between $f = D_1$ or D_2 and the Higgs field[1] there are four Lorentz and gauge invariant categories: ffH^3, $ff\mathscr{D}H^2$, $ff\mathscr{D}^2H$, $ff\mathscr{D}^3$, and of course $ffff$.

- ffH^3 : There are no such operators which preserve the Z_2-symmetry, or, as a matter of fact, the charge conjugation or custodial symmetry or lepton number , e.g. there is $(H^\dagger D_1 \bar{e})(H^\dagger H)$ and the one with triplets.
- $ff\mathscr{D}H^2$: There are quite a few invariant operators of this kind. The independent

[1] All others are identical to standard dimension-6 operators and can be found in [317, 319].

ones are

$$
\begin{aligned}
-\mathcal{L}_{\rm dim=6} \supset\ & \left(\frac{a_1}{\Lambda^2}\, D_1^{\dagger a}\, \bar\sigma^\mu\, D_{1a} \ +\ \frac{a_2}{\Lambda^2}\, D_2^{\dagger a}\, \bar\sigma^\mu\, D_{2a}\right) \left(i\, H^{\dagger b}\, (\overleftrightarrow{\mathscr{D}_\mu})_b{}^c\, H_c\right) \\
& + \left(\frac{a_1'}{\Lambda^2}\, D_1^{\dagger a}\, (\tau^A)_a{}^b\, \bar\sigma^\mu\, D_{1b} \ +\ \frac{a_2'}{\Lambda^2}\, D_2^{\dagger a}\, (\tau^A)_a{}^b\, \bar\sigma^\mu D_{2b}\right) \left(i\, H^{\dagger c}\, (\overleftrightarrow{\mathscr{D}_\mu^A})_c{}^d\, H_d\right) \\
& + \frac{b_1}{\Lambda^2}\, (D_2^{\dagger a}\, \bar\sigma^\mu\, D_{1a})\, [\epsilon^{bc} H_b\, (\overleftrightarrow{\mathscr{D}_\mu})_c{}^d\, H_d] \ +\ \frac{b_2}{\Lambda^2}\, (D_1^{\dagger a}\, \bar\sigma^\mu\, D_{2a})\, (\epsilon_{bc}\, H^{\dagger b}\, (\overleftrightarrow{\mathscr{D}_\mu}^\dagger)^c{}_d\, H^{\dagger d})
\end{aligned}
\tag{B.6}
$$

where $H^\dagger \overleftrightarrow{\mathscr{D}_\mu} H \equiv H^\dagger \overrightarrow{\mathscr{D}_\mu} H - H^\dagger \overleftarrow{\mathscr{D}_\mu} H$ and $H^\dagger \overleftrightarrow{\mathscr{D}_\mu^A} H \equiv H^\dagger \tau^A \overrightarrow{\mathscr{D}_\mu} H - H^\dagger \overleftarrow{\mathscr{D}_\mu} \tau^A H$, $a_{1,2}$ and $a'_{1,2}$ are real numbers, while $b_2 = b_1^*$. We can obtain new operators after changing $L \leftrightarrow D_1$ but these would violate Z_2 or they would belong to existing SM operators given in ref. [317].

- $ff\mathscr{D}^2H$: Because D_1, D_2 and the H are $SU(2)$-doublets only Z_2-breaking terms exist in this category, e.g., $(D_1\sigma_{\mu\nu}\bar e)F^{\mu\nu}H^\dagger$ or when the Higgs receives VEV they reduce to $d=5$ operators already given in (B.5).
- $ff\mathscr{D}^3$: We found no new operators. Lorentz invariance says that they exist only if ff transforms as a vector e.g., $(D_1^\dagger\bar\sigma_\mu D_1)(\mathscr{D}_\rho B^{\rho\mu})$. By using equations of motion we get at most the operators of eq. (B.6), or the four fermion operators, $ffff$, given below and/or other like previously violating Z_2-symmetry. Acting with the covariant derivative to the left (on fermion current) we obtain operators as in eq. (B.5).
- $ffff$: we found the following independent operators:

$$
\begin{aligned}
-\mathcal{L}_{\rm dim=6} \supset\ & \frac{c_{12}}{\Lambda^2}\, (\epsilon^{ab} D_{1a} D_{2b})\, (\epsilon^{cd} D_{1c} D_{2d}) \ +\ \sum_{k,\ell=1}^{2} \frac{d_{k\ell}}{\Lambda^2}\, (D_k^{\dagger a}\, \bar\sigma^\mu\, D_{k\,a})\, (D_\ell^{\dagger b}\, \bar\sigma_\mu\, D_{\ell\, b}) \\
& + \sum_{i,j=1}^{3} \sum_{k=1}^{2} \frac{1}{\Lambda^2}\, (D_k^{\dagger a}\, \bar\sigma^\mu\, D_{k\,a}) \left[f^\ell_{kij} (\ell_i^\dagger \bar\sigma_\mu \ell_j) + f^q_{kij} (q_i^\dagger \bar\sigma_\mu q_j)\right] \ + \\
& + \sum_{i,j=1}^{3} \sum_{k=1}^{2} \frac{1}{\Lambda^2}\, (D_k^{\dagger a}\, \bar\sigma^\mu\, (\tau^A)_a{}^b D_{k\, b}) \left[c^L_{kij} (L_i^{\dagger\, c} \bar\sigma_\mu (\tau^A)_c{}^d L_{j\, d}) + c^Q_{kij} (Q_i^{\dagger\, c} \bar\sigma_\mu (\tau^A)_c{}^d Q_{j\, d})\right] \\
& + \frac{c'_{12}}{\Lambda^2}\, (D_1^{\dagger a}\, \bar\sigma^\mu\, (\tau^A)_a{}^b D_{1\, b})\, (D_2^{\dagger c}\, \bar\sigma^\mu\, (\tau^A)_c{}^d D_{2\, d}) + \text{H.c.}\,,
\end{aligned}
\tag{B.7}
$$

not counting operators that violate Z_2. Note that $\ell \equiv L, \bar e$ and $q \equiv Q, \bar u, \bar d$ and i, j indices stand for lepton or quark flavour. Furthermore, there is only one scalar $d=6$ four-fermion operator, the one containing DM-self interactions proportional to c_{12}. In addition, there are lepton number violating *scalar* operators like:

$$
(D_{1a} D_{1b})(L^{\dagger\, a} L^{\dagger\, b}) \ +\ \epsilon^{ac}\epsilon^{bd}\, (D_{2a} D_{2b})(L_c L_d) \ +\ \epsilon^{ab}\epsilon^{cd}\, (D_{2a} L_b)(D_{2c} L_d)\,. \tag{B.8}
$$

Other four-fermion *scalar* operators between quarks/leptons and DM fields appear first at $d=7$ level and have the form $D_1 D_2 (QH\bar u + QH^\dagger \bar d + LH^\dagger \bar e)$. All other operators in eq. (B.7) are vector-like, and, many of them lead to spin-dependent interactions in DM-nuclei collisions.

Bibliography

[1] S. L. Glashow, *Partial Symmetries of Weak Interactions*, *Nucl. Phys.* **22** (1961) 579–588.

[2] S. Weinberg, *A Model of Leptons*, *Phys. Rev. Lett.* **19** (1967) 1264–1266.

[3] A. Salam, *Weak and Electromagnetic Interactions*, *Conf. Proc.* **C680519** (1968) 367–377.

[4] D. J. Gross and F. Wilczek, *Asymptotically Free Gauge Theories. 1*, *Phys. Rev.* **D8** (1973) 3633–3652.

[5] D. J. Gross and F. Wilczek, *Asymptotically Free Gauge Theories. 2.*, *Phys. Rev.* **D9** (1974) 980–993.

[6] H. D. Politzer, *Asymptotic Freedom: An Approach to Strong Interactions*, *Phys. Rept.* **14** (1974) 129–180.

[7] J. D. Bjorken and S. D. Drell, *Relativistic Quantum Fields*. McGraw-Hill, 1965.

[8] F. Halzen and A. D. Martin, *Quarks And Leptons: An Introductory Course In Modern Particle Physics*. Wiley, 1984.

[9] C. Itzykson and J. Zuber, *Quantum Field Theory*. International series in pure and applied physics. McGraw-Hill, 1985.

[10] T. P. Cheng and L. F. Li, *Gauge theory of elementary particle physics*. 1984.

[11] V. D. Barger and R. J. N. Phillips, *Collider physics*. 1987.

[12] S. Pokorski, *Gauge field theories*. Cambridge University Press, 2005.

[13] M. E. Peskin and D. V. Schroeder, *An Introduction to quantum field theory*, .

[14] S. Weinberg, *The Quantum theory of fields. Vol. 1: Foundations*. Cambridge University Press, 2005.

[15] S. Weinberg, *The quantum theory of fields. Vol. 2: Modern applications*. Cambridge University Press, 2013.

[16] S. Weinberg, *The quantum theory of fields. Vol. 3: Supersymmetry*. Cambridge University Press, 2013.

[17] J. L. Hewett, *The Standard model and why we believe it*, in *Supersymmetry, supergravity and supercolliders. Proceedings, Theoretical Advanced Study Institute in elementary particle physics, TASI'97, Boulder, USA, June 2-27, 1997*, pp. 3–83, 1997. `hep-ph/9810316`.

[18] D. Griffiths, *Introduction to Elementary Particles*. Wiley, 2008.

[19] M. Srednicki, *Quantum Field Theory*. Cambridge Univ. Press, Cambridge, 2007.

[20] F. Mandl and G. Shaw, *Quantum Field Theory*. Wiley, 2010.

[21] J. C. Romao and J. P. Silva, *A resource for signs and Feynman diagrams of the Standard Model*, *Int. J. Mod. Phys.* **A27** (2012) 1230025, [`arXiv:1209.6213`].

[22] M. D. Schwartz, *Quantum Field Theory and the Standard Model*. Cambridge University Press, 2014.

[23] **CMS** Collaboration, S. Chatrchyan et al., *Observation of a new boson at a mass of 125 GeV with the CMS experiment at the LHC*, *Phys. Lett.* **B716** (2012) 30–61, [arXiv:1207.7235].

[24] **ATLAS** Collaboration, G. Aad et al., *Observation of a new particle in the search for the Standard Model Higgs boson with the ATLAS detector at the LHC*, *Phys.Lett.* **B716** (2012) 1–29, [arXiv:1207.7214].

[25] P. W. Higgs, *Broken Symmetries and the Masses of Gauge Bosons*, *Phys. Rev. Lett.* **13** (1964) 508–509.

[26] F. Englert and R. Brout, *Broken Symmetry and the Mass of Gauge Vector Mesons*, *Phys. Rev. Lett.* **13** (1964) 321–323.

[27] G. S. Guralnik, C. R. Hagen, and T. W. B. Kibble, *Global Conservation Laws and Massless Particles*, *Phys. Rev. Lett.* **13** (1964) 585–587.

[28] H. K. Dreiner, H. E. Haber, and S. P. Martin, *Two-component spinor techniques and Feynman rules for quantum field theory and supersymmetry*, *Phys.Rept.* **494** (2010) 1–196, [arXiv:0812.1594].

[29] **Planck** Collaboration, P. A. R. Ade et al., *Planck 2015 results. XIII. Cosmological parameters*, *Astron. Astrophys.* **594** (2016) A13, [arXiv:1502.01589].

[30] S. Weinberg, *Gravitation and Cosmology: Principles and Applications of the General Theory of Relativity*. Wiley, New York, NY, 1972.

[31] E. W. Kolb and M. S. Turner, *The Early Universe*, *Front. Phys.* **69** (1990) 1–547.

[32] S. Dodelson, *Modern Cosmology*. Academic Press, Amsterdam, 2003.

[33] S. Weinberg, *The First Three Minutes. A Modern View of the Origin of the Universe*. 1977.

[34] U. A. Yajnik, *Cosmology for Particle Physicists*, in *21st SERC School in Theoretical High Energy Physics Ahmedabad, India, February 11-March 3, 2006*, 2006. arXiv:0808.2236.

[35] A. R. Liddle, *An Introduction to cosmological inflation*, in *Proceedings, Summer School in High-energy physics and cosmology: Trieste, Italy, June 29-July 17, 1998*, pp. 260–295, 1999. astro-ph/9901124.

[36] D. Baumann, *Inflation*, in *Physics of the large and the small, TASI 09, proceedings of the Theoretical Advanced Study Institute in Elementary Particle Physics, Boulder, Colorado, USA, 1-26 June 2009*, pp. 523–686, 2011. arXiv:0907.5424.

[37] J. M. Cline, *Baryogenesis*, in *Les Houches Summer School - Session 86: Particle Physics and Cosmology: The Fabric of Spacetime Les Houches, France, July 31-August 25, 2006*, 2006. hep-ph/0609145.

[38] D. E. Morrissey and M. J. Ramsey-Musolf, *Electroweak baryogenesis*, *New J. Phys.* **14** (2012) 125003, [arXiv:1206.2942].

[39] F. Zwicky, *Die Rotverschiebung von extragalaktischen Nebeln*, *Helv. Phys. Acta* **6** (1933) 110–127. [Gen. Rel. Grav.41,207(2009)].

[40] V. C. Rubin, W. K. Ford, Jr., and N. Thonnard, *Extended rotation curves of high-luminosity spiral galaxies. IV. Systematic dynamical properties, Sa through Sc*, *Astrophys. J.* **225** (1978) L107–L111.

[41] L. A. Moustakas and R. B. Metcalf, *Detecting dark matter substructure spectroscopically in strong gravitational lenses*, *Mon. Not. Roy. Astron. Soc.* **339** (2003) 607, [astro-ph/0206176].

[42] E. van Uitert, H. Hoekstra, T. Schrabback, D. G. Gilbank, M. D. Gladders, and H. K. C. Yee, *Constraints on the shapes of galaxy dark matter haloes from weak gravitational lensing*, *Astron. Astrophys.* **545** (2012) A71, [arXiv:1206.4304].

[43] K. Umetsu, A. Zitrin, D. Gruen, J. Merten, M. Donahue, and M. Postman, *CLASH: Joint Analysis of Strong-Lensing, Weak-Lensing Shear and Magnification Data for 20 Galaxy Clusters*, *Astrophys. J.* **821** (2016), no. 2 116, [arXiv:1507.04385].

[44] D. Clowe, M. Bradac, A. H. Gonzalez, M. Markevitch, S. W. Randall, C. Jones, and D. Zaritsky, *A direct empirical proof of the existence of dark matter*, *Astrophys. J.* **648** (2006) L109–L113, [astro-ph/0608407].

[45] **Fermi-LAT** Collaboration, M. Ackermann et al., *Search for gamma-ray spectral lines with the Fermi large area telescope and dark matter implications*, *Phys. Rev.* **D88** (2013) 082002, [arXiv:1305.5597].

[46] **Fermi-LAT** Collaboration, M. Ackermann et al., *Updated search for spectral lines from Galactic dark matter interactions with pass 8 data from the Fermi Large Area Telescope*, *Phys. Rev.* **D91** (2015), no. 12 122002, [arXiv:1506.00013].

[47] K. Kadota, T. Sekiguchi, and H. Tashiro, *A new constraint on millicharged dark matter from galaxy clusters*, arXiv:1602.04009.

[48] V. Iršič et al., *New Constraints on the free-streaming of warm dark matter from intermediate and small scale Lyman-α forest data*, arXiv:1702.01764.

[49] P. J. E. Peebles, *How the Nonbaryonic Dark Matter Theory Grew*, arXiv:1701.05837.

[50] B. W. Lee and S. Weinberg, *Cosmological Lower Bound on Heavy Neutrino Masses*, *Phys. Rev. Lett.* **39** (1977) 165–168.

[51] P. Hut, *Limits on Masses and Number of Neutral Weakly Interacting Particles*, *Phys. Lett.* **B69** (1977) 85.

[52] G. Jungman, M. Kamionkowski, and K. Griest, *Supersymmetric dark matter*, *Phys.Rept.* **267** (1996) 195–373, [hep-ph/9506380].

[53] S. Weinberg, *Cosmology*. Oxford Univ. Press (2008), 2008.

[54] D. Hooper, *Particle Dark Matter*, in *Proceedings of Theoretical Advanced Study Institute in Elementary Particle Physics on The dawn of the LHC era (TASI 2008)*, pp. 709–764, 2010. arXiv:0901.4090.

[55] G. Gelmini and P. Gondolo, *DM Production Mechanisms*, arXiv:1009.3690.

[56] M. Lisanti, *Lectures on Dark Matter Physics*, in *Theoretical Advanced Study Institute in Elementary Particle Physics: New Frontiers in Fields and Strings (TASI 2015) Boulder, CO, USA, June 1-26, 2015*, 2016. arXiv:1603.03797.

[57] J. Edsjo and P. Gondolo, *Neutralino relic density including coannihilations*, *Phys. Rev.* **D56** (1997) 1879–1894, [hep-ph/9704361].

[58] K. Griest and M. Kamionkowski, *Unitarity Limits on the Mass and Radius of Dark Matter Particles*, *Phys. Rev. Lett.* **64** (1990) 615.

[59] K. Griest and D. Seckel, *Three exceptions in the calculation of relic abundances*, *Phys. Rev.* **D43** (1991) 3191–3203.

[60] **Particle Data Group** Collaboration, C. Patrignani et al., *Review of Particle Physics*, *Chin. Phys.* **C40** (2016), no. 10 100001.

[61] L. J. Hall, K. Jedamzik, J. March-Russell, and S. M. West, *Freeze-In Production of*

FIMP Dark Matter, *JHEP* **03** (2010) 080, [arXiv:0911.1120].

[62] F. Elahi, C. Kolda, and J. Unwin, *UltraViolet Freeze-in*, *JHEP* **03** (2015) 048, [arXiv:1410.6157].

[63] A. R. Zhitnitsky, *On Possible Suppression of the Axion Hadron Interactions. (In Russian)*, *Sov. J. Nucl. Phys.* **31** (1980) 260. [Yad. Fiz.31,497(1980)].

[64] M. Dine, W. Fischler, and M. Srednicki, *A Simple Solution to the Strong CP Problem with a Harmless Axion*, *Phys. Lett.* **B104** (1981) 199–202.

[65] R. D. Peccei, *The Strong CP problem and axions*, *Lect. Notes Phys.* **741** (2008) 3–17, [hep-ph/0607268]. [,3(2006)].

[66] W. Hu, R. Barkana, and A. Gruzinov, *Cold and fuzzy dark matter*, *Phys. Rev. Lett.* **85** (2000) 1158–1161, [astro-ph/0003365].

[67] J. R. Ellis, D. V. Nanopoulos, and S. Sarkar, *The Cosmology of Decaying Gravitinos*, *Nucl. Phys.* **B259** (1985) 175–188.

[68] H. Goldberg and L. J. Hall, *A New Candidate for Dark Matter*, *Phys. Lett.* **B174** (1986) 151. [,467(1986)].

[69] A. Ringwald, *Exploring the Role of Axions and Other WISPs in the Dark Universe*, *Phys. Dark Univ.* **1** (2012) 116–135, [arXiv:1210.5081].

[70] G. Steigman and M. S. Turner, *Cosmological Constraints on the Properties of Weakly Interacting Massive Particles*, *Nucl. Phys.* **B253** (1985) 375–386.

[71] E. W. Kolb, D. J. H. Chung, and A. Riotto, *WIMPzillas!*, in *Trends in theoretical physics II. Proceedings, 2nd La Plata Meeting, Buenos Aires, Argentina, November 29-December 4, 1998*, pp. 91–105, 1998. hep-ph/9810361. [,91(1998)].

[72] S. P. Martin, *A Supersymmetry primer*, hep-ph/9709356. [Adv. Ser. Direct. High Energy Phys.18,1(1998)].

[73] H.-C. Cheng, J. L. Feng, and K. T. Matchev, *Kaluza-Klein dark matter*, *Phys. Rev. Lett.* **89** (2002) 211301, [hep-ph/0207125].

[74] G. Servant and T. M. P. Tait, *Is the lightest Kaluza-Klein particle a viable dark matter candidate?*, *Nucl. Phys.* **B650** (2003) 391–419, [hep-ph/0206071].

[75] R. Mahbubani and L. Senatore, *The Minimal model for dark matter and unification*, *Phys.Rev.* **D73** (2006) 043510, [hep-ph/0510064].

[76] B. Patt and F. Wilczek, *Higgs-field portal into hidden sectors*, hep-ph/0605188.

[77] J. March-Russell, S. M. West, D. Cumberbatch, and D. Hooper, *Heavy Dark Matter Through the Higgs Portal*, *JHEP* **07** (2008) 058, [arXiv:0801.3440].

[78] M. Cirelli, N. Fornengo, and A. Strumia, *Minimal dark matter*, *Nucl.Phys.* **B753** (2006) 178–194, [hep-ph/0512090].

[79] T. Cohen, J. Kearney, A. Pierce, and D. Tucker-Smith, *Singlet-Doublet Dark Matter*, *Phys. Rev.* **D85** (2012) 075003, [arXiv:1109.2604].

[80] L. Calibbi, A. Mariotti, and P. Tziveloglou, *Singlet-Doublet Model: Dark matter searches and LHC constraints*, *JHEP* **10** (2015) 116, [arXiv:1505.03867].

[81] J. Abdallah et al., *Simplified Models for Dark Matter Searches at the LHC*, *Phys. Dark Univ.* **9-10** (2015) 8–23, [arXiv:1506.03116].

[82] A. Dedes and D. Karamitros, *Doublet-Triplet Fermionic Dark Matter*, *Phys. Rev.* **D89** (2014), no. 11 115002, [arXiv:1403.7744].

[83] Q.-H. Cao, C.-R. Chen, C. S. Li, and H. Zhang, *Effective Dark Matter Model: Relic*

density, CDMS II, Fermi LAT and LHC, *JHEP* **08** (2011) 018, [arXiv:0912.4511].

[84] F. D'Eramo and M. Procura, *Connecting Dark Matter UV Complete Models to Direct Detection Rates via Effective Field Theory*, *JHEP* **04** (2015) 054, [arXiv:1411.3342].

[85] S. Matsumoto, S. Mukhopadhyay, and Y.-L. S. Tsai, *Effective Theory of WIMP Dark Matter supplemented by Simplified Models: Singlet-like Majorana fermion case*, arXiv:1604.02230.

[86] N. Nagata and S. Shirai, *Higgsino Dark Matter in High-Scale Supersymmetry*, *JHEP* **01** (2015) 029, [arXiv:1410.4549].

[87] N. Weiner and I. Yavin, *UV completions of magnetic inelastic and Rayleigh dark matter for the Fermi Line(s)*, *Phys. Rev.* **D87** (2013), no. 2 023523, [arXiv:1209.1093].

[88] A. Dedes, D. Karamitros, and V. C. Spanos, *Effective Theory for Electroweak Doublet Dark Matter*, *Phys. Rev.* **D94** (2016), no. 9 095008, [arXiv:1607.05040].

[89] T. Asaka, S. Blanchet, and M. Shaposhnikov, *The nuMSM, dark matter and neutrino masses*, *Phys. Lett.* **B631** (2005) 151–156, [hep-ph/0503065].

[90] A. Kusenko, *Sterile neutrinos: The Dark side of the light fermions*, *Phys. Rept.* **481** (2009) 1–28, [arXiv:0906.2968].

[91] C. Boehm and P. Fayet, *Scalar dark matter candidates*, *Nucl. Phys.* **B683** (2004) 219–263, [hep-ph/0305261].

[92] J.-H. Huh, J. E. Kim, J.-C. Park, and S. C. Park, *Galactic 511 keV line from MeV milli-charged dark matter*, *Phys. Rev.* **D77** (2008) 123503, [arXiv:0711.3528].

[93] C. Cheung, J. T. Ruderman, L.-T. Wang, and I. Yavin, *Kinetic Mixing as the Origin of Light Dark Scales*, *Phys. Rev.* **D80** (2009) 035008, [arXiv:0902.3246].

[94] A. Dedes, D. Karamitros, and A. Pilaftsis, *Radiative Light Dark Matter*, *Phys. Rev.* **D95** (2017), no. 11 115037, [arXiv:1704.01497].

[95] **CDMS** Collaboration, R. Agnese et al., *Silicon Detector Dark Matter Results from the Final Exposure of CDMS II*, *Phys. Rev. Lett.* **111** (2013), no. 25 251301, [arXiv:1304.4279].

[96] **SuperCDMS** Collaboration, R. Agnese et al., *Search for Low-Mass Weakly Interacting Massive Particles with SuperCDMS*, *Phys. Rev. Lett.* **112** (2014), no. 24 241302, [arXiv:1402.7137].

[97] **PandaX-II** Collaboration, A. Tan et al., *Dark Matter Results from First 98.7 Days of Data from the PandaX-II Experiment*, *Phys. Rev. Lett.* **117** (2016), no. 12 121303, [arXiv:1607.07400].

[98] **DarkSide** Collaboration, P. Agnes et al., *Results from the first use of low radioactivity argon in a dark matter search*, *Phys. Rev.* **D93** (2016), no. 8 081101, [arXiv:1510.00702]. [Addendum: Phys. Rev.D95,no.6,069901(2017)].

[99] **XENON100** Collaboration, E. Aprile et al., *Dark Matter Results from 225 Live Days of XENON100 Data*, *Phys. Rev. Lett.* **109** (2012) 181301, [arXiv:1207.5988].

[100] **LUX** Collaboration, D. S. Akerib et al., *Results from a search for dark matter in the complete LUX exposure*, *Phys. Rev. Lett.* **118** (2017), no. 2 021303, [arXiv:1608.07648].

[101] M. W. Goodman and E. Witten, *Detectability of Certain Dark Matter Candidates*,

Phys.Rev. **D31** (1985) 3059.

[102] J. Hisano, S. Matsumoto, M. M. Nojiri, and O. Saito, *Direct detection of the Wino and Higgsino-like neutralino dark matters at one-loop level*, *Phys.Rev.* **D71** (2005) 015007, [hep-ph/0407168].

[103] J. Hisano, K. Ishiwata, N. Nagata, and T. Takesako, *Direct Detection of Electroweak-Interacting Dark Matter*, *JHEP* **1107** (2011) 005, [arXiv:1104.0228].

[104] **LUX** Collaboration, D. S. Akerib et al., *Limits on spin-dependent WIMP-nucleon cross section obtained from the complete LUX exposure*, arXiv:1705.03380.

[105] E. Aprile et al., *First Dark Matter Search Results from the XENON1T Experiment*, arXiv:1705.06655.

[106] **XENON** Collaboration, E. Aprile et al., *Physics reach of the XENON1T dark matter experiment*, *JCAP* **1604** (2016), no. 04 027, [arXiv:1512.07501].

[107] **XENON100** Collaboration, E. Aprile et al., *XENON100 Dark Matter Results from a Combination of 477 Live Days*, *Phys. Rev.* **D94** (2016), no. 12 122001, [arXiv:1609.06154].

[108] A. Dedes, I. Giomataris, K. Suxho, and J. D. Vergados, *Searching for Secluded Dark Matter via Direct Detection of Recoiling Nuclei as well as Low Energy Electrons*, *Nucl. Phys.* **B826** (2010) 148–173, [arXiv:0907.0758].

[109] R. Essig, J. Mardon, and T. Volansky, *Direct Detection of Sub-GeV Dark Matter*, *Phys. Rev.* **D85** (2012) 076007, [arXiv:1108.5383].

[110] R. Essig, T. Volansky, and T.-T. Yu, *New Constraints and Prospects for sub-GeV Dark Matter Scattering off Electrons in Xenon*, arXiv:1703.00910.

[111] G. B. Gelmini, *TASI 2014 Lectures: The Hunt for Dark Matter*, in *Theoretical Advanced Study Institute in Elementary Particle Physics: Journeys Through the Precision Frontier: Amplitudes for Colliders (TASI 2014) Boulder, Colorado, June 2-27, 2014*, 2015. arXiv:1502.01320.

[112] M. Klasen, M. Pohl, and G. Sigl, *Indirect and direct search for dark matter*, *Prog. Part. Nucl. Phys.* **85** (2015) 1–32, [arXiv:1507.03800].

[113] J. M. Gaskins, *A review of indirect searches for particle dark matter*, *Contemp. Phys.* **57** (2016), no. 4 496–525, [arXiv:1604.00014].

[114] N. Fornengo, *Dark matter overview*, in *25th European Cosmic Ray Symposium (ECRS 2016) Turin, Italy, September 04-09, 2016*, 2016. arXiv:1701.00119.

[115] G. Bertone, D. Hooper, and J. Silk, *Particle dark matter: Evidence, candidates and constraints*, *Phys. Rept.* **405** (2005) 279–390, [hep-ph/0404175].

[116] **Snowmass 2013 Cosmic Frontier Working Groups 1–4** Collaboration, D. Bauer et al., *Dark Matter in the Coming Decade: Complementary Paths to Discovery and Beyond*, *Phys. Dark Univ.* **7-8** (2015) 16–23, [arXiv:1305.1605].

[117] **Fermi-LAT** Collaboration, M. Ackermann et al., *Searching for Dark Matter Annihilation from Milky Way Dwarf Spheroidal Galaxies with Six Years of Fermi-LAT Data*, *Phys. Rev. Lett.* **115** (2015), no. 23 231301, [arXiv:1503.02641].

[118] **DES, Fermi-LAT** Collaboration, A. Albert et al., *Searching for Dark Matter Annihilation in Recently Discovered Milky Way Satellites with Fermi-LAT*, *Astrophys. J.* **834** (2017), no. 2 110, [arXiv:1611.03184].

[119] **H.E.S.S.** Collaboration, A. Abramowski et al., *Search for dark matter annihilation signatures in H.E.S.S. observations of Dwarf Spheroidal Galaxies*, *Phys. Rev.* **D90**

(2014) 112012, [arXiv:1410.2589].

[120] **H.E.S.S.** Collaboration, H. Abdalla et al., *H.E.S.S. Limits on Linelike Dark Matter Signatures in the 100 GeV to 2 TeV Energy Range Close to the Galactic Center*, *Phys. Rev. Lett.* **117** (2016), no. 15 151302, [arXiv:1609.08091].

[121] **VERITAS** Collaboration, J. Holder, *Latest Results from VERITAS: Gamma 2016*, *AIP Conf. Proc.* **1792** (2017), no. 1 020013, [arXiv:1609.02881].

[122] A. U. Abeysekara et al., *Sensitivity of the High Altitude Water Cherenkov Detector to Sources of Multi-TeV Gamma Rays*, *Astropart. Phys.* **50-52** (2013) 26–32, [arXiv:1306.5800].

[123] **HAWC** Collaboration, R. López-Coto, *Very high energy gamma-ray astronomy with HAWC*, in *9th International Workshop on Ring Imaging Cherenkov Detectors (RICH 2016) Bled, Slovenia, September 5-9, 2016*, 2016. arXiv:1612.09078.

[124] H. A. Clark, P. Scott, R. Trotta, and G. F. Lewis, *Substructure considerations rule out dark matter interpretation of Fermi Galactic Center excess*, arXiv:1612.01539.

[125] S. K. Lee, M. Lisanti, B. R. Safdi, T. R. Slatyer, and W. Xue, *Evidence for Unresolved γ-Ray Point Sources in the Inner Galaxy*, *Phys. Rev. Lett.* **116** (2016), no. 5 051103, [arXiv:1506.05124].

[126] R. Bartels, S. Krishnamurthy, and C. Weniger, *Strong support for the millisecond pulsar origin of the Galactic center GeV excess*, *Phys. Rev. Lett.* **116** (2016), no. 5 051102, [arXiv:1506.05104].

[127] **IceCube** Collaboration, M. G. Aartsen et al., *Improved limits on dark matter annihilation in the Sun with the 79-string IceCube detector and implications for supersymmetry*, *JCAP* **1604** (2016), no. 04 022, [arXiv:1601.00653].

[128] **IceCube** Collaboration, M. G. Aartsen et al., *Search for annihilating dark matter in the Sun with 3 years of IceCube data*, *Eur. Phys. J.* **C77** (2017), no. 3 146, [arXiv:1612.05949].

[129] **ANTARES** Collaboration, S. Adrian-Martinez et al., *Limits on Dark Matter Annihilation in the Sun using the ANTARES Neutrino Telescope*, *Phys. Lett.* **B759** (2016) 69–74, [arXiv:1603.02228].

[130] **Super-Kamiokande** Collaboration, K. Choi et al., *Search for neutrinos from annihilation of captured low-mass dark matter particles in the Sun by Super-Kamiokande*, *Phys. Rev. Lett.* **114** (2015), no. 14 141301, [arXiv:1503.04858].

[131] L. M. Krauss, K. Freese, W. Press, and D. Spergel, *Cold dark matter candidates and the solar neutrino problem*, *Astrophys. J.* **299** (1985) 1001.

[132] M. Kamionkowski, *Energetic neutrinos from heavy neutralino annihilation in the sun*, *Phys. Rev.* **D44** (1991) 3021–3042.

[133] K. Griest and D. Seckel, *Cosmic Asymmetry, Neutrinos and the Sun*, *Nucl. Phys.* **B283** (1987) 681–705. [Erratum: Nucl. Phys.B296,1034(1988)].

[134] P. Baratella, M. Cirelli, A. Hektor, J. Pata, M. Piibeleht, and A. Strumia, *PPPC 4 DMν: a Poor Particle Physicist Cookbook for Neutrinos from Dark Matter annihilations in the Sun*, *JCAP* **1403** (2014) 053, [arXiv:1312.6408].

[135] **AMS** Collaboration, M. Aguilar et al., *First Result from the Alpha Magnetic Spectrometer on the International Space Station: Precision Measurement of the*

Positron Fraction in Primary Cosmic Rays of 0.5–350 GeV, *Phys. Rev. Lett.* **110** (2013) 141102.

[136] **PAMELA** Collaboration, O. Adriani et al., *An anomalous positron abundance in cosmic rays with energies 1.5-100 GeV*, *Nature* **458** (2009) 607–609, [arXiv:0810.4995].

[137] D. Hooper, I. Cholis, T. Linden, and K. Fang, *HAWC Observations Strongly Favor Pulsar Interpretations of the Cosmic-Ray Positron Excess*, *Submitted to: JCAP* (2017) [arXiv:1702.08436].

[138] J. Feng and H.-H. Zhang, *Pulsar interpretation of lepton spectra measured by AMS-02*, *Eur. Phys. J.* **C76** (2016), no. 5 229, [arXiv:1504.03312].

[139] S. Profumo, *Dissecting cosmic-ray electron-positron data with Occam's Razor: the role of known Pulsars*, *Central Eur. J. Phys.* **10** (2011) 1–31, [arXiv:0812.4457].

[140] D. Hooper, P. Blasi, and P. D. Serpico, *Pulsars as the Sources of High Energy Cosmic Ray Positrons*, *JCAP* **0901** (2009) 025, [arXiv:0810.1527].

[141] P. Blasi and P. D. Serpico, *High-energy antiprotons from old supernova remnants*, *Phys. Rev. Lett.* **103** (2009) 081103, [arXiv:0904.0871].

[142] F. Kahlhoefer, *Review of LHC Dark Matter Searches*, *Int. J. Mod. Phys.* **A32** (2017) 1730006, [arXiv:1702.02430].

[143] V. A. Mitsou, *Overview of searches for dark matter at the LHC*, *J. Phys. Conf. Ser.* **651** (2015), no. 1 012023, [arXiv:1402.3673].

[144] V. A. Bednyakov, *Is it possible to discover a dark matter particle with an accelerator?*, *Phys. Part. Nucl.* **47** (2016), no. 5 711–774, [arXiv:1505.04380].

[145] A. Crivellin, U. Haisch, and A. Hibbs, *LHC constraints on gauge boson couplings to dark matter*, *Phys. Rev.* **D91** (2015) 074028, [arXiv:1501.00907].

[146] D. Abercrombie et al., *Dark Matter Benchmark Models for Early LHC Run-2 Searches: Report of the ATLAS/CMS Dark Matter Forum*, arXiv:1507.00966.

[147] M. E. Peskin and T. Takeuchi, *Estimation of oblique electroweak corrections*, *Phys.Rev.* **D46** (1992) 381–409.

[148] D. C. Kennedy and B. W. Lynn, *Electroweak Radiative Corrections with an Effective Lagrangian: Four Fermion Processes*, *Nucl. Phys.* **B322** (1989) 1–54.

[149] D. C. Kennedy, B. W. Lynn, C. J. C. Im, and R. G. Stuart, *Electroweak Cross-Sections and Asymmetries at the Z0*, *Nucl. Phys.* **B321** (1989) 83–107.

[150] J. R. Ellis, M. K. Gaillard, and D. V. Nanopoulos, *A Phenomenological Profile of the Higgs Boson*, *Nucl.Phys.* **B106** (1976) 292.

[151] A. Djouadi, *The Anatomy of electro-weak symmetry breaking. I: The Higgs boson in the standard model*, *Phys.Rept.* **457** (2008) 1–216, [hep-ph/0503172].

[152] Y. G. Kim and K. Y. Lee, *The Minimal model of fermionic dark matter*, *Phys. Rev.* **D75** (2007) 115012, [hep-ph/0611069].

[153] **ATLAS** Collaboration, G. Aad et al., *Search for invisible decays of a Higgs boson using vector-boson fusion in pp collisions at $\sqrt{s} = 8$ TeV with the ATLAS detector*, *JHEP* **01** (2016) 172, [arXiv:1508.07869].

[154] Z. Fodor and A. Hebecker, *Finite temperature effective potential to order g**4, lambda**2 and the electroweak phase transition*, *Nucl. Phys.* **B432** (1994) 127–146, [hep-ph/9403219].

[155] V. A. Kuzmin, V. A. Rubakov, and M. E. Shaposhnikov, *On the Anomalous Electroweak Baryon Number Nonconservation in the Early Universe*, *Phys. Lett.* **B155** (1985) 36.

[156] A. G. Cohen, D. B. Kaplan, and A. E. Nelson, *Progress in electroweak baryogenesis*, *Ann. Rev. Nucl. Part. Sci.* **43** (1993) 27–70, [hep-ph/9302210].

[157] A. Pilaftsis, *CP violation and baryogenesis due to heavy Majorana neutrinos*, *Phys. Rev.* **D56** (1997) 5431–5451, [hep-ph/9707235].

[158] A. Pilaftsis and T. E. J. Underwood, *Resonant leptogenesis*, *Nucl. Phys.* **B692** (2004) 303–345, [hep-ph/0309342].

[159] C. Cheung, L. J. Hall, D. Pinner, and J. T. Ruderman, *Prospects and Blind Spots for Neutralino Dark Matter*, *JHEP* **05** (2013) 100, [arXiv:1211.4873].

[160] A. Bharucha, F. Brümmer, and R. Ruffault, *Well-tempered n-plet dark matter*, arXiv:1703.00370.

[161] **XENON100** Collaboration, E. Aprile et al., *Dark Matter Results from 225 Live Days of XENON100 Data*, *Phys.Rev.Lett.* **109** (2012) 181301, [arXiv:1207.5988].

[162] **LUX** Collaboration, D. Akerib et al., *First results from the LUX dark matter experiment at the Sanford Underground Research Facility*, arXiv:1310.8214.

[163] P. Panci, *New Directions in Direct Dark Matter Searches*, arXiv:1402.1507.

[164] **Planck** Collaboration, P. A. R. Ade et al., *Planck 2013 results. XVI. Cosmological parameters*, *Astron. Astrophys.* **571** (2014) A16, [arXiv:1303.5076].

[165] P. Sikivie, L. Susskind, M. B. Voloshin, and V. I. Zakharov, *Isospin Breaking in Technicolor Models*, *Nucl.Phys.* **B173** (1980) 189.

[166] F. del Aguila, A. Carmona, and J. Santiago, *Tau Custodian searches at the LHC*, *Phys.Lett.* **B695** (2011) 449–453, [arXiv:1007.4206].

[167] K. Agashe, R. Contino, L. Da Rold, and A. Pomarol, *A Custodial symmetry for Zb anti-b*, *Phys.Lett.* **B641** (2006) 62–66, [hep-ph/0605341].

[168] R. Sekhar Chivukula, S. Di Chiara, R. Foadi, and E. H. Simmons, *The Limits of Custodial Symmetry*, *Phys.Rev.* **D80** (2009) 095001, [arXiv:0908.1079].

[169] A. Carmona and F. Goertz, *Custodial Leptons and Higgs Decays*, arXiv:1301.5856.

[170] H. E. Haber and G. L. Kane, *The Search for Supersymmetry: Probing Physics Beyond the Standard Model*, *Phys.Rept.* **117** (1985) 75–263.

[171] M. S. Carena, A. Megevand, M. Quiros, and C. E. Wagner, *Electroweak baryogenesis and new TeV fermions*, *Nucl.Phys.* **B716** (2005) 319–351, [hep-ph/0410352].

[172] F. D'Eramo, *Dark matter and Higgs boson physics*, *Phys.Rev.* **D76** (2007) 083522, [arXiv:0705.4493].

[173] N. Arkani-Hamed and S. Dimopoulos, *Supersymmetric unification without low energy supersymmetry and signatures for fine-tuning at the LHC*, *JHEP* **0506** (2005) 073, [hep-th/0405159].

[174] G. Giudice and A. Romanino, *Split supersymmetry*, *Nucl.Phys.* **B699** (2004) 65–89, [hep-ph/0406088].

[175] **CMS** Collaboration, S. Chatrchyan et al., *Searches for long-lived charged particles in pp collisions at $\sqrt{s}$=7 and 8 TeV*, arXiv:1305.0491.

[176] **XENON100** Collaboration, E. Aprile et al., *The XENON100 Dark Matter Experiment*, *Astropart.Phys.* **35** (2012) 573–590, [arXiv:1107.2155].

[177] C. Cheung and D. Sanford, *Simplified Models of Mixed Dark Matter*, arXiv:1311.5896.

[178] M. Drees, M. M. Nojiri, D. Roy, and Y. Yamada, *Light Higgsino dark matter*, *Phys.Rev.* **D56** (1997) 276–290, [hep-ph/9701219].

[179] M. Pospelov and A. Ritz, *Higgs decays to dark matter: beyond the minimal model*, *Phys.Rev.* **D84** (2011) 113001, [arXiv:1109.4872].

[180] P. B. Pal, *Cold Dark Matter in the doublet - triplet Model*, *Phys.Lett.* **B205** (1988) 65.

[181] T. Araki, C. Geng, and K. I. Nagao, *Dark Matter in Inert Triplet Models*, *Phys.Rev.* **D83** (2011) 075014, [arXiv:1102.4906].

[182] S. S. Law and K. L. McDonald, *Inverse seesaw and dark matter in models with exotic lepton triplets*, *Phys.Lett.* **B713** (2012) 490–494, [arXiv:1204.2529].

[183] M. Aoki, J. Kubo, T. Okawa, and H. Takano, *Impact of Inert Higgsino Dark Matter*, *Phys.Lett.* **B707** (2012) 107–115, [arXiv:1110.5403].

[184] Y. G. Kim, K. Y. Lee, and S. Shin, *Singlet fermionic dark matter*, *JHEP* **0805** (2008) 100, [arXiv:0803.2932].

[185] E. Ma and D. Suematsu, *Fermion Triplet Dark Matter and Radiative Neutrino Mass*, *Mod.Phys.Lett.* **A24** (2009) 583–589, [arXiv:0809.0942].

[186] K. Hamaguchi, S. Shirai, and T. Yanagida, *Cosmic Ray Positron and Electron Excess from Hidden-Fermion Dark Matter Decays*, *Phys.Lett.* **B673** (2009) 247–250, [arXiv:0812.2374].

[187] Y. G. Kim and S. Shin, *Singlet Fermionic Dark Matter explains DAMA signal*, *JHEP* **0905** (2009) 036, [arXiv:0901.2609].

[188] C. de S. Pires, F. Queiroz, and P. Rodrigues da Silva, *Singlet Majorana fermion dark matter, DAMA, CoGeNT, and CDMS-II*, *Phys.Rev.* **D82** (2010) 105014, [arXiv:1002.4601].

[189] J.-M. Zheng, Z.-H. Yu, J.-W. Shao, X.-J. Bi, Z. Li, et al., *Constraining the interaction strength between dark matter and visible matter: I. fermionic dark matter*, *Nucl.Phys.* **B854** (2012) 350–374, [arXiv:1012.2022].

[190] K. Fukushima, J. Kumar, and P. Sandick, *Detection Prospects for Majorana Fermion WIMPless Dark Matter*, *Phys.Rev.* **D84** (2011) 014020, [arXiv:1103.5068].

[191] B. Bellazzini, C. Csaki, J. Hubisz, J. Shao, and P. Tanedo, *Goldstone Fermion Dark Matter*, *JHEP* **1109** (2011) 035, [arXiv:1106.2162].

[192] C.-H. Chen and S. S. Law, *Exotic fermion multiplets as a solution to baryon asymmetry, dark matter and neutrino masses*, *Phys.Rev.* **D85** (2012) 055012, [arXiv:1111.5462].

[193] E. Ma, *Dark-Matter Fermion from Left-Right Symmetry*, *Phys.Rev.* **D85** (2012) 091701, [arXiv:1202.5828].

[194] W. Chao, *Dark Matter, LFV and Neutrino Magnetic Moment in the Radiative Seesaw Model with Triplet Fermion*, arXiv:1202.6394.

[195] L. Lopez-Honorez, T. Schwetz, and J. Zupan, *Higgs portal, fermionic dark matter, and a Standard Model like Higgs at 125 GeV*, *Phys.Lett.* **B716** (2012) 179–185,

[arXiv:1203.2064].

[196] W.-M. Yang, *An Unification Model of Fermion Flavor and Baryon asymmetry and Dark Matter with The TeV Scale $U(1)_{B-L}$*, arXiv:1206.5353.

[197] H. Okada and T. Toma, *Fermionic Dark Matter in Radiative Inverse Seesaw Model with $U(1)_{B-L}$*, *Phys.Rev.* **D86** (2012) 033011, [arXiv:1207.0864].

[198] S. Baek, P. Ko, W.-I. Park, and E. Senaha, *Vacuum structure and stability of a singlet fermion dark matter model with a singlet scalar messenger*, arXiv:1209.4163.

[199] C. Arbelaez, R. Longas, D. Restrepo, and O. Zapata, *Fermion dark matter from SO(10) GUTs*, *Phys. Rev.* **D93** (2016), no. 1 013012, [arXiv:1509.06313].

[200] J. Fan and M. Reece, *Probing Charged Matter Through Higgs Diphoton Decay, Gamma Ray Lines, and EDMs*, *JHEP* **1306** (2013) 004, [arXiv:1301.2597].

[201] R. A. Horn and C. R. Johnson, *Matrix Analysis*, *Cambridge University Press* (1995) p. 595.

[202] G. F. Giudice and A. Strumia, *Probing High-Scale and Split Supersymmetry with Higgs Mass Measurements*, *Nucl.Phys.* **B858** (2012) 63–83, [arXiv:1108.6077].

[203] N. Arkani-Hamed, K. Blum, R. T. D'Agnolo, and J. Fan, *2:1 for Naturalness at the LHC?*, *JHEP* **1301** (2013) 149, [arXiv:1207.4482].

[204] **Particle Data Group** Collaboration, J. Beringer et al., *Review of Particle Physics (RPP)*, *Phys.Rev.* **D86** (2012) 010001.

[205] C. Cai, Z.-H. Yu, and H.-H. Zhang, *CEPC Precision of Electroweak Oblique Parameters and Weakly Interacting Dark Matter: the Fermionic Case*, arXiv:1611.02186.

[206] M. Drees and M. Nojiri, *Neutralino - nucleon scattering revisited*, *Phys.Rev.* **D48** (1993) 3483–3501, [hep-ph/9307208].

[207] A. Crivellin, M. Hoferichter, and M. Procura, *Accurate evaluation of hadronic uncertainties in spin-independent WIMP-nucleon scattering: Disentangling two- and three-flavor effects*, *Phys.Rev.* **D89** (2014) 054021, [arXiv:1312.4951].

[208] J. Gasser, H. Leutwyler, and M. Sainio, *Sigma term update*, *Phys.Lett.* **B253** (1991) 252–259.

[209] P. Junnarkar and A. Walker-Loud, *Scalar strange content of the nucleon from lattice QCD*, *Phys.Rev.* **D87** (2013), no. 11 114510, [arXiv:1301.1114].

[210] A. Vainshtein, V. I. Zakharov, and M. A. Shifman, *Higgs Particles*, *Sov.Phys.Usp.* **23** (1980) 429–449.

[211] B. A. Kniehl and M. Spira, *Low-energy theorems in Higgs physics*, *Z.Phys.* **C69** (1995) 77–88, [hep-ph/9505225].

[212] A. Pilaftsis, *Higgs boson low-energy theorem and compatible gauge fixing conditions*, *Phys.Lett.* **B422** (1998) 201–211, [hep-ph/9711420].

[213] R. J. Hill and M. P. Solon, *WIMP-nucleon scattering with heavy WIMP effective theory*, arXiv:1309.4092.

[214] R. J. Hill and M. P. Solon, *Standard Model anatomy of WIMP dark matter direct detection I: weak-scale matching*, arXiv:1401.3339.

[215] J. Hisano, K. Ishiwata, and N. Nagata, *Direct Search of Dark Matter in High-Scale Supersymmetry*, *Phys.Rev.* **D87** (2013) 035020, [arXiv:1210.5985].

[216] J. Hisano, K. Ishiwata, and N. Nagata, *QCD Effects on Direct Detection of Wino Dark Matter*, *JHEP* **06** (2015) 097, [arXiv:1504.00915].

[217] T. Appelquist and J. Carazzone, *Infrared Singularities and Massive Fields*, *Phys.Rev.* **D11** (1975) 2856.

[218] A. Dedes and K. Suxho, *Anatomy of the Higgs boson decay into two photons in the unitary gauge*, *Adv.High Energy Phys.* **2013** (2013) 631841, [arXiv:1210.0141].

[219] A. Joglekar, P. Schwaller, and C. E. Wagner, *Dark Matter and Enhanced Higgs to Di-photon Rate from Vector-like Leptons*, *JHEP* **1212** (2012) 064, [arXiv:1207.4235].

[220] **CMS** Collaboration, S. Chatrchyan et al., *Observation of a new boson at a mass of 125 GeV with the CMS experiment at the LHC*, *Phys.Lett.* **B716** (2012) 30–61, [arXiv:1207.7235].

[221] **ATLAS, CMS** Collaboration, G. Aad et al., *Measurements of the Higgs boson production and decay rates and constraints on its couplings from a combined ATLAS and CMS analysis of the LHC pp collision data at $\sqrt{s} = 7$ and 8 TeV*, *JHEP* **08** (2016) 045, [arXiv:1606.02266].

[222] S. R. Coleman, *The Fate of the False Vacuum. 1. Semiclassical Theory*, *Phys.Rev.* **D15** (1977) 2929–2936.

[223] G. Isidori, G. Ridolfi, and A. Strumia, *On the metastability of the standard model vacuum*, *Nucl.Phys.* **B609** (2001) 387–409, [hep-ph/0104016].

[224] C. Cheung, M. Papucci, and K. M. Zurek, *Higgs and Dark Matter Hints of an Oasis in the Desert*, *JHEP* **1207** (2012) 105, [arXiv:1203.5106].

[225] **ATLAS** Collaboration, *Search for direct production of charginos and neutralinos in events with three leptons and missing transverse momentum in 21 fb^{-1} of pp collisions at $\sqrt{s} = 8$ TeV with the ATLAS detector*, ATLAS-CONF-2013-035, ATLAS-COM-CONF-2013-042.

[226] **CMS** Collaboration, *Search for electroweak production of charginos, neutralinos, and sleptons using leptonic final states in pp collisions at 8 TeV*, CMS-PAS-SUS-13-006.

[227] W. Beenakker, M. Klasen, M. Kramer, T. Plehn, M. Spira, et al., *The Production of charginos / neutralinos and sleptons at hadron colliders*, *Phys.Rev.Lett.* **83** (1999) 3780–3783, [hep-ph/9906298].

[228] J. F. Gunion and H. E. Haber, *Two-body decays of Neutralinos and Charginos*, *Phys.Rev.* **D37** (1988) 2515.

[229] A. Delgado, G. Nardini, and M. Quiros, *Large diphoton Higgs rates from supersymmetric triplets*, *Phys.Rev.* **D86** (2012) 115010, [arXiv:1207.6596].

[230] T. Abe, R. Kitano, and R. Sato, *Discrimination of dark matter models in future experiments*, *Phys. Rev.* **D91** (2015), no. 9 095004, [arXiv:1411.1335].

[231] A. Freitas, S. Westhoff, and J. Zupan, *Integrating in the Higgs Portal to Fermion Dark Matter*, *JHEP* **09** (2015) 015, [arXiv:1506.04149].

[232] A. Betancur, R. Longas, and O. Zapata, *Doublet-triplet dark matter with neutrino masses*, arXiv:1704.01162.

[233] A. De Simone and T. Jacques, *Simplified Models vs. Effective Field Theory Approaches in Dark Matter Searches*, arXiv:1603.08002.

[234] **Particle Data Group** Collaboration, K. A. Olive et al., *Review of Particle*

Physics, *Chin. Phys.* **C38** (2014) 090001.

[235] L. Roszkowski, *Light neutralino as dark matter*, *Phys.Lett.* **B262** (1991) 59–67.

[236] S. Banerjee, S. Matsumoto, K. Mukaida, and Y.-L. S. Tsai, *WIMP Dark Matter in a Well-Tempered Regime: A case study on Singlet-Doublets Fermionic WIMP*, arXiv:1603.07387.

[237] N. Nagata, K. A. Olive, and J. Zheng, *Weakly-Interacting Massive Particles in Non-supersymmetric SO(10) Grand Unified Models*, *JHEP* **10** (2015) 193, [arXiv:1509.00809].

[238] S. M. Boucenna, M. B. Krauss, and E. Nardi, *Dark matter from the vector of SO (10)*, *Phys. Lett.* **B755** (2016) 168–176, [arXiv:1511.02524].

[239] C. Garcia-Cely and J. Heeck, *Phenomenology of left-right symmetric dark matter*, arXiv:1512.03332. [JCAP1603,021(2016)].

[240] F. D'Eramo and M. Procura, *Connecting Dark Matter UV Complete Models to Direct Detection Rates via Effective Field Theory*, *JHEP* **04** (2015) 054, [arXiv:1411.3342].

[241] Y. Mambrini, K. A. Olive, J. Quevillon, and B. Zaldivar, *Gauge Coupling Unification and Nonequilibrium Thermal Dark Matter*, *Phys. Rev. Lett.* **110** (2013), no. 24 241306, [arXiv:1302.4438].

[242] C.-K. Chua and G.-G. Wong, *Study of Majorana Fermionic Dark Matter*, 2015. arXiv:1512.01991.

[243] E. Del Nobile, R. Franceschini, D. Pappadopulo, and A. Strumia, *Minimal Matter at the Large Hadron Collider*, *Nucl. Phys.* **B826** (2010) 217–234, [arXiv:0908.1567].

[244] S. Chang, N. Weiner, and I. Yavin, *Magnetic Inelastic Dark Matter*, *Phys. Rev.* **D82** (2010) 125011, [arXiv:1007.4200].

[245] N. Weiner and I. Yavin, *How Dark Are Majorana WIMPs? Signals from MiDM and Rayleigh Dark Matter*, *Phys. Rev.* **D86** (2012) 075021, [arXiv:1206.2910].

[246] T. W. B. Kibble, *Symmetry breaking in nonAbelian gauge theories*, *Phys. Rev.* **155** (1967) 1554–1561.

[247] T. W. B. Kibble, G. Lazarides, and Q. Shafi, *Strings in SO(10)*, *Phys. Lett.* **B113** (1982) 237–239.

[248] M. Frigerio and T. Hambye, *Dark matter stability and unification without supersymmetry*, *Phys. Rev.* **D81** (2010) 075002, [arXiv:0912.1545].

[249] **LEP2 SUSY Working Group** Collaboration, *Combined lep chargino results, up to 208 gev for low dm (2001)*, . http://lepsusy.web.cern.ch/lepsusy/www/inoslowdmsummer02/charginolowdm_pub.html.

[250] **L3** Collaboration, P. Achard et al., *Search for heavy neutral and charged leptons in e^+e^- annihilation at LEP*, *Phys. Lett.* **B517** (2001) 75–85, [hep-ex/0107015].

[251] **DELPHI** Collaboration, J. Abdallah et al., *Searches for supersymmetric particles in e+ e- collisions up to 208-GeV and interpretation of the results within the MSSM*, *Eur. Phys. J.* **C31** (2003) 421–479, [hep-ex/0311019].

[252] J. Hisano, D. Kobayashi, N. Mori, and E. Senaha, *Effective Interaction of Electroweak-Interacting Dark Matter with Higgs Boson and Its Phenomenology*, *Phys. Lett.* **B742** (2015) 80–85, [arXiv:1410.3569].

[253] **LUX** Collaboration, D. S. Akerib et al., *Improved WIMP scattering limits from*

the LUX experiment, arXiv:1512.03506.

[254] **LUX** Collaboration, D. S. Akerib et al., *First results from the LUX dark matter experiment at the Sanford Underground Research Facility*, *Phys. Rev. Lett.* **112** (2014) 091303, [arXiv:1310.8214].

[255] V. Barger, W.-Y. Keung, and D. Marfatia, *Electromagnetic properties of dark matter: Dipole moments and charge form factor*, *Phys. Lett.* **B696** (2011) 74–78, [arXiv:1007.4345].

[256] T. Banks, J.-F. Fortin, and S. Thomas, *Direct Detection of Dark Matter Electromagnetic Dipole Moments*, arXiv:1007.5515.

[257] J.-F. Fortin and T. M. P. Tait, *Collider Constraints on Dipole-Interacting Dark Matter*, *Phys. Rev.* **D85** (2012) 063506, [arXiv:1103.3289].

[258] **ATLAS, CMS** Collaboration, G. Aad et al., *Combined Measurement of the Higgs Boson Mass in pp Collisions at $\sqrt{s} = 7$ and 8 TeV with the ATLAS and CMS Experiments*, *Phys. Rev. Lett.* **114** (2015) 191803, [arXiv:1503.07589].

[259] R. Barbieri, A. Pomarol, R. Rattazzi, and A. Strumia, *Electroweak symmetry breaking after LEP-1 and LEP-2*, *Nucl. Phys.* **B703** (2004) 127–146, [hep-ph/0405040].

[260] H. Mebane, N. Greiner, C. Zhang, and S. Willenbrock, *Constraints on Electroweak Effective Operators at One Loop*, *Phys. Rev.* **D88** (2013), no. 1 015028, [arXiv:1306.3380].

[261] **IceCube** Collaboration, M. G. Aartsen et al., *Search for dark matter annihilations in the Sun with the 79-string IceCube detector*, *Phys. Rev. Lett.* **110** (2013), no. 13 131302, [arXiv:1212.4097].

[262] G. Belanger, F. Boudjema, and A. Pukhov, *micrOMEGAs : a code for the calculation of Dark Matter properties in generic models of particle interaction*, in *The Dark Secrets of the Terascale*, pp. 739–790, 2013. arXiv:1402.0787.

[263] A. Semenov, *LanHEP: A package for automatic generation of Feynman rules from the Lagrangian*, *Comput. Phys. Commun.* **115** (1998) 124–139.

[264] D. Hooper, C. Kelso, and F. S. Queiroz, *Stringent and Robust Constraints on the Dark Matter Annihilation Cross Section From the Region of the Galactic Center*, *Astropart. Phys.* **46** (2013) 55–70, [arXiv:1209.3015].

[265] J. F. Navarro, C. S. Frenk, and S. D. M. White, *The Structure of cold dark matter halos*, *Astrophys. J.* **462** (1996) 563–575, [astro-ph/9508025].

[266] A. Sommerfeld, *ber die beugung und bremsung der elektronen*, *Annalen der Physik* **403** no. 3.

[267] J. Hisano, S. Matsumoto, and M. M. Nojiri, *Explosive dark matter annihilation*, *Phys. Rev. Lett.* **92** (2004) 031303, [hep-ph/0307216].

[268] J. Hisano, S. Matsumoto, M. M. Nojiri, and O. Saito, *Non-perturbative effect on dark matter annihilation and gamma ray signature from galactic center*, *Phys. Rev.* **D71** (2005) 063528, [hep-ph/0412403].

[269] M. Cirelli, A. Strumia, and M. Tamburini, *Cosmology and Astrophysics of Minimal Dark Matter*, *Nucl. Phys.* **B787** (2007) 152–175, [arXiv:0706.4071].

[270] **LUX** Collaboration, D. S. Akerib et al., *Results on the Spin-Dependent Scattering of Weakly Interacting Massive Particles on Nucleons from the Run 3 Data of the LUX Experiment*, *Phys. Rev. Lett.* **116** (2016), no. 16 161302, [arXiv:1602.03489].

[271] **ATLAS** Collaboration, G. Aad et al., *Search for dark matter in events with a Z boson and missing transverse momentum in pp collisions at $\sqrt{s}$=8 TeV with the ATLAS detector*, *Phys. Rev.* **D90** (2014), no. 1 012004, [arXiv:1404.0051].

[272] **ATLAS** Collaboration, G. Aad et al., *Search for new particles in events with one lepton and missing transverse momentum in pp collisions at $\sqrt{s}$ = 8 TeV with the ATLAS detector*, *JHEP* **09** (2014) 037, [arXiv:1407.7494].

[273] **CMS** Collaboration, V. Khachatryan et al., *Search for physics beyond the standard model in final states with a lepton and missing transverse energy in proton-proton collisions at sqrt(s) = 8 TeV*, *Phys. Rev.* **D91** (2015), no. 9 092005, [arXiv:1408.2745].

[274] **ATLAS** Collaboration, G. Aad et al., *Search for dark matter in events with a hadronically decaying W or Z boson and missing transverse momentum in pp collisions at $\sqrt{s}$ = 8 TeV with the ATLAS detector*, *Phys. Rev. Lett.* **112** (2014), no. 4 041802, [arXiv:1309.4017].

[275] A. G. Delannoy et al., *Probing Dark Matter at the LHC using Vector Boson Fusion Processes*, *Phys. Rev. Lett.* **111** (2013) 061801, [arXiv:1304.7779].

[276] A. Berlin, T. Lin, M. Low, and L.-T. Wang, *Neutralinos in Vector Boson Fusion at High Energy Colliders*, *Phys. Rev.* **D91** (2015), no. 11 115002, [arXiv:1502.05044].

[277] **CMS** Collaboration, S. Chatrchyan et al., *Search for invisible decays of Higgs bosons in the vector boson fusion and associated ZH production modes*, *Eur. Phys. J.* **C74** (2014) 2980, [arXiv:1404.1344].

[278] **CMS** Collaboration, V. Khachatryan et al., *Search for dark matter, extra dimensions, and unparticles in monojet events in proton–proton collisions at $\sqrt{s} = 8$ TeV*, *Eur. Phys. J.* **C75** (2015), no. 5 235, [arXiv:1408.3583].

[279] **ATLAS** Collaboration, G. Aad et al., *Search for new phenomena in events with a photon and missing transverse momentum in pp collisions at $\sqrt{s} = 8$ TeV with the ATLAS detector*, *Phys. Rev.* **D91** (2015), no. 1 012008, [arXiv:1411.1559]. [Erratum: Phys. Rev.D92,no.5,059903(2015)].

[280] J. Brooke, M. R. Buckley, P. Dunne, B. Penning, J. Tamanas, and M. Zgubic, *Vector Boson Fusion Searches for Dark Matter at the LHC*, arXiv:1603.07739.

[281] A. Belyaev, N. D. Christensen, and A. Pukhov, *CalcHEP 3.4 for collider physics within and beyond the Standard Model*, *Comput. Phys. Commun.* **184** (2013) 1729–1769, [arXiv:1207.6082].

[282] A. Ismail, E. Izaguirre, and B. Shuve, *Illuminating New Electroweak States at Hadron Colliders*, *Phys. Rev.* **D94** (2016), no. 1 015001, [arXiv:1605.00658].

[283] G. Busoni, A. De Simone, E. Morgante, and A. Riotto, *On the Validity of the Effective Field Theory for Dark Matter Searches at the LHC*, *Phys. Lett.* **B728** (2014) 412–421, [arXiv:1307.2253].

[284] G. Busoni, A. De Simone, J. Gramling, E. Morgante, and A. Riotto, *On the Validity of the Effective Field Theory for Dark Matter Searches at the LHC, Part II: Complete Analysis for the s-channel*, *JCAP* **1406** (2014) 060, [arXiv:1402.1275].

[285] O. Buchmueller, M. J. Dolan, and C. McCabe, *Beyond Effective Field Theory for Dark Matter Searches at the LHC*, *JHEP* **01** (2014) 025, [arXiv:1308.6799].

[286] M. Endo and Y. Yamamoto, *Unitarity Bounds on Dark Matter Effective Interactions at LHC*, *JHEP* **06** (2014) 126, [arXiv:1403.6610].

[287] N. Bell, G. Busoni, A. Kobakhidze, D. M. Long, and M. A. Schmidt, *Unitarisation of EFT Amplitudes for Dark Matter Searches at the LHC*, arXiv:1606.02722.

[288] J. Billard, L. Strigari, and E. Figueroa-Feliciano, *Implication of neutrino backgrounds on the reach of next generation dark matter direct detection experiments*, *Phys. Rev.* **D89** (2014), no. 2 023524, [arXiv:1307.5458].

[289] N. E. Mavromatos and A. Pilaftsis, *Anomalous Majorana Neutrino Masses from Torsionful Quantum Gravity*, *Phys. Rev.* **D86** (2012) 124038, [arXiv:1209.6387].

[290] R. Adhikari et al., *A White Paper on keV Sterile Neutrino Dark Matter*, *JCAP* **1701** (2017), no. 01 025, [arXiv:1602.04816].

[291] L. Heurtier and D. Teresi, *Dark matter and observable lepton flavor violation*, *Phys. Rev.* **D94** (2016), no. 12 125022, [arXiv:1607.01798].

[292] R. Essig et al., *Working Group Report: New Light Weakly Coupled Particles*, in *Proceedings, 2013 Community Summer Study on the Future of U.S. Particle Physics: Snowmass on the Mississippi (CSS2013): Minneapolis, MN, USA, July 29-August 6, 2013*, 2013. arXiv:1311.0029.

[293] J. Alexander et al., *Dark Sectors 2016 Workshop: Community Report*, 2016. arXiv:1608.08632.

[294] R. D. Peccei and H. R. Quinn, *Constraints Imposed by CP Conservation in the Presence of Instantons*, *Phys. Rev.* **D16** (1977) 1791–1797.

[295] R. D. Peccei and H. R. Quinn, *CP Conservation in the Presence of Instantons*, *Phys. Rev. Lett.* **38** (1977) 1440–1443.

[296] P. S. Bhupal Dev, P. Millington, A. Pilaftsis, and D. Teresi, *Flavour Covariant Transport Equations: an Application to Resonant Leptogenesis*, *Nucl. Phys.* **B886** (2014) 569–664, [arXiv:1404.1003].

[297] A. Achelashvili and Z. Tavartkiladze, *Calculable Cosmological CP Violation and Resonant Leptogenesis*, arXiv:1611.07956.

[298] M. Viel, G. D. Becker, J. S. Bolton, and M. G. Haehnelt, *Warm dark matter as a solution to the small scale crisis: New constraints from high redshift lyman-α forest data*, *Phys. Rev.* **D88** (2013) 043502, [arXiv:1306.2314].

[299] G. C. Branco, P. M. Ferreira, L. Lavoura, M. N. Rebelo, M. Sher, and J. P. Silva, *Theory and phenomenology of two-Higgs-doublet models*, *Phys. Rept.* **516** (2012) 1–102, [arXiv:1106.0034].

[300] H. Georgi and D. V. Nanopoulos, *Suppression of Flavor Changing Effects From Neutral Spinless Meson Exchange in Gauge Theories*, *Phys. Lett.* **B82** (1979) 95–96.

[301] J. F. Gunion and H. E. Haber, *The CP conserving two Higgs doublet model: The Approach to the decoupling limit*, *Phys. Rev.* **D67** (2003) 075019, [hep-ph/0207010].

[302] I. F. Ginzburg and M. Krawczyk, *Symmetries of two Higgs doublet model and CP violation*, *Phys. Rev.* **D72** (2005) 115013, [hep-ph/0408011].

[303] P. S. Bhupal Dev and A. Pilaftsis, *Maximally Symmetric Two Higgs Doublet Model with Natural Standard Model Alignment*, *JHEP* **12** (2014) 024, [arXiv:1408.3405]. [Erratum: JHEP11,147(2015)].

[304] A. Pilaftsis, *Symmetries for standard model alignment in multi-Higgs doublet models*, *Phys. Rev.* **D93** (2016), no. 7 075012, [arXiv:1602.02017].

[305] B. Grzadkowski, O. M. Ogreid, and P. Osland, *Spontaneous CP violation in the 2HDM: physical conditions and the alignment limit*, *Phys. Rev.* **D94** (2016), no. 11 115002, [arXiv:1609.04764].

[306] M. Gorbahn, J. M. No, and V. Sanz, *Benchmarks for Higgs Effective Theory: Extended Higgs Sectors*, *JHEP* **10** (2015) 036, [arXiv:1502.07352].

[307] H. Bélusca-Maïto, A. Falkowski, D. Fontes, J. C. Romão, and J. P. Silva, *Higgs EFT for 2HDM and beyond*, arXiv:1611.01112.

[308] J. E. Kim and G. Carosi, *Axions and the Strong CP Problem*, *Rev. Mod. Phys.* **82** (2010) 557–602, [arXiv:0807.3125].

[309] S. Weinberg, *A New Light Boson?*, *Phys. Rev. Lett.* **40** (1978) 223–226.

[310] F. Wilczek, *Problem of Strong p and t Invariance in the Presence of Instantons*, *Phys. Rev. Lett.* **40** (1978) 279–282.

[311] G. G. Raffelt, *Astrophysical axion bounds*, *Lect. Notes Phys.* **741** (2008) 51–71, [hep-ph/0611350]. [,51(2006)].

[312] M. S. Turner, *Cosmic and Local Mass Density of Invisible Axions*, *Phys. Rev.* **D33** (1986) 889–896.

[313] K. Pedersen and Z. Sullivan, *Probing the two Higgs doublet wedge region with charged Higgs boson decays to boosted jets*, *Phys. Rev.* **D95** (2017), no. 3 035037, [arXiv:1612.03978].

[314] G. Passarino and M. Veltman, *One Loop Corrections for e^+e^- Annihilation Into $\mu^+\mu^-$ in the Weinberg Model*, *Nucl.Phys.* **B160** (1979) 151.

[315] A. Axelrod, *Flavor Changing Z^0 Decay and the Top Quark*, *Nucl.Phys.* **B209** (1982) 349.

[316] M. Duch, B. Grzadkowski, and J. Wudka, *Classification of effective operators for interactions between the Standard Model and dark matter*, *JHEP* **05** (2015) 116, [arXiv:1412.0520].

[317] B. Grzadkowski, M. Iskrzynski, M. Misiak, and J. Rosiek, *Dimension-Six Terms in the Standard Model Lagrangian*, *JHEP* **10** (2010) 085, [arXiv:1008.4884].

[318] W.-C. Huang and F. F. Deppisch, *Dark matter origins of neutrino masses*, *Phys. Rev.* **D91** (2015) 093011, [arXiv:1412.2027].

[319] A. Dedes, W. Materkowska, M. Paraskevas, J. Rosiek, and K. Suxho, *Feynman Rules for the Standard Model Effective Field Theory in R_ξ-gauges*, arXiv:1704.03888.